Università degli Studi di Roma
"La Sapienza"

Doctoral School "Vito Volterra"

PhD Thesis in Earth Sciences

XXX Cycle

The impact of isotopic events on the Central Mediterranean carbonate successions between late Eocene and Miocene

Irene Cornacchia

February 2018

Supervisor:

Prof. Marco Brandano
Dipartimento di Scienze della Terra,
Università degli Studi di Roma "La Sapienza"
P.le Aldo Moro 5, 00185 Roma (Italy)

Co-Supervisors:

Prof. Isabella Raffi
Dipartimento di Ingegneria e Geologia,
Università degli Studi "G. d'Annunzio"
Chieti- Pescara
Via dei Vestini 31, 66013 Chieti (Italy)

Dr. Samuele Agostini
Istituto di Geoscienze e Georisorse (IGG)
CNR Via Moruzzi 1, 56124 Pisa (Italy)

Revised by:

Prof. Helmut Weissert
Department of Earth Sciences,
ETH Zürich
Sonnegstrasse 5, 8092 Zürich (Switzerland)

Prof. Nereo Preto
Departimento di Geoscienze,
Unversity of Padua via G. Gradenigo 6,
35131 Padova (Italy)

Dr. Telm Bover-Arnal
Departament de Mineralogia, Petrologia i
Geologia Aplicada Facultat de Ciències de la
Terra, Universitat de Barcelona 08028
Barcelona (Spain)

Table of contents

Abstract

The late Eocene-Miocene is a key interval in the evolution of the global climate. At the Eocene-Oligocene boundary, the Earth faced the transition from a greenhouse period, to the present icehouse climate. This transition culminated with the onset of the Antarctica polar ice cap, testified by a positive oxygen isotope shift recorded in the deep-sea carbonate successions, known in literature as Oi-1 Event (~33.5 Ma). At the Oligocene-Miocene boundary (~23 Ma) another positive oxygen isotope excursion, the Mi-1 Event, testifies for the increase of the Antarctica ice-volume. Conversely, a long-term negative $\delta^{18}O$ excursion documents the Mid Miocene Climatic Optimum (17-13.5 Ma). These climatic events were associated to two sharp positive $\delta^{13}C$ shifts recorded contemporary to the Oi-1 and Mi-1 events, and a long-term positive carbon isotope excursion recorded in the middle Miocene, known in literature as Monterey Event.

On a regional scale, the Eocene-Miocene interval is extremely dynamic too. In fact, the Mediterranean evolved from a wide open to the modern closed basin, and the Apennine orogenesis, coupled with the associated volcanism, affected the Central Mediterranean area.

This work aims to identify how the Central Mediterranean shallow- and deep-sea carbonate successions responded to the major carbon-cycle perturbations, and recorded the main carbon isotope events between late Eocene and middle Miocene. Furthermore, this study intends to discriminate the global and the regional factors controlling carbonate production and changes, to understand which one prevailed in affecting the Central Mediterranean water chemistry and its isotope signature during the interval of interest.

Both shallow-water and basinal carbonate successions have been investigated. The shallow-water record has been investigated in the Central Apennines platforms, the Latium-Abruzzi Platform and the Apula Platform, while the basinal isotope signature has been investigated in the Umbria-Marche hemipelagic succession, in the Northern Apennines.

A robust chronostratigraphic framework of the platform successions has been assessed through calcareous nannofossil biostratigraphy coupled with Strontium Isotope Stratigraphy. The reconstruction of the stratigraphic architecture of the platforms and the high-resolution biostratigraphy allowed to correlate the shallow-water isotope signals with the Mediterranean hemipelagic record and the global deep-sea isotope curves.

The carbon-cycle perturbation related to the Eocene-Oligocene transition and the Oi-1 Event has been analysed in the northern extension of the Apula Platform, cropping out in the Majella Mountain (Santo Spirito Formation), and in the contemporary Umbria-Marche basinal succession (Massignano section, Conero area, Northern Apennines). The shallow-water $\delta^{13}C$ has been measured on whole-rock samples and correlated with the $\delta^{13}C_{TOC}$ of the hemipelagic succession. The results show that the upper Eocene carbon isotope record of the Central Mediterranean follows the global trend, but that local factors related to the oceanography of the Mediterranean affected the hemipelagic carbon isotope record. Furthermore, no major carbon isotope shifts are recorded contemporary to the Oi-1 Event in the Santo Spirito Formation since the normal bedding is interrupted by extensive slumps, which are interpreted as the main consequence of the sea-level drop occurred due to the establishment

of the Antarctica ice-sheet. Lastly, no significant changes in the carbonate factory of the Santo Spirito Formation are recorded at the Eocene-Oligocene transition since the sampled sections represent an outer ramp setting, thus colonised only by photo-independent organisms. However, the observation of skeletal assemblages within the resedimented material across the Eocene-Oligocene transition document the demise of the Larger Benthic Foraminifera, the disappearance of the ortophragminids and the reduction of the nummulitids, and a contemporary increase of the organisms related to the seagrass and the spread of the corals.

The Monterey Event has been investigated in both the Central Apennine carbonate platforms: the Latium-Abruzzi Platform (*Lithothamnion* and Bryozoan Limestone Formation) and the Apula Platform (Bolognano Formation), and correlated with the contemporary Umbria-Marche pelagic signal. Differently from the carbon isotope record of the Eocene-Oligocene transition, the middle Miocene $\delta^{13}C$ curves show a wider positive excursion in the shallow-water records in comparison to the hemipelagic one. This amplification of the signal has been interpreted as due to the photosynthetic activity within the oligophotic zone. Furthermore, in both the carbonate platforms, the Monterey Event coincides with the spread of bryozoans within the lower portion of the middle ramp and in the outer ramp settings. Filter-feeding biota must have been favoured by the increased nutrient availability related to the Mid Miocene Climatic Optimum and enhanced by regional factors, e.g. the volcanism of the Sardinia-Corsica Block and the closure of the Indo-Pacific gateway between the late Burdigalian and the Langhian. The high productivity of the bryozoan-dominated carbonate factory, in turn, led to the development of low-angle ramps.

The complex interplay between global and regional factors in controlling the Central Mediterranean seawater chemistry has been investigated through the integrated study of the Sr and the Nd isotope signatures of the Miocene hemipelagic Umbria-Marche and Apula successions. The results document that the geodynamic evolution of the Mediterranean had an unequivocal control on the seawater chemistry of this basin. The Sr isotope record shows three critical intervals: the late Aquitanian, the middle to late Burdigalian and the Messinian. During late Aquitanian, the increased runoff in a moment of sea-level low-stand related to a glaciation affected the Sr isotope record of the Central Mediterranean. During Burdigalian, the highly explosive subduction-related volcanism of the Western Mediterranean led the Sr isotope ratios to fall below the global ocean signal. Lastly, during late Miocene, the Sr isotope record testifies for the onset of restricted water exchanges between several marginal basins, e.g the proto-Adriatic basins, and the main Central Mediterranean water body.

The onset of restricted water conditions has been documented not only in the hemipelagic record of the Majella Mountain succession (*Turborotalita multiloba* marls, Messinian), but also in the shallow-water record of the *Lithothamnion* Limestone (late Tortonian-early Messinian). In fact, the *Lithothamnion* Limestone Sr isotope signature falls significantly below the global ocean record during lower Messinian due to the eastward migration of the Apennine accretionary wedge, which led to an increased freshwater input and sediment runoff into the basin.

The Miocene Nd isotope record testifies for the evolution of the Mediterranean from a wide open to the modern closed basin. The volcanic influence on the Nd isotopes is recorded during Aquitanian, when the Cenozoic volcanism affected the northern Indian Ocean, and the subduction-related volcanism of the Western Mediterranean was active. During middle Miocene, the Nd isotope ratios document a Central Mediterranean exchanging with the Paratethys, especially during the sea-level

high-stand contemporary to the Middle Miocene Climatic Optimum. During the Messinian, the Nd isotope datum is coherent with the Sr isotope record, showing a good affinity with the Atlantic Ocean signal, but also contamination by the local freshwater input. Lastly, the Nd isotope record of the Mediterranean reflects the physiography of this basin, where the proximity of the land is a major controlling factor on its water chemistry due to runoff and freshwater input. Thus, the Nd isotope signature of the Mediterranean could never be the same as the surrounding Oceans, but it will always be a mix of two opposite controlling factors: the main oceanic masses entering the basin and its oceanography, and the local geodynamic evolution coupled with volcanism.

This work states that the Central Mediterranean carbonate successions recorded the main carbon isotope trends and the global carbon-cycle perturbations occurred between late Eocene and middle Miocene, but that the local factors related to the geodynamic and oceanographic evolution of the Mediterranean area affected the local water chemistry, complicating the isotope signature of the carbonate successions. For these reasons, this study stresses out how caution must be taken prior to drive any conclusion on the global climatic and the trophic events analysing the signal of a closed basin. Secondly, this work proves that Strontium Isotope Stratigraphy must be applied very carefully on carbonate successions of marginal basins, even when fully marine conditions are established, and diagenetic overprint is ruled out. Therefore, this work reaffirms the necessity to asses a good biostratigraphic framework prior to apply chemostratigraphy, especially on carbonate successions belonging a closed basin, because the local factors superimposed to the global signal can lead to mistakes and misinterpretations of the isotope curves.

Riassunto

L'intervallo compreso tra l'Eocene superiore e il Miocene è estremamente interessante e dimanico a livello globale come alla scala regionale del Mediterraneo. Al passaggio Eocene-Oligocene si registra la transizione da una fase di *greenhouse*, in cui la Terra era priva di calotte polari e la concentrazione di CO_2 in atmosfera raggiungeva le 1000 ppm, al periodo di *icehouse* attuale, caratterizzato dalla presenza di due calotte polari stabili e concentrazioni di gas serra dell'ordine delle centinaia di ppm. È, infatti, in questo momento che ha inizio la glaciazione della calotta polare Antartica, così come testimoniato da un picco positivo nel record globale del $\delta^{18}O$, registrato nell'Oligocene basale (33.5 Ma) e noto in letteratura come *Oi-1 Event*. Un secondo picco positivo di $\delta^{18}O$, denominato *Mi-1 Event*, viene registrato al passaggio Oligocene-Miocene (~23 Ma), mentre il Miocene medio è caratterizzato da un'escursione negativa dei rapporti isotopici dell'ossigeno che attestano un aumento delle temperature delle acque a livello globale. Questa fase di riscaldamento culmina nel *Middle Miocene Climatic Optmimum* (17-13.5 Ma), momento in cui si stima che le temperature delle acque superifciali alle latitudini temperate abbiano raggiunto valori fino a 6°C superiori a quelli odierni. Questi cambiamenti climatici hanno influenzato il ciclo del carbonio innescando perturbazioni di diversa entità. La curva globale del $\delta^{13}C$ mostra, infatti, due picchi positivi, rispettivamente in corrispondenza dell'*Oi-1 Event* e del *Mi-1 Event*, e una lunga escursione positiva durante il Miocene medio, nota in letterature come *Monterey Event*.
A scala regionale, l'intervallo stratigrafico in esame è ancora più dinamico a causa della complessa evoluzione geodinamica e oceanografica del Mediterraneo, ed in particolare del Mediterraneo Centro-Occidentale, dove si sviluppa l'orogenesi appenninica ed un forte vulcanismo ad essa associata.
Lo scopo di questo studio è quindi quello di identificare la risposta dei sistemi carbonatici del Mediterraneo Centrale ai principali eventi di perturbazione del ciclo del carbonio registrati a livello globale tra l'Eocene superiore e il Miocene medio. Inoltre, analizzando il record isotopico di Sr e Nd delle successioni carbonatiche del Mediterraneo Centrale, si intende discriminare i fattori di controllo globali da quelli locali, legati all'evoluzione geodinamica ed oceanografica dell'area Mediterranea, che possono aver influenzato il chimismo delle acque di questo bacino, concorrendo quindi ad innescare delle crisi o dei cambi della produzione carbonatica.
A tal fine sono stati analizzati i record isotopici del carbonio dei due domini di piattaforma dell'Appennino Centrale (la Piattaforma Laziale-Abruzzese e la Piattaforma Apula), ed il record isotopico del carbonio della successione emipelagica umbro-marchigiana (Appennino Settentrionale).
Al fine di indentificare l'influenza dei fattori di controllo regionali sul chimismo delle acque del Mediterraneo durante il Miocene, inoltre, si propone lo studio integrato del record isotopico dello Sr e del Nd, misurato nella successione Umbro-Marchigiana (Aquitaniano-Tortoniano inferiore), e in quella Apula (Tortoniano-Messiniano).
Il segnale isotopico del carbonio durante la transizione Eocene-Oligocene è stato investigato nella porzione settentrionale della Piattaforma Apula (Montagna della Majella), dove l'intervallo in esame corrisponde alla Formazione di Santo Spirito (Daniano-Rupeliano). Il $\delta^{13}C$ della Formazione di Santo Spirito è stato correlato al $\delta^{13}C_{TOC}$ della contemporanea successione bacinale Umbro-Marchigiana, misurata nella sezione di Massignano, GSSP del limite Eocene-Oligocene. Entrambe

le curve del carbonio analizzate per l'Eocene superiore seguono il trend globale, che attesta una ridotta produttività primaria delle acque. Tuttavia, la curva del $\delta^{13}C_{TOC}$ della sezione di Massignano mostra delle anomalie negative di breve durata, innescate da picchi momentanei della produttività delle acque tra i 36.5 e i 36.0 Ma. Queste perturbazioni transienti sono legate all'attività della *Subtropical Eocene Neo-Tethys current* (STENT), la quale, entrando nel Mediterraneo attraverso l'*Indian Gateway*, portava nel Mediterraneo Centrale acque ricche in ferro, innescando così un aumento della produttività primaria nelle acque superficiali. Il segnale isotopico di piattaforma non registra queste perturbazioni di breve durata, così come non registra l'anomalia del carbonio contemporanea all'*Oi-1 Event*. La mancata registrazione di questo evento è legata alla presenza di *slump* che interrompono la normale sedimentazione della Formazione di Santo Spirito nell'Oligocene basale. Questi *slump*, identificati sull'intera rampa carbonatica nello stesso intervallo stratigrafico, vengono qui interpretati come conseguenti alla caduta del livello del mare dovuta alla formazione della calotta polare Antartica. Una caduta del livello marino, infatti, comporta un abbassamento del limite inferiore di risentimento dell'onda di tempesta, andando a far aumentare l'instabilità della rampa. In ultimo, le sezioni stratigrafiche analizzate per la Formazione di Santo Spirito non permettono di vedere qualora ci siano stati cambi importanti della *carbonate factory* tra l'Eocene e l'Oligocene, poiché i depositi studiati identificano un ambiente di rampa esterna, colonizzato dai soli organismi foto-indipendenti. Tuttavia, l'analisi dei componenti scheletrici ritrovati nei conglomerati e nei depositi risedimentati mostra una diminuzione dei macroforaminiferi bentonici nell'Oligocene, ed un contemporaneo aumento degli organismi legati al *seagrass* e dei coralli.

Il segnale isotopico del Miocene inferiore e medio è stato analizzato nella successione della Montagna della Majella (Formazione di Bolognano), rappresentativa del dominio della Piattaforma Apula, e in quella della Piattaforma Laziale-Abruzzese (Calcari a Briozoi e Litotamni). Il record di piattaforma è stato poi correlato con il contemporaneo segnale isotopico del bacino umbro-marchigiano. A differenza di quanto visto per la transizione Eocene-Oligocene, il *Monterey Event* mostra un'anomalia positiva del $\delta^{13}C$ ben quattro volte più ampia nel record di piattaforma che in quello di bacino. In entrambi i domini di piattaforma il *Monterey Event* coincide con un momento di massima diffusione dei briozoi tra la porzione inferiore della rampa intermedia e la rampa esterna. A sua volta, una produttività così elevata nella zona afotica è andata a determinare la geometria complessiva di queste piattaforme, che infatti evolvono come rampe carbonatiche a basso angolo.

Lo studio integrato di Sr e Nd nelle successioni emipelagiche mioceniche del Mediterraneo Centrale mostra come sia assolutamente evidente l'influenza dell'evoluzione geodinamica dell'area Mediterranea sul chimismo delle acque di questo bacino. Il segnale isotopico dello Sr indica tre intervalli critici, durante i quali il segnale del Mediterraneo devia rispetto a quello globale: l'Aquitaniano superiore, il Burdigaliano medio e superiore e il Messiniano. Nell'Aquitaniano superiore, durante una fase di caduta del livello del mare legata ad una glaciazione, l'aumento del *runoff* nel Mediterraneo viene registrato dagli isotopi dello Sr, che mostrano un $^{87}Sr/^{86}Sr$ molto più alto di quello globale. Al contrario, durante il Burdigaliano, lo $^{87}Sr/^{86}Sr$ del Mediterraneo Centrale cade al di sotto della curva globale a causa del vulcanismo altamente esplosivo che interessava il Mediterraneo Occidentale. Infine, nel Messiniano il record isotopico dello Sr delle Marne a *T. multiloba* (Montagna della Majella, Appennino Centrale) indica l'*onset* di una circolazione ristretta nel proto-Adriatico. La deviazione del segnale isotopico dello Sr nel bacino proto-Adriatico viene

registrata nel Dominio della Piattaforma Apula già a partire dai *Lithothamnion* Limestone (Tortoniano-Messiniano inferiore). I rapporti isotopici dello Sr, misurati su gusci di bivalvi e brachiopodi, mostrano una deviazione dalla curva globale nel Messiniano inferiore, significativamente prima della crisi di salinità messiniana. L' abbassamento del rapporto $^{87}Sr/^{86}Sr$ nel bacino del proto-Adriatico è legato al verificarsi di condizioni di circolazione ristretta dovute alla fisiografia del bacino stesso. L'avanzamento del fronte appenninico ha, infatti, provocato un progressivo restringimento del bacino ed un concomitante aumento del *runoff*, ed una maggiore influenza delle acque dolci, fluviali nel bacino.
Il record isotopico del Nd durante il Miocene testimonia perfettamente l'evoluzione del Mediterraneo da bacino aperto ed alimentato principalmente dall'Oceano Indiano, all'attuale bacino chiuso, in connessione con il solo Oceano Atlantico. Nell'Aquitaniano il segnale isotopico del Nd attesta l'influenza del vulcanismo, attivo sia nell'Oceano Indiano settentrionale che nel Mediterraneo Occidentale, sul chimismo delle acque del Mediterraneo. Durante il Miocene medio, invece, il rapporto $^{144}Nd/^{143}Nd$ della successione Umbro-Marchigiana testimonia degli scambi di masse d'acqua tra il Mediterraneo Centrale e il bacino della Paratetide durante la fase di alto stazionamento del livello del mare connessa al *Mid Miocene Climatic Optimum*. Infine, il dato isotopico del Nd del Miocene superiore è coerente con quanto visto nel record dello Sr, testimoniando un bacino Mediterraneo in comunicazione con l'Oceano Atlantico, e un bacino proto-Adriatico contaminato dall'apporto di acque dolci e dal *runoff* continentale. Un dato estremamente interessante che si evince dall'analisi del record del Nd è che questo riflette la fisiografia del Mediterraneo stesso. In un mare interno, infatti, la vicinanza dei continenti non può non influire sul chimismo delle sue acque, il quale segnale isotopico sarà il risultato di due fattori distinti: l'assetto oceanografico e le principali masse oceaniche che entrano in questo mare interno da un lato, e l'evoluzione geodinamica e del vulcanismo dall'altro.
In conclusione, questa tesi dimostra che il record isotopico del carbonio delle successioni del Mediterraneo Centrale segue i trend globali registrati tra l'Eocene superiore e il Miocene medio. Allo stesso modo però, risulta evidente che diversi fattori locali, legati all'evoluzione geodinamica del Mediterraneo, ne hanno influenzato il chimismo delle acque, controllando il record isotopico delle successioni carbonatiche. Secondariamente, questo lavoro intende porre l'attenzione su quanto sia rischioso applicare la stratigrafia isotopica dello Sr su successioni carbonatiche di mari interni o bacini chiusi, anche dopo aver stabilito, per mezzo di un'accurata analisi di facies, condizioni marine franche, escluso variazioni significative di salinità, o qualsiasi sovraimpronta diagenetica sui campioni analizzati. Infine, sebbene forse non necessario, questa tesi afferma l'assoluta necessità di costruire un robusto *framework* stratigrafico, basato prima di tutto su dati biostratigrafici, prima di analizzare il record isotopico di successioni carbonatiche rappresentative di mari interni. Questo lavoro dimostra, infatti, come siano molteplici i fattori locali che, sovrapposti al segnale globale, possono complicare la risposta delle successioni locali al *forcing* climatico globale, e come questo possa portare a facili errori o interpretazioni sbagliate delle curve isotopiche locali.

1 Introduction

Anthropogenic increase of greenhouse gases and consequent climate change is one of the most important and urgent issues that challenges scientists and society nowadays. To build accurate and reliable predictive models, a detailed study of past climate changes and pre-industrial carbon cycle dynamics is needed. In this framework, the Cenozoic climatic evolution is the perfect case study, since it draws the transition from the warm Mesozoic greenhouse, to the modern glaciated climate.

The Eocene-Miocene global climatic evolution

The last greenhouse-icehouse transition faced by the Earth occurred at the Eocene-Oligocene boundary (Zachos et al., 2001; Coxall and Pearson, 2007 and references therein). The Cretaceous-middle Eocene time interval was, in fact, characterised by warm water temperatures and only minor and transient ice sheets (Pagani et al., 2005), where CO_2 concentrations in the atmosphere were as much as thousands of ppm (Beerling and Royer, 2011; Pagani et al., 2014 and references therein). After the Middle Eocene Climatic Optimum (MECO) (Zachos et al., 2008), CO_2 concentrations decreased, together with temperatures, until the Eocene-Oligocene transition, when the glaciation on Antarctica began, and CO_2 concentrations fell to ~400 ppm, the same values that we measure nowadays (Coxall and Pearson, 2007; Lear et al., 2008; Beerling and Royer, 2011; Lear and Lunt, 2016; Galeotti et al., 2016). A major positive oxygen isotope excursion marks the Eocene-Oligocene transition, known in literature as Oi-1 event (Zachos et al., 2001; Cramer et al., 2009). This major climatic transition led to a complete oceanographic reorganization, due to the stronger latitudinal gradients and the onset of a wind-driven thermohaline circulation, enhanced upwelling and consequent higher rates of the oceanic overturn (Coxall and Pearson, 2007; Miller et al., 2009). In turn, this climatic change affected the global carbon cycle, as testified by the deep-sea global $\delta^{13}C$ positive shift recorded in the early Oligocene (Zachos et al., 1996; 2001; Cramer et al., 2009), and a subsequent major drop of the Calcite Compensation Depth (CCD) (Coxall et al., 2005). Many hypotheses have been proposed that link the greenhouse-icehouse transition to the carbon cycle (Coxall and Wilson, 2011, and reference therein). Some models link the ice-sheet coverage and the silicate weathering to CO_2 fluctuations (Zachos and Kump, 2005); others rely on the increased marine organic carbon burial/cyclicity, and the increased oceanic overturning due to upwelling (Miller et al., 2009); others are based on changes in the chemical riverine input, the deepening of the carbonate sedimentation, or changes in the ecology of plankton (Coxall and Wilson, 2011 and reference therein). The CCD deepened to compensate the reduction of $CaCO_3$ in comparison to the organic carbon burial rates. In turn, the deepening of the CCD led to the recovery from the huge carbon cycle perturbation concomitant to the Oi-1 event (Coxall et al., 2005).

Two other major oxygen isotope shifts characterise the Cenozoic deep-sea record, respectively known as Mi-1 event and Mid Miocene Climatic Optimum (MMCO) (Zachos et al., 2001; 2008; Holbourn et al., 2015). The first one is a sharp positive peak recorded at the Oligocene-Miocene boundary (24.0-23.5 Ma), interpreted as a brief expansion of the Antarctica polar ice cap (Zachos et al., 2001). On the contrary, the MMCO is represented by a long-term negative oxygen isotope excursion, that marks the warmest time interval of the last 35 Myrs, with deep-water temperatures at mid latitudes ~2°C higher than today, whereas surface temperatures were estimated to be as much as ~6°C higher (Flower et al., 1999; Foster et al., 2012).

As the Oi-1 event, these climatic changes affected the carbon cycle. A sharp positive $\delta^{13}C$ peak is recorded at the Oligocene-Miocene boundary, named Early Miocene Carbon Maximum (EMCM) (Hodell and Woodruff, 1994; Zachos et al., 1997; 2001). Whereas, a long-term carbon isotope perturbation characterises the MMCO, known in literature as Monterey Carbon Isotope Excursion (Woodruff and Savin, 1991; Zachos et al., 2001; Houlbourn et al., 2004; 2007). Both these carbon isotope shifts have been linked to an enhanced primary productivity of surface waters due to increased nutrient availability.

The increased nutrient availability during the Mi-1 event might have been intensified by an increased continental-derived runoff (Hodell and Woodruff, 1994; Zachos et al., 1997). Furthermore, Föllmi et al. (2008) point out how the Oligocene-Miocene boundary has been a moment of enhanced upwelling within the Mediterranean area, that brought into surface waters huge amounts of phosphorous, leading to a bloom in primary productivity. Posphogenesis is recorded at the Oligocene-Miocene transition also in the Pacific (Kim and Barron, 1986; Grimm, 2000), while increased terrigenous input is recorded in the Carribean area (Mutti et al., 2005). On the other hand, the Monterey Carbon Isotope Excursion has been recorded during a climatic optimum. It derives its name from the type locality of the Monterey Formation, California, USA, where the storage of large amounts of organic carbon has been identified (Vincent and Berger, 1985). The Monterey Event is a long-term positive carbon isotope excursion (17 to 13.5 Ma), within which 7 different carbon maxima, orbitally paced, have been identified in the deep-sea record (Holbourn et al., 2004; 2007). In this case, the increase of primary productivity is contemporary to a major greenhouse moment, even if CO_2 remained under 300 ppm for most of this carbon cycle perturbation (Flower, 1999; Pagani et al., 1999; Pearson and Palmer, 2000; Beerling and Royer, 2011). During the climatic optimum, the increased humidity sustained enhanced nutrient availability within surface waters, due to enhanced weathering rates, as testified by many phosphate-rich deposits within the organic carbon-rich sediments of the Monterey Formation (Föllmi et al., 2005).

Lastly, the late Miocene is characterised by an overall cooling trend, marked by a gradual increase of the deep-sea oxygen isotope record, until the Pliocene, when also a stable Northern hemisphere ice sheet established (Zachos et al., 2001; 2008).

The geodynamic and oceanographic evolution of the Mediterranean

Within the global, highly dynamic scenario, the Mediterranean evolution during the Eocene-Miocene interval was extremely puzzling due to major tectonics and oceanographic changes. The Central-Western Mediterranean area is the result of the complex interplay between Europe and Africa plates, together with several other microplates, among which Adria (Carminati and Doglioni, 2005;

Carminati et al., 2010; 2012). The Apennine subduction started in the Eocene, due to the inversion of the Alpine subduction, and the west-directed subduction of the remains of the Tethys beneath the southern margin of Europe (Lustrino et al., 2009; Carminati et al., 2012 and reference therein). The west-dipping slab led to the development of an extensional tectonic in the back-arc area, where several basins opened, on thin continental crust (Valencia Trough), and on oceanic crust (Provencal Basin, Tyrrhenian Basin) (Gueguen et al., 1998). Whereas, the Sardinia-Corsica Block made a ~60° counter-clockwise rotation between 21 and 15 Ma (Gattacceca et al., 2007). Furthermore, the tectonic evolution of the Apennine fold-and-thrust belt is associated with an important volcanism, that affected the Western Mediterranean area from Eocene to Recent (Carminati et al., 2010; Lustrino et al. 2011). A highly explosive, subduction related volcanic activity developed within the Western Mediterranean from 38 to 15 Ma (Lustrino et al., 2009; 2011), reaching its climax between 21 and 18 Ma, contemporary to the moment of maximum rotation velocity of the Sardinia-Corsica Block (Gattacceca et al., 2007; Lustrino et al., 2011). Lastly, the subduction related volcanism was followed by an anorogenic type of volcanism from 12 Ma to Present (Lustrino and Wilson, 2007; Lustrino et al., 2011).

The complex tectonic evolution of the Mediterranean area during Cenozoic also affected its oceanographic evolution. During Miocene, in fact, the Mediterranean faced its major transition from a wide and open basin, well connected with both the Atlantic and the Indo-Pacific Oceans, to the modern closed sea, connected only with the Atlantic Ocean through a narrow strait (Rögl, 1999; Popov et al., 2004). Until early Miocene, the Indian Gateway was wide and open (Rögl, 1999), and the major water flux came into the Mediterranean from east and circulated westward (de la Vara et al., 2013). The Indian Gateway closed the first time during late Burdigalian due to the collision between the Arabia and the Eurasia plates and the formation of the Anatolia plate. The connection with the Indo-Pacific re-opened at least two times during Langhian, prior to its definitive closure in the basal Serravallian (Rögl, 1999; Popov et al., 2004). During late Miocene, the Betic and the Rifian corridors progressively narrowed due to tectonic uplift, leading eventually to the complete isolation of the Mediterranean and the Messinian salinity crisis (Martín et al., 2009). Furthermore, on a smaller scale, the Mediterranean water circulation is even more complex. The connection with the Paratethys has been intermittently open during early to middle Miocene, favouring water exchanges with the Central Mediterranean (Popov et al., 2004). Whereas, during late Miocene, several marginal basins developed within the eastern and the central Mediterranean area, e.g. the proto-Adriatic basin, evolving differently from the main central Mediterranean water body (Flecker and Ellam, 2006; Topper et al., 2011; Schildgen et al., 2014).

Outline

Climate, trophic and oceanographic changes affect carbonate production. In turn, carbonate-producing biota control the facies belts and the overall geometry and evolution of carbonate platforms (Pomar, 2001; Pomar et al., 2004; Pomar and Kendall, 2008; Westphal et al., 2010; Pomar and Haq, 2016). The Cenozoic long-term carbonate production changes are well-known. The warm Eocene was characterised by the spread of larger benthic foraminifera (Racey, 2001; Bassi, 2005; Beavington-Penney et al., 2005). They decreased during Oligocene, when seagrass meadows expanded in the euphotic zone and corals proliferated (Brandano et al., 2009; Pomar et al., 2014; Brandano et al., 2017a). In turn, corals declined from early to middle Miocene, as red algae spread in the middle ramp facies, together with bryozoans in the aphotic zone (Brandano and Corda, 2002; Civitelli and Brandano, 2005; Halfar and Mutti, 2005). Lastly, during the late Tortonian-early Messinian, different types of reefs flourished within the Western and Central Mediterranean (Braga et al., 1990; Braga and Martín, 1996; Esteban, 1996; Esteban et al., 1996; Pedley, 1996; Bosellini, 2006; Pomar et al., 2004; 2012).

Despite these long-term trends are known, the stratigraphic response to the global isotopic events on the Central Mediterranean area is still unclear. The carbon isotope anomaly related to the Oi-1 event has been studied in the pelagic Umbria-Marche Domain, at the Massignano stratigraphic section, Global Stratotype Section and Point (GSSP) for the Eocene-Oligocene (Premoli Silva and Jenkins, 1993), but little is known about the response of shallow-water carbonate systems (Jaramillo-Vogel et al., 2013; 2016). Likewise, little has been published on the EMCM in the Mediterranean (Reuter et al., 2013; Brandano et al., 2015), and sometimes the relative carbon isotope curves are unclear (Mutti et al., 1997). Conversely, it has been observed that the Monterey Event corresponds to the spread of bryozoans in the Apennine platforms, but the related carbon isotope curves are poorly age-constrained (Mutti et al., 1997; 1999; Auer et al., 2015).

Lastly, the role of volcanism in affecting carbonate production changes and demises has long been underrated. Volcanism can influence sea-water chemistry due to the fertilization potential of volcanic ashes (Duggen et al., 2007; 2010; Langman et al., 2010; Olgun et al., 2011). Secondly, CO_2 is one of the major propellants of volcanic eruptions. Repeated volcanic CO_2 pulses decrease water pH, limiting carbonate ion concentration, leading to a decrease of carbonate saturation state. Furthermore, an increased CO_2 concentration in atmosphere can trigger a greenhouse effect, enhancing humidity and rainfall, increasing, in turn, weathering and run-off (Larson and Erba, 1999; Brandano and Corda, 2011; Brandano et al., 2015; Erba et al., 2015). Lastly, the highly explosive Oligo-Miocene volcanism of the Western Mediterranean must have brought large amounts of silica into the Central Mediterranean waters, overall favouring the siliceous over the carbonate-producing organisms (Brandano and Corda, 2011; Brandano et al., 2015).

For these reasons, the purpose of this work is to identify the impact of the global carbon cycle perturbations, recorded between late Eocene and middle Miocene, on the Central Mediterranean. Thus, the aims are twofold: identify the stratigraphic response of the carbon cycle perturbations in the carbon isotope record of selected Central Mediterranean carbonate successions, and frame the carbonate production shifts within the geodynamic and oceanographic evolution of the Central Mediterranean, discriminating global from regional controlling factors.

The structure

To identify how the global carbon cycle perturbations have been recorded in the Central Mediterranean between late Eocene and middle Miocene, we focused on the two platform domains of the Central Apennines

(Latium-Abruzzi and the Apula platforms), and the contemporary Umbria-Marche pelagic domain (Northern Apennines). In fact, if, on the one hand, carbonate platforms are extremely sensitive to climate and trophic changes, shallow-water successions are often discontinuous, or lack in biostratigraphic markers. On the contrary, pelagic and hemipelagic successions are monotonous, but continuous and well age-constrained thanks to planktonic foraminifera and calcareous nannofossil biostratigraphy.

In this work, the Eocene-Oligocene transition has been investigated in the Apula Platform (Santo Spirito Formation, Majella Mountain), and in the Umbria-Marche pelagic record (Conero area, Northern Apennines). Whereas, the Miocene carbon isotope events have been investigated both in the Central Apennines platforms, Apula (Bolognano Formation) and Latium-Abruzzi Platform (*Lithothamnion* and Bryozoan Limestone Formation), and in the Umbria-Marche basinal domain (Northern Apennines).

As a preliminary step, the accurate stratigraphy of the shallow-water successions has been reconstructed. The stratigraphic constraints of the Santo Spirito and the Bolognano Formations are provided by nannofossil biostratigraphy (Raffi et al., 2016; Brandano et al., 2016a). Nannofossil assemblages found within marly layers or preserved in chalk within cherty nodules, in fact, proved to be extremely useful to date shallow-water deposits. Thanks to this new discovery, the stratigraphy of the Santo Spirito Formation has been refined, and the Eocene-Oligocene boundary identified (Raffi et al., 2016). Similarly, the stratigraphic architecture of the Bolognano Formation has been reconstructed. Six different units, three shallow-water units, separated by deep-water intervals, have been identified, and the Oligocene-middle Miocene portion of the Formation has been age-constrained (Brandano et al., 2016a).

These accurate stratigraphic studies allowed to correlate the Eocene-Oligocene (**Chapter 2**) and the lower-middle Miocene (**Chapter 3**) carbon isotope curves of the platform successions with the Mediterranean pelagic and the global records.

In **Chapter 2**, the impact of the carbon cycle perturbation related to the Eocene-Oligocene transition has been investigated in the Apula Platform and in the Umbria-Marche pelagic record. The shallow-water $\delta^{13}C$ was measured on whole-rock samples and correlated with the $\delta^{13}C_{TOC}$ of the pelagic succession, to provide new insights on the carbon cycle dynamics across the major greenhouse-icehouse transition. The upper Eocene carbon isotope record, of both platform and pelagic successions, overall matches the global curve, showing a decrease of the $\delta^{13}C$ and an increase of the $\delta^{13}C_{TOC}$ due to a reduced primary productivity within surface waters. However, the pelagic $\delta^{13}C_{TOC}$ curve is punctuated by negative spikes related to the Eocene palaeoceanography of the Mediterranean. This basin was, in fact, characterised by the alternation of low and high primary productivity moments, due to the influence of the westward subtropical Eocene Neo-Tethys (STENT) current (Jovane et al., 2007). The carbon cycle perturbation across the Eocene-Oligocene transition is more evident in the pelagic than in the shallow-water record, where the carbon isotope shift related to the Oi-1 event is not recorded due to the occurrence of slumps at the base of the Oligocene. These slumps are the main evidence of the sea-level drop related to the onset of the Antarctic ice sheet. However, the Santo Spirito ramp shows a change in the carbonate factory, since the larger benthic foraminifera, which proliferated during Eocene, reduced across the Eocene-Oligocene transition, while seagrass associations and red algae spread.

In **Chapter 3**, the Central Mediterranean record of the Monterey Event is presented and discussed. While the Bolognano Formation stratigraphy was established (Brandano et al., 2016a), the *Lithothamnion* and Bryozoan Limestone (L&B) Formation (Latium-Abruzzi Platform) lacked any preserved nannofossil marker, since it consists of extremely calcareous lithologies that do not allow the preservation of calcareous nannofossil assemblages. For this reason, the L&B Formation was dated through Sr Isotope Stratigraphy (SIS). Sr isotope ratios, measured on selected pectinid shells after a detailed diagenetic screening, allowed to refine the stratigraphy of the L&B Formation in the studied area, and to correlate its carbon isotope composition with the other Central Mediterranean successions and the global pelagic record (**Chapter 3**).

Unlike the carbon isotope excursion related to the Oi-1, the Monterey Event has been recorded more distinctly in the platform than in the pelagic record. The Central Mediterranean platforms, in fact, record a positive carbon isotope shift of $\Delta\delta^{13}C > 2.0‰$ in magnitude, that is four times wider than the contemporary Umbria-Marche pelagic record, and two times the deep-ocean record. In both the Central Apennines platforms, the Monterey Event coincides with a huge spread of bryozoans within the middle and outer ramp environments. The high productivity of these filter-feeding associations was sustained by the high trophic conditions of Mediterranean waters, enhanced by local factors, e.g. the active volcanism of the Sardinia-Corsica Block, the increasing continental runoff related to the migration of the Apennine accretionary wedge, the closure of the Indian Gateway between early and middle Miocene. Furthermore, the spread of bryozoan-dominated facies within the oligophotic and aphotic zones controlled the overall depositional profile of the Central Apennine ramps, producing low-angle ramps (**Chapter 3**).

Therefore, both late Eocene-early Oligocene and middle Miocene carbon isotope curves of the Central Mediterranean record the global carbon cycle perturbations. However, in both cases, regional causes, related to the geodynamic and oceanographic evolution of the Mediterranean, influence the carbonate systems response to the global forcing, overlapping or enhancing the global signal.

To investigate the role of regional controlling factors on Central Mediterranean waters, the Miocene Sr and Nd isotope record of the Umbria-Marche succession has been investigated (**Chapter 4**). $^{87}Sr/^{86}Sr$ can be considered homogenous within the oceans since the Sr residence time into marine water (10^6 years) is much longer than the oceans mixing time (10^3 years). On a global scale, the Sr isotope ratios are controlled by continental weathering and volcanism. The first tends to increase the $^{87}Sr/^{86}Sr$ ratio, while the second decreases it, releasing large amounts of ^{86}Sr. On the contrary, Nd residence time within the ocean water ranges between 200 and 1500 years, thus is considerably shorter than the oceans mixing time (Bertram and Elderfield, 1993; Tachikawa et al., 1999). This implies that each ocean is characterised by a distinct Nd isotope signature. Thus, the study of the Mediterranean Nd isotope record during Miocene helps to unravel the dynamics of water exchanges and circulation patterns within the basin, testing whether regional or global controlling factors mainly affected Mediterranean waters. In fact, the Miocene Sr and Nd isotope record documents the overall evolution of the Mediterranean, from a wide open basin mainly influenced by the Indo-Pacific Ocean, to the modern closed basin connected only with the Atlantic Ocean. However, some offset related to regional causes are recorded. During middle Burdigalian to basal Langhian, in fact, Sr isotope ratios deviate from the global ocean curve of McArthur and Howarth (2004) due to the highly explosive volcanism developed within Western Mediterranean. Whereas, during early Messinian different Mediterranean sub-basins, e.g. the Adriatic basin, suffered restricted water conditions from the larger Mediterranean water body, leading to a major mismatch of the local Sr isotope signature in comparison to the global curve (**Chapter 4**).

A deviation of the Sr isotope ratios of the Adriatic basin from the global signal is documented not only in the hemipelagic record (**Chapter 4**), but also in the upper Miocene unit of the Bolognano Formation: the *Lithothamnion Limestone* (LL) (**Chapter 5**). The LL represents an homoclinal ramp characterised by an inner ramp colonised by seagrass meadows, and a wide middle ramp dominated by red algae (Brandano et al., 2016b). Unlike the underlying portion of the Bolognano Formation, the LL lacked any preserved calcareous nannofossil marker. Thus, SIS has been applied on selected pectinid and brachiopod shells of LL, and compared with benthic foraminifera biostratigraphy. The results show that, in the upper Miocene, the Sr isotope ratios of the Apula platform deviate from the global reference line of McArthur and Howarth (2004). This deviation is due to local oceanographic conditions, related to the tectonic evolution of the Central Apennine, which affected not only the Sr isotope signature of the Adriatic basin, but the overall evolution of the LL ramp (**Chapter 5**).

To sum up, this work states that the global carbon isotope events have been recorded within the Central Mediterranean carbonate successions between late Eocene and middle Miocene, but that regional causes, related to the geodynamic and oceanographic evolution of the Central-Western Mediterranean basin, overlap these signals, hampering or complicating the Mediterranean isotope record. Thus, first, caution must be taken in drawing any inference on the global climatic and trophic changes through the study of only Mediterranean successions. Secondly, Sr Isotope Stratigraphy should be applied very carefully on marginal basins, even if fully marine conditions are verified and major diagenetic overprints ruled out. Lastly, this work proves how an accurate biostratigraphic framework is fundamental to apply chemostratigraphy in a closed basin, since regional controlling factors, superimposed to the global feedbacks, may distort the response of carbonate systems leading to possible mistakes and misinterpretations.

References

Auer, G., Piller, W. E., Reuter, M. and **Harzhauser, M.** (2015). Correlating carbon and oxygen isotope events in early to middle Miocene shallow marine carbonates in the Mediterranean region using orbitally tuned chemostratigraphy and lithostratigraphy. *Paleoceanography*, 30, 332-352.

Bassi, D. (2005). Larger foraminiferal and coralline algal facies in an Upper Eocene storm-influenced, shallow-water carbonate platform (Colli Berici, north-eastern Italy). *Palaeogeogr. Palaeoclimatol. Palaeoecol.*, 226, 17-35

Beavington-Penney, S.J., Wright, V.P. and **Racey, A.** (2005). Sediment production and dispersal on foraminifera-dominated early tertiary ramps: the Eocene El Garia Formation, Tunisia. *Sedimentology*, 52, 537-569.

Beerling, D. J. and **Royer, D. L.** (2011). Convergent cenozoic CO_2 history. *Nature Geoscience*, 4, 418.

Bertram, C. J., and **Elderfield, H.** (1993). The geochemical balance of the rare earth elements and neodymium isotopes in the oceans. *Geochim. Cosmochim. Acta, 57,* 1957-1986.

Bosellini, F.R. (2006). Biotic changes and their control on Oligocene-Miocene reefs: A case study from the Apulia Platform margin (southern Italy). *Palaeogeogr. Palaeoclimatol. Palaeoecol.,* 241, 393–409

Braga, J. C., Martin, J. M. and **Alcala, B.** (1990) Coral reefs in coarse-terrigenous sedimentary environments (Upper Tortonian, Granada Basin, southern Spain). *Sed. Geol.,* 66, 135-150.

Braga, J. C. and **Martín, J. M.** (1996). Geometries of reef advance in response to relative sea-level changes in a Messinian (uppermost Miocene) fringing reef (Cariatiz reef, Sorbas Basin, SE Spain). *Sed. Geol.,* 107, 61-81.

Brandano, M. and **Corda, L.** (2002). Nutrients, sea level and tectonics: constrains for the facies architecture of a Miocene carbonate ramp in central Italy. *Terra Nova*, 14, 257-262.

Brandano, M. and **Corda, L.** (2011). The Lower Miocene spongolitic sequence of the Central Apennines: a record of the Burdigalian siliceous event in the Central Mediterranean. *Annalen des Naturhistorischen Museums in Wien. Serie A für Mineralogie und Petrographie, Geologie und Paläontologie, Anthropologie und Prähistorie*, 145-166.

Brandano, M., Frezza, V., Tomassetti, L., Pedley, M. and **Matteucci, R.,** (2009). Facies analysis and palaeoenvironmental interpretation of the late Oligocene Attard Member (Lower Coralline Limestone Formation), Malta. *Sedimentology*, 56, 1138-1158.

Brandano, M., Lustrino, M., Cornacchia, I. and **Sprovieri, M.** (2015). Global and regional factors responsible for the drowning of the Central Apennine Chattian carbonate platforms. *Geological Journal*, 50, 575-591.

Brandano, M., Cornacchia, I., Raffi, I. and **Tomassetti, L.** (2016a). The Oligocene–Miocene stratigraphic evolution of the Majella carbonate platform (Central Apennines, Italy). *Sedimentary Geology*, 333, 1-14.

Brandano, M., Tomassetti, L., Sardella, R. and **Tinelli, C.** (2016b). Progressive deterioration of trophic conditions in a carbonate ramp environment: the *Lithothamnion* Limestone, Majella Mountain (Tortonian–early Messinian, central Apennines, Italy). *Palaios*, *31*, 125-140.

Brandano, M., Cornacchia, I. and **Tomassetti, L.** (2017). Global versus regional influence on the carbonate factories of Oligo-Miocene carbonate platforms in the Mediterranean area. *Marine and Petroleum Geology*, 87, 188-202.

Carminati, E. and **Doglioni C.** (2005). Mediterranean tectonics. *Encyclopedia of geology, 2,* 135-146.

Carminati, E., Lustrino, M., Cuffaro, M. and **Doglioni, C.** (2010). Tectonics, magmatism and geodynamics of Italy: what we know and what we imagine. *Journal of the Virtual Explorer,* 36*,* 1-59.

Carminati, E., Lustrino, M. and **Doglioni, C.** (2012), Geodynamic evolution of the central and western Mediterranean: Tectonics vs. igneous petrology constraints. *Tectonophysics,* 579*,* 173-192.

Civitelli, G. and **Brandano, M.** (2005). Atlante delle litofacies e modello deposizionale dei Calcari a Briozoi e Litotamni nella Piattaforma carbonatica laziale-abruzzese. *Boll. Soc. Geol. It.,* 124, 611.

Coxall, H. K. and **Pearson, P. N.** (2007). The Eocene-Oligocene transition. *Deep Time Perspectives on Climate Change: Marrying the Signal from Computer Models and Biological Proxies*, 351-387.

Coxall, H. K. and **Wilson, P. A.** (2011). Early Oligocene glaciation and productivity in the eastern equatorial Pacific: Insights into global carbon cycling. *Paleoceanography*, 26, PA2221, doi:10.1029/2010.

Coxall, H. K., Wilson, P. A., Palike, H., Lear, C. H. and **Backman, J.** (2005). Rapid stepwise onset of Antarctic glaciation and deeper calcite compensation in the Pacific Ocean. *Nature*, 433, 53-57.

Cramer, B.S., Toggweiler, J.R., Wright, J.D., Katz, M.E. and **Miller, K.G.** (2009). Ocean overturning since the Late Cretaceous: Inferences from a new benthic foraminiferal isotope compilation. *Paleoceanography*, 24 PA4216. DOI: 10.1029/2008PA001683.

de la Vara, A., Meijer, P. T. and **Wortel M. J. R.** (2013). Model study of the circulation of the Miocene Mediterranean Sea and Paratethys: closure of the Indian Gateway, *Climate of the Past Discussions,* 4385-4424.

Duggen, S., Croot, P.L., Schacht, U. and **Hoffmann, L.** (2007). Subduction zone volcanic ash can fertilize the surface ocean and stimulate phytoplankton growth: evidence from the biogeochemical experiments and satellite data. *Geophysical Research Letters*, 34. DOI: 10.1029/2006GL027522.

Duggen, S., Olgun, N., Croot, P.L., Hoffmann, L., Dietze, H., Delmelle, P. and **Teschner, C.** (2010). The role of airborne volcanic ash for the surface ocean biogeochemical iron-cycle: a review. *Biogeoscience*, 7, 827–844.

Erba, E., Duncan, R. A., Bottini, C., Tiraboschi, D., Weissert, H., Jenkyns, H. C. and **Malinverno, A.** (2015). Environmental consequences of Ontong Java Plateau and Kerguelen Plateau volcanism. *Geological Society of America Special Papers*, 511, 271-303.

Esteban, M. (1996). An overview of Miocene reefs from Mediterranean areas: general trends and facies models. In: E.K. Franseen, M. Esteban, W. Ward and J. Rouchy (Eds.) *Models for Carbonate Stratigraphy from Miocene Reef Complexes of Mediterranean Regions*. SEPM Concepts in Sedimentology and Paleontology, 5, 3-53.

Esteban, M., Braga, J.C., Martín, J. and **De Santisteban, C.** (1996). Western Mediterranean reef complexes. In: E.K. Franseen, M. Esteban, W. Ward and J. Rouchy

(Eds.) *Models for Carbonate Stratigraphy from Miocene Reef Complexes of Mediterranean Regions*. SEPM Concepts in Sedimentology and Paleontology, 5, 55-72.

Flecker, R., and **Ellam R. M.** (2006). Identifying late Miocene episodes of connection and isolation in the Mediterranean-Paratethyan realm using Sr isotopes, *Sed. Geol.*,188–189, 189–203.

Flower, B. P. (1999). Warming without high CO_2? *Nature*, *399*(6734), 313.

Föllmi, K. B., Badertscher, C., de Kaenel, E., Stille, P., John, C. M., Adatte, T. and **Steinmann, P.** (2005). Phosphogenesis and organic-carbon preservation in the Miocene Monterey Formation at Naples Beach, California—The Monterey hypothesis revisited. *Geological Society of America Bulletin*, 117, 589-619.

Föllmi, K.B., Gertsch, B., Renevey, J.-P., De Kaenel, E. and **Stilles, P.** (2008). Stratigraphy and sedimentology of phosphate-rich sediments in Malta and south-eastern Sicily (latest Oligocene to early Late Miocene). *Sedimentology*, 55, 1029–1051.

Foster, G. L., Lear, C. H. and **Rae, J. W.** (2012). The evolution of pCO_2, ice volume and climate during the middle Miocene. *Earth Planet. Sci. Lett.*, 341, 243-254.

Galeotti, S., DeConto, R., Naish, T., Stocchi, P., Florindo, F., Pagani, M., Barrett, P., Bohaty, S. M., Lanci, L., Pollard, D., Sandroni, S., Talarico, F. M. and **Zachos, J. C.** (2016). Antarctic Ice Sheet variability across the Eocene-Oligocene boundary climate transition. *Science*, 352, 76-80.

Gattacceca, J., Deino, A., Rizzo, R., Jones, D. S., Henry, B., Beaudoin, B. and **Vadeboin, F.** (2007). Miocene rotation of Sardinia: new paleomagnetic and geochronological constraints and geodynamic implications. *Earth Planet. Sci. Lett.*, 258, 359–377.

Grimm, K.A. (2000) Stratigraphic condensation and the redeposition of economic phosphorite. Allostratigraphy of Oligo-Miocene shelfal sediments, Baja California Sur, Mexico. In: *Marine Authigenesis; From Global to Microbial* (Eds C.R. Glenn, L. Pre´voˆt-Lucas and J. Lucas), *SEPM Spec. Publ.*, *66*, 325–347.

Halfar, J. and **Mutti, M.** (2005). Global dominance of coralline red-algal facies: a response to Miocene oceanographic events. *Geology*, 33, 481-484.

Hodell, D. A. and **Woodruff, F.** (1994). Variations in the strontium isotopic ratio of seawater during the Miocene: Stratigraphic and geochemical implications. *Paleoceanography*, *9*, 405-426.

Holbourn, A., Kuhnt, W., Simob, J.A. and **Li, Q.** (2004). Middle Miocene isotope stratigraphy and paleoceanographic evolution of the northwest and southwest Australian margins (Wombat Plateau and Great Australian Bight). *Palaeogeogr. Palaeoclimatol. Palaeoecol.*, 208, 1– 22

Holbourn, A., Kuhnt, W., Flores, J.-A. and **Andersen, N.** (2007). Orbitally-paced climate evolution during the middle Miocene "Monterey" carbon-isotope excursion. *Earth Planet. Sci. Lett.*, 261, 534-550.

Holbourn, A., Kuhnt, W., Kochhann, K. G., Andersen, N. and **Meier, K. S.** (2015). Global perturbation of the carbon cycle at the onset of the Miocene Climatic Optimum. *Geology*, 43, 123-126.

Jaramillo-Vogel, D., Strasser, A., Frijia, G. and **Spezzaferri, S.** (2013). Neritic isotope and sedimentary records of the Eocene–Oligocene greenhouse–icehouse transition: The Calcare di Nago Formation (northern Italy) in a global context. *Palaeogeogr. Palaeoclimatol. Palaeoecol.*, 369, 361-376.

Jaramillo-Vogel, D., Bover-Arnal, T. and **Strasser, A.** (2016). Bryozoan beds in northern Italy as a shallow-water expression of environmental changes during the Oligocene isotope event 1. *Sedimentary Geology*, 331, 148-161.

Jovane, L., Sprovieri, M., Florindo, F., Acton, G., Coccioni, R., Dall'Antonia, B. and Dinarès-Turell, J. (2007). Eocene-Oligocene paleoceanographic changes in the stratotype section, Massignano, Italy: Clues from rock magnetism and stable isotopes. Journal of Geophysical Research: Solid Earth, 112, doi:10.1029/2007JB004963.

Kim, W. H. and **Barron, J. A.** (1986). Diatom biostratigraphy of the upper Oligocene to lowermost Miocene San Gregorio Formation, Baja California Sur, Mexico. *Diatom Research*, *1*(2), 169-187.

Langmann, B., Zaksek, K., Hort, M. and **Duggen, S.** (2010). Volcanic ash as fertiliser for the surface ocean. *Atmospheric Chemistry and Physics*, 10, 3891–3899.

Larson, R. L. and **Erba, E.** (1999). Onset of the Mid-Cretaceous greenhouse in the Barremian-Aptian: Igneous events and the biological, sedimentary, and geochemical responses. *Paleoceanography*, *14*, 663-678.

Lear, C. H. and **Lunt, D. J.** (2016). How Antarctica got its ice. *Science*, *352*(6281), 34-35.

Lear, C. H., Bailey, T. R., Pearson, P. N., Coxall, H. K. and **Rosenthal, Y.** (2008). Cooling and ice growth across the Eocene-Oligocene transition. *Geology*, 36, 251-254.

Lustrino, M. and **Wilson, M.** (2007). The circum-Mediterranean anorogenic Cenozoic igneous province, *Earth-Sci. Rev.*, 81, 1-65.

Lustrino, M., Morra, V., Fedele, L. and **Franciosi, L.** (2009). Beginning of the Apennine subduction system in central western Mediterranean: constraints from Cenozoic "orogenic" magmatic activity of Sardinia, Italy. *Tectonics*, 28, TC5016, doi:10.1029/2008TC002419.

Lustrino, M., Duggen, S. and **Rosenberg, C. L.** (2011). The Central-Western Mediterranean: anomalous igneous activity in an anomalous collisional tectonic setting. *Earth-Sci. Rev.*, 104, 1-40.

Martín, J. M., Braga, J. C., Aguirre, J. and **Puga-Bernabéu, Á.** (2009). History and evolution of the North-Betic Strait (Prebetic Zone, Betic Cordillera): a narrow, early Tortonian, tidal-dominated, Atlantic–Mediterranean marine passage, *Sed. Geol.*, 216, 80-90.

McArthur, J.M., and **Howarth, R. J.** (2004). Strontium isotope stratigraphy. In: A *Geologic Time Scale*

(Gradstein, F., Ogg, J., Smith, A. eds), Cambridge University Press, Cambridge, 96-105.

Miller, K. G., Wright, J. D., Katz, M. E., Wade, B. S., Browning, J. V., Cramer, B. S. and **Rosenthal, Y.** (2009). Climate threshold at the Eocene-Oligocene transition: Antarctic ice sheet influence on ocean circulation. *Geological Society of America Special Papers*, 452, 169-178.

Mutti, M., Bernoulli, D. and **Stille, P.** (1997) Temperate carbonate platform drowning linked to Miocene oceanographic events: Maiella platform margin, Italy. *Terra Nova*, 9, 122–125.

Mutti, M., Bernoulli, D., Spezzaferri, S. and **Stille, P.** (1999). Lower and Middle Miocene carbonate facies in the central Mediterranean: the impact of paleoceanography on sequence stratigraphy. In: *Advances in Carbonate Sequence Stratigraphy: Application to Reservoirs, Outcrops and Models* (Eds P. Harris, A. Saller, J. Simo and C.R. Handford), *SEPM Spec. Publ.*, 63, 371–384.

Mutti, M., Droxler, A. W. and **Cunningham, A. D.** (2005). Evolution of the Northern Nicaragua Rise during the Oligocene–Miocene: drowning by environmental factors. *Sedimentary Geology*, *175*(1), 237-258.

Mutti, M., John, C.M. and **Knoerich, A.C.** (2006) Chemostratigraphy in Miocene heterozoan carbonate settings: applications, limitations and perspectives. *Geological Society, London, Special Publications*, 255, 307-322.

Pagani, M., Arthur, M. A. and **Freeman, K. H.** (1999). Miocene evolution of atmospheric carbon dioxide. *Paleoceanography*, 14, 273-292.

Pagani, M., Zachos, J. C., Freeman, K. H., Tipple, B. and **Bohaty, S.** (2005). Marked decline in atmospheric carbon dioxide concentrations during the Paleogene. *Science*, 309, 600-603.

Pagani, M., Huber, M. and **Sageman, B.** (2014). Greenhouse Climates. In: *Treatise on Geochemistry 2nd Eidtion*. Elsevier, Oxford, 281-304. DOI: 10.1016/B978-0-08-095975-7.01314-0.

Pearson, P. N. and **Palmer, M. R.** (2000). Atmospheric carbon dioxide concentrations over the past 60 million years. *Nature*, 406, 695-699.

Pedley, M. (1996). Miocene reef facies of the Pelagian region (Central Mediterranean). In: In: E.K. Franseen, M. Esteban, W. Ward and J. Rouchy (Eds.) *Models for Carbonate Stratigraphy from Miocene Reef Complexes of Mediterranean Regions*. SEPM Concepts in Sedimentology and Paleontology, 5, 247-260.

Pomar, L. (2001). Types of carbonate platforms: a genetic approach. *Basin Research*, 13, 313-334.

Pomar, L. and **Kendall, C. G. S. C.** (2008). Architecture of carbonate platforms: a response to hydrodynamics and evolving ecology. In *Controls on carbonate platform and reef development* SEPM S.P., 89, 187-216), Tulsa.

Pomar, L. and **Haq, B. U.** (2016). Decoding depositional sequences in carbonate systems: concepts vs experience. *Global and Planetary Change*, 146, 190-225.

Pomar, L., Brandano, M. and **Westphal, H.** (2004). Environmental factors influencing skeletal grain sediment associations: a critical review of Miocene examples from the western Mediterranean. *Sedimentology*, 51, 627-651.

Pomar, L., Bassant, P., Brandano, M., Ruchonnet, C., & **Janson, X.** (2012). Impact of carbonate producing biota on platform architecture: insights from Miocene examples of the Mediterranean region. *Earth-Sci. Rev.,* 113, 186-211.

Pomar, L., Mateu-Vicens, G., Morsilli, M. and **Brandano, M.** (2014). Carbonate ramp evolution during the late Oligocene (Chattian), Salento Peninsula, southern Italy. *Palaeogeogr. Palaeoclimatol. Palaeoecol.*, 404, 109-132.

Popov, S. V., Rögl, F., Rozanov, A. Y., Steininger, F. F., Shcherba, I. G. and **Kovac, M.** (2004). Lithological-Paleogeographic maps of Paratethys. Late Eocene to Pliocene. *Courier Forschungsinstitut Senckenberg, 250,* pp. 46, maps 1-10 (annex).

Premoli Silva, I. and **Jenkins, D. G.** (1993). Decision on the Eocene-Oligocene boundary stratotype. *Episodes*, 16, 379-382.

Olgun, N., Duggen, S., Croot, P. L., Delmelle, P., Dietze, H., Schacht, U., Óskarsson, N., Siebe, C., Auer, A. and **Garbe-Schönberg, D.** (2011). Surface ocean iron fertilization: the role of airborne volcanic ash from subduction zone and hot spot volcanoes and related iron fluxes into the Pacific Ocean. *Global Biogeochemical Cycles*, 25, GB4001, doi:10.1029/2009GB003761.

Racey, A. (2001). A review of Eocene nummulite accumulations: structure, formation and reservoir potential. *Journal of Petroleum Geology*, 24, 79-100.

Raffi, I., Ricci, C., Garzarella, A., Brandano, M., Cornacchia, I. and **Tomassetti, L.** (2016). Calcareous nannofossils as a dating tool in shallow marine environment: an example from an upper Paleogene carbonate platform succession in the Mediterranean. *Newsletters on Stratigraphy*, 49, 481-495.

Rögl, F. (1999). Mediterranean and Paratethys. Facts and hypotheses of an Oligocene to Miocene paleogeography (short overview). *Geol. Carpath., 50,* 339–349.

Schildgen, T. F., Cosentino, D., Frijia, G., Castorina, F., Dudas, F. Ö., Iadanza, A., Sampalmieri, G., Cipollari, P., Caruso, A. and **Strecker, M. R.** (2014). Sea level and climate forcing of the Sr isotope composition of late Miocene Mediterranean marine basins. *Geochemistry, Geophysics, Geosystems,* 15, 2964-2983.

Tachikawa, K., Jeandel, C. and **Roy-Barman, M.** (1999). A new approach to the Nd residence time in the ocean: the role of atmospheric inputs. *Earth Planet. Sci. Lett., 170,* 433-446.

Topper, R. P. M., Flecker, R., Meijer, P. T. and **Wortel, M. J. R.** (2011). A box model of the Late Miocene Mediterranean Sea: Implications from combined $^{87}Sr/^{86}Sr$ and salinity data. *Paleoceanography, 26,* PA3223, doi:10.1029/2010PA002063.

Vincent, E. and **Berger, W. H.** (1985) Carbon dioxide and polar cooling in the Miocene: the Monterey hypothesis. In: W.S. Broecker and E.T. Sundquis (Eds.), *The*

Carbon Cycle and Atmospheric CO: Natural Variations Archean to Present. *AGU Geophys. Mon.*, 32, pp. 455–468.

Westphal, H., **Halfar, J.** and **Freiwald, A.** (2010). Heterozoan carbonates in subtropical to tropical settings in the present and past. *Int. J. Earth Sci.*, 99, 153-169.

Woodruff, F. and **Savin, S.** (1991). Mid-Miocene isotope stratigraphy in the deep sea: high resolution correlations, paleoclimatic cycles, and sediment preservation. *Paleoceanography*, 6, 755–806.

Zachos, J. C. and **Kump, L. R.** (2005). Carbon cycle feedbacks and the initiation of Antarctic glaciation in the earliest Oligocene. *Global and Planetary Change*, 47, 51-66.

Zachos, J. C., **Quinn, T. M.** and **Salamy, K. A.** (1996). High-resolution (10^4 years) deep-sea foraminiferal stable isotope records of the Eocene-Oligocene climate transition. *Paleoceanography,* 11, 251-266.

Zachos, J. C., **Flower, B. P.**, and **Paul, H.**, (1997). Orbitally paced climate oscillations across the Oligocene/Miocene boundary. *Nature*, *388*, 567-570.

Zachos, J, **Pagani, M.**, **Sloan, L.**, **Thomas, E.** and **Billups, K.** (2001). Trends, rhythms, and aberrations in global climate 65 Ma to present. *Science*, 292, 686-693.

Zachos, J. C., **Dickens, G. R.** and **Zeebe, R. E.** (2008). An early Cenozoic perspective on greenhouse warming and carbon-cycle dynamics. *Nature,* 451, 279-283.

2 The Eocene-Oligocene transition in the C-isotope record of carbonate successions in the Central Mediterranean

Irene Cornacchia[1], Marco Brandano[1,2], Isabella Raffi[3], Laura Tomassetti[1], Isabella Flores[1]

1: Dipartimento di Scienze della Terra, La Sapienza Università di Roma, P. Aldo Moro 5, 00185 Roma, (Italy).
2: Istituto di Geologia Ambientale e Geoingegneria (IGAG) CNR, Sez. Sapienza, c/o Dipartimento Scienze della Terra, P. Aldo Moro 5, I-00185, Roma (Italy).
3: Dipartimento di Ingegneria e Geologia, Università degli Studi "G. d'Annunzio" Chieti- Pescara, via dei Vestini 31, 66013 Chieti.

Submitted to *Global and Planetary Change*

ABSTRACT

Upper Eocene to lower Oligocene $\delta^{13}C_{Carb}$ and $\delta^{13}C_{TOC}$ records of a shallow-water and an hemipelagic carbonate settings within the Central Mediterranean area have been studied and discussed. The shallow-water carbon isotope signal has been analysed in the northern portion of the Apula Platform, cropping out in the Majella Mountain, Central Apennines (Santo Spirito Formation). A coeval Umbria-Marche basinal succession has been investigated in the Massignano section (Conero area, Central Italy). The purposes of this work were multiple: to identify the impact of the C-cycle perturbation occurred during the Oi-1 event on the Mediterranean successions; to correlate the regional C-isotope signal with the global record; to evaluate the carbon cycle dynamics across the greenhouse-icehouse transition. The upper Eocene carbon isotope records of the analysed successions agree with the global signal. They show an overall negative trend, linked to a reduced primary productivity that characterised the interval between the Middle Eocene Climatic Optimum and the onset of the Oi-1 event. However, the upper Eocene basinal $\delta^{13}C_{TOC}$ record is marked by short-term negative spikes that possibly represent times of higher productivity, triggered by the westward subtropical Eocene Neo-tethys current entering from the Arabian-Eurasian gateway. The shallow-water record, instead, does not display these short-term productivity pulses. A change in the carbonate factory is only recorded at the Eocene-Oligocene transition, and is marked by reduction of the larger benthic foraminifera, while the spread of seagrass and red algae. Moreover, in the shallow-water record of the Santo Spirito Formation no major carbon isotope shift related to the Oi-1 event is displayed due to the presence of extensive slumps that disrupt the bedding. These slumps are the main evidence of the sea-level drop that occurred concomitantly to the onset of the Antarctica ice-sheet, which caused the deepening of the storm-weather wave base and increased the instability over the entire ramp.

2.1 INTRODUCTION

The Eocene-Oligocene transition represents the most important step in the evolution of the modern glaciated climate. It marks the transition between the warm "greenhouse world", when the atmospheric pCO_2 was higher than 1000 ppm (Beerling and Royer, 2011; Pagani et al., 2014) and only transient ice-sheets could develop at low latitudes (Carter et al., 2017), to the modern "icehouse" climate, characterised by stable polar ice caps and lower CO_2 concentrations (Pearson et al., 2009; Beerling and Royer, 2011). The onset of this oxygen isotope event is known in literature as the Eocene-Oligocene Transition (EOT) (Houben et al., 2012), and has a peak in the early Oligocene (33.55 Ma) known as Oi-1 event (Miller et al 1991; Zachos et al., 1996, 2001; Coxall and Pearson, 2007; Lear et al., 2008) that led to the development of a permanent ice sheet in Antarctica as much as 50% in volume of the present one (DeConto and Pollard, 2003; Liu et al., 2009; Miller et al., 2009; Bohaty et al., 2012). This major climatic shift resulted in a general global ocean reorganization and affected the global carbon cycle, as marked by a global positive $\delta^{13}C$ isotope excursion (Zachos et al., 1996; 2001; Cramer et al., 2009) associated with a major deepening of the CCD (Coxall et al., 2005). Different hypotheses have been suggested to explain this positive carbon isotope excursion, most of them related to changes in the oceanic trophic regime and the associated primary productivity, induced by sea level changes or change in the global oceanography (Salamy and Zachos, 1999; Zachos and Kump, 2005; Coxall et al., 2005; Coxall and Pearson, 2007; Miller et al., 2009; Coxall and Wilson, 2011).

The carbon cycle perturbation related to the Oi-1 event has been clearly identified in the global ocean record (Zachos et al., 1996; 2001; Cramer et al., 2009), whereas little is still known about the shallow-water carbonate systems response to this carbon cycle perturbation (Jaramillo-Vogel et al., 2013; 2016). During the transition from the warm Eocene to the Oligocene "icehouse", these major changes in climate, ice volume, and ocean circulation deeply influenced the composition and production of the carbonate factory (Nebelsick et al., 2005; Brandano et al., 2009; 2017a).

The larger benthic foraminifera, which dominated the Eocene carbonate platforms (Racey, 2001, and references therein; Bassi, 2005; Beavington-Penney et al., 2005), experienced a major decline. In turn, zooxanthellate corals and coralline algae spread as main biota-producing sediment, and seagrass environments expanded strongly in the euphotic zone, influencing the facies association of the Cenozoic carbonate platforms (Nebelsick et al., 2005; Pomar and Kendall, 2008; Brandano et al., 2017a).

In this work, the Eocene-Oligocene transition is studied in two different carbon isotope records from the Central Mediterranean area. The first case study refers to sedimentary succession from the Apula carbonate Platform in which the main lithofacies of the Santo Spirito Formation (Central Apennines, Central Italy), and $\delta^{13}C$ of the whole-rock signal are analysed and discussed. This shallow-water carbon isotope signal is here correlated with the $\delta^{13}C$ record obtained in the Massignano section (Scaglia Variegata and Scaglia Cinera Fm, Conero area, Central Italy), the well-known Global Stratotype Section and Point (GSSP) of the Eocene-Oligocene boundary (Premoli Silva and

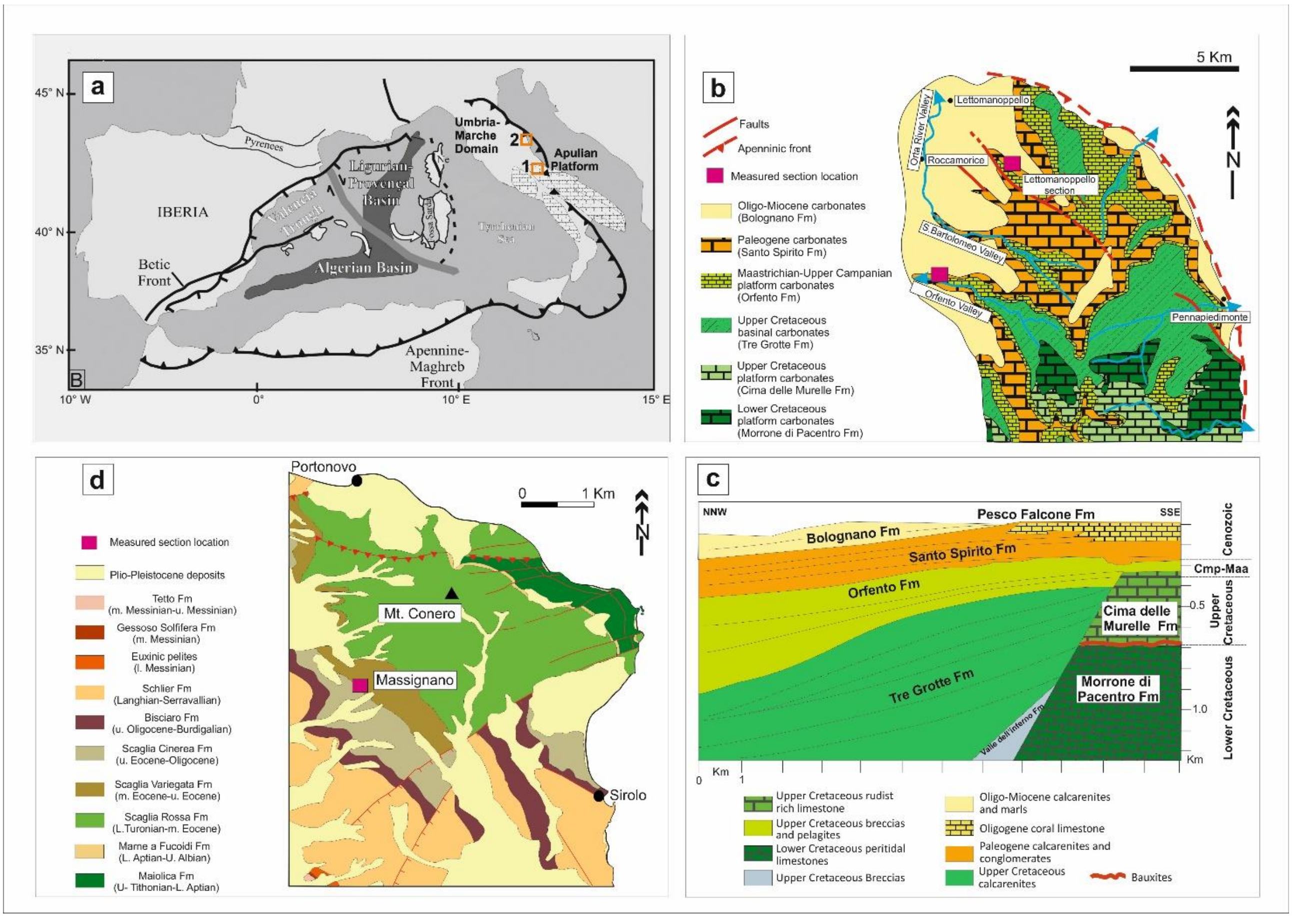

Fig. 2.1: a) Map of the Mediterranean area with the studied successions location. 1: Majella Mountain; 2: Conero area. Modified after Gueguen et al. (1998). b) Simplified geological map of the Majella Mountain (modified after Vecsei and Sanders, 1999) with section locations. c) Schematic stratigraphic architecture of the Majella carbonate platform, modified after Vecsei et al. (1998). d) Simplified geological map of the Conero area, with Massignano section location (modified after Coccioni et al., 1997).

Jenkins, 1993) that represents the Umbria-Marche basinal succession.

The aim of this study is (i) to identify the impact of the C-cycle perturbation related to the Oi-1 event on the shallow- and deep-water carbonate successions of the Central Mediterranean area; (ii) to correlate the C isotope records of the Mediterranean successions with the global signal; and (iii) to evaluate the carbon cycle dynamics across this major greenhouse-icehouse transition.

2.2 GEOLOGICAL SETTING

The Apennine fold-and-thrust belt is the result of the collision of the Adria plate with the southern margin of Europe (Carminati et al., 2012). The beginning of the Apennine subduction occurred during late Eocene (Lustrino et al., 2009), but its evolution mostly took place during the Neogene to Present interval. The westward-dipping Apennine slab led to an eastward migration of the deformation fronts and related foredeeps, and a subsequent extensional tectonics in the back-arc area, where several basins opened during the Oligocene-Miocene interval on thin continental (the València Through) and oceanic (Alborán, Provençal and Thyrrenian Basin) crust (Carminati et al., 2012 and references therein). The Central Apennine consists of Triassic to Miocene deposits that can be ascribed to three different paleogeographic domains: the Apennine carbonate platforms (Latium-Abruzzi and Apula platforms), the Umbria-Marche basin and the Molisano basin (Vezzani et al., 2010). In this study the northern extension of the Apula platform, represented by the Majella Mountain, and the Marche basinal successions are investigated (Fig. 2.1a).

2.2.1 The Majella Mountain

The Majella Mountain (Fig. 2.1b) is a 35 km-long anticline that is convex towards northeast and plunges both northward and southward (Patacca et al., 2008). Its outcropping succession consists of Upper Jurassic to upper Miocene limestones and dolostones (Crescenti et al., 1969). During the Mesozoic, a steep erosional escarpment separated the platform top from the basin, which extended northward (Fig. 2.1c). By the late Campanian, the platform prograded over the basin, filled up by onlapping sediments (Vecsei et al., 1998). Thus, the Paleogene evolution of the Majella carbonate platform, identified by the Santo Spirito Formation, is represented by a continuous sedimentation along the platform margin and the slope, while the platform top shows long-term hiatuses and discontinuous deposits. In the upper Rupelian a discontinuity surface occurs, separating the Santo Spirito Formation from the Bolognano Formation (upper Rupelian-lower Messinian) that represents a carbonate ramp developed above the former shallow deposits of the platform (Mutti et al., 1997; Brandano et al., 2012, 2016a). The evolution of the Oligocene-Miocene ramp ended in the Messinian with the deposition of the *Turborotalita multiloba* Marls (Carnevale et al., 2011), followed by the Gessoso-Solfifera Formation (Crescenti et al., 1969). Lastly, during the early Pliocene the Majella Mountain was involved into the foredeep system of the Apennine orogeny (Cosentino *et al.*, 2010).

2.2.2 The Umbria-Marche Domain

The Umbria-Marche Domain consists of an Upper Triassic-Miocene sedimentary succession deposited in the northern margin of the Tethys (Fig. 2.1a; 2.1d). During the Late Triassic, the rifting of the Tethys led to a marine transgression, testified by the evaporitic deposition of the Anidridi di Burano and, subsequently, by the development of the Calcare Massiccio carbonate platform (Pialli, 1971). During the Early Jurassic, the Calcare Massiccio platform drowned due to the rift-related extensional tectonics and the Umbria-Marche domain evolved into a wide basin, characterised by intrabasinal structural highs (Centamore et al., 1971; Bernoulli and Jenkins, 1974, Brandano et al., 2016b), until the Late Jurassic. This heterogeneous paleogeography ended with the deposition of pelagic mudstones (the Maiolica Formation, Titonian to Albian in age), that leveled the inherited topography (Alvarez, 1990). The evolution of the Umbria-Marche basin during the Cretaceous to Miocene interval resulted in the transition from pelagic to hemipelagic sedimentation, characterised by a constant increase of siliciclastic content, in a context of significant subsidence (Marchegiani et al., 1999; Guerrera et al., 2012). Lastly, the diachronic involvement of the Umbria-Marche basin into the Apennine foredeep system is witnessed by the onset of the deposition of the siliciclastic turbiditic deposits of the Marnoso Arenacea Formation during the middle to late Miocene from West to East (Alvarez, 1999; Guerrera et al., 2012).

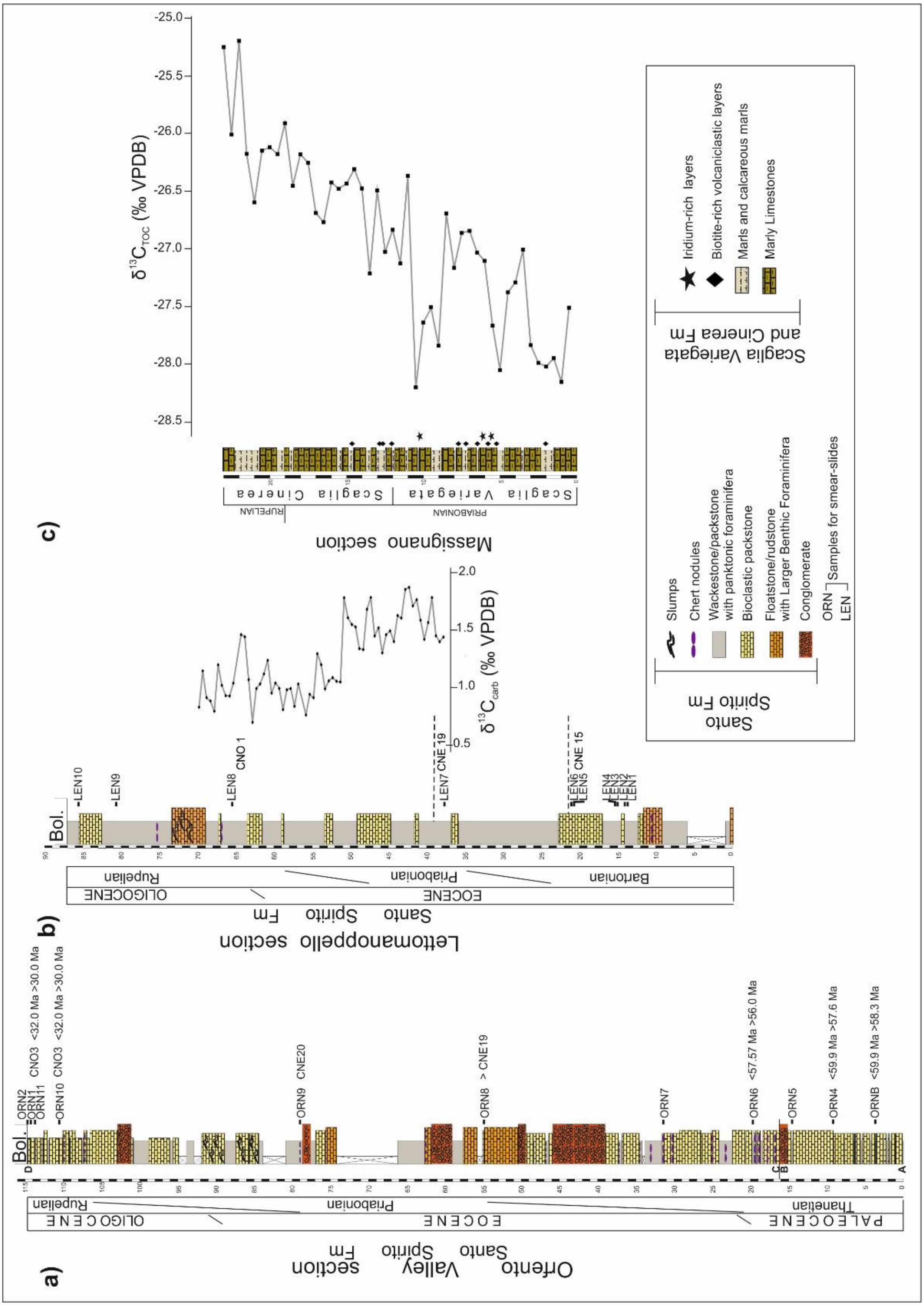
a)
Orfento Valley section
Santo Spirito Fm
b)
Lettomanoppello section
Santo Spirito Fm
c)
Massignano section
$\delta^{13}C_{TOC}$ (‰ VPDB)
$\delta^{13}C_{carb}$ (‰ VPDB)
PALEOCENE
EOCENE
OLIGOCENE
Thanetian
Bartonian
Priabonian
Rupelian
Scaglia Variegata
Scaglia Cinerea
Bol.
ORN2
ORN1
ORN11
ORN10
ORN9
ORN8
ORN7
ORN6
ORN5
ORN4
ORNB
CNO3 <32.0 Ma >30.0 Ma
CNE20
> CNE19
<57.57 Ma >56.0 Ma
<59.9 Ma >57.6 Ma
<59.9 Ma >58.3 Ma
LEN10
LEN9
LEN8
LEN7
LEN6
LEN5
LEN4
LEN3
LEN2
LEN1
CNO 1
CNE 19
CNE 15
Santo Spirito Fm
Slumps
Chert nodules
Wackestone/packstone with panktonic foraminifera
Bioclastic packstone
Floatstone/rudstone with Larger Benthic Foraminifera
Conglomerate
ORN
LEN
Samples for smear-slides
Scaglia Variegata and Cinerea Fm
Iridium-rich layers
Biotite-rich volcaniclastic layers
Marls and calcareous marls
Marly Limestones

Fig. 2.2: Stratigraphic sections with carbon isotope composition plotted against stratigraphic depth. a) Orfento Valley stratigraphic section; b) Lettomanoppello section; c) Massignano section. Age constraints for the Santo Spirito Formation (Orfento Valley and Lettomanoppello sections) are provided by calcareous nannofossil biostratigraphy (this work) and refer to the Paleogene Zonation of Agnini et al. (2014). Age constraints for the Massignano section are referred to Coccioni et al. (1988) and Premoli-Silva and Jenkins (1993).

2.3 METHODS

The studied materials originate from three different stratigraphic sections: the Lettomanoppello and the Orfento Valley sections (Majella Mountain, Central Italy), and the Massignano section (Conero area, Central Italy) (Fig. 2.2). Eighty-five thin sections of the Santo Spirito Formation, belonging to both the sections, were observed at the petrographic microscope for textural characterisation and skeletal components identification.

Previously published and newly generated data on calcareous nannofossil assemblages have been considered for biostratigraphic characterization. Eleven samples have been examined from Orfento Valley section, collected from marly layers and chalk inclusions within cherty nodules if present. Smear-slides for nannofossils analysis were obtained following the procedure defined by Bown and Young (1998) and observed at the polarizing microscope (X1200 magnification). The nannofossil biostratigraphic data of Lettomanoppello section are from Raffi et al. (2016). For biozones and biochronology we refer to the Paleogene Zonation of Agnini et al. (2014).

The Lettomanoppello and the Massignano sections have been sampled for carbon isotope stratigraphy. A 0.5-m sampling interval has been chosen. Stable isotope analyses have been carried out at the Isotope Geochemistry Laboratory of the Istituto di Geologia Ambientale e Geoingegneria (IGAG-CNR) of Rome. Carbon and oxygen stable isotope ratios have been measured on 63 bulk samples of the Lettomanoppello section. The whole-rock analyses have been performed with a Finnigan Delta Plus Mass spectrometer coupled with a gas chromatography-based Gas Bench II. Stable isotope ratios have been calibrated with the international NBS19 carbonate standard. All the results are expressed in Vienna Pee Dee Belemnite (VPDB) scale. The analytical error is ±0.1‰ (SD) based on replicate standards.

$\delta^{13}C_{TOC}$ was measured on 46 samples belonging to the Massignano section. Rock samples were hand-crushed in an agate mortar. To remove the carbonate fraction, 0.5 g of powder per sample have been treated with 40 ml of a HCl 1M solution and shaked with a magnetic stirrer for 20 minutes. After 20 minutes, the pH of the solution was ~2, indicating that the entire carbonate fraction was consumed, and the reaction completed. The residual powder has been rinsed with deionized water and oven-dried a 50°C. $\delta^{13}C_{TOC}$ analyses were performed with a Finnigan Delta Plus Mass spectrometer coupled with a Flash-1112 Thermo Elemental Analyzer. Organic matter carbon isotope ratios were calibrated with the IAEA-CH-6 and IAEA-CH-7 international standards. The analytical error is ±0.3‰ based on replicate standards.

2.4 RESULTS

2.4.1 The Orfento Valley section

The Orfento Valley section (Fig. 2.2a, 2.3a, Annex A.1, A.2) consists of the upper

Paleocene-lower Oligocene portion of the Santo Spirito Formation. The composite section is 114.6 m thick, the first section (A-B), is 16.2 m thick, the second (C-D) is 98.4 m thick (Fig. 2.2a). The first 15.1 m of the Orfento A-B section, are represented by planktonic-rich wackestones to packstones (Fig. 2.4a) alternated with laminated biocalstic packstones. The main components of the bioclastic packstones are highly fragmented

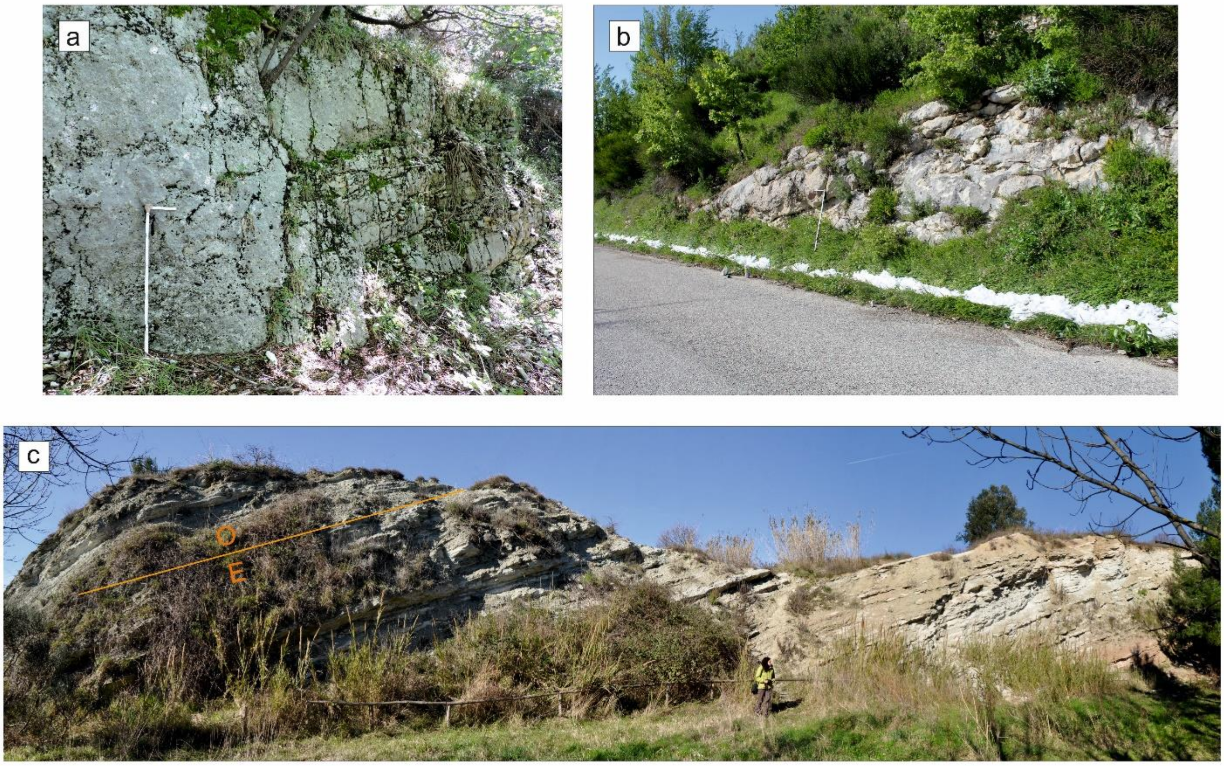

Fig. 2.3: a) Conglomerate interval interrupting the normal outer ramp sedimentation in the Orfento Valley section. b) Slumps within the lower Oligocene portion of the Lettomanoppello section. c) Massignano section, the Eocene-Oligocene boundary is marked with the orange line.

Larger Benthic Foraminifera (LBF) as *Nummulites*, *Discocyclina,* rotalids, and red algae crusts, together with echinoids and bivalve fragments (Fig. 2.4b; 2.4c; 2.4d). Thin marly layers alternate with this calcareous facies of Orfento A-B section that is interrupted by a 1.1-m thick conglomerate, characterised by an erosional basal surface with LBF and intraclasts. The base of the Orfento C-D section consists of 22.2 m of coarse packstones with LBF, alternated with planktonic-rich mudstones/wackestones. Cherty nodules are very abundant in this interval. At m 39.0, a 7-m thick conglomerate crops out. This conglomerate is chaotic and poorly sorted. LBF and coral fragments have been identified, together with intraclasts. The section continues with a 16.8-m thick interval dominated by bioclastic packstones with LBF, such as *Nummulites* and *Alveolina*, alternated with floastones with *Alveolina* in a grainstone matrix dominated by abundant miliolids and peneroplids, and with packstones with encrusting foraminifera such as *Gypsina moussaviani*, red algae crusts and nodules (Fig. 2.4e; 2.4f). These facies are interrupted by two conglomerate intervals, respectively 0.6- (m 49.5) and 2.8-m thick (m 59). This portion of the Orfento C-D section ends with a 3.50-m thick interval of wackestones with planktonic foraminifera. Cherty nodules are common. At m 74.2, after an 8-m covered interval, the upper portion of the Orfento C-D section crops out. It consists of an alternation of bioclastic packstones with LBF and wackestones with planktonic foraminifera. A 1.0 m-thick conglomerate interrupts the normal sedimentation at 77.5 m. From 84.5 m to 92.0 m an interval of biocalstic packstones with LBF characterised by extensive slumps

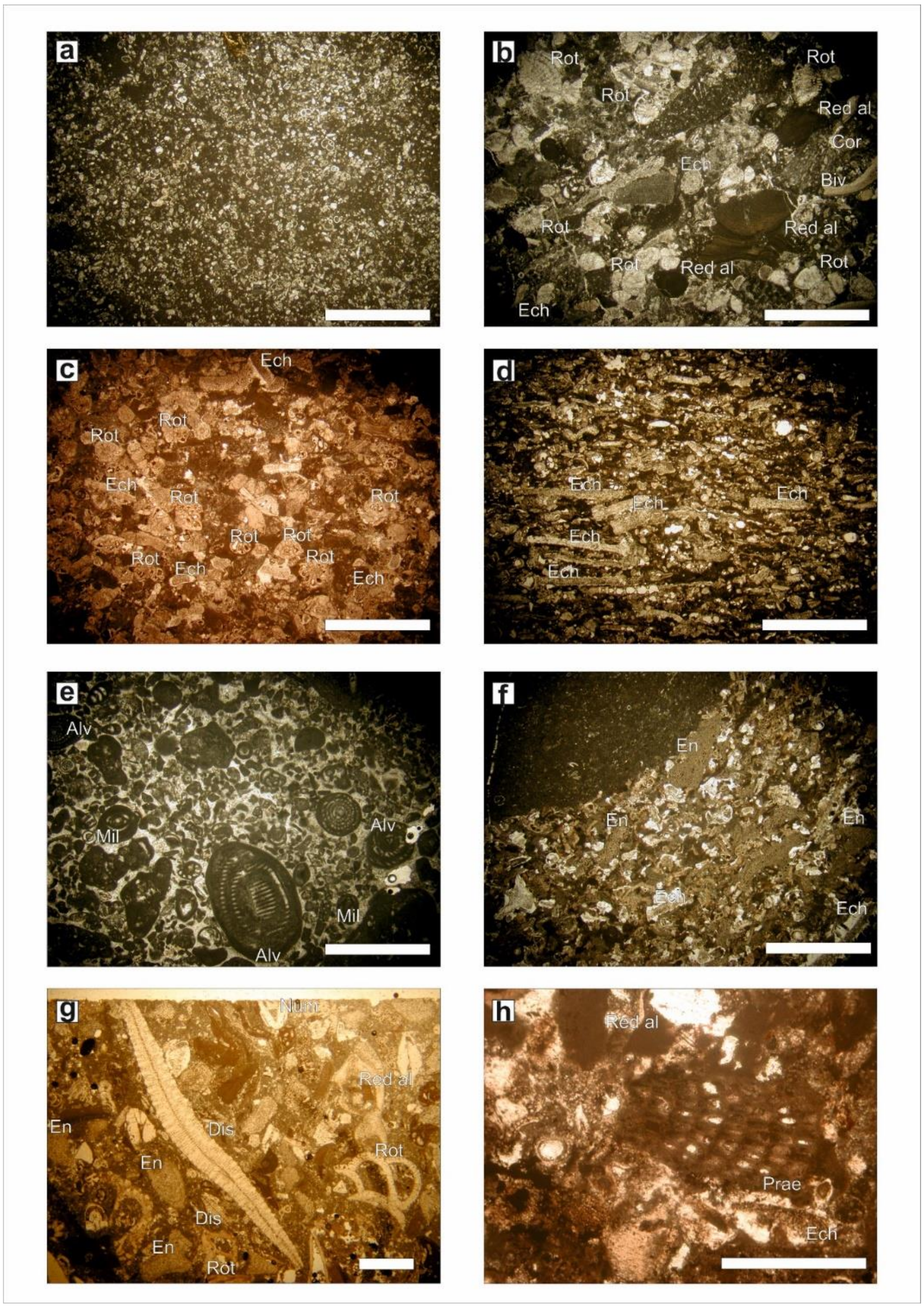

Fig. 2.4: Miocrofacies of the Santo Spirito Formation. a) Highly bioturbated packstone with planktonic foraminifera. b) Bioclastic packstone. C) Packstone with rotalids. d) Packstone with echinoid fragments. e) Grainstone with *Alveolina* and miliolids. f) Packstone with encrusting foraminifera and intraclasts. G) Floatstone with LBF. h) Floatstone with LBF. Alv: *Alveolina*. Biv: Bivalve fragments. Cor: coral fragments. Dis: *Discocyclina*. Ech: echinoid fragments. En: encrusting foraminifera. Mil: miliolids. Num: nummulitids. Prae: *Praerhapydionina* cf. *delicata*. Red al: red algae crusts and fragments. Rot: rotalids. Scale bar= 1mm.

occurs. The uppermost conglomerate, 1.9 m-thick, crops out at 101 m. The 13.6 m interval at the top of the section consists of alternation of very fine bioclastic packstones and planktonic-rich wackestones. Chert occurs in nodules and lists up to the top of the section (Fig. 2.2a).

2.4.1.1 Biostratigraphy and age constraints

Although the observed nannofossil assemblages in the sample from Orfento Valley composite section are generally scarce and show moderate to bad preservation, it was possible to obtain some biostratigraphic and biochronologic constraints based on the presence of some marker species. In few samples from Orfento A-B section and in a marly interlayer cropping out at m 3.4 of the Orfento C-D section (Fig. 2.2a), the presence of specimens belonging to the genus *Fasciculithus* (*F. ulii* group, *F. pileatus*, *F. tympaniformis*) indicate a biostratigraphic position included in the interval between Zones CNP7 and CNP9 of Agnini et al. (2014). Therefore, the lower part of the composite Orfento section corresponds to the interval Selandian-lower Thanetian (<59.9 Ma and >57.0 Ma) (Plate 2.1 1-10). In the interval from m 20 to m 55 in the composite section, the abundance of calcarenites and resedimented material limited the availability of samples suitable for biostratigraphy (Fig. 2.2a). The nannofossil assemblage observed in a marly interlayer at 55 m and in the chalk found a in a cherty nodule a 79 m, allows to ascribe this interval to the Priabonian (CNE 19 and CNE20 of Agnini et al., 2014) for the presence of very rare *Discoaster saipanensis* and *D. barbadiensis* and *Ericsonia formosa* (Plate 2.1 11-14). In the uppermost portion of the section (m 110.5 and m 113.5) the few samples show a scarce but typical lower Oligocene nannofossil assemblage, which places the top of the section in the CNO3 Zone (Agnini et al., 2014).

2.4.2 The Lettomanoppello section

The Lettomanoppello section represents the middle Eocene-lower Oligocene portion of the Santo Spirito Formation (Fig. 2.2b, Annex A.3). The section is 87 m thick. The first interval consists of 9 m of highly bioturbated planktonic-rich wackestones/packstones. The foraminiferal assemblage is dominated by globigeriniids, such as *Globigerina*, *Globigerinatheka* and *Turborotalia cerroazulensis*. Minor components are sponge spicules, echinoid and mollusk fragments. The following interval is represented by a 2.4 m thick interval of LBF floatstones to rudstones. The main components are LBF, such as *Nummulites*, *Assilina*, *Discocyclina* and rotalids (Fig. 2.2b; 2.4f). Other components are encrusting foraminifera, such as *Gypsina* and *Acervulina*, *Textularia, Nodosaria*, red algae, echinoid and mollusk fragments (Fig. 2.4g). From m 10.6 to m 69, the section consists of the alternation of bioclastic packstones and highly, planktonic-rich bioturbated wackestones (Fig. 2.2b). The main components of the bioclastic packstones are encrusting and epiphytic foraminifera such as *Gypsina moussaviani*, usually hooked, *Planorbulina*, *Lobatula lobatula* and nubecularids. Both articulated branches and non-articulated crusts of red algae, sometimes hook-shaped, among which *Sporolithon* and *Subterraniphyllum*, are frequent. Echinoid and mollusk, bryozoan and *Ditrupa* fragments are common, together with small benthic foraminifera (SBF), such as miliolids, small

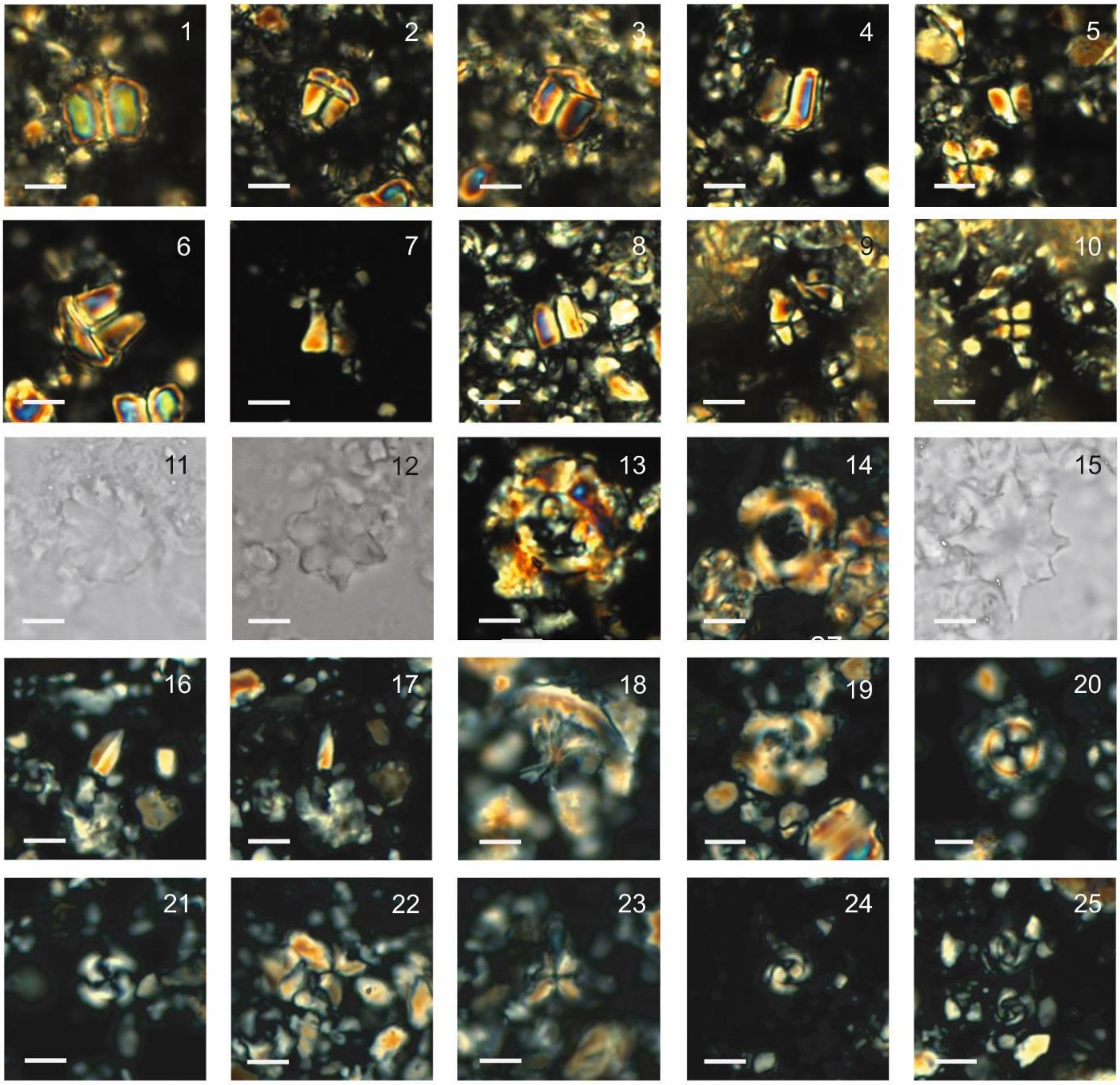

Plate 2.1: Microphotographs of selected calcareous nannofossils in samples from the Orfento (ORN) and Lettomanoppello (LEN) sections. Scale bar=5 μm.

1. *Fasciculithus* cf. *ulii* Perch-Nielsen, 1971; crossed nicols. Sample ORNB**. 2, 3, 6**. *Fasciculithus pileatus* Bukry; crossed nicols. 2) Sample ORN 2; 3,6) Sample ORN4. **4.** *Fasciculithus ulii* Perch-Nielsen, 1971; crossed nicols. Sample ORN4. **5, 8.** *Fasciculithus tympaniformis* Hay and Mohler in Hay et al., 1967; crossed nicols. Sample ORN4. **7.** *Fasciculithus* cf. *alanii* Perch-Nielsen, 1971; crossed nicols. Sample ORN4. **9,10.** *Sphenolithus anarrhopus* Bukry and Bramlette, 1969; 9) crossed nicols 45°, 10) crossed nicols 0°. Sample ORN6. **11.** *Discoaster mohleri* Bukry and Percival, 1971; parallel nicols. Sample ORN6. **12**. *Discoaster saipanensis* Bramlette and Riedel, 1954; parallel nicols. Sample ORN8. **13, 14.** *Reticulofenestra umbilicus* (Levin, 1965) Martini and Ritzkowski, 1968; crossed nicols. 13) Sample ORN8; 14) Sample LEN7. **15**. *Discoaster saipanensis* Bramlette and Riedel, 1954; parallel nicols. Sample LEN7. **16,17**. *Sphenolithus intercalaris* Martini, 1971; 16) crossed nicols 0°, 17) crossed nicols 45°. Sample LEN7. **18**. *Chiasmolithus oamaruensis* (Deflandre, 1954) Hay, Mohler and Wade, 1966; broken specimen, crossed nicols. Sample LEN7. **19, 20**. *Ericsonia formosa* (Kamptner, 1963) Haq, 1971; crossed nicols. 19) Sample LEN7; 20) Sample LEN5. **21**. *Cribrocentrum reticulatum* (Gartner and Smith, 1967) Perch-Nielsen 1971; crossed nicols. Sample LEN5. **22, 23**. *Sphenolithus radians* Deflandre in Gassé, 1952; 22) crossed nicols 45°, 23) crossed nicols 0°. Sample LEN5. **24, 25** *Clausicoccus subdistichus* Roth and Hay in Hay et al., 1967 Prins; crossed nicols. Sample LEN8.

rotaliids, *Lenticulina*, textularids and buliminacea such as *Bolivina*. At 69 m, a 4.50-m thick interval of floatstones/rudstones with LBF occurs. Among the LBF tests, *Phraerhapydionina* cf. *delicata* has been identified (Fig. 2.4h). This interval is characterised by extensive slumps. The last 13.6 m of the section consist of bioturbated, planktonic-rich wackestones, interrupted at 82.5 m by 3 m of bioclastic packstones. Cherty nodules occur at 75 m. A discontinuity surface marks the passage to the overlying Bolognano Formation at m 87.

2.4.2.1 Biostratigraphy and age constraints

Previously obtained nannofossil data in the Lettomanoppello section (Raffi et al., 2016) permitted to obtain a rather detailed biostratigraphic classification of the section, referring to Agnini et al. (2014) Zonation. The lower portion (up to 21.2 m) corresponds to mid-Eocene (Bartonian) Zone CNE15, based on the presence of *Cribrocentrum reticulatum, Sphenolithus obtusus, Sphenolithus spiniger* and *Dictyococcites bisectus* (Fig. 2.2b, Plate 2.1 20-23). Above, in a sample from a marly layer at 37.8 m, the observed nannofossil assemblage indicates Zone CNE19 (*Discoaster saipanensis* TZ) thus ascribing the central portion of the section to the upper Eocene (Priabonian) (Fig. 2.2b, Plate 2.1 15-19) . The biostratigraphic results from the upper portion of the section indicate the transition to the lower Oligocene. In fact, a marly layer at m 64.50 contains a nannofossil assemblage belonging to Zone CNO1 (*Ericsonia formosa* CRZ, age between 34 and 33 Ma) followed above (just below the boundary with the Bolognano Formation) by sediments of Zone CNO3 (*Dictyococcites bisectus* PRZ, age <32 Ma), with *D. bisectus*, *Sphenolithus predistentus* and *Sphenolithus celsus* (Plate 2.1 24-25).

2.4.2.2 The C isotope record

The upper Eocene-lower Oligocene $\delta^{13}C_{Carb}$ values of the Lettomanoppello section range between +0.7‰ and +1.9‰ (Fig. 2.2b) (see Annex B.1 for the detailed C and O isotope ratios). The lower portion of the carbon isotope curve, from m 37.8 m to m. 50.8 m in the section, shows a stationary trend with the values fluctuating between +1.4‰ and +1.8‰. A sharp negative shift is recorded starting from 50.8 m, with values falling first to +1.1‰ at 51.8 m, and then falling further to +0.7‰ at 62.8 m, in correspondence to the base of the Oligocene. A small positive shift is recorded above (from 62.8 to 64.3 m), with values rising to +1.5‰, fluctuating again around +1.0‰ up to the end of the measured interval in the section (at 69.8 m).

2.4.3 The Massignano section

The Massignano section represents the upper Eocene-lower Oligocene interval of the Umbria-Marche basinal succession. It is 23.0 m thick, and comprises the Scaglia Variegata and Scaglia Cinerea Formations (Fig. 2.2c; 2.3c). The Scaglia Variegata Formation consists of alternating reddish and greenish marls, calcareous marls and marly limestones. This interval is characterised by horizontal and homogeneous beds, ranging in thickness between 50 cm and few centimetres. Bioturbation is common. The Scaglia Cinerea consists of homogeneous hemipelagic grey marls and marly limestones. Beds are tabular and range between 80 and few centimetres. Bioturbation is present in all the lithologies. Ten biotite-rich layers, related to volcanic events, characterise the section, 6 in the Scaglia Variegata and 4 in the Scaglia Cinerea (Jovane et al., 2009). Lastly, three iridium-rich-layers, cropping out respectively at 5.61, 6.17 and 10.28 m, are interpreted as linked to impactoclastic events (Bodiselitsch et al., 2004) (Fig. 2.2c). The boundary between the Scaglia Variegata and the Scaglia Cinerea falls at 12.0 m (Coccioni et al., 1988).

2.4.3.1 Biostratigraphy and age constraints

Based on planktonic foraminifera biostratigraphy, the Massignano section spans from Priabonian to Rupelian (Coccioni et al., 1988; Premoli-Silva and Jenkins, 1993). The base of the section is placed in the upper P15 Zone of Blow (1969) and Berggren et al. (1995), or the E14 Zone Wade et al. (2011). The top of the section falls into the P18 Zone (Blow, 1969; Berggren, 1995), which corresponds to the O1 Zone of Wade et al. (2011). The Eocene/Oligocene boundary, marked by the extinction of the *Hantkeninidae,* is placed at 19 m (Coccioni et al., 1988). The calcareous nannofossils commonly used as markers for the late Eocene-early Oligocene are *Discoaster saipanensis* (last occurrence at 34.44 Ma; Pälike et al., 2006) and *Clausicoccus subdistichus* whose increase (equivalent to "Acme *Ericsonia obruta*") approximates the Eocene/Oligocene boundary at 33.88 Ma (Pälike et al., 2006). Both biohorizons are recognized in Massignano section (Premoli-Silva and Jenkins, 1993).

2.4.3.2 The C isotope record

The upper Eocene-lower Oligocene $\delta^{13}C_{TOC}$ record at Massignano ranges between -28.2‰ and -25.2‰ (Fig. 2.2c) (see Annex B.2 for the detailed C isotope ratios). An overall increasing trend is evident throughout the entire carbon isotope curve. The lowest portion of the curve (from 0 to 8.5 m) shows a stationary trend, with the values fluctuating around -27.5‰. An abrupt negative shift occurs between 8.5 and 10.5 m, with the values decreasing from -26.7‰ down to -28.2‰, and represents the lowest value recorded in the section. The distinct positive trend recorded from 10.5 to 19.0 m, with the values rising to -25.9‰, corresponds to the Eocene-Oligocene boundary interval. The carbon isotope record in the lowermost Oligocene shows the values fluctuating between -26.5‰ and -26.0‰ from 19.0 to 21.5 m, and rising to -25.2‰ at the top of the section.

2.5 DISCUSSION

2.5.1 Facies association and depositional model of the Santo Spirito Formation

The Santo Spirito formation represents a carbonate platform developed in the Majella Mountain during the Paleogene, and it can be referred to the standard model of Buxton and Pedley (1989) for Cenozoic carbonate ramps. The recognised lithofacies can be ascribed to an outer ramp and to the adjacent basin environments. In particular, the facies with highly bioturbated wackestones to packstones and planktonic foraminifera is interpreted as deposited within the aphotic zone and below the storm weather wave base of the outer ramp, where only photo-independent organisms accumulate. The outer ramp environment gradually passes to the basin, where marly wackestones to mudstones with planktonic foraminifera occur. In this lower portion of the ramp accumulation of abundant bioclastic turbidites and debris flow deposits occurs which constitute a complex fan system and interrupt the normal outer ramp and hemipelagic sedimentation (cf. Payros et al., 2007).

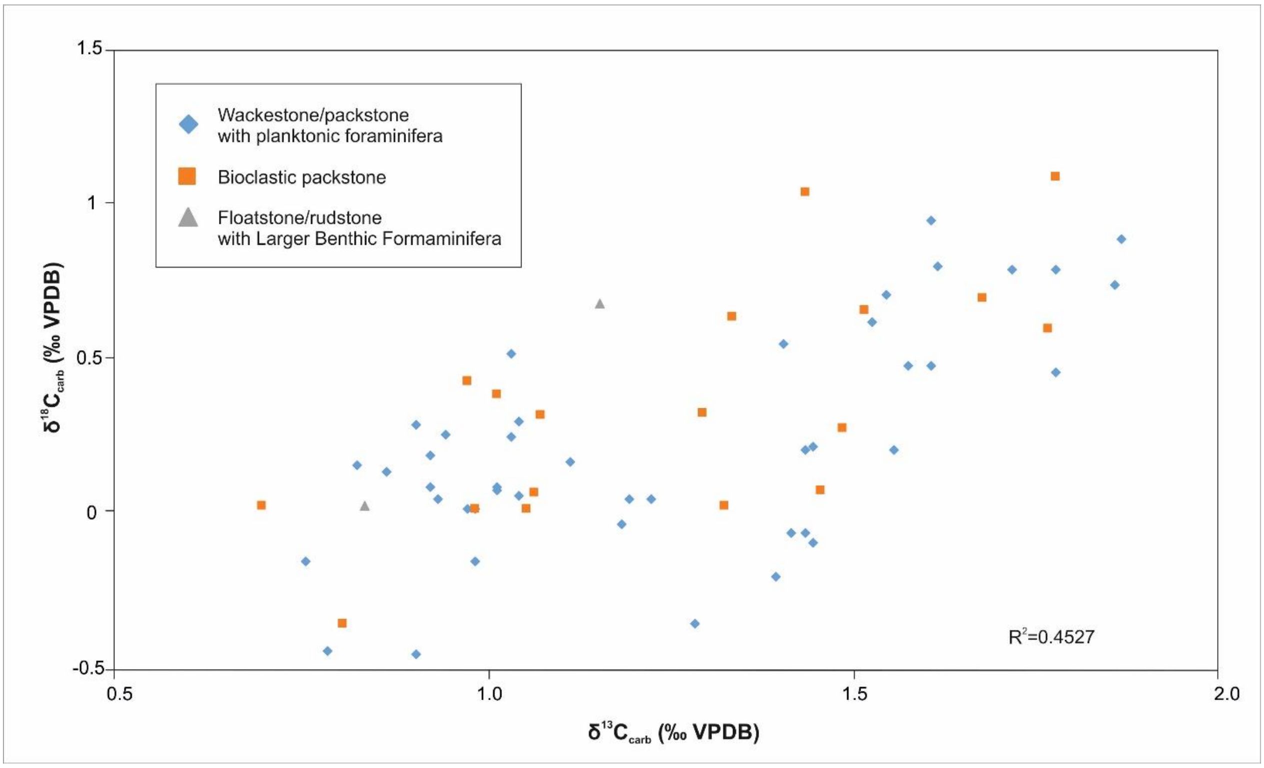

Fig. 2.5: Cross-plots of $\delta^{13}C$ and $\delta^{18}O$ of bulk rock samples of each lithofacies of the Lettomanoppello section, showing the broad isotope ratios distribution of each facies, indicating a negligible lithological and facies control on the isotope ratios.

Analysis of the skeletal components of the bioclastic packstones, the floatstones/rudstones lithofacies and the clasts of the conglomerates, permits to infer the different facies belts that constituted the inner portions of the platform. The major components identified in the bioclastic packstones, such as encrusting foraminifera, hooked-shaped red algae crusts, together with miliolids and alveolinids, indicate the presence of a vegetated environment developed within the euphotic zone, as in the inner ramp (Beavington-Penney et al., 2004; Tomassetti et al., 2016). Seagrass meadows hosted an important carbonate factory of the Cenozoic inner ramps, where encrusting, epiphytic and miliolids foraminifera lived, together with red algae and mollusks (Buxton and Pedley, 1989; Beavington-Penney et al., 2004; Brandano et al 2016c; Tomassetti et al., 2016; Tomás et al., 2016). The middle ramp was dominated by nummulitids in the upper portion, and distally by orthofragminids, as evident by the occurrence of common *Discocyclina* tests in the LBF-rich floatstones/rudstones. During late Eocene, zooxanthellate corals and red algae also occurred, as testified by the presence of these components in the conglomerates and in the LBF floatstones to rudstones lithofacies observed in the Orfento Valley section.

2.5.2 Diagenetic overprint over $\delta^{13}C_{Carb}$ and $\delta^{13}C_{TOC}$ records

Precipitation of carbonates is associated with only little carbon isotopic fractionation relative to the dissolved inorganic carbon (DIC). Therefore the $\delta^{13}C$ of both inorganic and biologically precipitated carbonate must be very close to the value of dissolved inorganic carbon in the ocean (Saltzman and Thomas, 2012). Furthermore, both $\delta^{13}C_{Carb}$ and $\delta^{13}C_{TOC}$

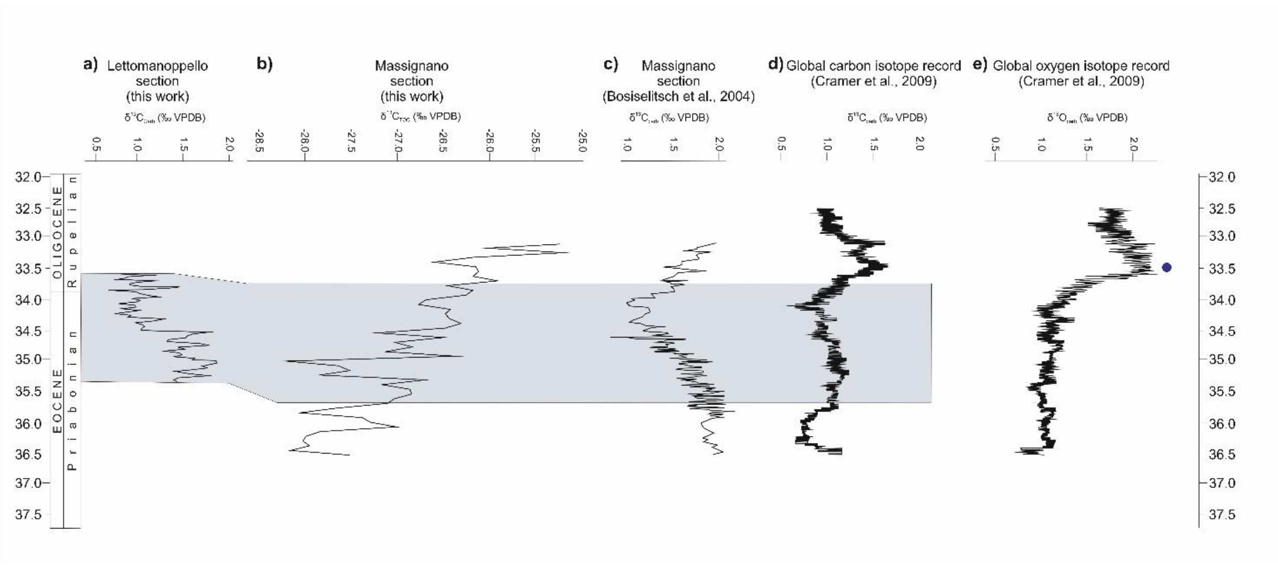

Fig. 2.6: Comparison of the carbon isotope record of the studied sections with the global carbon and oxygen isotope record. All the curves have been calibrated with the Geological Time Scale 2004.

are almost insensitive to temperature changes (Galimov, 2006; Burla et al., 2008; Saltzman and Thomas, 2012). Pelagic carbonates are considered the most reliable record to study carbon isotope stratigraphy, since they are not affected by meteoric diagenesis, and they are more continuous and better age-constrained (Weissert, 2008 and references therein). Several papers recently published demonstrated that shallow-water carbonates can preserve the original carbon isotope signature, (John et al., 2003; Mutti et al., 2005; Franceschi et al., 2014; Brandano et al., 2015; Frijia et al., 2015), and can possibly show even wider and clearer carbon isotope excursions in comparison to the coeval pelagic successions (Brandano et al., 2017b). Within the shallow-water skeletal associations, the heterozoan carbonates have a greater potential to preserve the original marine isotopic ratios than the photozoan skeletal assemblages (Mutti et al., 2006), due to their mineralogical composition, low-Mg calcite-dominated, which makes them more resistant to diagenetic alteration. The overall $\delta^{13}C_{Carb}$ values in modern oceans vary between -1.5‰ up to +2.0‰ (Weissert, 2008 and references therein). Therefore, the Santo Spirito Formation carbon isotope record falls precisely within the normal carbonate $\delta^{13}C_{Carb}$ range(Fig. 2.2b). Any lithological or facies control on the isotope record can be ruled out, since each facies shows broad values of both carbon and oxygen isotope ratios, and no specific facies ranges can be detected (Fig. 2.5). Lastly, the overall C and O isotope ratios show a covariance of R^2=0.4527 (Fig. 2.5), which is not here interpreted as a diagenetic overprint, but due to the fact that, also on a global scale, the upper Eocene carbon and oxygen isotope ratios show similar trends (Cramer et al., 2009) (Fig. 2.6). Likewise, the $\delta^{13}C_{TOC}$ record of the Massignano section is consistent with the mixing of continental organic matter and marine phytoplankton, and generally ranges between -20‰ and -30‰ (Saltzman and Thomas, 2012) (Fig. 2.2c).

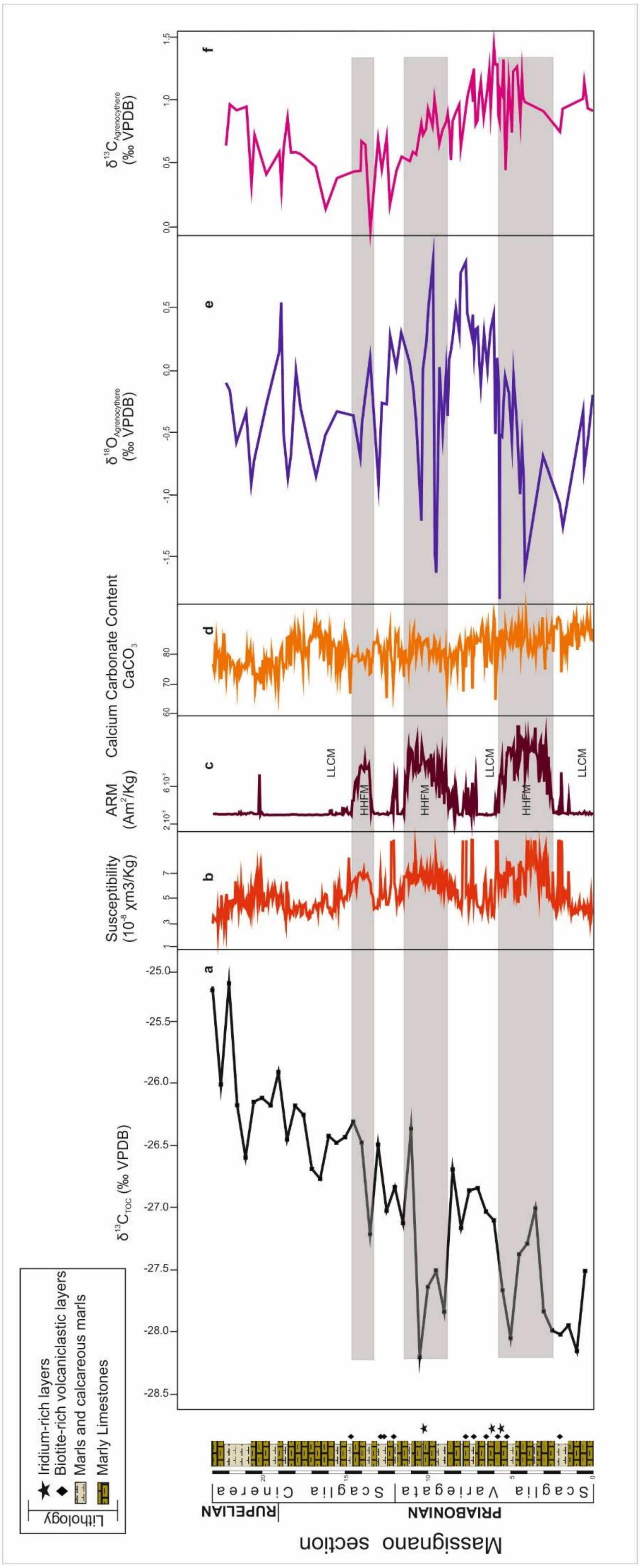
Massignano section
RUPELIAN
PRIABONIAN
Scaglia Cinerea
Scaglia Variegata
Lithology
Iridium-rich layers
Biotite-rich volcaniclastic layers
Marls and calcareous marls
Marly Limestones
δ13CTOC (‰ VPDB)
Susceptibility (10-8 χm3/Kg)
ARM (Am2/Kg)
Calcium Carbonate Content CaCO3
δ18OAgrenocythere (‰ VPDB)
δ13CAgrenocythere (‰ VPDB)
LLCM
HHFM

Fig. 2.7: a) Comparison of the $\delta^{13}C_{TOC}$ record of the Massignano (this work). B) Low-field magnetic susceptibility of the Massignano section. c) Anhysteretic Remanent Magnetization (ARM). D) Calcium Carbonate Content (CaCO3%), e) $\delta^{18}O$ and f) $\delta^{13}C$ isotope record measured on valves of the *Agrenocythere* ostracod genera throughout the Massignano section. (b), (c), (d), € and (f) are modified from Jovane et al. (2009). HHFM=high concentration, high coercivity, and fi ne-grained magnetic; LLCM=low concentration, low coercivity, and coarse-grained magnetic (modified from Jovane et al., 2004).

2.5.3 The Central Mediterranean carbon isotopes shifts at the Eocene-Oligocene transition

Short-lived C-cycle perturbations, representing short-lived warming events, characterise the Eocene interval (Cramer et al., 2003; Lourens et al., 2005). One of the major perturbation occurred during the Middle Eocene Climatic Optimum (MECO, 41.5 Ma in age), and it has been identified as a positive $\delta^{13}C$ anomaly (Bohaty and Zachos, 2003; Jovane et al., 2007b). The increased productivity of surface waters, and the subsequent high organic carbon burial immediately following the MECO, caused a reduction in the pCO_2 and the return to the general cooling trend in the late Eocene (Spofforth et al., 2010; Luciani et al., 2010), that culminated with the Oligocene glaciation. The c-cycle perturbation that occurred during the Oi-1 has long been debated. The different interpretations vary from feedbacks among atmospheric pCO_2 and ice sheet coverage, silicate weathering rates, to increased marine organic carbon burial/cycling. Different hypotheses regard a global switch in the ecology of plankton that favored siliceous organisms over calcareous ones, a shift in global carbonate sedimentation from the shelf to the deep ocean, changes in riverine chemical inputs, a heavier isotopic composition of the terrestrial biosphere, or an increase in the rain ratio of the inorganic/organic carbon from surface to deep ocean, to a reduced ocean acidity linked to an increased ocean overturning (see Coxall and Wilson, 2011 for a review). According to Goldner et al. (2014), the decrease of atmospheric pCO_2 during the Eocene-Oligocene transition produced the cooling phase that promoted the growth of the Antarctica ice cap, which in turn enhanced the ocean thermal gradient and invigorated its circulation. The increased wind-driven upwelling around Antarctica drove an increase in the ocean productivity, potentially drawing down carbon. Furthermore, it strengthened the cooling across the Eocene-Oligocene transition, pointing towards a C–cycle perturbation related to the enhanced burial rates of organic carbon in marine sediments, coupled with increased surface water productivity (Salamy and Zachos, 1999; Zachos and Kump, 2005; Dunkely Jones et al., 2008).

The upper Eocene-lower Oligocene $\delta^{13}C_{Carb}$ record of the Santo Spirito ramp and the coeval $\delta^{13}C_{TOC}$ record of the Massignano hemipelagic succession agree with the global signal (cf. Cramer et al., 2009) (Fig. 2.6). The $\delta^{13}C_{Carb}$ curves of Lettomanoppello and Massignano sections show a clear negative trend during the late Priabonian (Fig. 2.6a, 2.6c). This trend reflects the interval between the end of the c-cycle perturbation associated with the MECO and the onset of the carbon isotope anomaly contemporary to the Oi-1 event, marked by a cooling trend associated with a decrease of primary production. This decrease is well recorded by the Eocene $\delta^{13}C_{TOC}$ of the

Massignano section, which shows an overall positive trend. The decoupling of the $\delta^{13}C_{Carb}$ and the $\delta^{13}C_{TOC}$ curves during the late Priabonian is consistent with the decreasing values of CO_2 that characterise the upper Eocene (Beerling and Royer, 2011). The net isotopic fractionation between TOC and sedimentary carbonates depends on four processes: the fractionation associated with primary producers, the fractionation between Dissolved Inorganic Carbon (DIC) and dissolved CO_2, the fractionation between DIC and carbonate minerals, the fractionation associated with secondary biological processes (see Hayes et al., 1999 for a review). Among these processes, the first one is the most effective, and it has not been constant through time. In fact, Hayes et al. (1999) point out how the isotopic effect associated with primary production decreases as dissolved CO_2 lowers, affecting the Total Organic Carbon (TOC) sequestrated in sediments, thus increasing the difference between the TOC and the DIC. Within the overall positive $\delta^{13}C_{TOC}$ trend, negative spikes are present in the interval between 36.5 and 36.0 Ma of the Massignano record. These spikes may be related to the environmental changes produced by the alternating activity of the westward subtropical Eocene Neo-tethys (STENT) current, as proposed by Jovane et al., (2007a; 2009). According to the authors, the paleoceanography of the Neo-tethys was characterised by alternating periods of low productivity, represented by intervals of deposition driven by local terrigenous material, and expressed by the authors as coarser magnetite, and periods of high productivity and freshening, displayed by abundant fine-grained magnetite plus hematite layers. The high productivity and freshening periods represent times when the westward subtropical Eocene Neo-tethys current entered through the Arabia-Eurasian gateway, bringing large amounts of fresh and deep-sea waters, rich in dissolved iron. The negative spikes of $\delta^{13}C_{TOC}$ of the Massignano section show a good correspondence with the fine hematite-rich sediments interval recognized by Jovane et al. (2007a) and confirm the coexistence of the high biogenic productivity phases (Fig. 2.7). Lastly, in the Massignano section the onset of the positive carbon isotope excursion of the early Oligocene is recorded (Bodiselitsch et al., 2004), although in the section the entire perturbation is not displayed (Fig. 2.6c).

Likewise, the carbon isotope record of Lettomanoppello section shows the end of the negative trend, linked to the decrease of primary production, at the end of the Eocene. The prominent $\delta^{13}C$ excursion occurring in the early Oligocene, associated with the onset of Antarctic glaciation, is not recorded because the regular bedding is interrupted by the occurrence of extensive slumps. These slumps are indeed interpreted as the major consequence of the sea-level drop related to the cooling corresponding to the Oi-1 event. Slumps in the lower Oligocene (within Zone CNO1 of Agnini et al., 2014) have been identified not only in the Lettomanoppello and in the Orfento Valley sections (Fig. 2a; 2b; 3b), but also in the eastern sector of the Santo Spirito ramp, namely in the Pennapiedimonte stratigraphic section (Raffi et al., 2016), and testify an enhanced instability over the entire ramp. Houben et al. (2012), in a study of the Eocene-Oligocene succession of the Berici Mountain (Northern Italy), estimated a ~20 m sea-level drop in correspondence of the Eocene-Oligocene boundary, related to the EOT, and then a further ~60 m drop related to the Oi-1 event and the glaciation of Antarctica. Similarly, Miller et al. (2009)

suggest a sea level drop related to the Oi-1 event of 80 ± 25 m. In this framework, the occurrence of extensive slumps indicates the deepening of the storm weather wave base. It is widely accepted that slumps and soft-sediment deformation structures can be triggered by storm waves (Molina et al., 1998). The intensification and the more frequent occurrence of storm events on the Santo Spirito ramp could have been enhanced also by the onset of the new oceanographic conditions and strong wind-driven currents related to the stronger latitudinal gradient (Coxall and Pearson, 2007; Miller et al., 2009).

The high biogenic productivity phases recorded during late Eocene in the pelagic realm do not seem to be equally recorded in the platform domain. Apparently, no significant changes in the carbonate factory of the Santo Spirito ramp occurred concomitantly with the Eocene-Oligocene transition. On the other hand, since the depositional environment of Santo Spirito Fm ranges from outer ramp to pelagic settings, consequently, the carbonate factory was dominated by aphotic biota such as small benthic foraminifera, mollusk and echinoid fragments, coupled with the pelagic components, represented by the planktonic foraminifera accumulating in the outer ramp. Relevant compositional changes are observed only in the resedimented interval (floatstone to rudstone lithofacies) marked by the disappearance of *Discoyclina* specimens, reduced occurrence of *Nummulites*, and spreading of red algae. A drastic change of the carbonate factory is recorded in the western margin of the Lessini shelf (Jaramillo-Vogel et al., 2013; 2016). While red algae and LBF dominate in the lower portion of the succession, its uppermost part is characterized by bryozoan-rich beds. According to Jaramillo-Vogel et al. (2013; 2016), the disappearance of *Discocyclina* and *Asterocyclina,* and the replacement of phototrophic organisms by heterotrophic ones could be due to a significant change in the environmental conditions. This change corresponds to a sharp positive shift in $\delta^{13}C$ that starts just below the bryozoan beds and is interpreted as the main c-cycle perturbation occurring at Eocene-Oligocene transition. This perturbation is associated to a major change in trophic resources, indicated in the Lessini Shelf by a rise in the total phosphorus content, that triggered an increased primary productivity and, thus, a shallowing of the photic zone (Jaramilo-Vogel et al., 2016). Decreased water transparency would have limited light-dependent biota and left bryozoans as dominant benthic calcifying organisms. The coeval deposition of bryozoan beds reported from other several localities in northern Italy is interpreted to represent the regional response of a carbonate platform depositional system to global oceanographic changes related to the beginning of the Antarctic glaciation. In the Southern Tethys platforms (Hyblea, southern Apula, Malta), the progressive global cooling at Eocene-Oligocene Transition produced a major decline of larger benthic foraminiferal assemblages. The *Discocyclina* genus disappeared, as well as most of the *Nummulites* species, whereas coral bioconstructions underwent renewed development. Lastly, coralline algae became a dominant sediment-producing biota, and seagrass environments expanded, causing a change in the facies association of the Cenozoic carbonate platforms (Pedley, 1998; Nebelsick et al., 2005; Brandano et al., 2009; 2017a).

2.6 Conclusions

The Neo-thetys carbon isotope records of the Santo Spirito Formation (Majella Mountain, northern Apula Platform) and the coeval basinal succession of the Massignano section match with the global carbon isotope signal. The shallow-water $\delta^{13}C_{Carb}$ record of upper Eocene shows an overall negative trend, while the contemporary $\delta^{13}C_{TOC}$ records a positive one. This general trend is related to reduced fractionation by primary producers during the late Eocene, due to the decreasing pCO_2 after the C-cycle perturbation of the MECO and before the onset of the carbon anomaly linked to the Oi-1 event. However, regional factors influenced the Neo-thetys carbon isotope record, as suggested by sharp transient negative spikes that mark the $\delta^{13}C_{TOC}$ record of the Massignano section. These short-term anomalies are interpreted as short times of higher productivity linked to enhanced nutrient availability, and triggered by the westward subtropical Eocene Neo-tethys current entering from the Arabian-Eurasian gateway. Differently, the shallow-water carbon isotope signal does not record these short-term pulses of productivity. In fact, no significant changes in the carbonate factory of the Santo Spirito Formation are recorded, since the depositional environments range from the outer ramp to a pelagic setting where only photo-independent organisms occur and accumulate. However, the compositional characters of the resedimented sediments from the photic zone of the ramp through the Eocene-Oligocene transition evidence a change in the composition of the carbonate factory during the Oligocene, with the disappearance of orthophragminids, the reduction of *Nummulites*, and the expansion of biota associated with the seagrass together with the spread of red algae.

Finally, the Santo Spirito Formation does not record the major carbon isotope shift concomitantly to the Oi-1 event, since in the lowermost Oligocene the regular bedding of the sedimentary succession is interrupted by the occurrence of extensive slumps. The slumps represent the evidence of the sea-level drop that occurred at the onset of the Antarctica ice-sheet, that caused the deepening of the storm weather wave base, and eventually increased instability over the whole ramp.

Acknowledgements

The research leading to this paper benefitted from the financial support of the Sapienza, Università di Roma (Ateneo Project, MB; Avvio alla Ricerca Project, IC), from the Università degli Studi "G. d'Annunzio" di Chieti-Pescara (IR), and from the IAS Post-graduate Grant Scheme 2015 (IC). Many thanks go to Dr. Domenico Mannetta for providing the thin sections, and to Dr. Mauro Brilli and Dr. Francesca Giustini for their help in the isotope geochemistry laboratory. We are grateful to the Majella National Park, and to Dr. Elena Liberatoscioli in particular, for providing the license to sample within the park.

References

Agnini, C., Fornaciari, E., Raffi, I., Catanzariti, R., Pälike, H., Backman, J. and **Rio, D.** (2014). Biozonation and biochronology of Paleogene calcareous nannofossils from low and middle latitudes. *Newsletters on Stratigraphy*, 47, 131-181.

Alvarez, W. (1990). Pattern of extensional faulting in pelagic carbonates of the Umbria-Marche Apennines of central Italy. *Geology*, 18, 407-410.

Alvarez, W. (1999). Drainage on evolving fold-thrust belts: a study of transverse canyons in the Apennines. *Basin Research*, 11, 267-284.

Bassi, D. (2005). Larger foraminiferal and coralline algal facies in an Upper Eocene storm-influenced, shallow-water carbonate platform (Colli Berici, north-eastern

Italy). *Palaeogeogr. Palaeoclimatol. Palaeoecol.*, 226, 17-35.

Beavington-Penney, S. J., **Wright, V. P.** and **Woelkerling, W. J.** (2004). Recognising macrophyte-vegetated environments in the rock record: a new criterion using 'hooked' forms of crustose coralline red algae. *Sed. Geol.*, 166, 1-9.

Beavington-Penney, S.J., **Wright, V.P.** and **Racey, A.** (2005). Sediment production and dispersal on foraminifera-dominated early tertiary ramps: the Eocene El Garia Formation, Tunisia. *Sedimentology*, 52, 537-569.

Beerling, D. J. and **Royer, D. L.** (2011). Convergent cenozoic CO_2 history. *Nature Geoscience*, 4, 418.

Berggren, W.A., **Kent, D.V.**, **Swisher, C.C. III** and **Aubry, M.-P.** (1995). A revised Cenozoic geochronology and chronostratigraphy. In: Berggren, W.A., Kent, D.V., Swisher, C.C., III, Aubry, M.-P., and Hardenbol, J., eds., Geochronology, *Time Scales, and Global Stratigraphic Correlation*: *SEPM (Society for Sedimentary Geology) Spec. Publ.*, 54, 129–212.

Bernoulli, D. and **Jenkyns, H.** (1974). Alpine, Mediterranean, and central Atlantic Mesozoic facies in relation to the early evolution of the Tethys. In: *Modern and Ancient Geosynclinal Sedimentation* (Dott, R.H., Shaves, R.H. Eds.), *SEPM Spec. Publ.*, 19, 129-157.

Blow, W.H. (1969). Late middle Eocene to Recent planktonic foraminiferal biostratigraphy. In: Bronnimann, P., and Renz, H.H., eds., *Proceedings of the First International Conference on Planktonic Microfossils* (Geneva, 1967): Leiden, E.J. Brill, 199–421.

Bodiselitsch, B., **Montanari, A.**, **Koeberl, C.** and **Coccioni, R.** (2004). Delayed climate cooling in the Late Eocene caused by multiple impacts: high-resolution geochemical studies at Massignano, Italy. *Earth Planet. Sci. Lett.*, 223, 283-302.

Bohaty, S. M. and **Zachos, J. C.** (2003). Significant Southern Ocean warming event in the late middle Eocene. *Geology*, 31, 1017-1020.

Bohaty, S. M., **Zachos, J. C.** and **Delaney, M. L.** (2012). Foraminiferal Mg/Ca evidence for Southern Ocean cooling across the eocene–oligocene transition. *Earth Planet. Sci. Lett.*, 317, 251-261.

Bown, P. R. and **Young, J. R.** (1998). Techniques. In: Brown, P. R. (Eds), *Calcareous nannofossil biostratigraphy.* Micropaleontological Society Publication Series, Chapman & Hall, 16-28.

Bramlette, M. N. and **Riedel, W. R.** (1954). Stratigraphic value of discoasters and some other microfossils related to Recent coccolithophores. *Journal of Paleontology*, 385-403.

Brandano, M., **Frezza, V.**, **Tomassetti, L.** and **Cuffaro, M.** (2009). Heterozoan carbonates in oligotrophic tropical waters: the Attard member of the lower coralline limestone formation (Upper Oligocene, Malta). *Palaeogeogr. Palaeoclimatol. Palaeoecol.*, 274, 54-63.

Brandano, M., **Lipparini, L.**, **Campagnoni, V.** and **Tomassetti, L.** (2012). Downslope-migrating large dunes in the Chattian carbonate ramp of the Majella Mountains (Central Apennines, Italy). *Sed. Geol.*, 255, 29-41.

Brandano, M., **Lustrino, M.**, **Cornacchia, I.** and **Sprovieri, M.** (2015). Global and regional factors responsible for the drowning of the Central Apennine Chattian carbonate platforms. *Geological Journal*, 50, 575-591.

Brandano, M., **Corda, L.**, **Tomassetti, L.** and **Tagliavento, M.** (2016b). Frequency analysis across the drowning of a lower Jurassic Carbonate Platform: the Calcare Massiccio formation (Apennines, Italy). *Mar. Petrol. Geol.*, 78, 606-620.

Brandano, M., **Cornacchia, I.**, **Raffi, I.** and **Tomassetti, L.** (2016a). The Oligocene–Miocene stratigraphic evolution of the Majella carbonate platform (Central Apennines, Italy). *Sed. Geol.*, 333, 1-14.

Brandano, M., **Cuffaro, M.**, **Gaglianone, G.**, **Petricca, P.**, **Stagno, V.** and **Mateu-Vicens, G.** (2016c). Evaluating the Role of Seagrass in Cenozoic CO_2 Variations. *Frontiers in Environmental Science*, 4, 72, 1-9.

Brandano, M., **Cornacchia, I.**, **Raffi, I.**, **Tomassetti, L.** and **Agostini, S.** (2017b). The Monterey Event within the Central Mediterranean area: The shallow-water record. *Sedimentology*, 64, 286-310.

Brandano, M., **Cornacchia, I.** and **Tomassetti, L.** (2017a). Global versus regional influence on the carbonate factories of Oligo-Miocene carbonate platforms in the Mediterranean area. *Marine and Petroleum Geology*, 87, 188-202.

Bukry, D. and **Bramlette, M. N.** (1969). Some new and stratigraphically useful calcareous nannofossils of the Cenozoic. *Tulane studies in Geology and Paleontology*, 7, 131-142.

Bukry, D. and **Percival, S. F., Jr.** (1971). New Tertiary calcareous nannofossils. *Tulane Studies in Geology and Paleontology*, 8, 123–146.

Burla, S., **Heimhofer, U.**, **Hochuli, P.A.**, **Weissert, H.** and **Skelton, P.** (2008). Changes in sedimentary patterns of coastal and deep-sea successions from the North Atlantic (Portugal) linked to Early Cretaceous environmental change. *Palaeogeogr. Palaeoclimatol. Palaeoecol.*, 257, 38–57.

Buxton, M. W. N. and **Pedley, H. M.** (1989). Short Paper: A standardized model for Tethyan Tertiary carbonate ramps. *Journal of the Geological Society*, 146, 746-748.

Carminati, E., **Lustrino, M.** and **Doglioni, C.** (2012). Geodynamic evolution of the central and western Mediterranean Tectonics vs. igneous petrology constraints. *Tectonophysics*, 579, 173–192.

Carnevale, G., **Patacca, E.** and **Scandone, P.** (2011). Field guide to the post-conference excursions (Scontrone, Palena and Montagna della Majella). *R.C.M.N.S. Interim colloquium*, Scontrone (L'Aquila) 4-5 March 2011, Italy.

Carter, A., **Riley, T. R.**, **Hillenbrand, C. D.** and **Rittner, M.** (2017). Widespread Antarctic glaciation during the Late Eocene. *Earth Planet. Sci. Lett.*, 458, 49-57.

Centamore, E., **Chiocchini, G.**, **Deiana, A.**, **Micarelli, U.** and **Pieruccini, M.** (1971). Contributo alla conoscenza del Giurassico dell'Appennino umbro-marchigiano. *Studi Geol. Camerti.*, 1, 7-89.

Coccioni, R., Monaco, P., Monechi, S., Nocchi, M. and **Parisi, G.** (1988). Biostratigraphy of the Eocene/Oligocene boundary at Massignano (Ancona, Italy). In: Premoli Silva, I., Coccioni, R., and Montanari, A., eds., *The Eocene/Oligocene Boundary in the Marche-Umbria Basin (Italy)*: International Subcommission on Paleogene Stratigraphy Special Publication: Ancona, Industrie Grafi che Fratelli Aniballi, 59–80.

Coccioni, R., Moretti, E., Nesci, O., Savelli, D., Tramontana, M., Veneri, F. and **Astracedi, M.** (1997). *Carta Geologica con Itinerari Escursionistici—Parco Naturale del Conero*: Firenze, Società Elaborazioni Cartografiche.

Cosentino, D., Cipollari, P., Marsili, P. and **Scrocca, D.** (2010). Geology of the central Apennines: a regional review. In: *The Geology of Italy* (Eds M. Beltrando, A. Peccerillo, M. Mattei, S. Conticelli and C. Doglioni). *Journal of the Virtual Explorer, Electronic Edition*, 36, paper 11. ISSN 1441-8142.

Coxall, H. K. and **Pearson, P. N.** (2007). The Eocene-Oligocene transition. *Deep Time Perspectives on Climate Change: Marrying the Signal from Computer Models and Biological Proxies*, 351-387.

Coxall, H. K. and **Wilson, P. A.** (2011). Early Oligocene glaciation and productivity in the eastern equatorial Pacific: Insights into global carbon cycling. *Paleoceanography*, 26, PA2221, doi: 10.1029/2010PA002021.

Coxall, H. K., Wilson, P. A., Palike, H., Lear, C. H. and **Backman, J.** (2005). Rapid stepwise onset of Antarctic glaciation and deeper calcite compensation in the Pacific Ocean. *Nature*, 433, 53.

Cramer, B. S., Wright, J. D., Kent, D. V. and **Aubry, M. P.** (2003). Orbital climate forcing of δ13C excursions in the late Paleocene–early Eocene (chrons C24n–C25n). *Paleoceanography*, 18, 4, doi:10.1029/2003PA000909.

Cramer, B.S., Toggweiler, J.R., Wright, J.D., Katz, M.E. and **Miller, K.G.** (2009). Ocean overturning since the Late Cretaceous: Inferences from a new benthic foraminiferal isotope compilation. *Paleoceanography*, 24 PA4216. DOI: 10.1029/2008PA001683.

Crescenti, U., Crostella, A., Donzelli, G. and **Raffi, G.** (1969). Stratigrafia della serie calcarea dal Lias al Miocene nella regione marchigiano-abruzzese: Parte II. Litostratigrafia, biostratigrafia, paleogeografia. *Mem. Soc. Geol. It.*, 9, 343–420.

DeConto, R. M. and **Pollard, D.** (2003). Rapid Cenozoic glaciation of Antarctica induced by declining atmospheric CO2. *Nature*, 421, 245-249.

DeConto, R. M., Pollard, D., Wilson, P. A., Pälike, H., Lear, C. H. and **Pagani, M.** (2008). Thresholds for Cenozoic bipolar glaciation. *Nature*, 455, 652-657.

Deflandre, G. (1952). Classes de Coccolithophoridés. (Coccolithophoridae. Lohmann, 1902). In: *Grassé, P. P. (Ed.), Traite de Zoologie*. Masson, Paris, 439-470.

Deflandre, G. and **Fert, C.** (1954). Observations sur les coccolithophoridés actuels et fossiles en microscopie ordinaire et électronique. *Annales de Paléontologie*, 40, 115-176.

Franceschi, M., Dal Corso, J., Posenato, R., Roghi, G., Masetti, D. and **Jenkyns, H. C.** (2014). Early Pliensbachian (Early Jurassic) C-isotope perturbation and the diffusion of the Lithiotis Fauna: Insights from the western Tethys. *Palaeogeogr. Palaeoclimatol. Palaeoecol.*, 410, 255-263.

Frijia, G., Parente, M., Di Lucia, M. and **Mutti, M.** (2015). Carbon and strontium isotope stratigraphy of the Upper Cretaceous (Cenomanian-Campanian) shallow-water carbonates of southern Italy: Chronostratigraphic calibration of larger foraminifera biostratigraphy. *Cretaceous Research*, 53, 110-139.

Galimov, E. M. (2006). Isotope organic geochemistry. *Organic geochemistry*, 37, 1200-1262.

Gartner Jr, S. and **Smith, L. A.** (1967). Coccoliths and related calcareous nannofossils from the Yazoo Formation (Jackson, Late Eocene) of Louisiana. *Universtity of Kansas Paleontological Contributions*, 20, 1-7.

Goldner, A., Herold, N. and **Huber, M.** (2014). Antarctic glaciation caused ocean circulation changes at the Eocene-Oligocene transition. *Nature*, 511, 574-577.

Gueguen, E., Doglioni, C. and **Fernandez, M.** (1998). On the post-25 Ma geodynamic evolution of the western Mediterranean. *Tectonophysics*, 298, 259–269.

Guerrera, F., Tramontana, M., Donatelli, U. and **Serrano, F.** (2012). Space/time tectono-sedimentary evolution of the Umbria-Romagna-Marche Miocene Basin (Northern Apennines, Italy): a foredeep model. *Swiss Journal of Geosciences*, 105, 325-341.

Haq, B. U. (1971). Paleogene calcareous nannoflora, part IV. Paleogene nanno-plankton biostratigraphy and evolutionary rates in Cenozoic calcareous nannoplankton. *Stockholm Contribution in Geology*, 25, 129–158.

Hay, W.W., Mohler, H. P. and **Wade, M. E.** (1966). Calcareous nannofossils from Nal'chik (northwest Caucasus). *Eclogae Geologicae Helvetiae*, 59, 379–399.

Hay, W. W., Mohler, H. P., Roth, P. H., Schmidt, R. R. and **Boudreaux, J. E.** (1967). Calcareous Nannoplankton Zonation of the Cenozoic of the Gulf Coast and Caribbean-Antillean Area, and Transoceanic Correlation. *Transactions of the Gulf Coast Association of the Geological Societies*, 17, 428-480.

Hayes, J. M., Strauss, H. and **Kaufman, A. J.** (1999). The abundance of ^{13}C in marine organic matter and isotopic fractionation in the global biogeochemical cycle of carbon during the past 800 Ma. *Chemical Geology*, 161, 103-125.

Houben, A. J., van Mourik, C. A., Montanari, A., Coccioni, R. and **Brinkhuis, H.** (2012). The Eocene–Oligocene transition: Changes in sea level, temperature or both? *Palaeogeogr. Palaeoclimatol. Palaeoecol.*, 335, 75-83.

Jaramillo-Vogel, D., Strasser, A., Frijia, G. and **Spezzaferri, S.** (2013). Neritic isotope and sedimentary records of the Eocene–Oligocene greenhouse–icehouse transition: The Calcare di Nago Formation (northern Italy) in a global context. *Palaeogeogr. Palaeoclimatol. Palaeoecol.*, 369, 361-376.

Jaramillo-Vogel, D., Bover-Arnal, T. and **Strasser, A.** (2016). Bryozoan beds in northern Italy as a shallow-water expression of environmental changes during the Oligocene isotope event 1. *Sed. Geol.*, 331, 148-161.

John, C. M., Mutti, M. and **Adatte, T.** (2003). Mixed carbonate-siliciclastic record on the North African margin (Malta)—coupling of weathering processes and mid Miocene climate. *Geological Society of America Bulletin*, 115, 217-229.

Jovane, L., Florindo, F. and **Dinarès-Turell, J.** (2004). Environmental magnetic record of paleoclimate change from the Eocene-Oligocene stratotype section, Massignano, Italy. *Geophysical Research Letters*, 31 L15601, doi:10.1029/2004GL020554.

Jovane, L., Florindo, F., Coccioni, R., Dinarès-Turell, J., Marsili, A., Monechi, S., Roberts, A. P. and **Sprovieri, M.** (2007b). The middle Eocene climatic optimum event in the Contessa Highway section, Umbrian Apennines, Italy. *Geological Society of America Bulletin*, 119, 413-427.

Jovane, L., Sprovieri, M., Florindo, F., Acton, G., Coccioni, R., Dall'Antonia, B. and **Dinarès-Turell, J.** (2007a). Eocene-Oligocene paleoceanographic changes in the stratotype section, Massignano, Italy: Clues from rock magnetism and stable isotopes. *Journal of Geophysical Research: Solid Earth*, 112, doi:10.1029/2007JB004963.

Jovane, L., Coccioni, R., Marsili, A. and **Acton, G.** (2009). The late Eocene greenhouse-icehouse transition: Observations from the Massignano global stratotype section and point (GSSP). *Geol. Soc. Am. Spec. Pap.*, 452, 149-168.

Lear, C. H., Bailey, T. R., Pearson, P. N., Coxall, H. K. and **Rosenthal, Y.** (2008). Cooling and ice growth across the Eocene-Oligocene transition. *Geology*, 36, 251-254.

Levin, H. L. (1965). Coccolithoporidae and related microfossils from the Yazoo Formation (Eocene) of Mississippi. *Journal of Paleontology*, 265-272.

Liu, Z., Pagani, M., Zinniker, D., DeConto, R., Huber, M., Brinkhuis, H., Shah, S.R., Leckie, M. and **Pearson, A.** (2009). Global cooling during the Eocene-Oligocene climate transition. *Science*, 323, 1187-1190.

Lourens, L. J., Sluijs, A., Kroon, D. and **Zachos, J. C.** (2005). Astronomical pacing of late Palaeocene to early Eocene global warming events. *Nature*, 435, 1083-1087.

Lustrino, M., Morra, V., Fedele, L. and **Franciosi, L.** (2009). Beginning of the Apennine subduction system in central western Mediterranean: constraints from Cenozoic "orogenic" magmatic activity of Sardinia, Italy. *Tectonics*, 28, TC5016, doi:10.1029/2008TC002419.

Marchegiani, L., Bertotti, G., Cello, G., Deiana, G., Mazzoli, S. and **Tondi, E.** (1999). Pre-orogenic tectonics in the Umbria–Marche sector of the Afro-Adriatic continental margin. *Tectonophysics*, 315, 123-143.

Martini, E. (1971). Standard Tertiary and Quaternary calcareous nannoplankton zonation. In*: Proceedings of the Second Planktonic Conference*, Roma 1970, pp. 739-785.

Martini, E. and **Ritzkowski, S.** (1968). Was ist das "Unter-Oligocan"? Nachrichten der Akademie der Wissenschaften in Gottingen II. *Mathematisch-physikalische Klasse*, 13, 231–251.

Miller, K. G., Wright, J. D. and **Fairbanks, R. G.** (1991). Unlocking the ice house: Oligocene-Miocene oxygen isotopes, eustasy, and margin erosion. *Journal of Geophysical Research: Solid Earth*, 96, 6829-6848.

Miller, K. G., Wright, J. D., Katz, M. E., Wade, B. S., Browning, J. V., Cramer, B. S. and **Rosenthal, Y.** (2009). Climate threshold at the Eocene-Oligocene transition: Antarctic ice sheet influence on ocean circulation. *Geological Society of America Special Papers*, 452, 169-178.

Molina, J. M., Alfaro, P., Moretti, M. and **Soria, J. M.** (1998). Soft-sediment deformation structures induced by cyclic stress of storm waves in tempestites (Miocene, Guadalquivir Basin, Spain). *Terrra Nova*, 10, 145-150.

Mutti, M., Bernoulli, D. and **Stille, P.** (1997). Temperate carbonate platform drowning linked to Miocene oceanographic events: Maiella platform margin, Italy. *Terra Nova*, 9, 122–125.

Mutti, M., Droxler, A. W. and **Cunningham, A. D.** (2005). Evolution of the Northern Nicaragua Rise during the Oligocene–Miocene: drowning by environmental factors. *Sed. Geol.*, 175, 237-258.

Mutti, M., John, C.M. and **Knoerich, A.C.** (2006). Chemostratigraphy in Miocene heterozoan carbonate settings: applications, limitations and perspectives. *Geol. Soc. London Spec. Publ.*, 255, 307–322.

Nebelsick, J. H., Rasser, M. W. and **Bassi, D.** (2005). Facies dynamics in Eocene to Oligocene circumalpine carbonates. *Facies*, 51, 197-217.

Pälike, H., Norris, R. D., Herrle, J. O., Wilson, P. A., Coxall, H. K., Lear, C. H., Shackleton, N., Tripati, A.K. and **Wade, B. S.** (2006). The heartbeat of the Oligocene climate system. *Science*, 314, 1894-1898.

Pagani, M., Huber, M. and **Sageman, B.** (2014). Greenhouse Climates. In: *Treatise on Geochemistry 2nd Eidtion*. Elsevier, Oxford, 281-304. DOI: 10.1016/B978-0-08-095975-7.01314-0

Patacca, E., Scandone, P., Di Luzio, E., Cavinato, G. P. and **Parotto, M.** (2008). Structural architecture of the central Apennines: Interpretation of the CROP 11 seismic profile from the Adriatic coast to the orographic divide. *Tectonics*, 27, TC3006, 36 pp.

Payros, A., Pujalte, V. and **Orue-Etxebarria, X.** (2007). A point-sourced calciclastic submarine fan complex (Eocene Anotz Formation, western Pyrenees): facies architecture, evolution and controlling factors. *Sedimentology*, 54, 137-168.

Pearson, P. N., Foster, G. L. and **Wade, B. S.** (2009). Atmospheric carbon dioxide through the Eocene-Oligocene climate transition. *Nature*, 461, 1110.

Pedley, M. (1998). A review of sediment distributions and processes in Oligo-Miocene ramps of southern Italy and Malta (Mediterranean divide). *Geol. Soc. London Spec. Publ.*, 149, 163-179.

Perch-Nielsen, K. (1971). Elektronenmikroskopische Untersuchungen an Coccolithen und verwandten Formen aus dem Eozän von Dänemark. *Det Kongelige Danske Videnskabernes-Selskabs Skrivter*, 18, 1–76.

Pialli, G. (1971). Facies di piana cotidale nel Calcare Massiccio dell'Appennino Umbro-Marchigiano. *Boll. Soc. Geol. It.*, 90, 481-507.

Pomar, L. and **Kendall, C. G. S. C.** (2008). Architecture of carbonate platforms: a response to hydrodynamics and evolving ecology. In: *Controls on carbonate platform and reef development SEPM Spec.Publ.,* 89, 187-216, Tulsa.

Premoli Silva, I. and **Jenkins, D. G.** (1993). Decision on the Eocene-Oligocene boundary stratotype. *Episodes*, 16, 379-382.

Raffi, I., Ricci, C., Garzarella, A., Brandano, M., Cornacchia, I. and **Tomassetti, L.** (2016). Calcareous nannofossils as a dating tool in shallow marine environment: an example from an upper Paleogene carbonate platform succession in the Mediterranean. *Newsletters on Stratigraphy*, 49, 481-495.

Salamy, K. A. and **Zachos, J. C.** (1999). Latest Eocene–Early Oligocene climate change and Southern Ocean fertility: inferences from sediment accumulation and stable isotope data. *Palaeogeogr. Palaeoclimatol., Palaeoecol.*, 145, 61-77.

Saltzman, M.R. and **Thomas, E.** (2012). Carbon isotope stratigraphy. In: *The Geologic Time Scale 2012* (Eds F.M. Gradstein, J.G. Ogg, M.D. Schmitz and G.M. Ogg), pp. 207–232. Elsevier, Amsterdam.

Spofforth, D. J. A., Agnini, C., Pälike, H., Rio, D., Fornaciari, E., Giusberti, L., Luciani, V., Lanci, L. and **Muttoni, G.** (2010). Organic carbon burial following the middle Eocene climatic optimum in the central western Tethys. *Paleoceanography*, 25, PA3210, doi:10.1029/2009PA001738.

Racey, A. (2001). A review of Eocene nummulite accumulations: structure, formation and reservoir potential. *Journal of Petroleum Geology*, 24, 79-100.

Tomás, S., Frijia, G., Bömelburg, E., Zamagni, J., Perrin, C. and **Mutti, M.** (2016). Evidence for seagrass meadows and their response to paleoenvironmental changes in the early Eocene (Jafnayn Formation, Wadi Bani Khalid, N Oman). *Sed. Geol.*, 341, 189-202.

Tomassetti, L., Benedetti, A. and **Brandano, M.** (2016). Middle Eocene seagrass facies from Apennine carbonate platforms (Italy). *Sed. Geol.*, 335, 136-149.

Vecsei, A. and **Sanders, D. G.** (1997). Sea-level highstand and lowstand shedding related to shelf margin aggradation and emersion, Upper Eocene-Oligocene of Maiella carbonate platform, Italy. *Sed. Geol.*, 112, 219-234.

Vecsei, A. and **Sanders, D.G.K.** (1999). Facies analysis and sequence stratigraphy of a Miocene warm-temperate carbonate ramp, Montagna della Maiella, Italy. *Sed. Geol.*, 123, 103–127.

Vecsei, A., Sanders, D. G., Bernoulli, D., Eberli, G. P. and **Pignatti, J. S.** (1998). Cretaceous to Miocene sequence stratigraphy and evolution of the Maiella carbonate platform margin, Italy. In: *Mesozoic and Cenozoic Sequence Stratigraphy of European Basins* (Eds J. Hardenbol, J. Thierry, M.B. Farley, T. Jacquin, P.C. De Graciansky and P.R. Vail), *SEPM Spec. Publ.*, 60, 53–74.

Vezzani, L., Festa, A. and **Ghisetti, F.C.** (2010). Geology and tectonic evolution of the Central-Southern Apennines, Italy. *Geol. Soc. Am. Spec. Pap.*, 469, 1–58.

Wade, B. S., Pearson, P. N., Berggren, W. A. and **Pälike, H.** (2011). Review and revision of Cenozoic tropical planktonic foraminiferal biostratigraphy and calibration to the geomagnetic polarity and astronomical time scale. *Earth-Sci. Rev.*, 104, 111-142.

Weissert, H., Joachimski, M. and **Sarnthein, M.** (2008). Chemostratigraphy. *Newsl. Stratigr.*, 42, 145–179.

Zachos, J. C. and **Kump, L. R.** (2005). Carbon cycle feedbacks and the initiation of Antarctic glaciation in the earliest Oligocene. *Global and Planetary Change*, 47, 51-66.

Zachos, J. C., Quinn, T. M. and **Salamy, K. A.** (1996). High-resolution (10^4 years) deep-sea foraminiferal stable isotope records of the Eocene-Oligocene climate transition. *Paleoceanography*, 11, 251-266.

Zachos, J., Pagani, M., Sloan, L., Thomas, E. and **Billups, K.** (2001). Trends, rhythms, and aberrations in global climate 65 Ma to present. *Science*, 292, 686-693.

3 The Monterey event within the Central Mediterranean area: The shallow-water record

Marco Brandano[1,2], Irene Cornacchia[1], Isabella Raffi[3], Laura Tomassetti[1], Samuele Agostini[4]

1: Dipartimento di Scienze della Terra, La Sapienza Università di Roma, P. Aldo Moro 5, I-00185 Roma, Italy
2: Sez. Sapienza, c/o Dipartimento Scienze della Terra, Istituto di Geologia Ambientale e Geoingegneria (IGAG) CNR, P. Aldo Moro 5, I-00185 Roma, Italy
3: Dipartimento di Ingegneria e Geologia, Universita degli Studi "G. d'Annunzio" Chieti- Pescara, Via dei Vestini 31, 66013 Chieti, Italy
4: Istituto di Geoscienze e Georisorse (IGG) CNR, Via Moruzzi 1, 56124 Pisa, Italy

Published in *Sedimentology* (2017), 64 (1), 286-310

Abstract

The middle Miocene is an important time to understand modern global climate evolution and its consequences on marine systems. The Mid-Miocene Climatic Optimum (between 17.0 Ma and 13.5 Ma) was the warmest time interval of the past 35 million years during which atmospheric CO_2 concentrations were lower than today. In the Mid-Miocene Climatic Optimum, a significant carbon cycle perturbation occurred, expressed as a last long-term positive carbon isotope shift, known in literature as the Monterey Carbon Isotope Excursion and recorded in open-ocean settings. In this work, the lower to middle Miocene carbon isotope records from three different domains of the Central Mediterranean are analysed with the aim of identifying the local carbonate platform response to the major global carbon cycle perturbation of the Monterey Event. Carbon and oxygen isotope ratios have been measured on samples belonging to three different stratigraphic sections, two of them are representative of shallow-water settings (Latium–Abruzzi and Apula platforms), and the latter of a hemipelagic setting (Umbria–Marche Basin). A well-defined Monterey Carbon Isotope Excursion is recorded also in these shallow-water sections. Despite their expected problematic stratigraphic constraints, a reliable age model is provided by calcareous nannofossil biostratigraphy and strontium isotope stratigraphy. In both the carbonate platform successions examined, the Monterey Carbon Isotope Excursion coincides with a spread of bryozoans over other carbonate-producing biota. The high productivity of the bryozoan-dominated factory in the aphotic zone had an important control on the platform depositional profile. The high rates of sediment production in the deeper aphotic and oligophotic zones produced a depositional profile of a low-angle ramp.

3.1 INTRODUCTION

The middle Miocene is a key time for understanding of the modern global climate evolution and its consequences for the ocean system (for example, circulation and productivity). The warmest time interval in the last 35 Myr, the Mid-Miocene Climatic Optimum, was recorded from 17.0 to 13.5 Ma (Zachos et al., 2001) and was characterized by mid-latitude temperatures as much as 6°C higher than today (Flower, 1999). During this interval, the atmospheric CO_2 concentrations were surprisingly lower than today and a long-term positive carbon isotope shift is recorded that preceded the onset of the glacial–interglacial climatic mode (Woodruff and Savin, 1991; Holbourn et al., 2004, 2007). This large-scale carbon isotope maximum is known in the literature as the Monterey Carbon Isotope Excursion, because it has been linked by previous authors to the storage of large amounts of organic matter in the type locality of the Monterey Formation, California (USA) (Vincent and Berger, 1985). For these reasons, the middle Miocene is a time of extreme palaeoceanographic change that deeply affected carbonate production.

Carbonate systems are sensitive to global carbon cycle perturbations. The variations in the stable carbon isotope ratios ($^{13}C/^{12}C$) in the total dissolved inorganic carbon have been identified in the carbonate geological record, and linked to changes in partitioning of carbon between organic matter and carbonate (Saltzman and Thomas, 2012); thus, they are related strictly to both the biosphere and the global carbon cycle. Moreover, the carbon fractionation process is almost entirely related to carbon incorporation into organic matter through photosynthesis, and almost completely independent from temperature. These characteristics make the carbonate carbon isotope ratios a reliable proxy of the carbon isotope signature of the ambient waters at the moment of the precipitation of carbonates. Lastly, unlike the oxygen isotope ratios, the carbon isotope chemistry is little influenced by diagenesis (Weissert et al., 2008; Saltzman and Thomas, 2012, and references therein).

The most reliable record to identify carbon isotope signatures and changes is considered the marine pelagic carbonate record (Weissert et al., 1998, 2008; Weissert and Erba, 2004), because it is usually continuous, well age constrained and lacking in meteoric diagenesis. However, shallow-water carbonate systems have also proven to be a reliable tool to record global carbon cycle perturbations, especially if the chemostratigraphic analyses are correlated and compared with the facies changes recorded in these systems (Föllmi et al., 1994; Wissler et al., 2003; Mutti et al., 2006; Amodio et al., 2008; Parente et al., 2008; Brandano et al., 2015; Frijia et al., 2015). Furthermore, during the Miocene, the heterozoan (*sensu* James, 1997) dominated carbonate platforms can be considered a reliable association due to their predominantly low-Mg calcite mineralogy. The absence or low percentage of aragonite components in the skeletal assemblage lessens the likelihood of early diagenetic remineralization and allows preservation of the original water carbon isotope signature (Mutti et al., 2006). On the other hand, it is well-documented that exported platform aragonite into the deeper basin can also influence this signal, and consequently may induce a shift in the carbon isotope composition towards more positive values, due to the generally higher $\delta^{13}C$ values of aragonite relative to calcite (Swart and Eberli, 2005; Föllmi and Godet, 2013).

The Monterey Carbon Isotope Excursion has been distinctly recognized and widely studied in oceanic settings (e.g. Vincent and Berger, 1985; Woodruff and Savin, 1991), mostly through Ocean Drilling Program (ODP) Site data sets (Zachos et al., 2001; Holbourn et al., 2004, 2007), but still little is known about the response of Mediterranean carbonate systems to this global carbon cycle perturbation. In fact, the middle Miocene Mediterranean carbon isotope curves, currently available from the literature, usually have low resolution (Kocsis et al., 2008) or are poorly age constrained (Mutti et al., 1999; Reuter et al., 2013; Auer et al., 2015).

This work presents the lower to middle Miocene carbon isotope records of two different carbonate platforms of the Central Mediterranean. The first case study refers to the record of the *Lithothamnion* and Bryozoan Formation (Latium–Abruzzi Platform). The second case study is the carbon isotope record of the Bolognano Formation (Apula Platform, Majella Mountains). These two shallow-water carbonate records are correlated to the upper lower to middle Miocene record of the hemipelagic Schlier Formation (Umbria–Marche Basin).

The aims of this study are: (i) to correlate the lower to middle Miocene carbon isotope record of the Central Mediterranean shallow-water environments to the global record; (ii) to correlate the Mediterranean carbon isotope signature to changes in carbonate production, in order to discriminate between the global controlling factors on carbonate production and the local causes, related to the Mediterranean oceanographic evolution; and (iii) to evaluate the validity of the record of carbon perturbation in shallow water versus the pelagic realm in the Apennine domain during the Miocene.

3.2 GEOLOGICAL SETTING

The Miocene evolution of the Mediterranean area. The Mediterranean Sea represents the westernmost portion of the former Mesozoic Tethys Ocean (Rögl, 1999). At the end of the Eocene, the Tethys vanished due to the collision between the Indian and Asian plates; hence, at the Eocene–Oligocene boundary it was already reduced to the Mediterranean Sea, still connected to both Atlantic and Indo-Pacific oceans, and to the newly formed, isolated Paratethys Sea (Rögl, 1999). Apennine subduction started during the Eocene (Lustrino et al., 2009). The west-dipping subduction led to an east/north-east migration of the deformation belt fronts, together with an almost contemporaneous extensional wave, eastward migrating too, in the back-arc area (Gueguen et al., 1998). Extension resulted in the formation of several basins on both oceanic (Alboran, Provencal and Tyrrhenian basins) and thinned continental crust (Valencia Trough) (Carminati et al., 2010, 2012). Moreover, Apennine subduction triggered the development of a highly explosive, subduction-related volcanism, within the western Mediterranean, that reached its climax during the early Miocene (22 to 18 Ma according to Carminati et al., 2012), contemporary to the phase of maximum angular velocity of the anticlockwise rotation of the Sardinia–Corsica Block (Gattacceca et al., 2007). Subsequent anorogenic volcanism is recorded within the western Mediterranean (Lustrino and Wilson, 2007; Lustrino *et al.*, 2011).

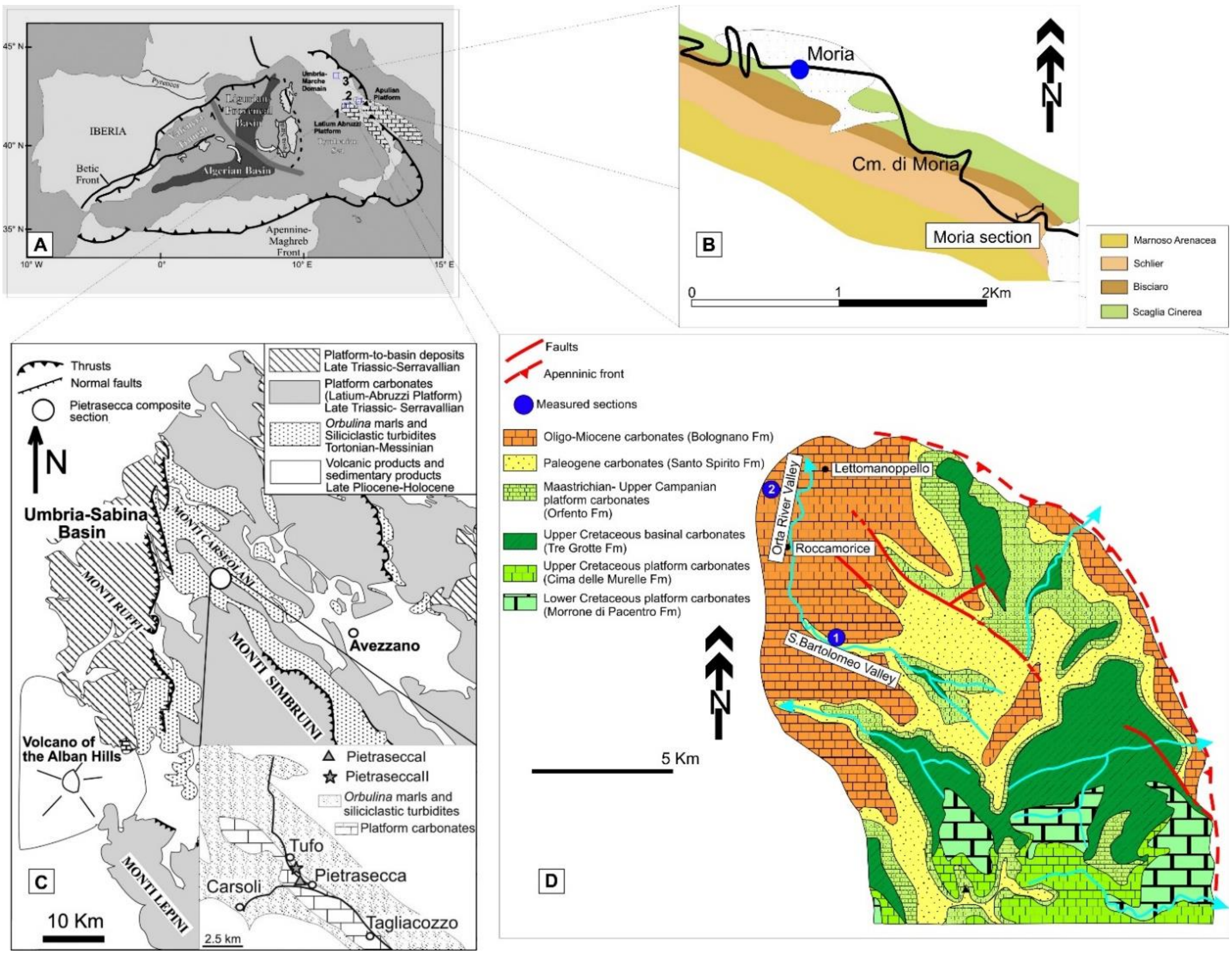

Fig. 3.1. (A) Map of the Mediterranean showing the location of the studied successions: 1, Latium–Abruzzi Platform; 2, Majella Mountains; 3, Umbria–Marche Domain, Northern Apennines (modified after Gueguen et al., 1998). (B) Simplified geological map of the Moria section (Northern Apennines), showing the studied section location. (C) Geological map of the area of the Pietrasecca section in the Central Apennines (after Corda and Brandano, 2003). (D) Simplified geological map of the Majella Mountains with locations of the measured stratigraphic sections (modified from Vecsei and Sanders, 1999); 1, San Bartolomeo Valley section; 2, Orta River section.

3.2.1 The Apennine platforms

The central portion of the Apennine Chain consists of Triassic to middle Miocene deposits once located along the western palaeo-margin of Adria. The main palaeogeographic domains are the Apennine carbonate platforms (the Latium–Abruzzi Platform and the Apula Platform) and the Umbria–Sabina Basin (Fig. 3.1A).

The Latium–Abruzzi Platform (Fig. 3.1A and C) consists of a Triassic to upper Miocene succession of shallow-water carbonates deposited in a tropical to subtropical environment. The Lower Cretaceous and the Upper Cretaceous portions of the Latium–Abruzzi Platform succession are separated by the first of three important, regionally distributed, bauxite layers which, together with significant karstification features, testify to a long-lasting subaerial exposure (Carbone, 1993). Another, long-term hiatus, encompassing the Palaeogene, characterizes most of the Latium–Abruzzi Platform, because Miocene carbonates lie directly in

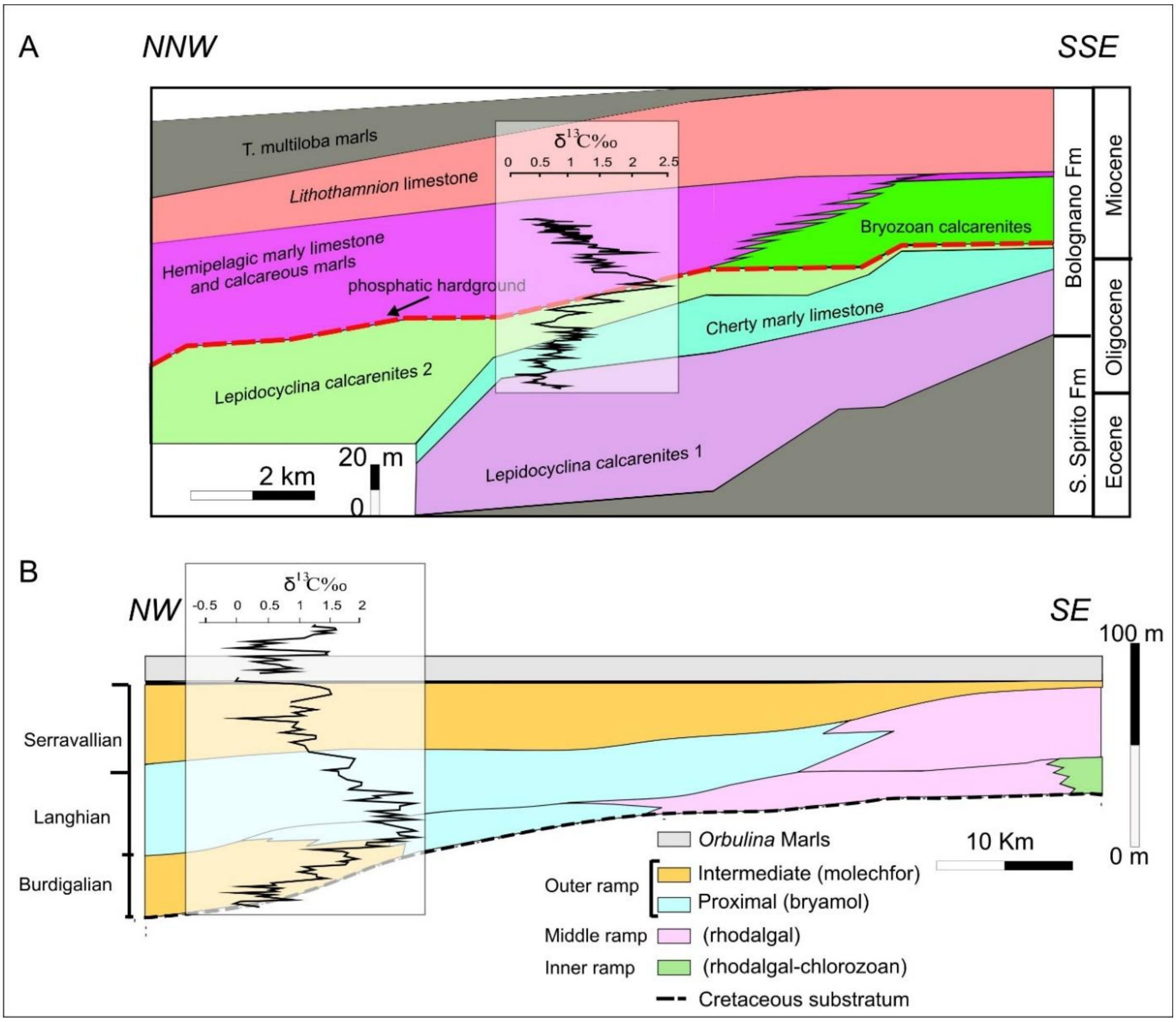

Fig. 3.2. (A) Stratigraphic architecture of the Bolognano Formation, Majella Mountains (after Brandano et al., 2016a), with the San Bartolomeo–Orta River carbon isotope curve. (B) Stratigraphic architecture of the Bryozoan and *Lithothamnion* Limestone Formation, Latium–Abruzzi Platform (after Brandano and Corda, 2002), with the Pietrasecca carbon isotope curve (after Brandano et al., 2010a).

paraconformity over the inner portions of the Cretaceous platform while, over the margins of the Mesozoic platform, thin, discontinuous Palaeocene–Eocene and upper Oligocene deposits are preserved (Accordi et al., 1967).
The Miocene portion of the Latium–Abruzzi succession is represented by the *Lithothamion* and Bryozoan (L&B) Formation (Aquitanian–Serravallian in age) (Civitelli and Brandano, 2005; Brandano et al., 2010b). The L&B Formation was deposited on a low-angle homoclinal ramp, developed in a persistent subtropical setting, dominated by rhodalgal (*sensu* Carannante et al., 1988) associations within the oligophotic zone and by bryomol (*sensu* Nelson, 1988) and molechfor (*sensu* Carannante et al., 1988) associations within the aphotic zone (Corda and Brandano, 2003; Brandano et al., 2010b) (Fig. 3.2B). The deposition of the L&B Formation ended in the late Miocene, due to the flexure of the foreland system and the consequent increase in the terrigenous input in the newly formed foredeep system of the Apennine Chain. The basal deposits of the foredeep system are represented by the *Orbulina* Marl Formation (Tortonian–

Messinian), which directly overlies the L&B Formation, and then by siliciclastic turbidites (Cipollari and Cosentino, 1992).

The northern portion of the Apula carbonate platform crops out in the Majella Mountain (Fig. 3.1D) where an Upper Jurassic to upper Miocene carbonate succession is exposed (Crescenti et al., 1969). The Upper Jurassic to upper Albian succession is represented by shallow subtidal to supratidal limestones (Vecsei et al., 1998). During the Late Cretaceous, a steep, erosional escarpment fully developed and, separating the platform from the basin, extended northward. In the uppermost Cretaceous, the depositional pattern of the shallow-water carbonates changed from aggradation to progradation because the basin was completely filled by the onlapping sediments (Vecsei et al., 1998). The K–Pg boundary is marked by a major unconformity, where *Microcodium* occurs, which testifies to the fact that the Majella platform faced another long-lasting interval of exposure (Vecsei and Moussavian, 1997). The Palaeogene evolution of the Majella carbonate platform is then represented by continuous sedimentation along the platform margin and the slope, while the platform top shows long-term hiatuses and discontinuous deposits up to the lower Oligocene, when the deposition the Bolognano Formation (upper Rupelian–Messinian) started.

The Bolognano Formation represents a homoclinal carbonate ramp that developed above the former shallow deposits of the platform (Mutti et al., 1997; Brandano et al., 2012, 2016a). The Bolognano Formation can be divided into six lithostratigraphic units, three of them representative of shallow-water carbonates, alternating with deeper units (Brandano et al., 2016a) (Fig. 3.2A). The first shallow-water phase is represented by the *Lepidocyclina* Calcarenite 1 that started to be deposited at the end of the Rupelian through to the Chattian. It is mainly represented by cross-bedded bioclastic packstones dominated by larger benthic foraminifera. This unit represents a large downslope migrating dune field, developed within the middle ramp environment. The second unit is the Cherty Marly Limestones (Chattian–upper Aquitanian), dominated by planktonic foraminifera and sponge spicules, and represents a drowning event that produced a sharp facies shift towards the low-energy outer ramp environment. During the early Burdigalian, the recovery of shallow-water sedimentation, confirmed by the deposition of the *Lepidocyclina* Calcarenites 2, again identifies the development of a well-developed dune field within the middle ramp environment. The *Lepidocyclina* Calcarenites 2 deposition ended with the occurrence of a hardground surface. In the late Burdigalian, a second drowning event is recorded, and marked by the deposition of two different lithostratigraphic units: the Bryozoan Calcarenites within the Orfento Valley, and the Hemipelagic Calcareous Marls and Marly Limestone in the northern sector of the Majella Mountains, both representing the upper Burdigalian–Serravallian interval. The hemipelagic marly limestones mainly consist of bioturbated packstones to packstones/wackestones dominated by planktonic foraminifera and, subordinately, by small benthic foraminifera, echinoids and mollusc fragments, thus indicating sedimentation within the aphotic zone. Lastly, a third shallow-water phase corresponds to the *Lithothamnion* Limestone unit (Tortonian), dominated by red algae assemblages. This unit is interpreted to represent an environment colonized by seagrass meadows developed between the distal inner ramp and in the middle ramp, while the distal portion of the latter was characterized by bioclastic packstone, together with red algal bindstone facies (Brandano et al., 2016b).

The evolution of the Oligo–Miocene ramp ended in Messinian time with the deposition of the Gessoso Solfifera Formation (Crescenti et al., 1969). Lastly, during the early Pliocene the northern portion of the Apula carbonate platform was involved into the foredeep system of the Apennine orogeny (Cosentino et al., 2010).

3.2.2 The Umbria–Marche Basin

During the Mesozoic, the Umbria–Marche Domain was located at the southern margin of the western Tethys. The Late Triassic rifting phase led to a marine transgression, as evidenced by evaporitic and marine restricted deposits, known as the Anidriti di Burano (Ciarapica and Passeri, 1976). In the earliest Jurassic, these deposits had already developed into a huge peritidal carbonate platform represented by the Calcare Massiccio Formation (Centamore et al., 1973), soon dismembered by Sinemurian rift tectonics, which led to the creation of fault-bounded platforms surrounded by deeper basins filled by Jurassic to Cretaceous pelagites. From the Late Cretaceous until the middle Miocene, the Umbria–Marche Basin has been filled by pelagic to hemipelagic sediments, with the continental derived siliciclastic fraction gradually increasing, starting from the Cretaceous Scaglia Bianca Formation to the Chattian–Aquitanian Scaglia Cinerea Formation. This evolution gives evidence of a progressive filling of the basin, with a concomitant decreasing bathymetry, and a more effective role of continental runoff (Montanari et al., 1994). The hemipelagic sedimentation during the Aquitanian to Langhian is represented by the Bisciaro Formation (Aquitanian–Burdigalian) and the Schlier Formation (Langhian), and was interrupted by the synorogenic turbiditic deposition of the flysch of the Marnoso Arenacea Formation (middle Miocene–Pliocene) that denotes the development of the Apennine foredeep system.

3.3 MATERIALS AND METHODS

The studied material comes from a composite stratigraphic section in the Apula Platform domain (San Bartolomeo–Orta River) cropping out in the Majella Mountains, a composite stratigraphic section of the Latium–Abruzzi Platform domain (Pietrasecca) and a stratigraphic section measured in the Umbria–Marche Basinal domain (Moria) (Figs 3.1B to D and 3.3A to C) (Annex A.1, A.8, A.9). The carbon and oxygen isotope compositions have been measured on 202 samples taken from two stratigraphic sections, the San Bartolomeo–Orta River and Moria sections (Figs 3.1B, 3.1D, 3.3A and

3.3C), whereas carbon and oxygen isotope compositions of the Pietrasecca section were measured by Brandano et al. (2010a) (Figs 3.1C and 3.3B).

The San Bartolomeo–Orta River composite section has been sampled with a 50 cm sampling interval in the initial 32 m, and a 1 m sampling interval in the following 88 m. Whole-rock analyses have been carried out at the isotope geochemistry laboratory of the Istituto of Geologia Ambientale e Geoingegneria (IGAG)-CNR of Rome, where stable carbon and oxygen isotope ratios have been measured with a gas chromatography-based Gas Bench II coupled with a Finnigan Delta Plus mass spectrometer (Thermo Fisher Scientific, Waltham, MA, USA).

The Moria section has been sampled with a 90-cm sampling interval. Whole-rock analyses have been performed on 38 samples. Carbon and oxygen stable isotope records have been measured with the Finnigan MAT 252 mass spectrometer at the isotope geochemistry laboratory of the Istituto per l'Ambiente Marino Costiero (IAMC)-CNR of Naples. The results were calibrated using the NBS carbonate standard. The values are reported on the Pee Dee Belemnite (PDB) scale. Analytical error is 0.1‰ based on replicate standards.

Fifteen samples for Strontium isotope stratigraphy (SIS) were collected from the Pietrasecca section. Eight out of fifteen pectinid samples have been selected for Sr isotope analysis after petrographic and geochemical analyses, in order to exclude any significant diagenetic overprint. Under petrographic microscope the examined shell material exhibited the typical cross-lamellar and fibrous microstructure of pectinid shells and lacked evidence of recrystallization (Fig. 3.4). The elemental composition of the shells was analysed as a further screening step. Concentration of Mg, Sr, Fe and Mn was determined through laser ablation at the laser ablation–inductively coupled plasma–mass spectrometry (LA-ICP-MS) laboratory of the Istituto di Geoscienze e Georisorse (IGG)-CNR of Pavia. The laser ablation apparatus consists of a Q-switched Nd: YAG laser source (Brilliant Quantel, Bozeman, Montana, USA) whose fundamental emission is converted into 266 nm by means of harmonic generators (Tiepolo et al., 2003). A fine alignment is provided by analysing the NIST 610 glass standard before any analytical session. The ablated material has then been analysed with an Element I, ThermoFinnigan MAT ICP-MS. Samples for Sr isotope analyses were obtained with a hand-operated microdrill, using 0 5 mm Ø tungsten drill bits. Samples were drilled from the polished surface in the same portion sampled by laser ablation.

Strontium isotopes were measured at IGG-CNR, Pisa (Italy), using a Finnigan MAT 262V multicollector mass spectrometer running in dynamic mode, after Sr purification with the conventional cation ion procedure. Measured $^{87}Sr/^{86}Sr$ ratios have been normalized to $^{86}Sr/^{88}Sr=0.1194$. During the collection of Sr isotopic data, 18 replicate analyses of standard NIST SRM 987 standard gave an average value

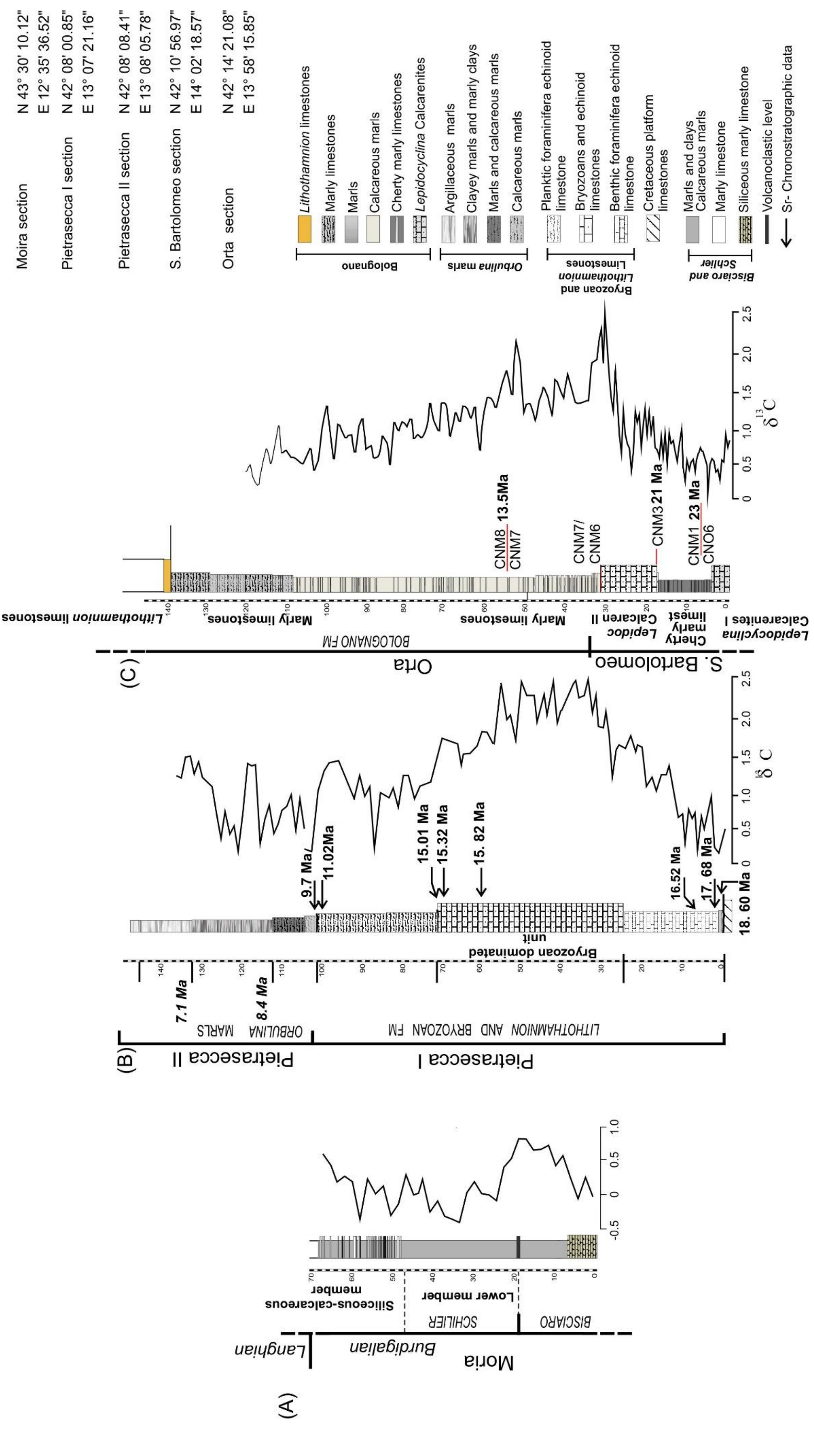
Moira section N 43° 30' 10.12" E 12° 35' 36.52"
Pietrasecca I section N 42° 08' 00.85" E 13° 07' 21.16"
Pietrasecca II section N 42° 08' 08.41" E 13° 08' 05.78"
S. Bartolomeo section N 42° 10' 56.97" E 14° 02' 18.57"
Orta section N 42° 14' 21.08" E 13° 58' 15.85"
Bolognano
Lithothamnion limestones
Marly limestones
Marls
Calcareous marls
Cherty marly limestones
Lepidocyclina Calcarenites
Orbulina marls
Argillaceous marls
Clayey marls and marly clays
Marls and calcareous marls
Calcareous marls
Bryozoan and Lithothamnion Limestones
Planktic foraminifera echinoid limestone
Bryozoans and echinoid limestones
Benthic foraminifera echinoid limestone
Cretaceous platform limestones
Bisciaro and Schlier
Marls and clays Calcareous marls
Marly limestone
Siliceous marly limestone
Volcanoclastic level
Sr- Chronostratographic data
(A)
Moria
Langhian
Burdigalian
BISCIARO
SCHLIER
Lower member
Siliceous-calcareous member
(B)
Pietrasecca II
Pietrasecca I
ORBULINA MARLS
LITHOTHAMNION AND BRYOZOAN FM
7.1 Ma
8.4 Ma
Bryozoan dominated unit
9.7 Ma
11.02Ma
15.01 Ma
15.32 Ma
15. 82 Ma
16.52 Ma
17. 68 Ma
18. 60 Ma
(C)
Orta
S. Bartolomeo
BOLOGNANO FM
Lithothamnion limestones
Marly limestones
Lepidoc Calcaren II
Cherty marly limest
Lepidocyclina Calcarenites I
CNM8 13.5Ma
CNM7
CNM7/ CNM6
CNM3 21 Ma
CNM1 23 Ma
CNO6
δ13C

Fig. 3.3. Comparison of the carbon isotope composition of the studied sections plotted against stratigraphic depth; (A) Moria section; (B) Pietrasecca compos- ite section; (C) San Bartolomeo Valley–Orta River composite section. All of the ages in the stratigraphic logs and related isotope curves have been calibrated with GTS 2004. The chronostratigraphic framework of the Moria section is from Di Stefano *et al.* (2015), based on biostratigraphy and magnetostratigraphy. The chronostratigraphic framework of the Pietrasecca section is provided by Sr isotope stratigraphy (this work). The $^{87}Sr/^{86}Sr$ values of the samples have been converted to numerical ages using Version 4B: 08/04 of the Look-Up Table of Howarth & McArthur (1997). The stratigraphic framework of the San Bartolomeo–Orta River section is based on calcareous nannofossil data (after Brandano *et al.*, 2016a), referred to the stratigraphic scheme of Backman *et al.* (2012).

of 0.710246 0.000011 (2 SE) which is, inside the error, indistinguishable from the value of 0.710248 reported in McArthur et al. (2001); thus, no any further adjustment was necessary.

The $^{87}Sr/^{86}6Sr$ values of the samples have been converted to numerical ages using Version 4B: 08/04 of the Look-Up Table of Howarth & McArthur (1997); for details of 4B: 08/04, see McArthur and Howarth (2004). Minimum and maximum ages were calculated by combining the long-term standard error (2 SE mean) of each measured $^{87}Sr/^{86}Sr$ ratio with the uncertainty related to the strontium isotope curve (Howarth and McArthur, 1997; Steuber, 2001).

3.4 RESULTS

3.4.1 The Pietrasecca section

The Pietrasecca section records the evolution of the Latium–Abruzzi domain during the Miocene, from foreland to subduction-related phases. The composite section comprises two formations: the Lithothamnion and Bryozoan Limestone (L&B) and Orbulina Marl (OM) formations (Fig. 3.3B). The L&B Formation corresponds to the initial 100 m and it is overlapped by the 48-m thick OM Formation. The L&B Formation comprises three main lithostratigraphic units that can be ascribed to an outer ramp environment. The first unit is a 25-m thick benthic

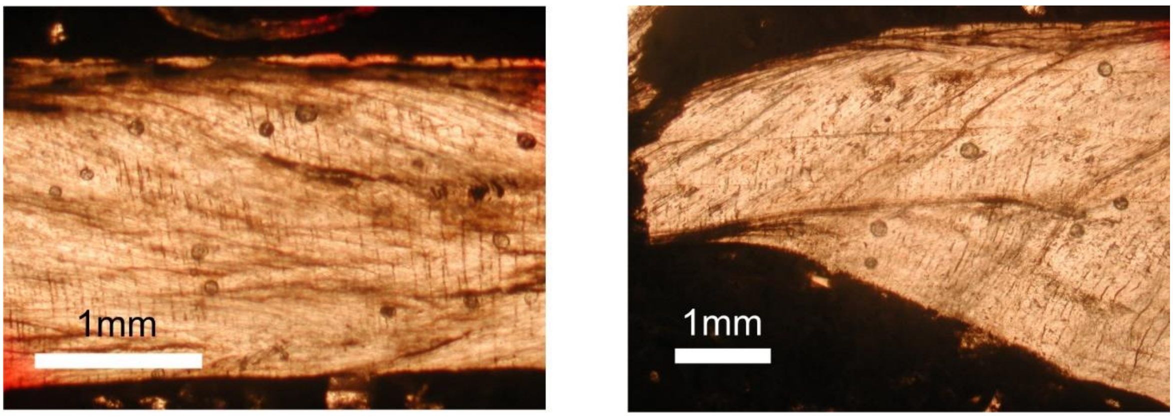

Fig. 3.4. Thin-section microphotographs of the analysed pectinids showing well-developed and well-preserved foliated microstructure.

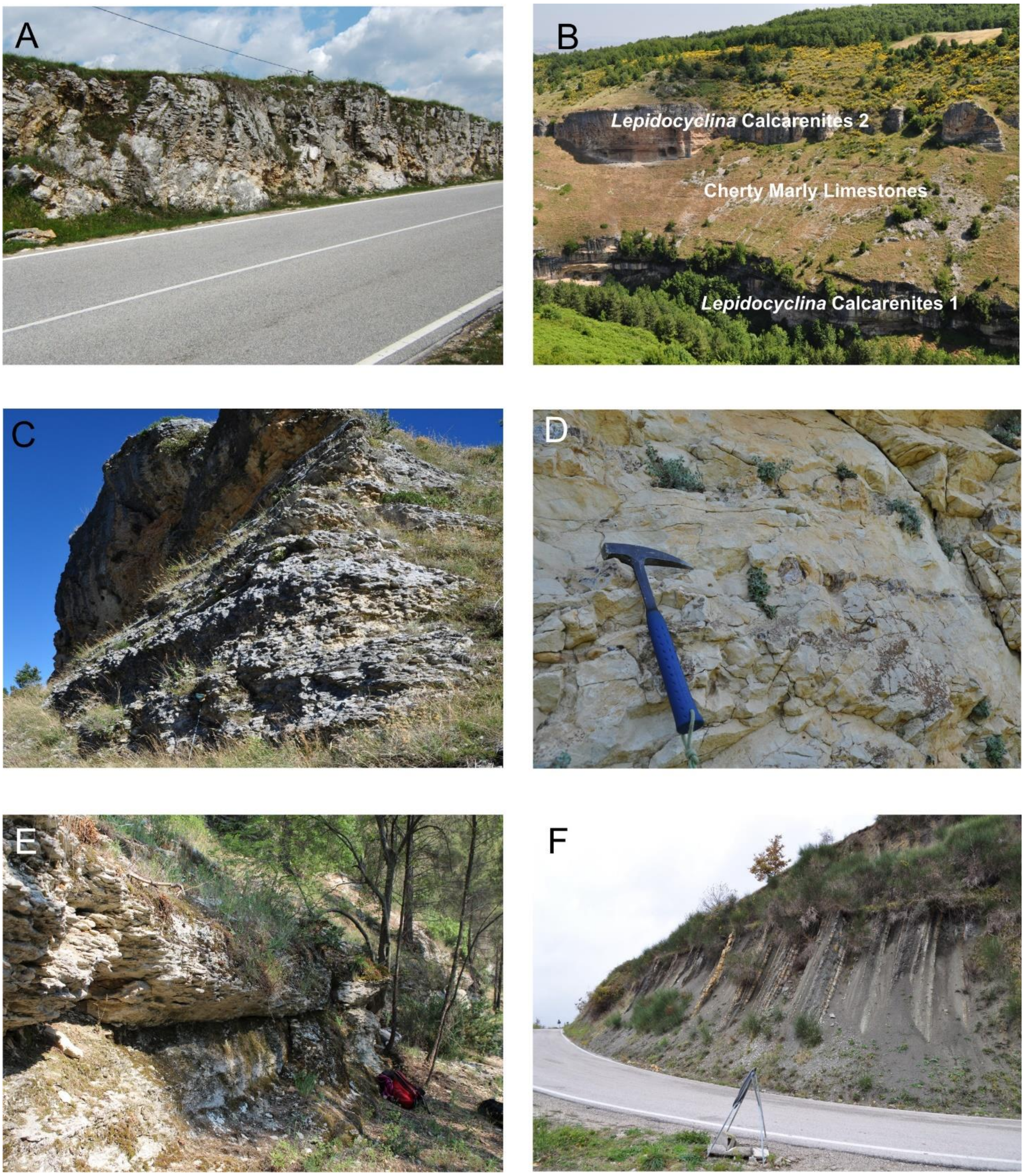

Fig. 3.5. Main lithofacies of the investigated outcrops. (A) to (D) Lithofacies association of Bolognano Formation. (A) *Lithothamnion* and Bryozoan Limestone unit overlain by medium-grained planktonic echinoid packstone unit cropping out at the Pietrasecca section. (B) Panoramic view of San Bartolomeo section showing the upper portion of the cross-bedded *Lepidocyclina* Calcarenites 1 unit overlain by the Cherty Marly Limestone unit that are lying under the cross-bedded *Lepidocyclina* Calcarenites 2 unit. (C) Detail of the cross-bedded bioclastic packstone of the *Lepidocyclina* Calcarenites 2 in the San Bartolomeo section. (D) Detail of the Cherty Marly Limestone unit characterized by cherty horizon and nodules (hammer for scale is 35 cm) (San Bartolomeo section). (E) Horizon- tally bedded hemipelagic calcareous marls and marly limestones cropping out in the Orta River section. (F) Mid- dle calcareous–siliceous member of the Schlier Formation of the Moria section characterizing by an alternation of clayey marls and calcareous marls.

foraminifer–echinoid packstone. This unit passes upward into a 44-m thick bryozoan and echinoid floatstone to packstone, and is overlain by 31 m of medium-grained planktonic-echinoid packstone (Fig. 5A). The hemipelagic OM Formation shows a thickness of 48 m and may be subdivided into four main intervals. The lowest interval consists of 3 m of calcareous marls and bioturbated marls with phosphate and glauconite, and bivalve and brachiopod shells. The interval above is 8 m thick and comprises bioturbated clayey or calcareous marls overlain by a third interval consisting of 20 m of marls and clays with planktonic foraminifera. The uppermost interval consists of 17 m thick argillaceous marls with silty to sandy levels (Fig. 3.3B).

The $\delta^{13}C$ values of the L&B Formation range between +0.1‰ and +2.48‰ (Fig. 3B). The $\delta^{13}C$ curve shows a positive shift from 0.1 to 1.71‰ in the lower unit, to 2.1 to 2.48‰ from 20 to 70 m, corresponding to the bryozoan-dominated and echinoid-dominated unit. The upper 20 m of the L&B Formation shows a negative shift of the $d^{13}C$ values, which decrease to fluctuating values around 0.5‰. Samples for carbon isotope analyses from the *Orbulina* Marl (OM) were collected only in the lowest 32 m. The overall $\delta^{13}C$ record of this interval spans from +0.2 to 1.2‰ (Fig. 3.3B). A sharp negative $\delta^{13}C$ shift marks the boundary between the L&B and OM formations, with values decreasing from +1.4 to +0.2‰. Two positive peaks occur around 120 m and slightly before the top of the section.

3.4.1.1 Screening of pectinid samples for diagenetic alteration, strontium isotope stratigraphy and numerical age

The degree of pectinid shell preservation was analysed for the 16 collected samples to select pristine samples for strontium isotope stratigraphy (See ANNEX B.3 for complete trace element concentration profiles) (SIS; Fig. 3.4). Low-Mg biogenic calcite is considered to be the best candidate for strontium isotope stratigraphy because it is relatively resistant to diagenetic alteration (Longman, 1980), meaning that well-preserved low-Mg calcite shells better retain the original seawater isotopic signature (McArthur, 1994; McArthur and Howarth, 2004; Steuber, 1999; Frijia and Parente, 2008; Brandano and Policicchio, 2012; Ullmann and Korte, 2015; Frijia et al., 2015). Usually the diagenesis of low-Mg calcite decreases Sr and increases Mn and Fe concentrations (Brand and Veizer, 1980; Veizer, 1983). In this study, the $^{87}Sr/^{86}Sr$ ratio has been analysed only on pectinids having Sr, Mn, Fe and Mg contents that are in agreement with those of well-preserved fossil pectinids and modern counterparts (McArthur, 1994; Steuber, 1999; Scasso et al., 2001; Kroeger et al., 2007). A Sr and Mn concentration above 650 ppm and below 100 ppm, respectively, has been chosen as the cut-off threshold (Steuber, 1999, 2001; Scasso et al., 2001) (Table 3.1). Several samples that, by Mn and Sr concentrations and from petrographic observation, appeared to be well-preserved had slightly higher Fe concentrations (up to 2000 ppm) than expected for pristine carbonate shell. According to Dingle et al. (1997), the concordance of the measured isotopic ratios, the monomineralic nature of the samples and their good petrographic preservation indicates that much of this soluble Fe could have been the result of dissolution of Fe oxyhydroxides on carbonate crystallites, rather than dissolution of recrystallised carbonate. Recently, Frijia et al. (2015) showed rudist shells with well-preserved pristine microstructure and high Sr, and Fe concentration higher than samples with petrographic evidence of recrystallization and low Sr concentration. These authors did not use Fe and Mn concentration as the prime criteria of diagenetic screening and relied mainly on Sr concentration. All of the pectinid shell samples used in this study have $\delta^{13}C$ and $\delta^{18}O$ that suggest precipitation from Miocene seawater Table 1) testifying to good preservation (See Annex B.4 for carbon and oxygen isotope ratios of the pectinid shells). The $^{87}Sr/^{86}Sr$ values together with the corresponding numerical ages of the samples are given in Table 2. The $^{87}Sr/^{86}Sr$ ratios of the samples range between 0.708542 and 0.708897 (Annex B.5). The derived ages range from to 18.60 Ma and 9.70 Ma. The ages obtained by Sr isotope analysis indicate that the lowest unit of the L&B Formation was deposited in the early to late Burdigalian interval, whereas the second bryozoan-rich unit was deposited between the late Burdigalian and Langhian. The third unit was deposited between Langhian and Tortonian, as confirmed by Sr chronostratigraphy of the top of this unit and of the base of the *Orbulina* Marl (Fig. 3.3B). The age–depth diagram in Fig. 3.6A was set to scale the stratigraphic thickness of the Pietrasecca section against numerical age. The age–depth control points are the seven strontium isotope dates obtained by bivalve samples of the Pietrasecca section. From the base of the section to the first 7 m, the sedimentation rates increase from 0.14 cm/ka to 0.49 cm/ka. Successively, the sedimentation rate increases up to 7.42 cm/ka in the bryozoan-dominated unit. In the upper part of this unit, the sedimentation rates reduce to 1.80 cm/ka, and attain a constant slow rate (0.72 cm/ka) in the upper 30 m of the section. The average sedimentation rate for the Pietrasecca section is 1.33 cm/ka.

3.4.2 The San Bartolomeo–Orta River composite section

The composite San Bartolomeo Valley–Orta River section records the Chattian–Serravallian evolution of the Bolognano Formation. The lowest 4.5 m consist of a cross-bedded bioclastic packstone with larger benthic foraminifera, which corresponds to the upper portion of the *Lepidocyclina* Calcarenites 1 unit (Figs 3.5B and 3.7A). This unit is overlain by 11.7 m of the Cherty Marly Limestone unit (Figs 3.3C, 3.5B, 3.5C and 3.7B). The base consists of a very fine calcarenite, with small benthic foraminifera (mostly textulariids) and glauconite grains, which grades upward into a marly limestone with planktonic foraminifera and cherty nodules (Fig. 3.5D).

Sample	Mg (ppm)	SD	Mn (ppm)	SD	Fe (ppm)	SD	Sr (ppm)	SD	Ba (ppm)	SD	$\delta^{13}C$ (‰ VPDB)	$\delta^{18}O$ (‰ VPDB)
PP0*	2286,34	722,77	32,55	54,15	30,06	85,04	659,47	386,34	209,99	236,67	0,39	-1,20
PP1*	1913,32	598,82	11,93	5,64	1359,92	624,47	1345,89	225,55	4,50	1,11	-0,18	-0,24
PP2*	1151,55	238,02	26,22	12,67	246,46	15,24	1317,43	94,21	5,42	1,23	0,46	-0,42
PP3	1456,99	294,58	12,04	1,94	664,94	97,61	571,87	79,53	3,12	0,33		
PP5*	2152,43	243,14	8,07	0,04	216,23	15,33	662,33	71,90	2,50	0,11	1,58	-0,38
PP6	2864,99	780,35	32,85	6,32	1326,273333	144,0179969	291,86	19,59	4,05	0,75		
PP7	4808,44	234,89	31,95	6,90	974,24	140,76	316,10	24,41	2,99	0,49		
PP9	5454,90	426,78	8,79	0,56	431,85	14,89	303,51	26,53	3,62	0,59		
PP10	6496,26	261,33	9,31	2,03	417,65	83,87	346,39	21,89	3,00	0,56		
PP11	2528,85	817,81	13,09	2,91	455,58	38,74	602,34	149,79	3,15	0,24		
PP12a*	1977,75	308,75	96,37	174,04	214,22	220,41	986,98	451,63	0,00	0,00	1,92	-0,56
PP13*	1481,35	42,94	3,64	1,18	231,70	44,10	997,27	139,43	2,92	1,38	1,92	-0,20
PP14	1697,39	800,72	196,31	15,17	2127,53	724,53	1358,39	183,22	< dl			
PP15*	7997,32	1573,86	92,96	29,70	2074,34	586,94	1333,18	307,22	7,22	0,55	1,42	1,04
PP16*	1303,63	370,50	62,66	14,34	1151,19	905,60	908,30	101,88	9,34	3,16	1,16	0,30

n= 3 from PP2 to PP16
n= 5 for PP1
n=9 for PP0
*=samples selected for SIS

Table 3.1. Trace element concentrations profiles of Mg, Mn, Fe, Sr and Ba, reported as mean values and standard deviations, of the pectinid shell samples. $\delta^{13}C$ and $\delta^{18}O$ values of the samples selected for SIS; n = number of measurements; dl = detection limit.

Sample	$^{87}Sr/^{86}Sr$	2s.e.(*10^{-6})	Minimum Age	Age	Maximum Age
PP0	**0.708542**	6	18,39	**18,60**	18,82
PP1	**0,708616**	9	17,43	**17,68**	17,89
PP2	**0,708689**	9	16,22	**16,52**	16,83
PP 2*	0,708684	17			
PP5	**0,708731**	9	15,55	**15,82**	16,09
PP12a	**0.708542**	5	14,99	**15,32**	15,57
PP13	**0,708780**	6	14,48	**15,01**	15,34
PP 13*	0,708754	15			
PP15	**0.708855**	4	10,41	**11,02**	11,95
PP16	**0,708897**	7	9,08	**9,70**	10,21
PP 16*	0,708898	9			
PP 16*	0,708896	8			
NIST 987 has a certified value of 0.710248. 18 replicate analyses of NIST 987 gave an average value of 0.710246±0.000011 (2 s.e.), thus no adjustment was necessarty for measured values.					
2s.e. errors are in run errors. The minimum and maximum ages have been recalculated considering an error of 0.000011, which is the standard reproducibility.					
* = repeated samples					

Table 3.2. $^{87}Sr/^{86}Sr$ values of the pectinid shell samples reported with related analytical error (2 SE); $^{87}Sr/^{86}Sr$ corrected ratios and the associated age values. Numerical ages are reported from McArthur et al. (2001; Look-Up Table Version 4B: 08/04). Minimum and maximum ages were calculated by combining the long-term standard error (2 SE mean) of each measured $^{87}Sr/^{86}Sr$ ratio with the uncertainty related to the strontium isotope curve Howarth & McArthur, 1997).

The marly content of this unit constantly increases upward. This unit is overlain by 14 m of a cross-bedded packstone with larger benthic foraminifera, echinoid and bryozoan fragments, and represents the *Lepidocyclina* Calcarenites 2 unit (Figs 3.5B and 3.7C). This unit is bound at the top by a hardground surface, characterized by abundant planktonic foraminifera and phosphate minerals which are widespread across the whole surface. The *Lepidocyclina* Calcarenites 2 unit is overlain by hemipelagic marly limestone and marl. This last unit has been measured and sampled in the Orta River Valley, where it reaches a maximum thickness of 88.3 m (Fig. 3.3C), and can be subdivided into three different portions. The lower 30 m thick portion consists of horizontally bedded calcareous marl, and marly limestone alternating with 2 to 3 cm thick marly interbeds. Scattered glauconite grains occur just above the hardground surface. In the central portion of the unit, the marly content increases significantly. This portion is almost 50 m thick and is characterized by very thinly stratified wackestone beds with planktonic foraminifera and cherty nodules (Fig. 3.7D). In the upper 10 m of this unit, a marly limestone interval occurs again, as in the lower part of the section (Fig. 3.5E). The gradual transition to the unit above, the *Lithothamnion* Limestone, consists of 18 m thick cross-bedded fine packstones with planktonic foraminifera and abundant fragments of a serpulid (*Ditrupa* sp) (Fig. 3.7E). Moreover, the upper portion of this interval is characterized by widespread phosphate particles and glauconite grains, and planktonic foraminifera shells appear almost entirely phosphatised, as well as large portions of the micritic matrix. The $\delta^{13}C$ values in the record from the Bolognano Formation range between +0.02‰ and +2.65‰ (Fig. 3.3C) (See Annex B.6 and B.7 for detailed carbon isotope ratios). A decrease in $\delta^{13}C$ characterizes the base of the section, because the values range between +0.81‰ in the upper portion of the *Lepidocyclina* Calcarenite 1 and +0.02‰ at the base of the Cherty Marly Limestones. This trend is followed by a mild positive shift which is recorded in the lower portion of the Cherty Marly Limestones, from 5 to 8 m, with values increasing from +0.02 to +0.99‰. A significant positive shift continues above, within the *Lepidocyclina* Calcarenites 2 unit, in which the $\delta^{13}C$ increases from +0.70‰ up to +2.65‰ towards the uppermost portion of the unit. A negative $\delta^{13}C$ trend characterizes the base of the hemipelagic marly limestones and calcareous marls, from 31 to 35 m, with $\delta^{13}C$ values that decrease from +2.28 to +1.35‰ and then fluctuate around +1.50‰ in the succeeding 15 m, below another abrupt positive spike with $\delta^{13}C$ values increasing sharply from +1.18‰ up to +2.25‰. Above, from 52 to 82 m, in the middle portion of the hemipelagic calcareous marls, the $\delta^{13}C$ record shows a slight negative trend, with values slowly decreasing to +0.63‰ and then fluctuating around +0.5‰ up to the top of the measured interval.

3.4.2.1 Stratigraphy

The *Lepidcocyclina* Calcarenites 1 unit has been attributed to the SBZ22A (shallow benthic zone of Cahuzac and Poignant, 1997), Rupelian to Chattian in age, on the basis of the larger benthic foraminifera assemblage (Benedetti et al., 2010). Age constraints of the other units of the San Bartolomeo–Orta River composite section are provided by the calcareous nannofossil biostratigraphy (Brandano et al., 2016a). The nannofossil index species *Sphenolithus delphix* (top of Zone CNO6 of Backman et al., 2012) was observed in the lower part of the Cherty Marly Limestone unit, while the assemblage observed in the upper part suggests an undifferentiated biostratigraphic interval between zones CNM1 and CNM3 (Backman et al., 2012), thus placing this unit in the stratigraphic interval from the upper Chattian to the upper Aquitanian. In the hemipelagic marly limestones/marls unit above, a nannofossil assemblage with *Sphenolithus heteromorphus* was observed in the lowermost part, indicating zones CNM6 and CNM7 (Backman et al., 2012), whereas at the top of the unit the nannofossil Zone CNM8 is recognized, indicating a Serravallian age, thus constraining the *Lepidocyclina* Calcarenite 2 unit to the upper Aquitanian–upper Burdigalian interval (Fig. 3.3C). In the age–depth diagram, set up to scale stratigraphic thickness to numerical age for the San Bartolomeo–Orta section (Fig. 3.6B), the age–depth control points are provided by nannofossil biostratigraphy from Brandano et al. (2016a). The sedimentation rate changes from 0.50 cm/ka in the Cherty Marly Limestones to 0.28 cm/ka in the *Lepidocyclina* Calcarenites 2 unit. It increases in the overlying hemipelagic marly limestones, reaching 0.92 cm/ka in the basal portion up to 4.36 cm/ka in the middle and upper part of this

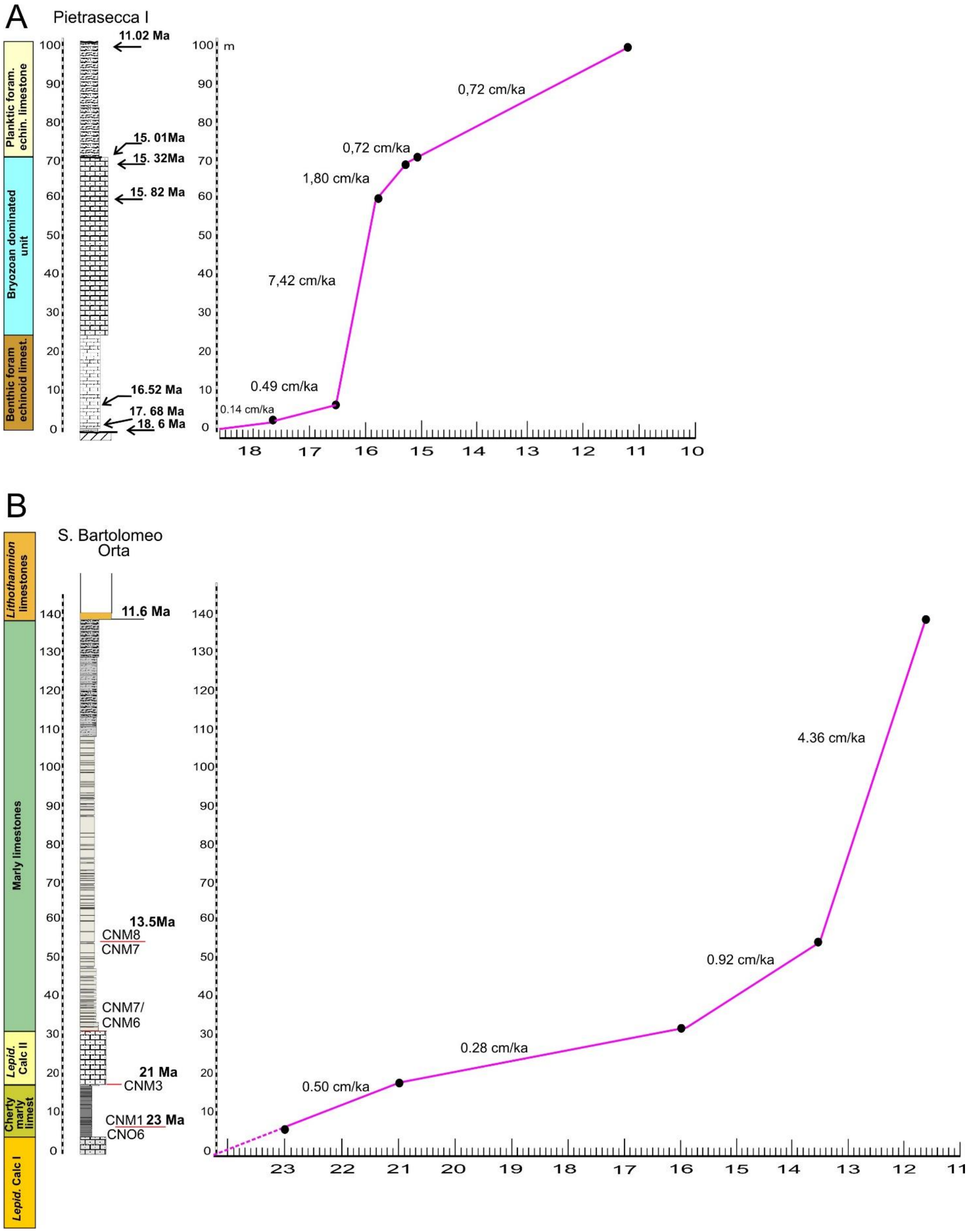

Fig. 3.6. Age–depth diagram and estimated sedimentation rates for the Pietrasecca section (A) and San Bartolomeo–Orta River section (B).

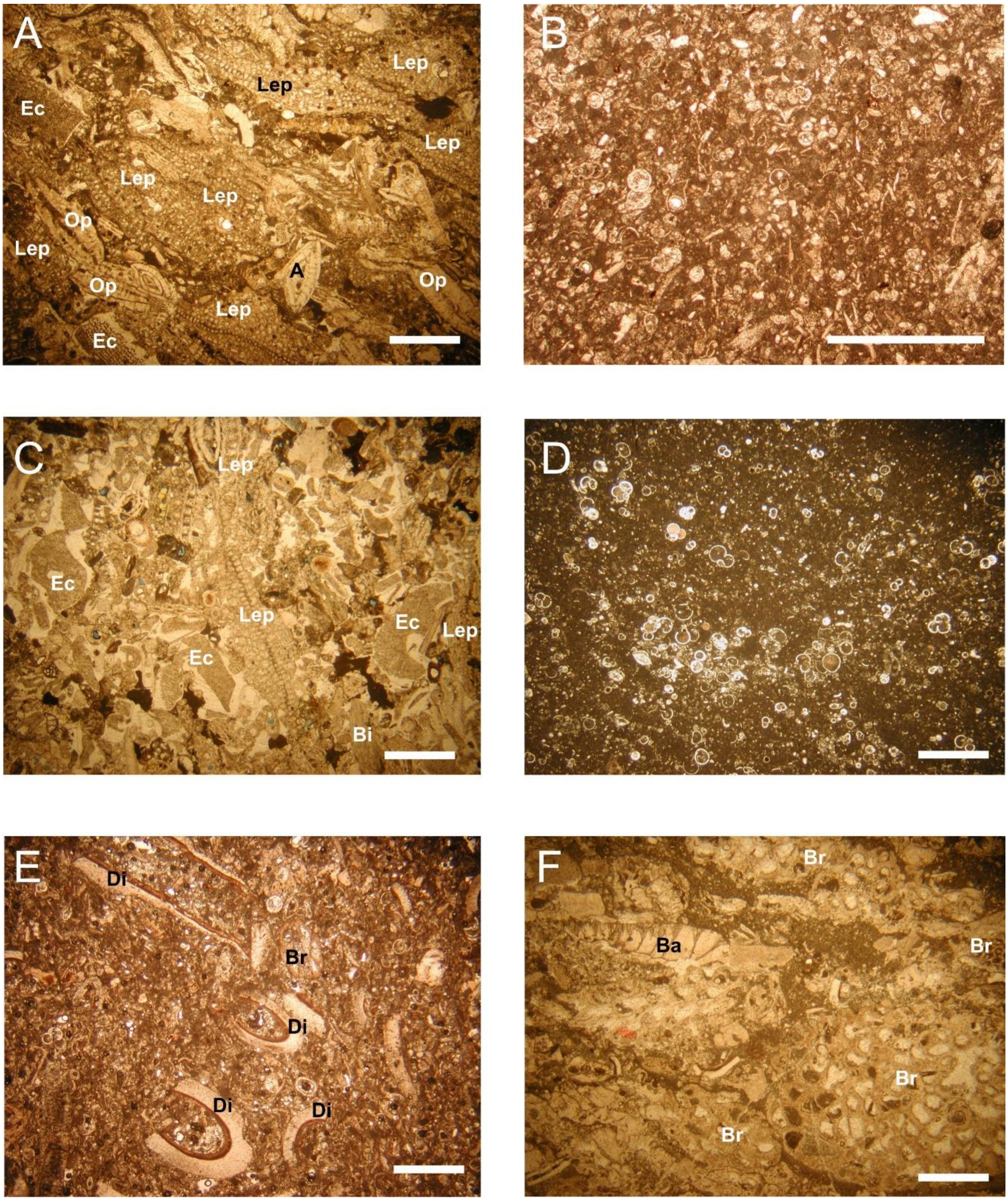

Fig. 3.7. Photomicrographs of the main microfacies of the investigated deposits. (A) to (E) Microfacies association of Bolognano Formation. (A) *Lepidocyclina* Calcarenites 1 characterized by abundant and tight packed lepidocyclinid specimens and subordinated *Operculina*, amphisteginids and echinoids (Lep=*Lepidocyclina*, Op=*Operculina*, A=*Amphistegina*, Ec=echinoid) (San Bartolomeo section; scale bar=1 mm). (B) Cherty Marly Limestone rich in planktonic foraminifera, mainly globigerinids and globigerinoids; locally iron oxides occur as brownish areas. (San Bartolomeo section; scale bar=500 lm). (C) *Lepidocyclina* Calcarenites 2 with *Lepidocyclina* specimens together with fragmented bioclastic fraction represented by echinoids, rotaliids, molluscs (Lep=*Lepidocyclina*, Bi=bivalve; Ec=echinoid) (San Bartolomeo section; scale bar=1 mm). (D) Hemipelagic marly limestone and calcareous marls with abundant planktonic foraminifera mainly orbulinids and globigerinids (Orta section; scale bar =500 lm). (E) Upper portion of the hemipelagic marly limestone at the Orta River section represented by a bioclastic fine-grained packstone with planktonic foraminifera and abundant fragments of *Ditrupa* (Di=*Ditrupa*; Br=bryozoan) (scale bar=1 mm). (F) Bryozoan and echinoid floatstone to packstone of the *Lithothamnion* and Bryozoan Limestone Formation. Bryozoans are mainly represented by celleporids, balanid fragments also occur (Br=bryozoan; Ba=balanid) (Pietrasecca section; scale bar=1 mm).

unit (Fig. 3.5B). The average sedimentation rate for the San Bartolomeo–Orta section of 1.15 cm/ka is comparable to the Pietrasecca section.

3.4.3 The Moria section

The Moria section belongs to the upper Burdigalian–Langhian interval and comprises the upper portion of the Bisciaro Formation and the lower members of the overlying Schlier Formation (Montanari et al., 1997; Di Stefano et al., 2015) (Fig. 3.3A). The Bisciaro Formation has been divided into three members: a lower marly member, a middle calcareous–siliceous–tuffitic member and an upper marly member, which represents the gradual transition to the overlying Schlier Formation (Montanari et al., 1997). The Schlier Formation has also been divided into three members (Deino et al., 1997): the lower and the upper marly members are separated by a 40-m thick alternation of siliceous–calcareous marly limestone and marl, with several intercalated bentonitic layers (Deino et al., 1997). Since the upper member of the Bisciaro Formation and the lower member of the Schlier Formation are lithologically identical, both consisting of greyish-blue marls, Coccioni and Montanari (1992) proposed placing the boundary between these two formations at a biotite-rich volcaniclastic layer, named "Piero della Francesca" and dated 17.08 ± 0.18 Ma with the $^{40}Ar/^{39}Ar$ on biotite crystals (Deino et al., 1997). At the base of the section, the upper marly member of the Bisciaro Formation, 13.5 m in thickness (Fig. 3.3A), consists of greyish-blue marls alternating sporadically with few thin calcareous strata.
The lower, marly member of the Schlier Formation, 27.5 m thick, consists of an alternation of marls and clay-rich marl strata, ca 70 to 90 cm thick. This member is overlain by 27 m of alternating clayey marls and calcareous marl corresponding to the middle member of the Schlier Formation (Fig. 3.5F). Bed thickness varies between 10 cm and 1 m. In this study, only 20 m of this member has been measured and sampled (Fig. 3.3A).
The $\delta^{13}C$ values of this section range between 0.43‰ and +0.82‰ (Fig. 3A). The upper member of the Bisciaro Formation records a positive trend of $\delta^{13}C$ values that increase from -0.01 to +0.82‰, which represents the strongest positive peak of the whole curve, recorded just above the Bisciaro/Schlier boundary. A sharp negative excursion follows this positive peak, evidenced by $\delta^{13}C$ values that fall to 0.43‰ within the middle member of the Schlier Formation. In the clayey marly upper member of the Schlier Formation the $\delta^{13}C$ values fluctuate between 0.37‰ and +0.27‰, while the upper portion of the section shows another positive excursion, with values increasing up to +0.59‰ at 1.5 m below the top of the measured section.

3.4.3.1 Stratigraphy

The age constraints of the Bisciaro and the Schlier formations in the Moria section refer to Di Stefano et al. (2015). The age model presented by these authors is based on bio-magnetostratigraphic data and provides a time interval of deposition between 17.7 Ma and 14.7 Ma for the Moria section. Consequently, the upper portion of the Bisciaro Formation corresponds to the upper Burdigalian. The radiometric age of the Bisciaro–Schlier boundary at 17.08 Ma (Deino et al., 1997) is consistent with the reconstruction by Di Stefano et al. (2015). The lower member, and the measured portion of the middle member of the Schlier Formation have been attributed to the upper Burdigalian. The Burdigalian–

Langhian boundary is not represented by the sampled section of this study (Fig. 3.3A).
To scale stratigraphic thickness to numerical age in the Moria section, the age model presented by Di Stefano et al. (2015) was used here. The average sedimentation rate obtained by these authors for the Moria section is 3.85 cm/ka, a value which is about three times higher than the average sedimentation rate for the Pietrasecca and San Bartolomeo–Orta sections.

3.5 DISCUSSION

3.5.1 Diagenetic overprint on carbon stable isotope

Precipitation of carbonates causes only little carbon isotopic fractionation relative to the dissolved inorganic carbon (DIC) (Saltzman and Thomas, 2012). Furthermore, $\delta^{13}C_{DIC}$ is practically unaffected by water temperature changes (Burla et al., 2008; Saltzman and Thomas, 2012). Therefore, the $\delta^{13}C_{DIC}$ of both inorganic and biologically precipitated carbonate can be considered to be very close to the value of dissolved inorganic carbon in the ocean at the moment of precipitation (Saltzman and Thomas, 2012). However, meteoric and late burial diagenesis, in particular, can completely mask the original water signature (Colombié et al., 2011). The general pattern of the carbon isotope signal measured in the investigated sections is not indicative of alteration during diagenesis or of restricted oceanographic conditions.
The overall $\delta^{18}O$ records of the Pietrasecca and San Bartolomeo–Orta River sections range, respectively, from 1.13‰ to +0.67‰ and from 0.24‰ to +1.53‰ (See Annex B.6 and B.7 for detailed oxygen isotope ratios of the San Bartolomeo-Orta River section). Therefore, the lowest recorded values are not so negative that they could indicate a strong diagenetic overprint by meteoric diagenetic environment, or by high temperatures within a deep-burial environment (Burla et al., 2008; Colombié et al., 2011). Furthermore, the low covariance between the carbon and oxygen isotopes in the two sections (R^2=0.0249 for the Pietrasecca section; R^2=0.0038 for the San Bartolomeo–Orta River section) can exclude a major diagenetic overprint of these carbonates and, consequently, this corroborates the $d^{13}C$ record as representative of the DIC at the moment of deposition of the studied successions (Fig. 3.8).
The overall $\delta^{18}O$ values of the Moria section are up to 1.5‰ lower than the values in the ther two studied sections, ranging from 2.91 to 1.15‰. In this case, the lowest values could be partly the result of a mild diagenetic overprint in a burial diagenetic environment. However, the R^2=0.2982 value indicates that there is a low covariance between the carbon and oxygen isotope values (Fig. 3.8), thus suggesting a negligible effect from the diagenetic overprint (cf. Burla et al., 2008).

3.5.2 The Monterey Event in the Mediterranean area and correlation with global records

The Monterey Event took place during a key time interval for the Mediterranean palaeogeographic evolution. During the early to middle Miocene, two large-scale palaeogeographic changes took place in the embryonic Mediterranean area: the gradual closure of the Tethyan passage between the Central Atlantic and Indian Oceans in the late Burdigalian (Rögl, 1999), and the contemporary counter-clockwise rotation of the Sardinia–Corsica block, which led to the formation of the Western Mediterranean (Gattacceca et al., 2007).
Despite the closure of the Mediterranean, documentation of the Monterey Event, in lower to middle Miocene carbonate

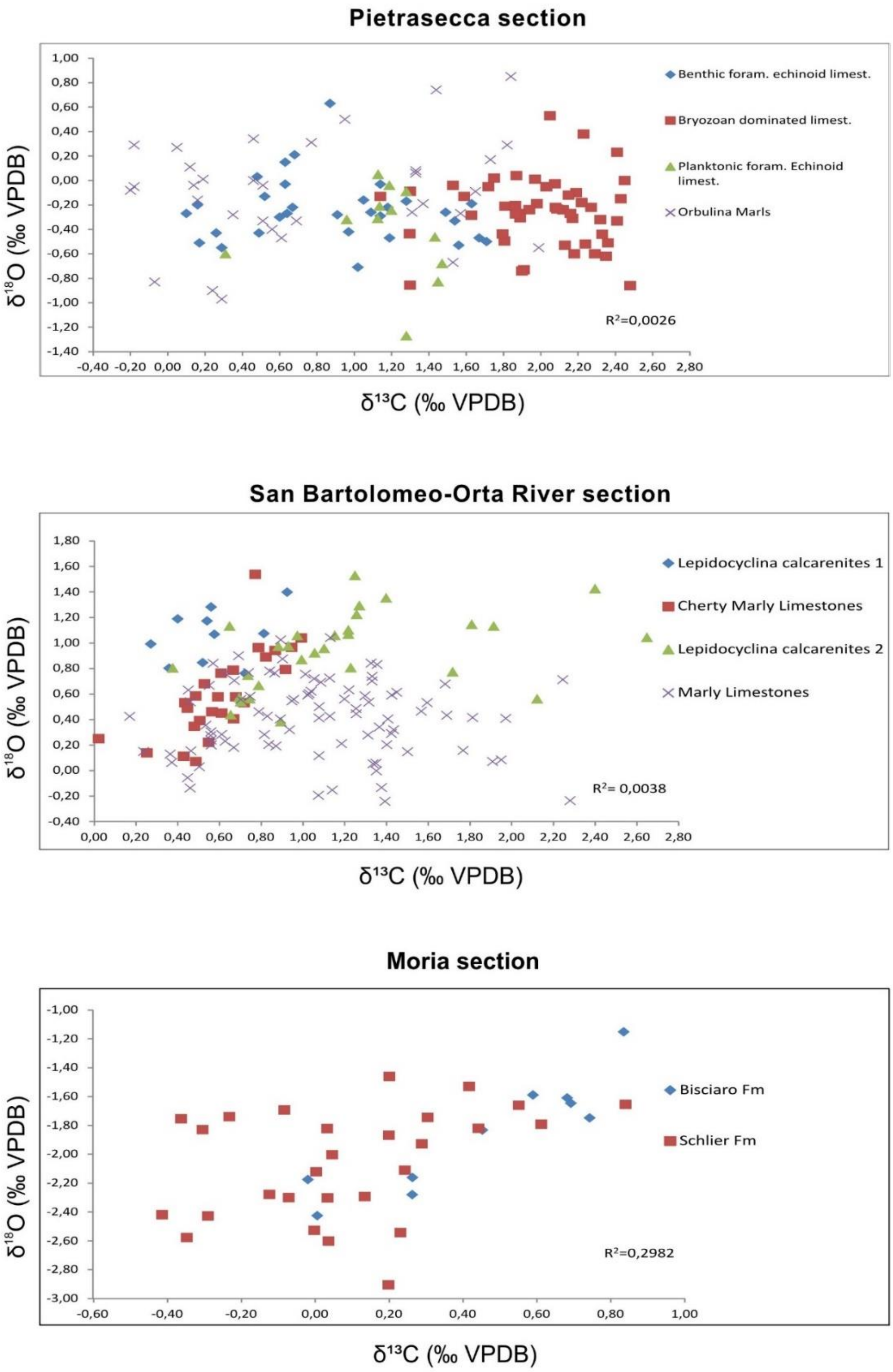

Fig. 3.8. Cross-plots of $\delta^{13}C$ and $\delta^{18}O$ of bulk rock samples of each lithostratigraphic unit of the Pietrasecca, San Bartolomeo–Orta River and Moria sections showing the low covariance between carbon and oxygen isotope values, probably indicating a negligible diagenetic overprint.

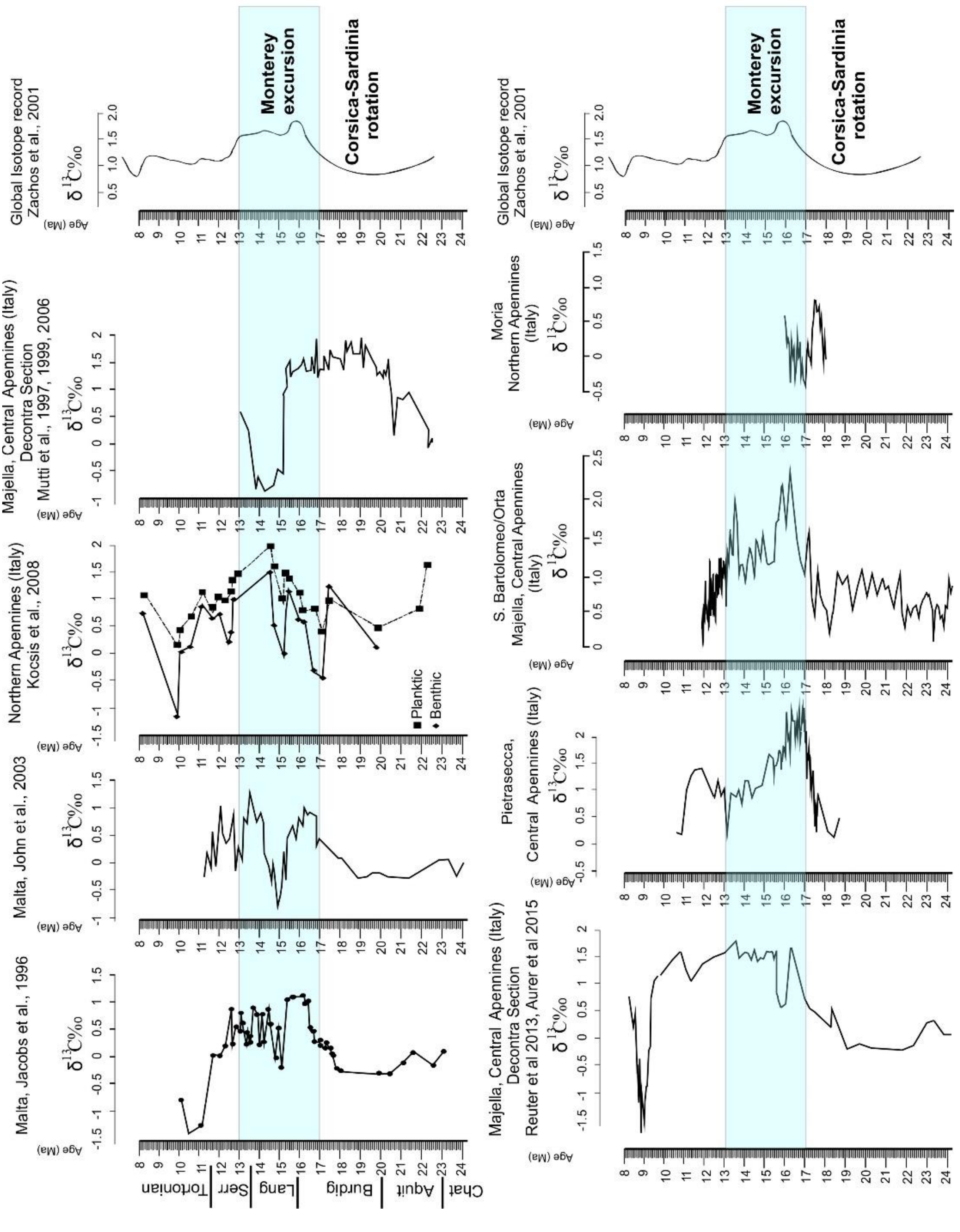

Malta, Jacobs et al., 1996
Malta, John et al., 2003
Northern Apennines (Italy)
Kocsis et al., 2008
Planktic
Benthic
Majella, Central Apennines (Italy)
Decontra Section
Mutti et al., 1997, 1999, 2006
Global Isotope record
Zachos et al., 2001
Monterey excursion
Corsica-Sardinia rotation
Majella, Central Apennines (Italy)
Decontra Section
Reuter et al 2013, Aurer et al 2015
Pietrasecca,
Central Apennines (Italy)
S. Bartolomeo/Orta
Majella, Central Apennines
(Italy)
Moria
Northern Apennines
(Italy)
Age (Ma)
$\delta^{13}C$‰
Tortonian
Serr
Lang
Burdig
Aquit
Chat

Fig. 3.9. Comparison of the carbon isotope composition of the studied sections with the other Central Mediter- ranean successions and the global pelagic record. All of the presented curves have scaled to numerical ages and been recalibrated with GTS 2004.

successions of shallow-water and pelagic settings, has been reported in several studies (Jacobs et al., 1996; John et al., 2003; Mutti et al., 2006; Kocsis et al., 2008; Auer et al., 2015). It is noteworthy that often, in the previous studies, the record of the Monterey Event was not revealed so clearly (Fig. 3.9).

Instead, the investigated sections of the Central Apennine carbonate platforms, presented in this study, display a good record of the Monterey Excursion (Figs 3.9 and 3.10). In fact, the carbon isotope record of the San Bartolomeo–Orta River composite section (Majella Mountains) is marked by a minor, but sharp, positive $\delta^{13}C$ shift at the Oligocene–Miocene boundary, because the values increase from +0.02‰ in the uppermost Chattian to +0.72‰ at the base of the Aquitanian, to increase further up to +0.99‰ in the Aquitanian (Fig. 3.10). This C-isotope shift has been interpreted by Mutti et al. (2006) as the ‘Early Miocene Carbon Isotope Excursion’ that occurred contemporaneously to the Mi-1 (Miocene isotope Event 1) glaciation (Zachos et al., 2001; Pekar and DeConto, 2006). This isotopic shift corresponds to the drowning of the *Lepidocyclina* Calcarenites 1 carbonate ramp, overlain by a Cherty Marly Limestone unit. A link between $\delta^{13}C$ positive shifts and carbonate platform drowning events is widely accepted (Föllmi et al., 1994; Wissler et al., 2003; Weissert and Erba, 2004). The increase in $\delta^{13}C$ values reflects an increased productivity of surface seawater. Eutrophic events may have caused the drowning of carbonate platforms due to the shift from photo-dependent–dominated to the filter feeding-dominated carbonate factory, and the associated weakened growth potential of the carbonate platforms (Mutti and Hallock, 2003). Furthermore, carbonate production crises which ultimately led to platform drowning are documented within the whole Mediterranean area at the Oligocene–Miocene transition (Mutti et al., 2005; Föllmi et al., 2008; Brandano et al., 2015). According to Wilson et al. (2009), the Mi-1 glaciation is punctuated by eustatic fall of 40 m, which is similar to the glacioeustasy predictions from oxygen isotopic and trace metal geochemical data (Paul et al., 2000; Lear et al., 2004). However, there is no record of such eustatic fall in the sedimentary record of either Apennine platform, and there is no record of any tectonic phase producing an increase of subsidence (Vecsei et al., 1998). Consequently, the shift from carbonate production dominated by larger benthic foraminifera towards planktonic and siliceous sponge spicule sedimentation cannot be related only to sea-level rise, and a change in the environmental conditions has to be hypothesized. Such conditions were characterized by a high silica content in seawater most probably induced by the coeval Mediterranean volcanism and the intense weathering during Alpine orogenesis (Lustrino et al., 2009; Brandano et al., 2015). Unfortunately, the long-term hiatus evident in by the Latium–Abruzzi carbonate platform in its innermost portion for the Palaeogene (Accordi et al., 1967) extends, in the Pietrasecca section, also to the Aquitanian, thus

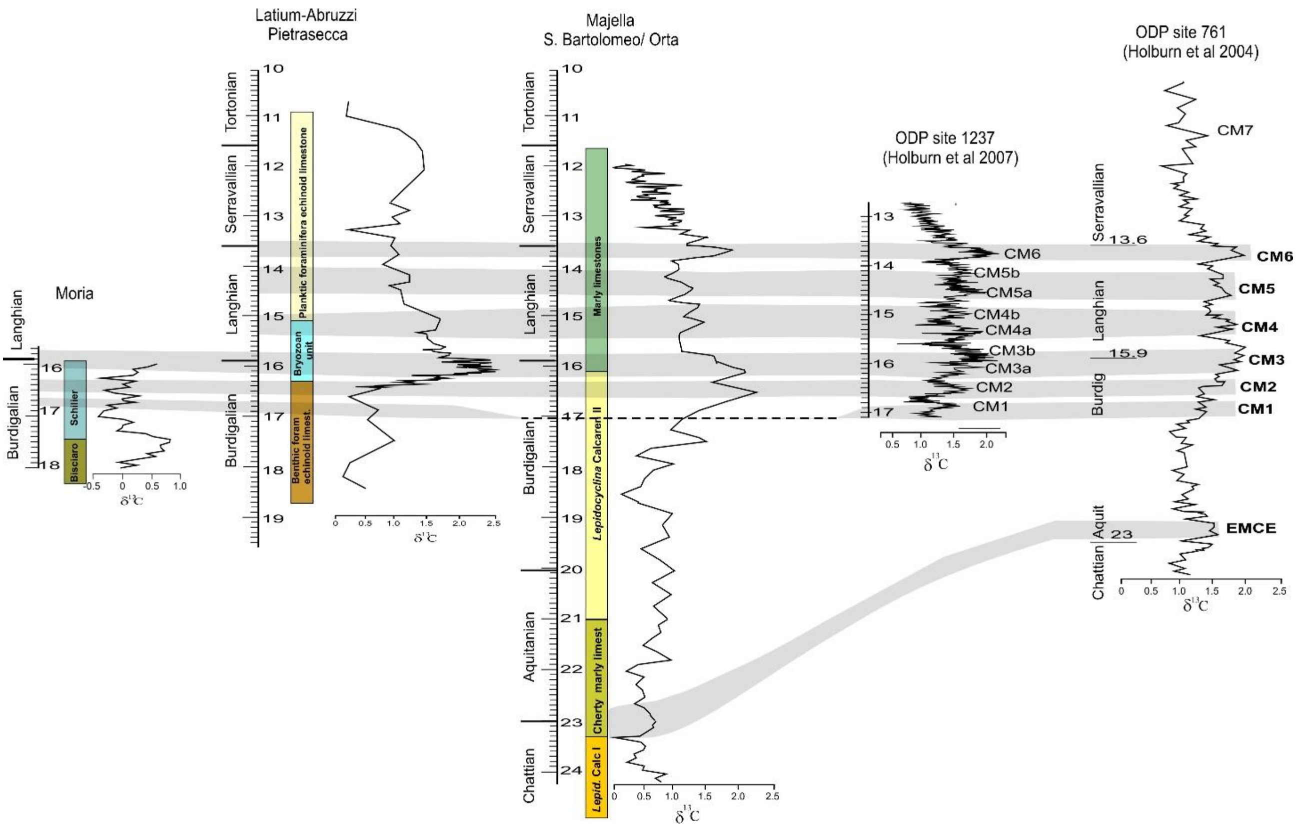

Fig. 3.10. Comparison of the carbon isotope curves of the studied sections, calibrated according the estimated sedimentation rates, with the lower to middle Miocene global carbon isotope curves of the ODP sites 1237 and 761. Sedimentation rates and age model of the Moria section are after Di Stefano *et al.* (2015). The carbon isotope curve of the ODP site 761 has been calibrated according to the carbon isotope curve of the ODP site 1237 (cali- brated on the ATNTS 2004 published in the GTS 2004), to make it consistent with the GTS 2004.

preventing any possible correlation between the San Bartolomeo–Orta River section and the Pietrasecca section in relation to Oligocene–Miocene boundary carbon isotope record.

In contrast to the Early Miocene Carbon Isotope Excursion, which results in only a minor carbon isotope shift within the Apula Platform record, the Monterey Carbon Isotope Excursion is well recorded within both the Bolognano and L&B formations (Figs 3.3B, 3.3C and 3.10). The upperportion of *Lepidocyclina* Calcarenites 2 is, in fact, characterized by two sharp $\delta^{13}C$ positive excursions, which reach their maxima during the late Burdigalian, and correspond to the ^{13}C maxima CM2 and CM3 of Holbourn et al. (2007). After these major peaks, the values shift back to +1.34‰ and then fluctuate around +1.5‰ during the middle Langhian until the late Langhian, when another major positive peak is recorded. According to the calcareous nannofossil assemblages found within the hemipelagic marl, this peak is recorded just before the base of the Serravallian (CNM8 Zone of Backman et al., 2012), and corresponds to CM6 (Woodruff and Savin, 1991; Holbourn et al., 2007). It is interesting to note that in the San Bartolomeo–Orta River section, the first major $\delta^{13}C$ positive shift, recorded in the upper Burdigalian, slightly predates the transition from the *Lepidocyclina* Calcarenites 2 to the hemipelagic marls (Figs 3.3C and 3.10).

Looking at the Latium–Abruzzi middle Miocene, it is evident that the L&B

Formation C-isotope record shows a trend very similar to that of the Apula Platform, which is directly correlated with the global Monterey Carbon Isotope Excursion (Figs 3.3B and 3.10). In the Pietrasecca composite section, the first positive carbon isotope excursion, characterized by an increase of $\delta^{13}C$ values from +0.1‰ up to +1.71‰ during the late Burdigalian followed by a maximum positive excursion (up to +2.48‰) at the base of bryozoan unit, can be correlated with CM3 (Woodruff and Savin, 1991; Holbourn et al., 2007). It is interesting to note that, in this section, the bryozoan-dominated facies coincides with the highest values of $\delta^{13}C$ and its deposition occurred during the major carbon cycle perturbation (Figs 3.3B and 3.10). As in the San Bartolomeo record, the Pietrasecca carbon isotope record shows a positive peak just before the Langhian–Serravallian boundary, thus corresponding to excursion CM6 of Holbourn et al. (2007) (Fig. 3.10). The bryozoan unit is overlain by Serravallian, planktonic foraminifera and echinoid-dominated facies that slightly predate the final drowning of the L&B Formation carbonate platform, resulting in deposition of the *Orbulina* Marl.

The onset of the Monterey Event in the Bolognano Formation is recorded by the *Lepidocyclina* Calcarenites 2 unit, which is characterized by the abundance of bryozoans and echinoid fragments in place of larger benthic foraminifera (Fig. 3.10). The spread of bryozoans in both of the studied platform settings has been linked to an increased nutrient availability in surface waters (Pomar et al., 2004; Brandano et al., 2010b). Under an enhanced nutrient flux, due to continental run-off or upwelling, phytoplankton blooms may increase the surface water turbidity, thus reducing the light available for the bottom-dwelling organisms, such as the larger benthic foraminifera. Moreover, primary production represents a very good resource for filter feeders, particularly photo-independent organisms such as the bryozoans, which proliferate in high trophic conditions (Mutti & Hallock, 2003). The two Apennine platforms, however, display a different facies belt evolution. In the Bolognano ramp, the *Lepidocyclina* Calcarenites 2 unit is overlain by the hemipelagic marly unit in the northern (basinward) portion of the ramp, while in the southern (landward) portion these calcarenites are overlain by the coeval and proximal Bryozoan calcarenites unit (Mutti et al., 1999; Reuter et al., 2013; Auer et al., 2015), which lies above the same phosphatic hardground as the hemipelagic marls. Therefore, this stratigraphic architecture reflects a backstepping trend of the ramp facies belt (Brandano et al., 2016a) (Fig. 3.2A). In the Latium–Abruzzi, the general stratigraphic architecture of the ramp evidences a progressive backstepping of the bryozoan unit, as a consequence of the (upward) landward migration of the shallow photic facies, and a contemporaneous progradation of the bryozoan unit basinward (Brandano and Corda, 2002; Corda and Brandano, 2003) (Fig. 3.2B).

In both Apennine ramps, the trophic resources played an important role in the efficiency of the bryozoan factory overall in the aphotic zone, exerting control on the depositional profile of the Apenninic platforms. On these platforms, the bryomol and molechfor-dominated sediments (Fig. 3.7F), produced in the aphotic outer ramp, exceed in volume the production of the photo-dependent factory, which, on the contrary, is less productive because of the high nutrient level (e.g. Hallock and Schlager, 1986; Mutti and Hallock, 2003). Generally, the high rates of sediment production in the deeper aphotic and oligophotic zones produce a depositional profile of a low-angle ramp (Brandano and Corda, 2002; Pomar et al., 2012). This type of carbonate factory influenced facies heterogeneities and stratigraphic architecture also. On a bryozoan-dominated platform, the absence of rigid framework and the volumetric importance of production below wave base (in the aphotic zone) reduced the impact of high-frequency sea-level fluctuations in creating facies architectural heterogeneities. As a consequence, only major sea-level fluctuations shifted facies belts sufficiently to create stratigraphic heterogeneities (Pomar et al., 2012). In the Majella region, the Bryozoan calcarenites show only a retrogradational pattern and they pass laterally into the hemipelagic marls (Brandano et al., 2016a), indicating that this platform was under the influence of a strong fine-grained terrigenous input that originated from northern sectors (Northern Apennines and Alps). Terrigenous accumulation exceeded the bryozoan production and accumulation, and hampered the progradation of this facies belt. Not surprisingly, the average sedimentation rate of the coeval hemipelagic formations (3.85 cm/ka for the Schlier Formation) of the nearby Umbria–Marche Basin is three times greater than that of the investigated ramps (1.3 cm/ka) (cf. Di Stefano et al., 2015).

The middle Miocene time, when high trophic conditions characterized the Mediterranean, coincides perfectly with the Monterey Event. The influence of this event on the trophic conditions of the central Mediterranean was added to other regional factors. In fact, during the late Burdigalian the closure of the Indo-Pacific passage (Rögl, 1999) led to a reversal of the deep-water circulation pattern in the whole Mediterranean (Mutti and Bernoulli, 2003), and favoured the upwelling activity (Föllmi et al., 2005, 2008, 2015). Moreover, the development of the Apennine accretionary wedge and foredeep system, together with its eastward migration, led to a constant increase of sediment run-off, whose finest portion would have reached the Latium–Abruzzi and Apula platforms (Brandano and Corda, 2002).

Kocsis et al. (2008) distinguished three different phases of the Miocene oceanographic evolution of the Mediterranean area, through the integrated study of Sr, Nd, C and O isotope records of both fossils and bulk sediments of different central-western Mediterranean carbonate successions. These authors state that during the latest Oligocene–early Miocene (25 to 19 Ma) Mediterranean waters were still strongly influenced by the Indo-Pacific influx, but that the relatively lighter $^{87}Sr/^{86}Sr$ and heavier $^{143}Nd/^{144}Nd$ isotope ratios, recorded in the central-western Mediterranean sediments, indicate a significant influence of subduction-related volcanism on Mediterranean seawater chemistry. In the subsequent phase, from 19 to 13 Ma, the Mediterranean isotope signature results in a mix of both Atlantic and Pacific signals, but sporadic high peaks of Nd indicate that volcanism was still a controlling factor on the Mediterranean water chemistry. The Sr isotope record indicates an increased weathering and erosion of Mesozoic carbonates, probably sustained by persistent subtropical climatic conditions. In the third identified phase, from 13 to 8 Ma, Mediterranean waters show a strong Atlantic influence, because both of their isotope signals seem totally comparable, until the Messinian salinity crisis and isolation of the Mediterranean, during which the isotope signals decouple again.

The investigated Miocene pelagic C-isotope record registers only the upper part of the Burdigalian interval, but it does not show the high values recorded in the Apennine ramps for the onset of the Monterey Event. In the time interval corresponding to the onset of the Monterey Event, the Moria section $\delta^{13}C$ record shows only a slight positive shift, with values increasing from 0.01‰ to +0.82‰ (Figs 3.3A and 3.10), while the main portion of the Monterey Event is missing, because the section ends at the beginning of the Langhian. Two main reasons could explain the lower amplitude C-isotope shift in the Moria section with respect to the shift observed in the platform records. Firstly, the carbon isotope signal of the Moria section could be diluted due to the large amount of continental derived sediments within the basin. This fact is indeed attested to by the sedimentation rates, which are as much as three times higher in the Umbria–Marche Basin (3.85 cm/ka according to Di Stefano et al., 2015) in comparison with the platform setting in which it was estimated as slightly more than 1 cm/ka. Furthermore, the continental derived sediments contain a significant fraction of Mesozoic–Palaeocene carbonates (Centamore et al., 2002) that may have influenced the result of isotope analysis on bulk sediment samples. The second reason lies in the carbon cycle itself: ^{13}C enrichment into surface waters is controlled by photosynthesis and production of organic matter which, in turn, is enriched in ^{12}C. Organic matter is oxidized in intermediate and deep waters, which are thus progressively enriched in ^{12}C (Weissert et al., 2008; and references therein). This light carbon enrichment of deep waters is recorded in the deep benthic calcareous shells. The $\delta^{13}C$ data of the Moira section have been obtained by analysis on bulk samples; consequently, these isotope values could contain the ^{13}C depleted signal of the deep benthic components. In contrast, in the shallow-water successions different models have been proposed to explain the occurrence of higher amplitude $\delta^{13}C$ shifts in comparison with pelagic and hemipelagic successions (Immenhauser et al., 2002, 2003; Colombié et al., 2011). In the shallow-water realm, early meteoric diagenesis or variations in local environmental conditions, such as restricted circulation, warmer waters and variations in salinity in shallow-water settings in comparison with coeval basinal, can produce changes in carbon isotopic values (Immenhauser et al., 2003; Colombié et al., 2011). In the Apennine platforms, both of these factors can be excluded. The low covariance between oxygen and carbon isotope ratios in the investigated sections rules out any major diagenetic overprints. Furthermore, because the main positive isotope shift is recorded within proximal outer ramp facies, a restricted circulation, due to limited water column thickness, can be also excluded. One possible controlling factor could be the vital effect related to the massive presence of photosynthetic organisms. The Miocene ramps within and outside the Mediterranean area had conspicuous carbonate production by red algae in deep parts of the photic zone (Halfar and Mutti, 2005), whereas in the inner ramps significant epiphytic carbonate production is supported by seagrasses (Brandano et al., 2010b). Important carbon isotopic fractionation in red algae and seagrass is well-documented (Maberly et al., 1992; Hemminga and Mateo, 1996). The observed amplification of the carbon isotope excursion recorded in the Apennine platforms ($\Delta\delta^{13}C$>2.0‰) with respect to the Moira section ($\Delta\delta^{13}C$ >0.5‰) and open-ocean settings ($\Delta\delta^{13}C$ >1.0‰) could be explained by intensification of photosynthetic activity in the photic zone of the ramp. This zone is placed in a well-oxygenated zone at water depth of –20/–50 m (Brandano et al., 2010b) and, therefore, it was not subjected to early diagenesis related to subaerial emersion, nor reduced circulation or fluvial input, which can alter the $\delta^{13}C$.

3.6 CONCLUSIONS

The Monterey Carbon Isotope Excursion has been identified in C-isotope records from Central Apennines carbonate platforms. A detailed biostratigraphy, together with the age constraints provided by the Sr isotope stratigraphy for the Latium–Abruzzi carbonate platform record, allows correlation of at least two of the six well-known $\delta^{13}C$ maxima recorded in the oceanic record of the lower to middle Miocene interval.

In the middle to outer ramp environments of the studied platform settings, the Monterey Event coincides with a spread of bryozoans. The spread of these filter feeding organisms within the central Mediterranean should be related to inception of high trophic conditions, probably enhanced by regional factors occurring during the late Burdigalian and Langhian, such as the closure of Indo-Pacific connection, Sardinia–Corsica volcanism and Apennine orogenesis. Because the Mediterranean pelagic setting shows a C-isotope record characterized by an attenuated signal when compared to the platform record, it is inferred that the photosynthetic activity in the oligophotic zone of the Apennine ramps could have amplified the carbon isotope signal.

The carbonate factories of the Apennine ramps were strongly influenced by trophic conditions. The high productivity of the bryozoan-dominated factory in the aphotic zone had an important influence on depositional profile. The high rates of sediment production in the deeper aphotic and oligophotic zones produced a low-angle ramp.

ACKNOWLEDGMENTS

We are grateful to Michele Lustrino for useful discussions. Criticisms from Mariano Parente, Gianluca Frijia and an anonymous reviewer are much appreciated. Comments and criticisms by Associate Editor Stephen Hesselbo greatly improved the manuscript. Financial support from the La Sapienza University of Rome (Fondi Ateneo 2014) and MIUR (PRIN 2010 Research Grant 20107ESMX9_001) are gratefully acknowledged. Irene Cornacchia was funded by an IAS postgraduate grant (2016).

REFERENCES

Accordi, B., Devoto, G., La Monica, G.B., Praturlon, A., Sirna, G. and **Zalaffi, M.** (1967). Il Neogene nell'Appennino laziale-abruzzese. *Commitee Mediterranean Neogene Stratigraphy (1969), Proc. IV Session, Bologna, Giorn. Geol.*,35, 235–268.

Amodio, S., Ferreri, V., D'Argenio, B., Weissert, H. and **Sprovieri, M.** (2008). Carbon-isotope stratigraphy and cyclostratigraphy of shallow-marine carbonates: the case of San Lorenzello, Lower Cretaceous of southern Italy. *Cretaceous Res.*, 29, 803–813.

Auer, G., Piller, W.E., Reuter, M. and **Harzhauser, M.** (2015). Correlating carbon and oxygen isotope events in earl to middle miocene shallow marine carbonates in the Mediterranean region using orbitally tuned chemo- and lithostratigraphy. *Paleoceanography*, 30, doi:10.1002/2014 PA002716.

Backman, J., Raffi, I., Rio, D., Fornaciari, E. and Palike, H. (2012). Biozonation and biochronology of Miocene through Pleistocene calcareous nannofossils from low and middle latitudes. *Newsl. Stratigr.*, 45, 221–244.

Benedetti, A., Di Carlo, M. and **Pignatti, J.** (2010). Embryo size variation in larger foraminiferal lineages: stratigraphy versus paleoecology in *Nephrolepidina praemarginata* (R. Douvillé, 1908) from the Majella Mt. (Central Appennines). *J. Med. Earth Sci.*, 2, 19–29.

Brand, U. and **Veizer, J.** (1980). Chemical diagenesis of a multicomponent carbonate system-1: trace elements. *J. Sed. Res.*, 50, 1219–1236.

Brandano, M. and **Corda, L.** (2002). Nutrients, sea level and tectonics: constrains for the facies architecture of a Miocene carbonate ramp in central Italy. *Terra Nova*, 14, 257–262.

Brandano, M. and **Policicchio, G.** (2012). Strontium stratigraphy of the Burdigalian transgression in the Western Mediterranean. *Lethaia*, 45, 315–328.

Brandano, M., Brilli, M., Corda, L. and **Lustrino, M.** (2010a). Miocene C-isotope signature from the central Apennine successions (Italy): monterey vs. regional controlling factors. *Terra Nova*, 22, 125–130.

Brandano, M., Westphal, H. and **Mateu-Vicens, G.** (2010b). The sensitivity of a tropical foramol-rhodalgal carbonate ramp to relative sea-level change: miocene of the central Apennines, Italy. *Int. Assoc. Sedimentol. Spec. Publ.*, 42, 89–106.

Brandano, M., Lipparini, L., Campagnoni, V. and **Tomassetti, L.** (2012). Downslope-migrating large dunes in the Chattian carbonate ramp of the Majella Mountains (Central Apennines, Italy). *Sed. Geol.*, 255–256, 29–41.

Brandano, M., Lustrino, M., Cornacchia, I. and **Sprovieri, M.** (2015). Global and regional factors responsible for the drowning of the Central Apennine Chattian carbonate platforms. *Geol. J.*, 50, 575–591.

Brandano, M., Cornacchia, I., Raffi, I. and **Tomassetti, L.** (2016a). The Oligocene-Miocene stratigraphic evolution of the Majella carbonate platform (Central Apennines, Italy). *Sed. Geol.*, 333, 1–14.

Brandano, M., Tomassetti, L., Sardella, R. and **Tinelli, C.** (2016b). Progressive deterioration of trophic conditions in a carbonate ramp environment: the *Lithothamnion* Limestone, Majella Mountain (Tortonian–early Messinian, central Apennines, Italy). *Palaios*, 31, 125–140.

Burla, S., Heimhofer, U., Hochuli, P.A., Weissert, H. and **Skelton, P.** (2008). Changes in sedimentary patterns of coastal and deep-sea successions from the North Atlantic (Portugal) linked to Early Cretaceous environmental change. *Palaeogeogr. Palaeoclimatol. Palaeoecol.*, 257, 38–57.

Cahuzac, B. and **Poignant, A.** (1997). Essai de biozonation de l'Oligo-Miocène dans les bassins européens a l'aide des grands foraminiferes néritiques. *Bull. Soc. Géol. Fr.*, 168, 155–169.

Carannante, G., Esteban, M., Milliman, J.D. and **Simone, L.** (1988). Carbonate lithofacies as paleolatitude indicators: problems and limitations. *Sed. Geol.*, 60, 333–346.

Carbone, F. (1993). Cretaceous depositional system of the evolving Mesozoic carbonate platform of Central Apennine thrust belt, Italy. *Geol. Romana*, 29, 31–58.

Carminati, E., Lustrino, M., Cuffaro, M. and **Doglioni, C.** (2010). Tectonics, magmatism and geodynamics of Italy: what we know and what we imagine, In: *The Geology of Italy* (Eds M. Beltrando, A. Peccerillo, M. Mattei, S. Conticelli and C. Doglioni), Journal of the Virtual Explorer, Electronic Edition, 36, paper 9. ISSN 1441–8142.

Carminati, E., Lustrino, M. and **Doglioni, C.** (2012). Geodynamic evolution of the central and western Mediterranean Tectonics vs. igneous petrology constraints. *Tectonophysics*, 579, 173–192.

Centamore, E., Jacobacci, A. and **Martelli, G.** (1973). Modello strutturale Umbro-Marchigiano, correlazioni con le regioni adiacenti. *Boll. Serv. Geol. Ital.*, 93, 25–40.

Centamore, E., Fumanti, F. and **Nisio, S.** (2002). The central-northern Apennines geological evolution from Triassic to Neogene time. *Boll. Soc. Geol. It.*, 1, 181–197.

Ciarapica, G. and **Passeri, L.** (1976). Deformazione da fluidificazione ed evoluzione diagenetica della formazione evaporitica di Burano. *Boll. Soc. Geol. Ital.*, 95, 1175–1199.

Cipollari, P. and **Cosentino, D.** (1992). La linea Olevano- Antrodoco: contributo della biostratigrafia alla sua caratterizzazione. In: *Studi Preliminari all'Acquisizione Dati del Profilo CROP 11 Civitavecchia-Vasto* (Eds M. Tozzi, G.P. Cavinato and M. Parotto), pp. 143–149. Studi Geologici Camerti Volume Speciale 1991/2. University of Camerino, Camerino, Italy.

Civitelli, G. and **Brandano, M.** (2005). Atlante delle litofacies e modello deposizionale dei Calcari a Briozoi e Litotamni nella Piattaforma carbonatica laziale-abruzzese. *Boll. Soc. Geol. Ital.*, 124, 611–643.

Coccioni, R. and **Montanari, A.** (1992). The 'Livello Piero della Francesca' in the Umbria-Marche Apennines, Italy: a regional volcaniclastic marker bed at the boundary between the Bisciaro and the Schlier/Marne con Cerrogna formations (Lower Miocene). In: *Volume of Abstracts and Field Trips, Interdisciplinary Geological Conference on the Miocene Epoch with emphasis on the Umbria-Marche sequence (I.U.G.S., Subcommission on Geochronology, Miocene Columbus Project)* (Eds A. Montanari, R. Coccioni and G.S. Odin), pp. 41–42, Ancona, November 11-15, 1992.

Colombié, C., Lécuyer, C. and **Strasser, A.** (2011). Carbon- and oxygen-isotope records of palaeoenvironmental and carbonate production changes in shallow-marine carbonates (Kimmeridgian, Swiss Jura). *Geol. Mag.*, 148, 133–153.

Corda, L. and **Brandano, M.** (2003). Aphotic zone carbonate production on a Miocene ramp, Central Apennines, Italy. *Sed. Geol.*, 161, 55–70.

Cosentino, D., Cipollari, P., Marsili, P. and **Scrocca, D.** (2010). Geology of the central Apennines: a regional review. In: *The Geology of Italy* (Eds M. Beltrando, A. Peccerillo, M. Mattei, S. Conticelli and C. Doglioni). Journal of the Virtual Explorer, Electronic Edition, 36, paper 11. ISSN 1441-8142.

Crescenti, U., Crostella, A., Donzelli, G. and **Raffi, G.** (1969). Stratigrafia della serie calcarea dal Lias al Miocene nella regionemarchigiano abruzzese: Parte II. Litostratigrafia, biostratigrafia, paleogeografia. *Mem. Soc. Geol. It.*, 9, 343–420.

Deino, A., Channell, J., Coccioni, R., De Grandis, G., DePaolo, D.J., Fornaciari, E., Emmanuel, L., Laurenzi, M.A., Montanari, A., Rio, D. and **Renard, M.** (1997). Integrated stratigraphy of the upper Burdigalian-lower Langhian section at Moria (Marche region, Italy). In: *Miocene Stratigraphy: An Integrated Approach* (Eds A. Montanari, G.S. Odin and R. Coccioni), pp. 315–341. Elsevier Science B.V, Amsterdam, the Netherlands.

Di Stefano, A., Baldassini, N., Maniscalco, R., Speranza, F., Maffione, M., Cascella, A. and **Foresi, L.M.** (2015). New bio-magnetostratigraphic data on the Miocene Moria section (Northern Apennines, Italy): connections between the Mediterranean region and the North Atlantic Ocean. *Newsl. Stratigr.*, 48, 135–152.

Dingle, R.V., McArthur, J.M. and **Vroon, P.** (1997). Oligocene and Pliocene interglacial events in the Antarctic Peninsula dated using strontium isotope stratigraphy. *J. Soc. Geol. London*, 154, 257–264.

Flower, B.P. (1999). Warming without high CO_2? *Nature*, 399, 313–314.

Föllmi, K.B. and **Godet, A.** (2013). Palaeoceanography of Lower Cretaceous Alpine platform carbonates. *Sedimentology*, 60, 131–151.

Föllmi, K.B., Weissert, H., Bisping, M. and **Funk, H.** (1994). Phosphogenesis, carbon-isotope stratigraphy, and carbonate-platform evolution along the Lower Cretaceous northern Tethyan margin. *Geol. Soc. Am. Bull.*, 106, 729– 746.

Föllmi, K.B., Badertscher, C., de Kaenel, E., Stille, P., John, C.M., Adatte, T. and **Steinmann, P.** (2005). Phosphogenesis and organic-carbon preservation in the Miocene Monterey Formation at Naples Beach, California—The Monterey hypothesis revisited. *Geol. Soc. Am. Bull.*, 117, 589–619.

Föllmi, K.B., Gertsch, B., Renevey, J.-P., De Kaenel, E. and **Stilles, P.** (2008). Stratigraphy and sedimentology of phosphate-rich sediments in Malta and south-eastern Sicily (latest

Oligocene to early Late Miocene). *Sedimentology*, 55, 1029–1051.

Föllmi, K.B., K.B., Hofmann, H., Chiaradia, M., Kaenel, E., Frijia, G. and **Parente, M.** (2015). Miocene phosphate-rich sediments in Salento (southern Italy). *Sed. Geol.*, 327, 55–71.

Frijia, G. and **Parente, M.** (2008) Strontium isotope stratigraphy in the upper Cenomanian shallow-water carbonates of the southern Apennines: short-term perturbations of marine 87 Sr/86 Sr during the oceanic anoxic event 2. *Palaeogeogr. Palaeoclimatol. Palaeoecol.*, 261, 15–29.

Frijia, G., Parente, M., Di Lucia, M. and **Mutti, M.** (2015). Carbon and strontium isotope stratigraphy of the Upper Cretaceous (Cenomanian-Campanian) shallow-water carbonates of southern Italy: chronostratigraphic calibration of larger foraminifera biostratigraphy. *Cretaceous Res.*, 53, 110–139.

Gattacceca, J., Deino, A., Rizzo, R., Jones, D.S., Henry, B., Beaudoin, B. and **Vadeboin, F.** (2007). Miocene rotation of Sardinia: new paleomagnetic and geochronological constraints and geodynamic implications. *Earth Planet. Sci. Lett.*, 258, 359–377.

Gueguen, E., Doglioni, C. and **Fernandez, M.** (1998). On the post-25 Ma geodynamic evolution of the western Mediterranean. *Tectonophysics*, 298, 259–269.

Halfar, J. and **Mutti, M.** (2005). Global dominance of coralline red-algal facies: a response to Miocene oceanographic events. *Geology*, 33, 481–484.

Hallock, P. and **Schlager, W.** (1986). Nutrient excess and the demise of coral reefs and carbonate platforms. *Palaios*, 1, 389–398.

Hemminga, M.A. and **Mateo, M.A.** (1996). Stable carbon isotopes in seagrasses: variability in ratios and use in ecological studies. *Mar. Ecol. Prog. Ser.*, 140, 285–298.

Holbourn, A., Kuhnt, W., Simob, J.A. and **Li, Q.** (2004). Middle Miocene isotope stratigraphy and paleoceanographic evolution of the northwest and southwest Australian margins (Wombat Plateau and Great Australian Bight). *Palaeogeogr. Palaeoclimatol. Palaeoecol.*, 208, 1–22.

Holbourn, A., Kuhnt, W., Flores, J.-A. and **Andersen, N.** (2007). Orbitally-paced climate evolution during the middle Miocene "Monterey" carbon-isotope excursion. *Earth Planet. Sci. Lett.*, 261, 534–550.

Howarth, R.J. and **McArthur, J.M.** (1997). Statistics for strontium isotope stratigraphy with a look-up table version. *J. Geol.*, 105, 441–456.

Immenhauser, A., Kenter, J.A., Ganssen, G., Bahamonde, J.R., Van Vliet, A. and **Saher, M.H.** (2002). Origin and significance of isotope shifts in Pennsylvanian carbonates (Asturias, NW Spain). *J. Sed. Res.*, 72, 82–94.

Immenhauser, A., Della Porta, G., Kenter, J.A. and **Bahamonde, J.R.** (2003). An alternative model for positive shifts in shallow-marine carbonate d13C and d18O. *Sedimentology*, 50, 953–959.

Jacobs, E., Weissert, H., Shields, G. and **Stille, P.** (1996). The Monterey event in the Mediterranean: a record from shelf sediments of Malta. *Paleoceanography*, 11, 717–728.

James, N.P. (1997). The cool-water carbonate depositional realm. In: *Cool-Water Carbonates*. (Eds N.P. James and J.A.D. Clarke), *SEPM Spec. Publ.*, 56, 1–20.

John, C.M., Mutti, M. and **Adatte, T.** (2003). Mixed carbonate-siliciclastic record on the North African margin (Malta)—coupling of weathering processes and mid Miocene climate. *Geol. Soc. Am. Bull.*, 1152, 217–229.

Kocsis, L., Vennemann, T.W., Fontignie, D., Baumgartner, C. and **Montanari, A.** (2008). Oceanographic and climatic evolution of the Miocene Mediterranean deduced from Nd, Sr, C e O isotope compositions of marine fossils and sediments. *Paleoceanography*, 23, PA4211.

Kroeger, K.F., Reuter, M., Forst, M.H., Breisig, S., Hartmann, G. and **Brachert, T.C.** (2007). Eustasy and sea water Sr composition: application to high-resolution Sr- isotope stratigraphy of Miocene shallow-water carbonates. *Sedimentology*, 54, 565–585.

Lear, C.H., Rosenthal, Y., Coxall, H.K. and **Wilson, P.A.** (2004). Late Eocene to early Miocene ice sheet dynamics and the global carbon cycle. *Paleoceanography*, 19, PA4015. doi: 10.1029/2004PA001039.

Longman, M.W. (1980). Carbonate diagenetic textures from nearsurface diagenetic environments. *AAPG Bull.*, 64, 461– 487.

Lustrino, M. and **Wilson, M.** (2007). The circum-Mediterranean anorogenic Cenozoic igneous province. *Earth-Sci. Rev.*, 81, 1–65.

Lustrino, M., Morra, V., Fedele, L. and **Franciosi, L.** (2009). Beginning of the Appenine subduction system in central western Mediterranean: constraints from Cenozoic "orogenic" magmatic activity of Sardinia, Italy. *Tectonics*, 28, TC5016.

Lustrino, M., Duggen, S. and **Rosenberg, C.L.** (2011). The Central-Western Mediterranean: anomalous igneous activity in an anomalous collisional tectonic setting. *Earth-Sci. Rev.*, 104, 1–40.

Maberly, S.C., Raven, J.A. and **Johnston, A.M.** (1992). Discrimination between ^{12}C and ^{13}C by marine plants. *Oecologia*, 91, 481–492.

McArthur, J.M. (1994). Recent trends in strontium isotope stratigraphy. *Terra Nova*, 6, 331–358.

McArthur, J.M. and **Howarth, R.J.** (2004). Strontium isotope stratigraphy. In: *A Geologic Time Scale* (Eds F. Gradstein, J. Ogg and A. Smith), pp. 96–105. Cambridge University Press, Cambridge.

McArthur, J.M., Howarth, R.J. and **Bailey, T.R.** (2001). Strontium isotope stratigraphy: LOWESS version 3: best fit to the marine Sr-isotope curve for 0–509 Ma and accompanying look-up table for deriving numerical age. *J. Geol.*, 109, 155–170.

Montanari, A., Carey, S., Coccioni, R. and **Deino, A.** (1994). Early Miocene in the Appenine pelagic sequence: an inferred Sardinian provenance and implications for western Mediterranean tectonics. *Tectonics*, 13, 1120–1134.

Montanari, A., Beaudoin, B., Chan, L.S., Coccioni, R., Deino, A., DePaolo, D.J., Emmanuel, L., Fornaciari, E., Kruge, M., Lundblad, S., Mozzato, C., Portier, E., Renard, M., Rio, D., Sandroni, P. and **Stankiewicz, A.** (1997). Integrated stratigraphy of the middle to upper Miocene pelagic sequence of Conero Riviera (Marche region, Italy). In: *Miocene Stratigraphy: An Integrated Approach* (Eds A. Montanari, G.S. Odin and R. Coccioni), pp. 410–450. Elsevier Science B.V, Amsterdam, the Netherlands.

Mutti, M. and **Bernoulli, D.** (2003). Early marine lithification and hardground development on a Miocene ramp (Majella, Italy) key surfaces to track changes in trophic resources in non tropical carbonate settings. *J. Sed. Res.*, 73, 296–308.

Mutti, M. and **Hallock, P.** (2003). Carbonate systems along nutrient and temperature gradients: some sedimentological and geochemical constraints. *Int. J. Earth Sci.*, 92, 465– 475.

Mutti, M., Bernoulli, D. and **Stille, P.** (1997). Temperate carbonate platform drowning linked to Miocene oceanographic events: Maiella platform margin, Italy. *Terra Nova*, 9, 122–125.

Mutti, M., Bernoulli, D., Spezzaferri, S. and **Stille, P.** (1999). Lower and Middle Miocene carbonate facies in the central Mediterranean: the impact of paleoceanography on sequence stratigraphy. In: *Advances in Carbonate Sequence Stratigraphy: Application to Reservoirs, Outcrops and Models* (Eds P. Harris, A. Saller, J. Simo and C.R. Handford), *SEPM Spec. Publ.*, 63, 371–384.

Mutti, M., Droxler, A.W. and **Cunningham, A.D.** (2005). Evolution of the Northern Nicaragua Rise during the Oligocene–Miocene: drowning by environmental factors. *Sed. Geol.*, 175, 237–258.

Mutti, M., John, C.M. and **Knoerich, A.C.** (2006). Chemostratigraphy in Miocene heterozoan carbonate settings: applications, limitations and perspectives. *Geol. Soc. London. Spec. Publ.*, 255, 307–322.

Nelson, C.S. (1988). An introductory perspective on non tropical shelf carbonates. *Sed. Geol.*, 60, 3–12.

Parente, M., Frijia, G., Di Lucia, M., Jenkyns, H.C., Woodfine, R.G. and **Baroncini, F.** (2008). Stepwise extinction of larger foraminifers at the Cenomanian-Turonian boundary: a shallow-water perspective on nutrient fluctuations during Oceanic Anoxic Event 2 (Bonarelli Event). *Geology*, 36, 715–718.

Paul, H.A., Zachos, J.C., Flower, B.P. and **Tripati, A.** (2000). Orbitally induced climate and geochemical variability across the Oligocene/Miocene boundary. P*aleoceanography*, 15, 471–485.

Pekar, S.F. and **DeConto, R.** (2006). High-resolution ice- volume estimates for the early Miocene: evidence for a dynamic ice sheet in Antarctica. *Palaeogeogr. Palaeoclimatol. Palaeoecol.*, 231, 101–109.

Pomar, L., Brandano, M. and **Westphal, H.** (2004). Environmental factors influencing skeletal grain sediment associations: a critical review of Miocene examples from the western Mediterranean. *Sedimentology*, 51, 627–651.

Pomar, L., Bassant, P., Brandano, M., Ruchonnet, C. and **Janson, X.** (2012). Impact of carbonate producing biota on platform architecture: insights from Miocene examples of the Mediterranean region. *Earth-Sci. Rev.*, 113, 186–211.

Reuter, M., Piller, W.E., Brandano, M. and **Harzhauser, M.** (2013). Correlating Mediterranean shallow water deposits with global Oligocene-Miocene stratigraphy and oceanic events. *Global Planet. Change*, 111, 226–236.

Rögl, F. (1999). Mediterranean and Paratethys. Facts and hypotheses of an Oligocene to Miocene paleogeography (short overview). *Geol. Carpath.*, 50, 339–349.

Saltzman, M.R. and **Thomas, E.** (2012). Carbon isotope stratigraphy. In: *The Geologic Time Scale 2012* (Eds F.M. Gradstein, J.G. Ogg, M.D. Schmitz and G.M. Ogg), pp. 207–232. Elsevier, Amsterdam.

Scasso, R.A., McArthur, J.M., Del Rıo, C.J., Martınez, S. and **Thirlwall, M.F.** (2001). $^{87}Sr/^{86}Sr$ Late Miocene age of fossil molluscs in the

'Entrerriense' of the Valdés Peninsula (Chubut, Argentina). *J. S. Am. Earth Sci.*, 14, 319–329.

Steuber, T. (1999). Isotopic and chemical intra-shell variations in low-Mg calcite of rudist bivalves (Mollusca-Hippuritacea): disequilibrium fractionations and late Cretaceous seasonality. *Int. J. Earth Sci.*, 88, 551–570.

Steuber, T. (2001). Strontium isotope stratigraphy of Turonian-Campanian Gosau-type rudist formations in the Northern Calcareous and Central Alps (Austria and Germany). *Cretaceous Res.*, 22, 429–441.

Swart, P.K. and **Eberli, G.** (2005). The nature of the d 13 C of periplatform sediments: implications for stratigraphy and the global carbon cycle. *Sed. Geol.*, 175, 115–129.

Tiepolo, M., Bottazzi, P., Palenzona, M. and **Vannucci, R.** (2003) A laser probe coupled with ICP–double-focusing sector-field mass spectrometer for *in situ* analysis of geological samples and U-Pb dating of zircon. *Can. Mineral.*, 41, 259–272.

Ullmann, C.V. and **Korte, C.** (2015). Diagenetic alteration in low-Mg calcite from macrofossils: a review. *Geol. Q.*, 591, 3–20. doi:10.7306/gq.1217.

Vecsei, A. and **Moussavian, E.** (1997). Paleocene reefs on the Maiella platform margin, Italy: an example of the effects of the Cretaceous/Tertiary boundary events on reefs and carbonate platforms. *Facies*, 36, 123–140.

Vecsei, A. and **Sanders, D.G.K.** (1999). Facies analysis and sequence stratigraphy of a Miocene warm-temperate carbonate ramp, Montagna della Maiella, Italy. *Sed. Geol.*, 123, 103–127.

Vecsei, A., Sanders, D.G.K., Bernoulli, D., Eberli, G.P. and **Pignatti, J.** (1998). Cretaceous to Miocene sequence stratigraphy and evolution of the Maiella carbonate platform margin, Italy. In: *Mesozoic and Cenozoic Sequence Stratigraphy of European Basins* (Eds J. Hardenbol, J. Thierry, M.B. Farley, T. Jacquin, P.C. De Graciansky and P.R. Vail), *SEPM Special Publication*, 60, 53–74.

Veizer, J. (1983). Trace elements and stable isotopes in sedimentary carbonates. In: *Carbonates: Mineralogy and Chemistry* (Ed. R.J. Reeder) *Rev. Mineral.*, 11, pp. 265–300. Mineralogical Society of America, Washington DC.

Vincent, E. and **Berger, W.H.** (1985). Carbon dioxide and polar cooling in the Miocene: the Monterey hypothesis. In: *The Carbon Cycle and Atmospheric CO: Natural Variations Archean to Present* (Eds W.S. Broecker and E.T. Sundquis), *AGU Geophys. Mon.*, 32, 455–468.

Weissert, H. and **Erba, E.** (2004). Volcanism, CO_2 and paleoclimate: A Late Jurassic-Early Cretaceous carbon and oxygen isotope record. *J. Geol. Soc. London*, 161, 695–702.

Weissert, H., Lini, A., Föllmi, K.B. and **Kuhn, O.** (1998). Correlation of Early Cretaceous carbon isotope stratigraphy and platform drowning events: a possible link? *Palaeogeogr. Palaeoclimatol. Palaeoecol.*, 137, 189–203.

Weissert, H., Joachimski, M. and **Sarnthein, M.** (2008). Chemostratigraphy. *Newsl. Stratigr.*, 42, 145–179.

Wilson, G.S., Pekar, S.F., Naish, T.R., Passchier, S. and **DeConto, R.** (2009). The Oligocene–Miocene Boundary– Antarctic Climate Response to Orbital Forcing. In: *Developments in Earth and Environmental Sciences* (Eds F. Florido and M. Siegert), 8, 369–400.

Wissler, L., Funk, H. and **Weissert, H.** (2003). Response of Early Cretaceous carbonate platforms to changes in atmospheric carbon dioxide levels. *Palaeogeogr. Palaeoclimatol. Palaeoecol.*, 200, 187–205.

Woodruff, F. and **Savin, S.** (1991). Mid-Miocene isotope stratigraphy in the deep sea: high resolution correlations, paleoclimatic cycles and sediment preservation. *Paleoceanography*, 6, 755–806.

Zachos, J., Pagani, M., Sloan, L., Thomas, E. and **Billups, K.** (2001). Trends, rhythms, and aberrations in global climate 65 Ma to present. *Science*, 292, 686–693.

4 Miocene oceanographic evolution based on the Sr and Nd isotope record of the Central Mediterranean

Irene Cornacchia[1], Samuele Agostini[2], Marco Brandano[1, 3]

1: Dipartimento di Scienze della Terra, Sapienza Università di Roma, P. Aldo Moro 5, 00185 Roma, (Italy).

2: Istituto di Geoscienze e Georisorse (IGG) CNR, Via Moruzzi 1, 56124 Pisa (Italy).

3: Istituto di Geologia Ambientale e Geoingegneria (IGAG) CNR, Sez. Sapienza, c/o Dipartimento Scienze della Terra, P. Aldo Moro 5, I-00185, Roma (Italy).

Accepted by *Paleocenaography,* DOI: 10.1002/2017PA003198.

ABSTRACT

The Miocene is a key interval in the geodynamic and oceanographic evolution of the Mediterranean marking the transition from a wide open basin to the modern closed basin. We used the Sr and Nd isotope records of two Miocene carbonate successions in the Adriatic to document that the evolution of the Mediterranean basin controlled its seawater chemistry. During the late Aquitanian (~21 Ma), a time of glaciation and sea-level low-stand, increased runoff affected the Sr isotope ratios of Mediterranean waters, whereas during the Burdigalian (20.44-15.97 Ma) volcanism in the circum-Mediterranean area mainly influenced the Sr isotopic signature. During the Langhian (15.97-13.82 Ma), a time of sea level high-stand associated with the Middle Miocene Climatic Optimum, the Nd isotope values indicate that waters exchanged between the Paratethys and the Central Mediterranean. The Central Mediterranean was well connected with the Atlantic Ocean between the Langhian and the early Tortonian (15.97-11.5 Ma), but exchange of water with the Paratethys declined. In the Messinian (6.3 Ma), connections between some marginal Mediterranean basins, e.g. the proto-Adriatic basin, and the Central Mediterranean, became restricted. In this basin, the Sr isotope~~s~~ values fell below the global reference line, while Nd isotope ratios show a strong affinity with the Atlantic Ocean, but also indicate freshwater input. We conclude that the Mediterranean Nd isotope signature differs from that in the open oceans and reflects the basin physiography, reflecting a mix of signals derived from the adjacent oceans and local signals.

4.1 INTRODUCTION

The Miocene oceanographic evolution of the Mediterranean basin represents the long-term transition from an open basin to its modern, closed basin shape. During the early Miocene (23.03-15.97 Ma), the Mediterranean was connected to both the Indo-Pacific and the Atlantic oceans (Rögl, 1999; Popov et al., 2004). The collision between the Arabia and the Eurasia plates led to the formation of the Anatolian microplate, and the closure of the Indian Gateway at the end of the early Miocene (Rögl, 1999; Popov et al., 2004). During the late Miocene (11.63-6 Ma), the Betic and the Rifian corridors in the West progressively narrowed due to tectonic uplift, leading to the onset of the restriction of exchanges of waters between the Mediterranean basin and the Atlantic Ocean and, eventually, to the Messinian Salinity crisis (5.96 Ma) (Krijgsman and Meijer, 2008; Martín et al., 2009; Dela Pierre et al., 2011; Manzi et al., 2013). Furthermore, volcanism developed within the Western Mediterranean area (Lustrino and Wilson, 2007; Lustrino et al., 2009; 2011), coupled with increased continental runoff linked to the Apennine orogenesis (Carminati et al., 2010; 2012), affected the Central Mediterranean water chemistry. Lastly, the Miocene is an extremely interesting time because of its climatic evolution. The Oligocene-Miocene boundary (~23 Ma) is marked by a global positive oxygen isotope shift, known as the Mi-1 event, and interpreted as a transient glaciation of Antarctica (Miller et al., 1991; Zachos et al., 2001; Lear et al., 2004; Pekar and De Conto, 2006). The early Miocene (~23-17 Ma) is characterized by a constant increase of global water temperatures, although punctuated by minor glaciation events that reflect a dynamic eastern Antarctic ice sheet (Paul et al., 2000; Lear et al., 2004; Zachos et al., 2008), until the Mid Miocene Climate Optimum (MMCO), marked by a long-term oxygen isotope negative excursion between 17 and 14.7 Ma (Holbourn et al., 2013, 2015). The latter event is known as the warmest time interval of the last 35 Ma, with average water temperatures at mid latitudes 6°C higher than today (Flower, 1999; Zachos et al., 2001; 2008). The MMCO was followed by a long-term cooling phase, between 12.9 and 8.4 Ma, punctuated only by a minor warm peak between 10.8 and 10.7 Ma (Holbourn et al., 2013).

Radiogenic isotopes are a reliable proxy in paleoceanographic studies (O'Nions et al., 1998; Burton and Vance, 2000; Frank, 2002; Scher and Martin, 2008; Kocsis et al., 2008). Integrated study of Sr and Nd isotope records are useful because of the different oceanic residence times of these elements, as compared to the oceans' mixing time. The $^{87}Sr/^{86}Sr$ ratio is homogeneous in the global ocean (McArthur et al., 2001; 2012) because the Sr residence time of ~10^6 years is much longer than the average ocean mixing time of 10^3 years. The global oceanic Sr isotope signature varied over the geological past due to two major controlling factors: volcanism and continental runoff (McArthur et al., 2012). Volcanism brings into the oceans a large input of the light ^{86}Sr isotope, lowering the seawater $^{87}Sr/^{86}Sr$ ratio, whereas the second raises the overall $^{87}Sr/^{86}Sr$ signature of the global ocean due to the weathering of old, continental crust (McArthur et al., 2012). Based on these assumptions, a global reference $^{87}Sr/^{86}Sr$ curve, calibrated with biostratigraphy and magnetostratigraphy, has been developed for the entire Phanerozoic (McArthur et al., 2001; 2012), and has been used extensively to date and correlate carbonate successions (McArthur and Howarth, 2004; Frijia and Parente, 2008; Brandano and Policicchio, 2012; Brandano et al., 2017a). However, it has become increasingly evident that the Sr isotope signature of marginal basins may deviate from the global ocean signature due to salinity changes, runoff and local volcanism, coupled with restricted conditions (Ingram and Sloan, 1992; Kocsis et al., 2008; Schildgen et al., 2014; Cornacchia et al., 2017).

Combined with Sr isotope ratios, $^{143}Nd/^{144}Nd$ ratios are useful to study circulation patterns and reconstruct paleoceanographic conditions (Stille et al., 1996; Frank et al., 2002; Pucéat et al., 2005; Scher et al., 2008; Dera et al., 2009). Nd isotopes show a strong provinciality due to the short residence time of Nd (between 200-1500 years) in the oceans (Bertram and Elderfield, 1993; Tachikawa et al., 1999). This implies that the Nd isotope signature of each ocean is significantly different from that of others (O'Nions et al., 1998; Burton and Vance, 2000; Frank, 2002; Scher and Martin, 2008). The Nd isotope signature of seawater is mainly controlled by continental erosional sources in rivers which drain into the basins (Goldstein and Jacobsen, 1987) as well as by ocean circulation and water mass distribution (Stille et al., 1996; Frank et al., 2002; Scher et al., 2008). The Atlantic Ocean is characterized by a non-radiogenic ε_{Nd} -13 signature due to its northern catchment that drains the old Canadian Shield (Piepgras and Wasserburg, 1987). On the contrary, the Pacific Ocean ε_{Nd}, ranging between -6 and -4, reflects the more radiogenic rocks of the volcanic arcs of the circum-Pacific area (Piepgras and Jacobsen, 1988). The Modern Mediterranean Sea is characterized by a ε_{Nd} -9.4 (Spivack and Wasserburg, 1988), which partly reflects the water exchange with the Atlantic Ocean, partly the freshwater input within the basin (Frost et al., 1986).

Therefore the Sr and Nd isotope signatures of the Miocene Central Mediterranean carbonate successions are extremely useful to highlight the factors that affected water chemistry. We thus analyzed the isotope sedimentary record of the proto-Adriatic basin to test which global and regional factors controlled the isotope signature. Our objectives are twofold: to highlight whether Sr Isotope stratigraphy may be applied to records from a marginal basin, e.g. the proto-Adriatic basin, and to test whether Nd isotope ratios can provide new insights in the exchange of water between the main Mediterranean Basin and the surrounding oceans, as well as within the different sub-basins of the Mediterranean area.

4.2 GEOLOGICAL SETTING AND SECTIONS LOCATION

4.2.1 The Central-Western Mediterranean

The Central-Western Mediterranean area is shaped by interaction between the European and African plates together with several other microplates, among which the Adria plate. It mainly evolved during the Cenozoic, specifically in the Neogene (Carminati and Doglioni, 2005; Carminati et al., 2012). Apennine subduction started during the late Eocene (Lustrino et al., 2009), and evolved mostly from Miocene to Recent. The eastward migration of the Apennine accretionary wedge was followed by an eastward extensional wave, which led to the opening of several basins on the thin continental (Valencia trough) and oceanic crust (Provençal basin, Tyrrhenian basin) in the Western Mediterranean (Gueguen et al., 1998). The Apennine subduction led to the development of highly explosive, subduction-related volcanism within

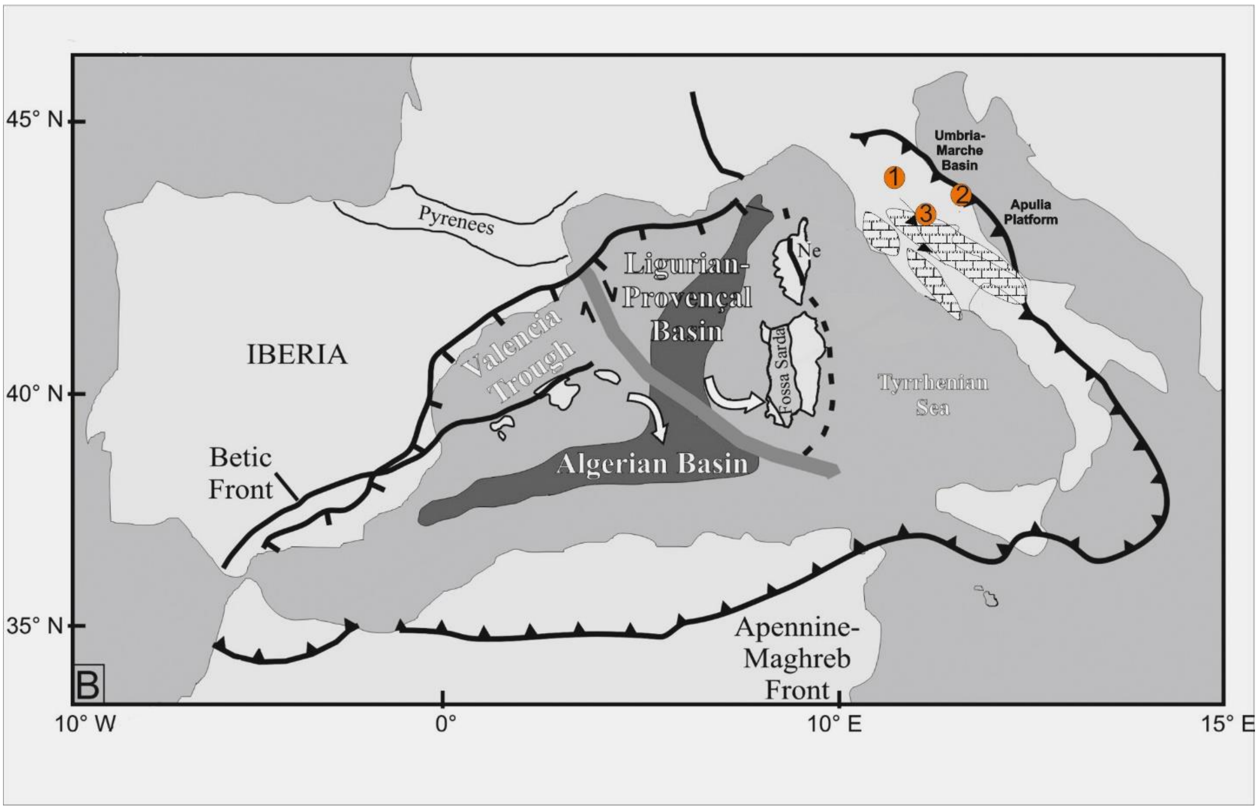

Fig. 4.1. Map of the Mediterranean area showing the location of the studied sections. 1: Contessa and Moria-Palcano sections. 2: La Vedova-Monte dei Corvi Section (Conero Riviera). 3: Roccamorice section (Majella Mountain). Modified after Gueguen et al. (1998).

the Western Mediterranean between 38 and 15 Ma (Carminati et al., 2010; Lustrino et al., 2011). This subduction-related volcanism peaked between 21 and 18 Ma, coeval with the most rapid phase of the counterclockwise rotation of the Sardinia-Corsica Block (Gattacceca et al., 2007; Lustrino et al., 2011). Anorogenic magmatism developed, and migrated from west to east from 12 Ma to Recent (Lustrino and Wilson, 2007; Lustrino et al., 2011).

This complex geodynamic evolution affected the Cenozoic oceanography of the Mediterranean. Until the early Miocene the main Mediterranean water body was connected to both the Atlantic and the Indo-Pacific Oceans, and characterized by an estuarine circulation (Rögl, 1999; Popov et al., 2004; Harzhauser et al., 2007; Harzhauser and Piller, 2007; Sant et al., 2017). The Indo-Pacific connection first closed in the late Burdigalian (~16 Ma), but reopened at least two times before its definitive closure in the late Langhian (~15 Ma) (Rögl, 1999). From the Oligocene to the middle Miocene (~29-13 Ma), Carpathian subduction indirectly affected Mediterranean circulation, through control of the exchanges between the Mediterranean and the Paratethys (Popov et al., 2004). In the early Miocene the Paratethys was connected to the Mediterranean by both a northern and an eastern passage (Popov et al., 2004). In the middle Miocene (15.97-11.63 Ma), Carpathian subduction led to the closure of the northern connection, leaving the Mediterranean to exchange only with the Pannonian basin to the north, and the Paratethys to the east. Shallow seaways opened and closed between the Mediterranean and the Paratethys during the middle Miocene as a

result of Carpathian orogenesis and sea level fluctuations (Rögl, 1999; Popov et al., 2004). Lastly, during the late Miocene, the Atlantic passage gradually narrowed (Popov et al., 2004). From Tortonian times on, this complex geodynamic evolution led to the isolation of different marginal Mediterranean basins from the larger Central Mediterranean water body (Flecker and Ellam, 2006; Topper et al., 2011, Schildgen et al., 2014; Cornacchia et al., 2017). It eventually led to the isolation of the entire Central Mediterranean basin during the Messinian, caused by the tectonic uplift of the Betic corridor and a coeval major sea-level fall, leading to the 'Messinian salinity crisis' (Popov et al., 2004; Krijgsman and Meijer, 2008; Martín et al., 2009; Manzi et al., 2013; Roveri et al., 2014).
Here, we analyzed two carbonate successions: the hemipelagic succession of the Umbria-Marche Domain in the Northern Apennines (upper Chattian-middle Miocene, ~25-11 Ma) and the upper Miocene (Messinian, ~6 Ma) formation of the *Turborotalita multiloba* Marls cropping out in the Majella Mountain (Central Apennines) (Fig. 4.1).

4.2.2 The Northern Apennine

The Northern Apennine succession consists of Lower Jurassic to upper Miocene pelagic to hemipelagic sediments. During Oligo-Miocene, a marly, pelagic to hemipelagic succession was deposited in the Northern Apennines, characterized by progressive increase in the siliciclastic fraction and decrease in bathymetry (Montanari et al., 1994; 1997a; 1997b; Deino et al., 1997; Guerrera et al., 2012). During the late Miocene, the area became the foredeep of the Apennine orogeny, as reflected by deposition of the siliciclastic turbidites of the Marnoso-Arenacea Formation (Guerrera et al., 2012; Carminati et al., 2013).

4.2.2.1 The Contessa stratigraphic section

The Contessa section includes the upper Chattian-middle Burdigalian (25-17 Ma) in two formations: the Scaglia Cinerea and the Bisciaro (Fig. 4.2a, 4.3a) (Montanari et al., 1997a). The first consists of homogeneous pelagic marly limestones with common biotite-rich volcaniclastic levels. The Bisciaro Formation consists of an alternation of pelagic marly limestones and calcareous marls interrupted by frequent volcaniclastic layers, and is divided into three members: a lower marly member, a middle calcareous-siliceous member and an upper marly member that represents the gradual transition to the overlying hemipelagic deposits of the Schlier Formation (Coccioni and Montanari, 1994; Montanari et al., 1997a). The boundary between the Scaglia Cinerea and the Bisciaro Formations is marked by a volcaniclastic layer, the "Livello Raffaello", which has been recognized regionally (Montanari et al., 1994), and is dated at 21.88 ± 0.32 Ma ($^{40}Ar/^{39}Ar$ on plagioclase minerals) (Montanari et al., 1997a). We used the age/depth conversion model proposed by Montanari et al. (1997a) based on the radiometrically dated volcanic ash layers (fig. 4.2a).
We used four samples from the Contessa section (CT3, CT8, CT36, CT 47) spanning the Aquitanian to lower Burdigalian (22.0-18.5 Ma) (Tab. 4.1). Sample CT3 is from the upper part of the Scaglia Cinerea, just below the limit with the overlying Bisciaro Formation. CT8 is from the lower member of the Bisciaro Formation, at 2.10 m above the Raffaello level. CT36 and CT47 are from the middle member of the Bisciaro formation,

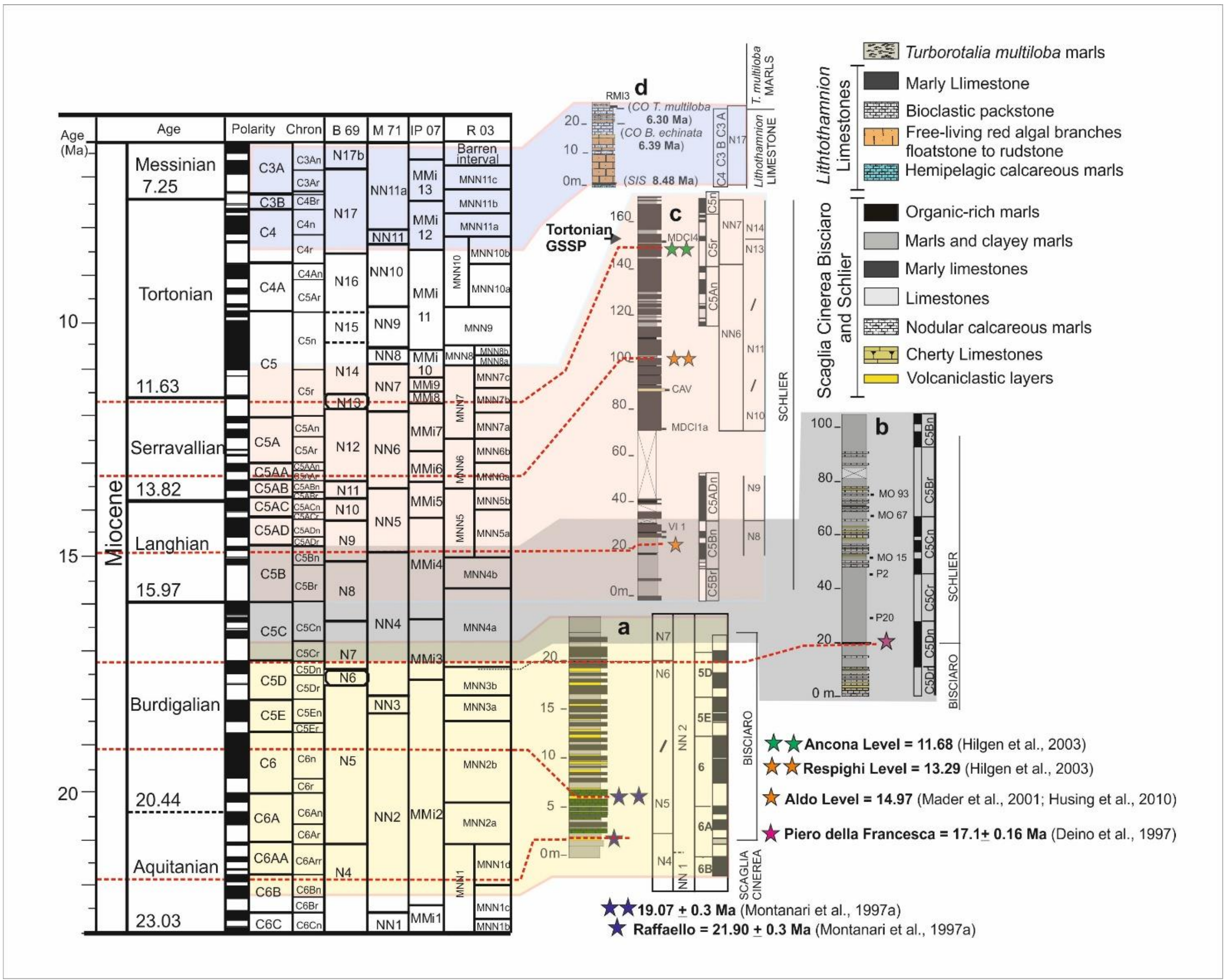

Fig. 4.2. Simplified stratigraphic sections plotted against stratigraphic depth and correlated with the Geological Time Scale. The age model of the of the Contessa section is from Montanari et al. (1997a); the age model of the Moria section is referred to Di Stefano et al. (2008, 2015). The age model of the La Vedova-Monte dei Corvi section is from Montanari et al. (1997b), Hilgen et al. (2003, 2005) and Husing et al. (2007, 2009, 2010). Age constraints for the Roccamorice sections are referred to by Cornacchia et al. (2017). B 69= planktonic foraminifera biozones of Blow (1969). M 71= calcareous nanoplankton biozones of Martini (1971) IP 07= Mediterranean planktonic foraminifera biozonation of Iaccarino and Premoli Silva (2007). R 03= Mediterranean calcareous nannofossil zonation of Raffi et al. (2003).

respectively at 10.40 m and 13.70 m in the Contessa section. CT36 is from a thin marly layer, CT47 from a volcaniclastic layer (Fig. 4.2a).

4.2.2.2 The Moria-Palcano stratigraphic section

The Moria stratigraphic section comprises the upper Burdigalian-Langhian (17.7-14.7 Ma) (Deino et al., 1997; Di Stefano et al., 2008; 2015). At the base of the section the siliceous-calcareous middle member of the Bisciaro Formation occurs, overlain by the upper marly member (Fig 2b; 3b). The transition to the Schlier Formation is gradual since the upper marly member of the Bisciaro Formation and the lower marly member of the overlying Schlier are lithologically indistinguishable. Therefore, Coccioni and Montanari (1992) proposed to place the limit between the formations in a biotite-rich volcaniclastic layer, recognized on a regional scale, and named “Piero della Francesca Level”. This level has been radiometrically dated with the $^{40}Ar/^{39}Ar$ method at 17.1 ± 0.16 Ma. The Schlier Formation has been divided into three members. The lower member consists of homogeneous marls, the middle member of an alternation of siliceous-calcareous marly limestones and marls, and the upper member is represented by marls (Deino et al., 1997). Six volcaniclastic layers are intercalated within the middle member of the Schlier Formation, two of which have been radiometrically dated by Deino et al. (1997) at 16.18 ± 0.16 Ma and 15.5 ± 0.16 Ma (Fig. 4.2b).

We use the recently revised age model proposed by Di Stefano et al. (2008, 2015) based on new biostratigraphic and magnetostratigraphic data for the Moria section. These authors ascribe the Moria section to the upper Burdigalian-Langhian, from 17.7 to 14.7 Ma, in agreement with the radiometric ages of the three volcaniclastic levels (Deino et al. 1997).

Five samples were collected from the Moria-Palcano section (P20, P2, MO15, MO67, MO93), from upper Burdigalian to lower Langhian (17-15.6 Ma) (Tab. 4.1). P20 is from the lower member of the Schlier Formation cropping out at Palcano, at 29.50 m. P2 and MO15 are from the calcareous middle member, cropping out respectively at 45.40 m and 51.70 m. MO67 and MO93 are representative of the upper marly member of the Schlier Formation and crop out at 67.1 m and 75 m respectively (Fig. 4.2b).

4.2.2.3 The La Vedova-Monte dei Corvi stratigraphic section

The upper Langhian-lower Tortonian (14.9-11.5 Ma) has been investigated at the La Vedova-Monte dei Corvi stratigraphic section along the coastal cliff of the Conero Riviera (central Italy) (Fig. 4.1). This section contains the Schlier Formation, consisting of three members: the lower marly member, the middle calcareous member, and the upper marly member (Fig. 4.2c). The upper Langhian-lower Tortonian is represented by the lower and middle members. According to Montanari et al. (1997b), the first member is massive, 22 m thick and composed of 7 massive layers of hemipelagic marls (Fig. 4.2c, 4.3c). A biotite-rich volcaniclastic layer, named “Aldo Level” crops out at the limit between the lower and the middle members (Fig. 4.2c), and has been dated with the $^{40}Ar/^{39}Ar$ method at 14.9 ± 0.2 Ma (Mader et al., 2001), in agreement with Hüsing et al. (2010). The calcareous member consists of 148 m of alternating marly limestones and marls, interrupted by a sandy turbiditic layer at 86.85 m (Cavolo sandstones). Two biotite-rich clayey layers occur in the middle calcareous member-known as the Respighi Level and Ancona Level (Fig. 4.2c), and dated ($^{40}Ar/^{39}Ar$) at 12.86 ± 0.16 and 11.43 ± 0.20 Ma respectively (Montanari et al., 1997b). However, Husing et al. (2007) supported the astronomically tuned age of 13.29 Ma for Respighi and 11.82 Ma for Ancona Level as proposed by Hilgen et al. (2003).

For the lower portion of the La Vedova-Monte dei Corvi section, we use the age model in Husing et al. (2010), who integrate biostratigraphy, magnetostratigraphy, and the radiometric date of the Aldo Level to provide the astronomical tuning of the Langhian portion of the section (15.29-14.17 Ma). For the middle Langhian-lower Serravallian portion of the section (14.17-13.29 Ma), we use the age model by Montanari et al. (1997b) based on planktonic foraminiferal biostratigraphy. For the upper portion of the La Vedova-Monte dei Corvi section, we refer to Hilgen et al. (2003) for the Tortonian GSSP and to Hüsing et al. (2007, 2009). The latter provides a high-resolution age model of the upper Serravallian-lower Tortonian portion of the Monte dei Corvi section. The composite section has then been plotted vs time scale (fig. 4.2c).

Four samples have been collected from the La Vedova-Monte dei Corvi section (VI1, CAVOLO, MDCI1a, MDCI4), spanning from the upper Langhian to the base of the Tortonian (14.9-11.6 Ma) (Tab. 4.1). Sample VI1 is from the base of the calcareous member of the Schlier Formation, above the "Aldo" volcaniclastic level. Sample MDCI1a is from the base of the Monte dei Corvi section, sample CAVOLO from just below the homonymous turbidite level, and sample MDCI4 from the top of the section cropping out along Monte dei Corvi beach. They occur at 70.0 m, 86.0 m and 151.0 m of the section, respectively (Fig. 4.2c).

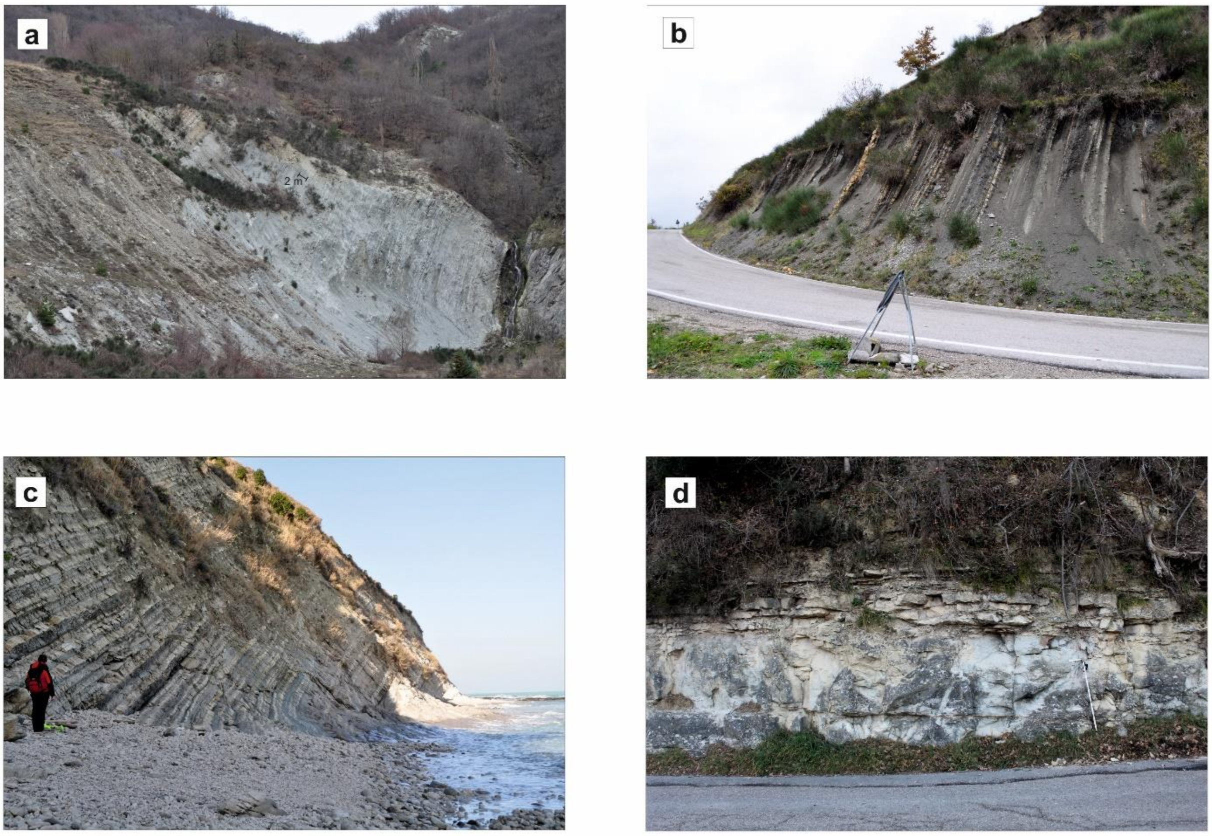

Fig. 4.3. Investigated sections and outcrops. a: Scaglia Cinerea-Bisciaro boundary cropping out within the Contessa Quarry. b: Middle calcareous-siliceous member of the Schlier Formation cropping out at Moria section. c: Lower Member of the Schlier Formation cropping out in the upper portion of the La Vedova section (Conero Riviera). d: *Lithothamnion* Limestone-*T. multiloba* Marls boundary cropping out in the upper portion of the Roccamorice section (Majella Mountain).

4.2.3 The Central Apennine

The Central Apennine succession consists of the Latium-Abruzzi carbonate platform and the Apulia Carbonate platform, deposited along the western margin of the Adria plate. The northern portion of the Apulian Carbonate Platform is represented by the Majella Mountain (Patacca and Scandone, 2007; Patacca et al., 2008; Vezzani et al., 2010). Here the carbonate succession consists of Upper Jurassic to upper Miocene limestones and dolostones (Crescenti et al., 1969). The Bolognano Formation consists of sediments deposited on a carbonate ramp in the late Rupelian-Messinian (Mutti et al., 1997; Vecsei et al., 1998; Brandano et al., 2012; 2016a), and contains an alternation of shallow-water carbonate and deeper marly units. The upper unit of the Bolognano Formation, named *Lithothamnion* Limestone unit, is upper Tortonian-lower Messinian (Brandano et al., 2016b; Cornacchia et al., 2017). The *Turborotalita multiloba* marls (Carnevale et al., 2011) cap the *Lithothamnion* Limestone unit, and predate the gypsum deposition, representing the lower Messinian interval before the onset of the salinity crisis. Lastly, during the early Pliocene, the Majella Mountain was part of the foredeep system of the Apennine orogeny, as shown by flysch deposition (Cosentino et al., 2010).

4.2.3.1 The Roccamorice stratigraphic section

The Roccamorice stratigraphic section contains the upper Miocene (8.5-6.3 Ma) portion of the Bolognano Formation (Fig. 4.2d, 4.3d), with the 25-m thick *Lithothamnion* Limestone unit (Brandano et al., 2016b). These authors divide the *Lithothamnion* Limestone unit into two intervals. The lower interval consists of a 0.20 m thick bed of a *Heterostegina* floatstone to rudstone followed by a 15-m free-living branches floatstone to rudstone alternated with a bioclastic packstone facies. The upper interval consists of 10 m of medium-grained bioclastic packstone. The terrigenous input increases evidently in the upper portion of the section. The *T. multiloba* marls cap the *Lithothamnion* Limestone unit, reflecting the drowning of the Bolognano ramp and the onset of a deeper water sedimentation.

For the stratigraphy of the Roccamorice section, the reader is referred to Cornacchia et al. (2017), who propose an integrated Sr Isotope Stratigraphy and biostratigraphy of the *Lithothamnion* Limestones. The base of the *Lithtothamnion* Limestone can be ascribed to the upper Tortonian (~8.50 Ma). The occurrence of *Bulimina echinata* at m 20 of the Roccamorice section places the upper *Lithothamnion* Limestone in the lower Messinian (the *Bulimina echinata* increases in abundance within the Mediterranean at 6.4 Ma according to Sprovieri et al., 1996; Kouwenhoven et al., 2006). Lastly, the base of the *T. multiloba* marls can be placed at 6.30 Ma, due to the abundance of the *T. multiloba* (Sierro et al., 2003; Kouwenhoven et al., 2006). The *T. multiloba* marls have been sampled 0.10 m above the limit with the underlying *Lithothamnion* Limestone unit (sample RMI3) (Fig. 4.2d).

4.3 MATERIALS AND METHODS

The above described 14 samples cover the entire Miocene. Samples were first disaggregated in acetic acid 80% for four to six hours, depending on the lithology of the sample, and then in an ultrasonic cleaner following Lirer (2000). The disaggregated material was wet-sieved in a 63μm sieve. The sand-sized material was observed through an optical microscope. Planktonic foraminifera were hand-picked, avoiding encrusted or altered shells. In contrast to the samples belonging to the Umbria-Marche succession, in the RMI3 sample (Roccamorice section, Majella Mountain), planktonic foraminifera have been analyzed for Sr isotopes while benthic foraminifera have been analyzed for Nd isotopes. In the latter case, benthic foraminifera shells have been selected since they are significantly more abundant than planktonic ones.

There is an ongoing debate on the main sources of Nd within the foraminifera tests. Mineralization for most planktonic foraminifera occurs within the upper 100 m of the water column. However, after the organism's death, it falls through the water column and might be affected by different chemical or physical processes, leading to ion exchanges, partial dissolution or partial secondary calcite overgrowth (Lohman, 1995). Scher and Martin (2008) state that fossils and marine sediments incorporate most of the Nd at or near the sediment-water interface, thus, both planktonic and benthic records are proxies of deep-waters Nd isotope composition. Pomiés et al. (2002), testing the Nd/Ca ratios on different planktonic foraminifera collected from 20 to 3400 m depth, concluded that the Nd in foraminifera from deep-waters (1500-200m) is partly (15%) incorporated in the calcite tests by the living organism and partly (85%) incorporated in the Mn coating formed after death, thus a mixture of the water column Nd isotope signature. In contrast, Vance et al. (2004) state that the main controlling factor on Nd concentration into calcite is the oxygenation level into the waters and not primary diagenesis. However, the same authors state that usually the Nd concentrations measured on dead specimens are too high to have been incorporated directly into the calcite tests, but do not discuss the possible sources of the excess Nd. However, the difference between the surface and the deep-water signature of the Nd is an issue only if the shallow water has a different Nd isotope ratio than the deeper water column. We use both planktonic and benthic foraminifera, since the main objective is to test whether Nd isotopes can provide new information on the main water exchange between the Mediterranean and the surrounding oceans. Similarly, when analyzing the Nd water signature of marine waters for paleoceanographic purposes, Kocsis et al. (2008) measured Nd isotope ratios on mixed planktonic and benthic foraminifera, and bivalves.

A diagenetic screening, based on Sr element concentrations and C and O stable isotope ratios measurements, was performed on the separated planktonic foraminifera. Sr concentrations were measured on polished thin sections using the CAMECA electron microprobe of the Istituto di Geologia Ambientale e Geoingegneria (IGAG-CNR) at Sapienza, University of Rome.

Carbon and oxygen stable isotopes were measured in the isotope geochemistry laboratory of the Istituto of Geologia Ambientale e Geoingegneria (IGAG-CNR) of Rome using a gas chromatography-based Gas Bench II coupled with a FINNIGAN Delta Plus mass-spectrometer. All the results were calibrated using the international NBS19 carbonate standard. The analytical error is ± 0.1‰ based on replicate standards. All the $\delta^{13}C$ and $\delta^{18}O$ values are reported on the Pee Dee Belemnite (PDB) scale.

Sr and Nd isotopes were measured at the Istituto di Geoscienze e Georisorse (IGG-CNR) of Pisa (Italy) using a Finnigan MAT 262 multicollector mass-spectrometer running in dynamic mode, after Sr and Nd purification with the conventional cation-ion procedure. Measured $^{87}Sr/^{86}Sr$ and $^{143}Nd/^{144}Nd$ ratios have been normalized, respectively to $^{86}Sr/^{88}Sr=0.1194$ and $^{146}Nd/^{144}Nd=0.7219$. During the collection of the Sr data, 51 replicate analyses of the standard NIST 987 gave an average value of 0.710232 ± 0.000019

(2 SE). All the $^{87}Sr/^{86}Sr$ isotope ratios have been corrected to the value of 0.710248 reported in McArthur et al. (2001). In total, 25 replicate analyses of the J Nd i 1 standard, measured during the $^{143}Nd/^{144}Nd$ data collection, gave an average value of 0.512105 ± 0.000010 (2 SE). Nd isotope values are corrected by age, assuming the Sm/Nd ratio of the samples is the same as the seawater ratio of 0.122 (Piepgrass and Wasserburg, 1980).

Age of samples

We selected samples from well-known and well dated sections (Montanari et al., 1997a; 1997b; Deino et al., 1997; Hilgen et al., 2003; 2005; Husing et al., 2007, 2009, 2010; Di Stefano et al., 2008, 2015). The age model of these sections has been established using integrated biostratigraphic and magnetostratigraphic analyses, as well as the occurrence of several volcanic layers, as described above. All sections have been plotted vs time scale (fig. 4.2).

4.4 RESULTS

4.4.1 Diagenetic screening

Foraminifera have been extensively used to study the chemical composition of seawater, their low-Mg calcite shell is resistant to diagenetic alteration (Brand and Veizer, 1980; Morse and Mckenzie, 1990) thus a reliable proxy of the ambient seawater chemistry (Palmer and Elderfield, 1985; McArthur, 1994; Veizer et al., 1997; 1999; Burton and Vance, 2000; Henderson, 2002; McArthur and Howarth, 2004; Kocsis et al., 2008; Frijia and Parente, 2008; Brandano and Policicchio, 2012; Frijia et al., 2015). Diagenesis of carbonates tends to decrease the Sr concentration in the tests (Brand and Veizer, 1980; Brown and Elderfield, 1996). We applied diagenetic screening prior to measuring Sr and Nd isotope ratios. According to Carpenter and Lohmann (1992) and Steuber et al. (1999), a cut-off threshold of 700 ppm of Sr has been chosen to determine diagenetic alteration of the foraminifera shells (Tab. 4.1, Annex B.8). Once established, we can state that diagenetic alteration did not affect the selected foraminifera tests. The Sr/Ca ratios confirm the lack of major diagenetic alteration. The Sr/Ca of the measured samples ranges between 0.9 to 1.3 mmol/mol (Tab. 4.1, Annex B.8). These values fit perfectly within the range recorded in both planktonic and benthic foraminifera (Martin et al., 1999).

Oxygen isotope ratios vary from -2.46‰ and +0.88‰, while carbon isotope ratios span from -0.55‰ to +1.07‰ (Tab. 4.1, Annex B.8). These stable isotope ratios fall entirely within the range of marine carbonates (Weissert, 2008 and reference therein), thus a strong diagenetic overprint on the shells can be ruled out.

Both the Sr concentrations and the stable isotope results imply that the digestion in cold acetic acid did not affect the chemical composition of the foraminifera. The acetic acid, in fact, causes a very slow reaction which disaggregates the matrix of lithified samples without corroding or destroying the fossil content (Lirer, 2000).

4.4.2 Sr isotopes

The measured $^{87}Sr/^{86}Sr$ ratios range between 0.708243 and 0.708869 (Tab. 4.2, Annex B.9). The samples from the Contessa section show very different Sr isotope ratios, ranging from 0.708243 to 0.708480 (Tab. 4.2, Annex B.9). Samples CT3 and CT36 fall within the global reference line of McArthur and Howarth

Sample	Sr (ppm)	SD	Sr/Ca (mmmol/mol)	SD	δ ^{13}C (‰ VPDB)	δ ^{18}O (‰ VPDB)	Age
RMI3	894,64	164,95	1,06	0,009	0,55	0,69	6,3
MDCI4	835,45	100,38	1,14	0,014	0,53	0,88	11,6
CAVOLO	1183,84	321,55	0,92	0,014	0,8	0,17	13,4
MDCI1a	1057,00	278,19	1,19	0,012	1,07	0,09	13,7
VI1	1138,74	271,42	1,29	0,054	0,02	0,03	14,9
MO93	1133,10	296,06	1,28	0,061	0,08	-1,54	15,6
MO67	885,76	224,89	1,33	0,025	-0,4	-1,82	15,9
MO15	1138,17	260,38	1,18	0,022	-0,34	-2,04	16,5
P2	1155,09	187,56	1,30	0,037	-0,47	-1,45	16,7
P20	1021,48	94,26	1,02	0,008	-0,16	-1,8	17,1
CT47	786,41	298,67	1,37	0,064	-0,55	-2,08	18,5
CT36	1036,70	284,06	1,22	0,029	-0,09	-2,46	19,1
CT8	995,69	375,57	0,98	0,012	0,13	-1,96	21,8
CT3	938,61	157,56	1,03	0,010	0,98	-1,55	22,0
n= 4 for CT8, MO67, MO93							
n=5 for CT3, CT36, CT47, MO15, P2, P20, CAVOLO, MDCI1a, MDCI4, RMI3							
n= 6 for VI1							

Tab. 4.1. Sr element concentration profiles of the measured samples reported as mean values and as Sr/Ca (mmol/mol) ratios. $\delta^{13}C$ and $\delta^{18}O$ values reported on the VPDB scale. Age data for samples CT3, CT8, CT36 and CT47 refer to the age/depth conversion proposed by Montanari et al. (1997a) for the Contessa section. Age data for samples P20, P2, MO15, MO67, and MO93 refer to Di Stefano et al. (2008, 2015). Age datum for sample VI1 is referred to by Hüsing et al. (2010). Age data for samples CAV, MDCI1a, and MDC4 are referred to by Montanari et al. (1997b), Hilgen (2003), and Hüsing et al. (2007, 2009). The age RMI3 is constrained by the *Turborotalita multiloba* according to Kouwenhoven et al. (2006).

(2004), whereas samples CT8 and CT47 show very different values (Fig. 4.4a). The samples from the Moria-Palcano stratigraphic section show Sr isotope ratios ranging between 0.708415 to 0.708702 (Tab. 2). Sample P20 and sample MO93 fall within the global reference line, whereas samples P2, MO15 and MO67 show a lower Sr isotope signal (Fig. 4.4a).

Samples VI1, CAV, MDCI1a, and MDCI4, from the La Vedova-Monte dei Corvi section, show $^{87}Sr/^{86}Sr$ ratios between 0.708717 and 0.708832 (Tab. 4.2), falling within the global reference line (Fig. 4.4a). Lastly, sample RMI3, representative of the lower Messinian has a Sr isotope value of 0.708869, deviating from the global reference line (Fig. 4.4a).

4.4.3 Nd isotopes

The $^{143}Nd/^{144}Nd$ isotope ratios range from 0.512212 and 0.512445, corresponding to a $\varepsilon_{Nd(t)}$ range between -3.5 and -14.4 (Tab. 4.2, Annex B.9). Samples CT8 and CT36 of the Contessa stratigraphic section show a very similar Nd isotope signal, namely an $\varepsilon_{Nd(t)}$ of -5.3 and 5.2, respectively. Samples from the Moria-Palcano section show lower $\varepsilon_{Nd(t)}$ values on average. P20, P2 and MO15 range from $\varepsilon_{Nd(t)}$ -8.0 and $\varepsilon_{Nd(t)}$ -6.9, whereas MO93 shows the highest measured value of $\varepsilon_{Nd(t)}$ -3.5. Samples VI1, CAV, MDCI1a and MDCI4, from the La Vedova-Monte dei Corvi section, show fluctuating $\varepsilon_{Nd(t)}$ values between -7.5 and 5.5 (Tab. 4.2, Annex B.9). Lastly, early lower Messianian sample RMI3 shows the lowest

Nd isotope value of $\varepsilon_{Nd(t)}$ -14.4 (Tab. 4.2, Annex B.9).

4.5 DISCUSSION

The isotope composition of marine carbonates in the Central Mediterranean during the Miocene approximates the global changes, but offsets may be interpreted as the result of the regional geodynamic evolution of the area.

Aquitanian (23.03-20.44 Ma)

The lower Aquitanian Sr isotope record falls within the global Sr isotope reference line of McArthur and Howarth (2004), indicating a Mediterranean water body exchanging with the global ocean (Fig. 4.4a). During the Aquitanian, the proto-Mediterranean was connected both with the Indo-Pacific and the Atlantic Oceans (Fig. 4.5a) (Rögl, 1999; Popov et al., 2004). On the contrary, the upper portion of the Aquitanian interval (CT8 sample) shows a Sr isotope ratio significantly higher than the global ocean (Fig. 4.4a). Its age is between 21.88 ± 0.32 Ma (the Raffaello Level) and 21.12 Ma (*Paragloborotalia kugleri Datum)* (Wade et al., 2011 calibrated with the Gradstein et al., 2004 timescale), thus it may be considered coeval with the Mi-1a event (21.1 Ma) (Fig. 4.6b) (Schackleton et al., 1999; Pekar and de Conto, 2006). Mi-events are positive oxygen isotope shifts representative of transient glaciations of Eastern Antarctica (Zachos et al., 2001; Pekar and De Conto, 2006). During these glacial maxima, continental derived runoff increased due to enhanced weathering. In this scenario, the locally increased continental-derived input from the Alps may have affected the $^{87}Sr/^{86}Sr$ isotope signature of seawater. Evidence of increased runoff related to the Mi-1 events lies in enhanced nutrient availability as recorded by basinal successions (Mutti et al., 2005; Föllmi et al., 2008; Brandano et al., 2015). At the time, Mediterranean carbonate platforms experienced a shift from photic to photo-independent skeletal assemblages (Foresi et al., 2007; Föllmi et al., 2008; Brandano et al., 2015; 2017b).

The Aquitanian Nd isotope record of the Central Mediterranean fits with the Pacific signal, reflecting that the major water mass into the Mediterranean came through its eastern gateway. The Pacific signal should result from an Indian Ocean signal whose ε_{Nd} is shifted towards higher values due to the extensive volcanism and volcanic runoff affecting the region of the Indian Gateway throughout the Cenozoic (e.g. Innocenti et al., 1982). A broad volcanic arc developed in the region from late Eocene to early Miocene (Azizi and Moinevaziri, 2009 and references therein). On the other hand, recent palaeoceanographic studies pointed out that a deep Indian Gateway affected Central and Eastern Mediterranean circulation due to an antiestuarine circulation pattern, where the major water mass entered into the basin from the east, and circulated westward (de la Vara et al., 2013).

The volcanism may have affected the northern Indian Ocean waters, and, in turn, the Nd isotope signature of the Mediterranean. Kocsis et al. (2008) document a Nd isotope signature for the Central Mediterranean which fluctuates between the Indian and the Pacific Ocean signature (Fig. 4.4b), and they interpreted it to represent short-lived signatures of the volcanism within the Western Mediterranean (Kocsis et al., 2008).

Burdigalian (20.44-15.97 Ma)

Lighter Sr isotope values than the global Sr reference curve occur during the middle Burdigalian to the base of the Langhian

Sample	Sr	2s.e. ($*10^{-6}$)	Nd	2s.e. ($*10^{-6}$)	$(\varepsilon_{Nd})_t$	±
RMI3	0,708869	10	0,511895	47	-14,4	0,9
MDCI4	0,708832	9	0,512341	13	-5,6	0,3
CAVOLO	0,708793	9	0,512251	13	-7,3	0,3
MDCI 1a	0,708824	21	0,512344	19	-5,5	0,4
VI 1	0,708717	11	0,512244	10	-7,5	0,2
MO 93	0,708702	19	0,512445	7	-3,5	0,1
MO 67	0,708529	7				
MO 15	0,708415	7	0,51223	27	-7,7	0,5
P 2	0,708466	9	0,512271	13	-6,9	0,3
P 20	0,708656	18	0,512212	47	-8,0	0,9
CT 47	0,708252	6				
CT 36	0,708565	12	0,512355	19	-5,2	0,4
CT 8	0,708480	37	0,512348	7	-5,3	0,1
CT 3	0,708243	16				
Standard values	NIST 987	0,710232	19 2s.e. ($*10^{-6}$)	N=51		
	J Nd i 1	0,512105	10 2s.e. ($*10^{-6}$)	N=25		
All Sr isotope values are corrected to 0.710248, as reported by McArthur et al., 2001						
Sr isotope values are not corrected by age, given very low Rb/Sr of analyzed samples						
Nd isotope values are corrected by age assuming Sm/Nd ratio of samples same as seawater (0.122), as reported by Piepgras and Wasserburg [1980]						

Tab.4.2. $^{87}Sr/^{86}Sr$ values of the measured samples, corrected for the standard values, are reported with the analytical error ($2\sigma_{mean}$). $^{143}Nd/^{144}Nd$ are reported with the analytical error ($2\sigma_{mean}$). Deviation of Nd isotopes (ε_{Nd}) from a chondritic uniform reservoir (ChUR) in parts per 10^4 with relative error.

(18.49-15.9 Ma) (Fig. 4.4a). The lowest value recorded in the studied successions falls in the lower portion of the Burdigalian, and corresponds to one of the volcaniclastic levels in the Contessa section (Fig. 4.2a). The light $^{87}Sr/^{86}Sr$ isotope ratios may be attributed to the strong contemporary volcanism that affected the Central Mediterranean and carbonate successions (Fig. 4.6a) (*Lustrino et al.,* 2009). The Bisciaro, as well as the Schlier Formations are characterized by the presence of volcanic ash layers (Deino et al., 1997). *Guerrera et al.* (2015) stated that the Bisciaro Formation is the result of mainly volcaniclastic deposition since its hemipelagic marine content is subordinate to the volcaniclastic one. The authors refer to this formation as the "Bisciaro volcaniclastic event" since it can be correlated with several others volcaniclastic deposits in the Central-Western Mediterranean (Apennines-Maghrebian chains and the Bethic Cordillera). It is not easy to identify the source region of the volcanism that affected the Central Mediterranean. Volcanism was active during Burdigalian in several different circum-Mediterranean zones: the Iberian margin, the Rif and Tell chains, the Maghrebian chain, the Sardinia and Corsica Block, and the Pannonian basin (Lustrino and Wilson, 2007; Lustrino et al., 2009). The highly explosive, Oligo-Miocene subduction-related volcanism in Sardinia was believed to be the source of the

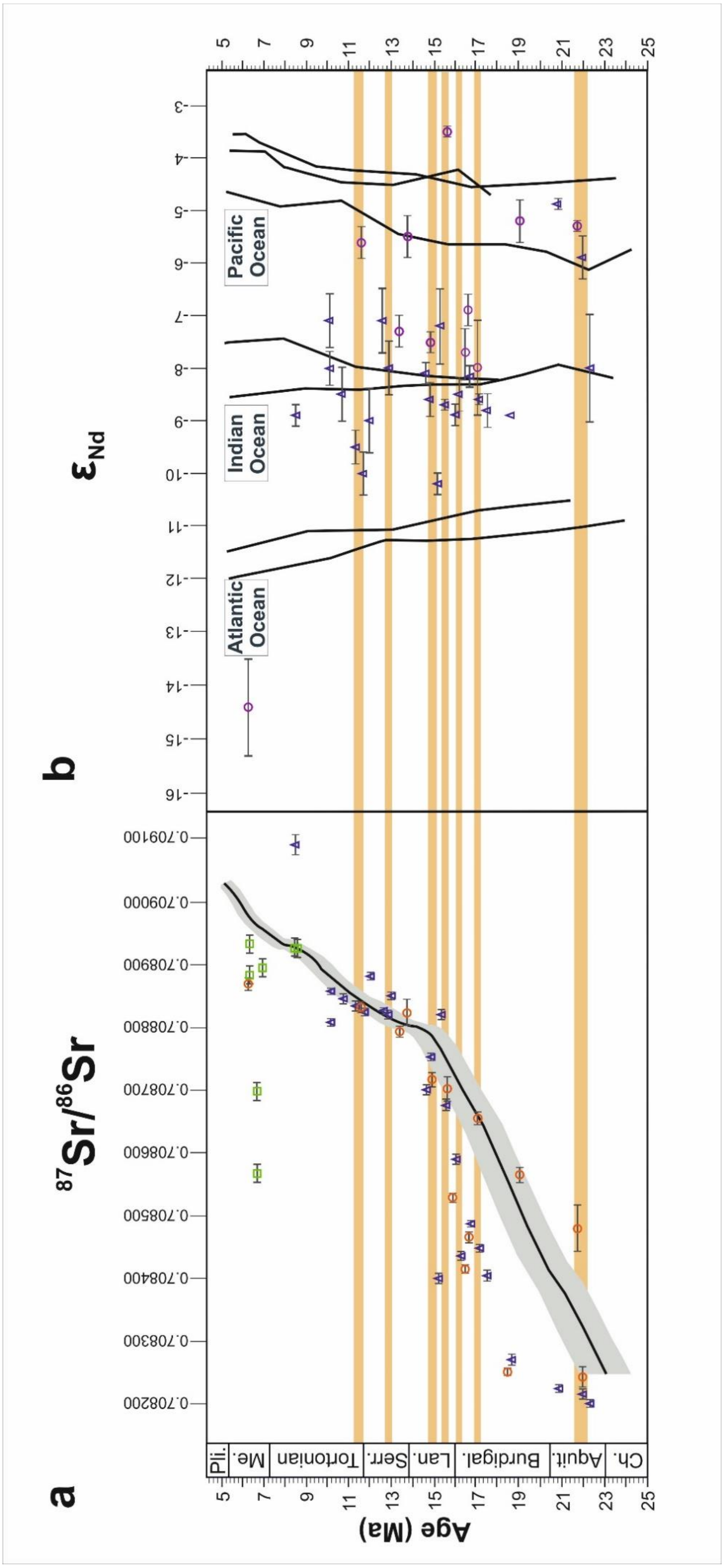

a
b
87Sr/86Sr
εNd
Age (Ma)
Pacific Ocean
Indian Ocean
Atlantic Ocean
Pli.
Me.
Tortonian
Serr.
Lan.
Burdigal.
Aquit.
Ch.

Fig. 4.4. a: Compilation of the Sr isotope data from this work (orange circles) plotted against age. The green squares are Sr isotope data from Cornacchia et al. (2017); the blue triangles are the Sr isotope composition of mixed fossils from Kocsis et al. (2008). The Sr isotope reference line is from McArthur and Howarth (2004). b: Compilation of Nd isotope data from this work (purple circles, in ε notation) plotted against age. The blue triangles are the Nd isotope data of mixed fossils from Kocsis et al. (2008). The reference line for Atlantic, Indian and Pacific Oceans are from O'Nions et al. (1998). Orange bars represent radiometrically dated volcaniclastic layers. The ages of the volcaniclastic levels are from (Montanari et al., 1997a; 1997b; Deino et al., 1997; Mader et al., 2001).

Bisciaro volcaniclastic deposits (Montanari et al., 1994), but Guerrera et al. (2015) proposed the southern margin of the Mesomediterranean plate (Rifian and Kabilian areas) as the source region. The volcanic activity also affected the shallow-water sedimentation where siliceous deposits rich in sponge spicules accumulated in the outer ramp of Apennine domain platforms (Brandano and Corda, 2011)

On the contrary, at 17 Ma, Sr isotope values fall within the global reference line of McArthur and Howart (2004), potentially due to a major sea level rise (Pekar and De Conto, 2006; De Boer et al., 2010) that favoured influx of Indian Ocean waters, as confirmed by the Nd isotope record (Fig. 4.4a; 4.6d).

The Burdigalian Nd signal indicates that the Mediterranean was still mainly connected with the Indo-Pacific Ocean (Fig. 4.4b; 4.5b). The modern Mediterranean Sea has a Nd isotope signature of ε_{Nd} -9.4 (Spivack and Wasserburg, 1988), whereas the Pacific Ocean is characterized by significantly higher ε_{Nd} values. The Burdigalian Nd isotope record of the Central Mediterranean falls within a mixing line between the Mediterranean and the Pacific Nd signatures as end members. Furthermore, it shows a great similarity with the Indian Ocean Nd isotope signatures, indicating that the major water mass entered the Mediterranean by the Indian Gateway (de la Vara et al., 2013). However, during the Burdigalian, the Indian Gateway narrowed and became progressively shallower due to the complex tectonic interplay between the Arabia and Eurasia plates. The Indo-Pacific connection closed for the first time during late Burdigalian and reopened at least two times during middle Miocene prior to its definitive closure in early Serravallian (*Popov et al.,* 2004).

Langhian-Serravallian (15.97-11.63 Ma)

The Langhian-Serravallian Sr isotope record indicates a Central Mediterranean water mass well connected with the Atlantic Ocean, with the Mediterranean Sr isotope values fitting the global curve of McArthur and Howarth (2004). The Nd isotope record remains significantly more radiogenic than the modern Mediterranean signature, suggesting an open connection with the Paratethys. During major sea level rise of the Mid Miocene Climate Optimum (Fig. 4.6b; 4.6d) (Flower et al., 1999; Zachos et al., 2001; 2008), the shallow Carpathian connection between the Central Mediterranean and the Paratethys may have affected the Mediterranean water body (Fig. 4.5c). Kocsis et al. (2009) report an average Nd isotope signature of the Paratethys between early and middle Miocene spanning from ε_{Nd} -9.0 to -4.8, with an average value of ε_{Nd} -7.0, exactly comparable with our Mediterranean middle Miocene Nd isotope record.

Tortonian-Messinian (11.63-5.333 Ma)

Sr and Nd isotope records document a Mediterranean well connected with the Atlantic Ocean during the Tortonian, whereas there was a progressive onset of restricted conditions in the Central Mediterranean sub-

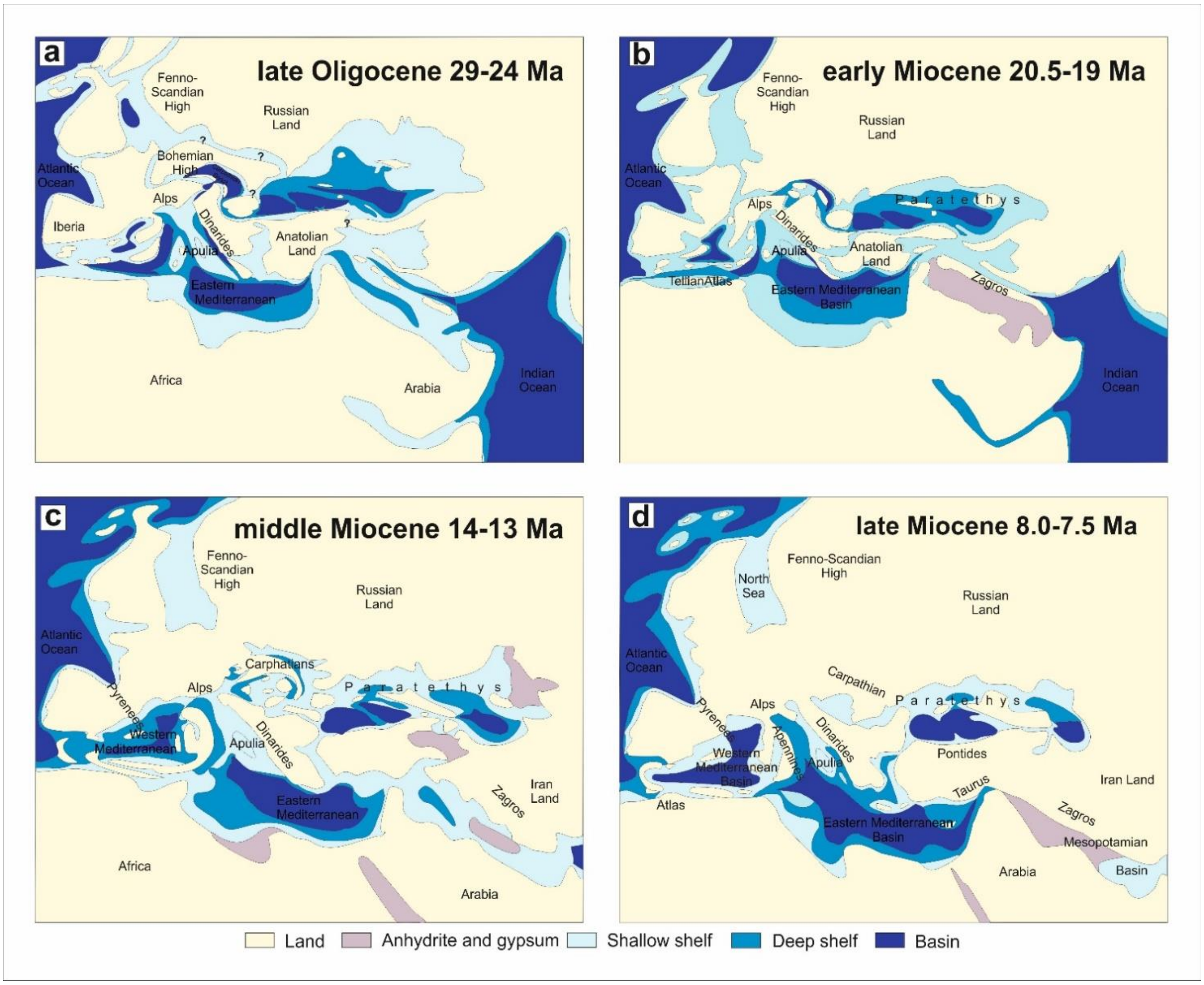

Fig.4.5: Simplified paleogeographic maps of the Mediterranean area (modified from Popov et al., 2004). a: schematic paleogeographic map of the Mediterranean area during Chattian. b: schematic paleogeographic map of the Mediterranean area during Burdigalian. c: schematic paleogeographic map of the Mediterranean area during Serravallian. d: schematic paleogeographic map of the Mediterranean area during Tortonian.

basins during the early Messinian. The Tortonian Sr isotope signature of the Central Mediterranean falls within the global reference line, indicating that the connection with the Atlantic Ocean was open (Fig. 4.4a). In contrast, the Messinian Sr isotope record indicates that a restricted water circulation developed within the proto-Adriatic basin, since the $^{87}Sr/^{86}Sr$ ratio is significantly lower than the global one (Fig. 4.4a). This mismatch has been observed in the Apulia Platform succession not only in the *T. multiloba* Marls, but also in the underlying unit of the *Lithothamnion* Limestones (upper Tortonian-lower Messinian) in lower Messinian sediment, dating from significantly before the Messinian salinity crisis (Fig. 4.4a) (Cornacchia et al., 2017). The authors have interpreted this deviation as due to the onset of a restricted water circulation in the elongated and narrow Adriatic basin (Fig. 4.5d). The restricted water exchanges, associated with an increased continental derived-runoff due to the migration of the Apennine accretionary wedge, led to the lowering of the Sr isotope values. Comparing the upper Tortonian-lower

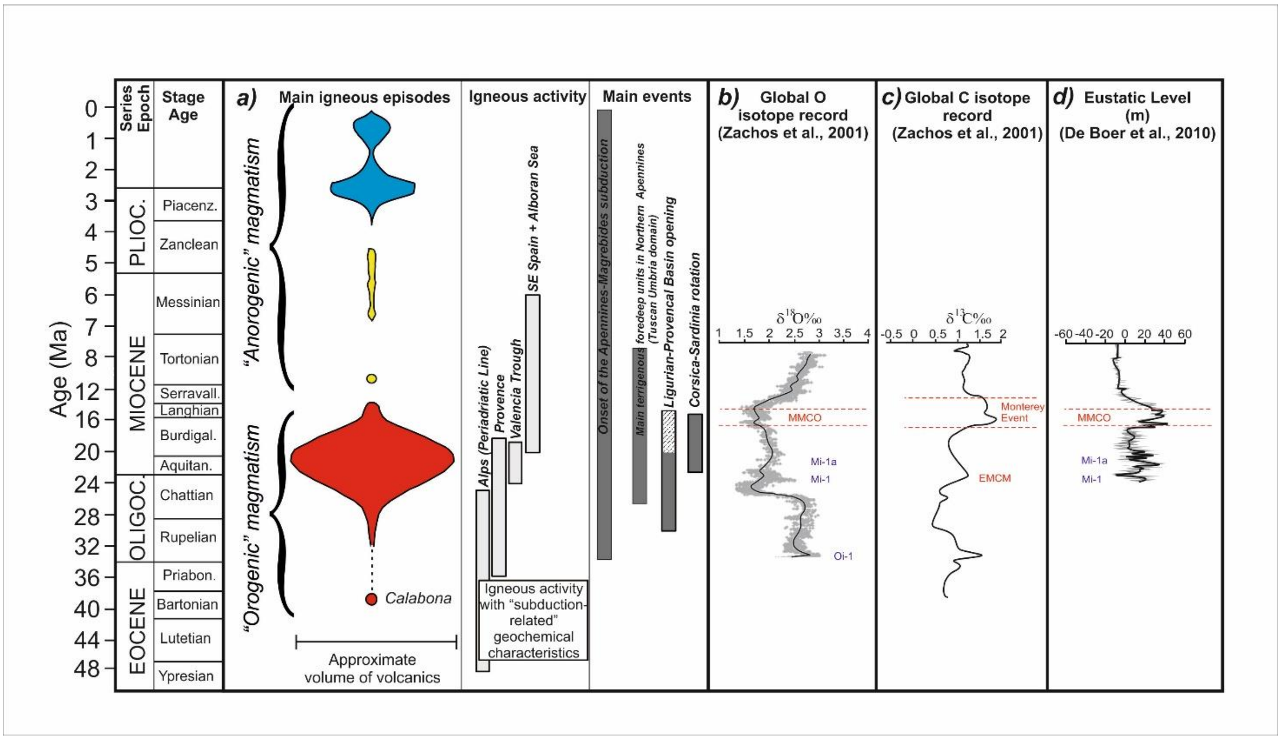

Fig. 4.6. Chrono-diagram showing the correlation between regional and global events during the Eocene-Recent time interval. a: qualitative volumes of the subduction–related and anorogenic type volcanism developed within the Central-Western Mediterranean area during the late Eocene-Recent time interval, correlated with the main igneous activity and geodynamic related events occurring in the studied area (modified after Lustrino et al., 2009). b: Global $\delta^{18}O$ isotope record of the Oligocene-Miocene time interval (modified after Zachos et al., 2001); MMCO= Mid Miocene Climatic Optimum. c: Global $\delta^{13}C$ isotope record of the Oligocene-Miocene time interval (modified after Zachos et al., 2001). EMCM= Early Miocene Carbon Maximum. d: Eustatic Sea level record during Miocene (modified from De Boer et al., 2010).

Messinian Sr isotope record of different Mediterranean sub-basins (the northern and the eastern marginal basins), Flecker and Ellam (2006) inferred that only 50% of the water of the proto-Adriatic sub-basin came from the Atlantic Ocean, the other 50% from riverine input; the salinity remained marine due to strong evaporation. On a global scale continental runoff raises $^{87}Sr/^{86}Sr$ ocean isotope ratios, but within the Mediterranean basin the opposite occurs because rivers that drain mostly Mesozoic shallow-water carbonates successions with lower $^{87}Sr/^{86}Sr$ ratios than the late Miocene mean ones (Topper et al., 2011), together with sedimentary formations containing a significant amount of volcanoclastic component (e.g. Mattioli et al., 2012). Thus, in the elongated Adriatic basin, the increased freshwater input and runoff related to the eastward migration of the Apennine accretionary wedge lowered the Sr isotope ratio compared to the Atlantic Ocean–and Central Mediterranean waters.

The Messinian Nd isotope record shows a strong affinity with that of the Atlantic Ocean, indicating the presence of enhanced Atlantic influx into the Mediterranean basin. However, the proto-Adriatic ε_{Nd} value falls below the Atlantic reference line (O'Nions et al., 1998) due to the influence of fresh-water input from the hinterland in this restricted sub-basin.

In conclusion, the long-term trend of the Sr and Nd isotope records of Miocene Central

Mediterranean carbonate successions shows the shift from a large Mediterranean water body mainly influenced by the Indo-Pacific Ocean during the early Miocene to an enhanced influence of the Atlantic waters during the late Miocene. However, on shorter timescales, the regional geodynamic evolution strongly affected the Central Mediterranean water body and its sub-basins, leading to deviations of the Mediterranean Sr isotope signals from the global ocean signature.

The Mediterranean Sr isotope signal was affected by isolation of the basin related to sea level low-stand phases and/or paleogeographic changes. In the first case, the signal is affected by increased continental runoff (late Aquitanian and early Messinian) and by volcanism during isolation of the basin from the adjacent oceans (Burdigalian).

The overall discrepancy in the Nd data of the Mediterranean and the surrounding oceans reflects the very nature of the Mediterranean, which has always been a distinct basin between the Atlantic Ocean and the Indo-Pacific Ocean. Since the Late Cretaceous, and mostly from the late Eocene on, the relative motion of Africa and Iberia towards Europe controlled the shape of the Mediterranean (Rosenbaum et al., 2002). Furthermore, the occurrence of only hemipelagic deposits, and not open-ocean successions, proves how the proximity of the land is a major controlling factor on Mediterranean waters. Thus, the Nd isotope record of Mediterranean waters was never the same as the open ocean signature, but always be a mix of two opposite signals: the main circulation patterns and the local geodynamic evolution. However, the comparison of the local Nd isotope signal with the open ocean curves yields the information on which ocean mainly affected Mediterranean waters during the different stages of its evolution.

4.6 Conclusions

The Sr isotope data here presented indicate that the dynamic evolution of the Mediterranean area during the Miocene unequivocally controlled seawater chemistry. The critical intervals are the late Aquitanian, middle to late Burdigalian, and the Messinian. During the late Aquitanian (21.8 Ma), a low-sea level phase related to glacial maxima led to an increased continental derived runoff due to an enhanced weathering affecting the $^{87}Sr/^{86}Sr$ isotope signature of Mediterranean seawater. The Burdigalian (18.5-15.9 Ma) Sr isotope record is significantly lighter than the contemporary global ocean signal, showing that the highly explosive subduction-related volcanism in the circum-Mediterranean area was the main controlling factor on Central Mediterranean water chemistry during a progressive isolation of the Mediterranean basin. During the late Miocene the Mediterranean sub-basins, e.g. the proto-Adriatic basin, suffered restricted water conditions due to the elongated and shallow physiography of this basin, and accordingly, the Sr isotopes fell below the global reference line. In contrast, the long-term Nd isotopes trend approximates the transition from a wide-open basin, where the major water mass was mainly controlled by the Indo-Pacific Ocean, to the modern closed basin connected only with the Atlantic Ocean. The Nd isotope record testifies the major water mass flow from the deep Indian Gateway, and the Indo-Pacific Ocean mainly controlled the Central Mediterranean water body. The Nd isotope record indicates that the open connection with the Paratethys significantly influenced the Mediterranean waters in the middle Miocene, in particular during the sea level high-stand related to the Mid Miocene Climatic Optimum. There was a volcanic influence on

Nd isotope signature during the Aquitanian, when northern Indian Ocean waters affected by Cenozoic volcanism entered in the Mediterranean while the volcanism of Western Mediterranean area was active.

Lastly, the early Messinian Nd data are coherent with the Sr isotope record, confirming an influence of Atlantic waters partly contaminated by local freshwater input. In this context, increased freshwater input and continental derived runoff, enhanced by the eastward migration of the Apennine accretionary wedge, mainly controlled this sub-basin's water chemistry.

Lastly, the Nd isotope signature of the Mediterranean with respect to the surrounding oceans reflects the physiographic characters of the Mediterranean area, which evolved following the relative motion of Africa and Iberia towards Europe. The relatively short distance between continents strongly influenced the Nd isotope record. The Mediterranean records never were the same as the open ocean records, but always were a mix of signals from the adjacent oceans influenced by the main circulation patterns and the local geodynamic evolution with related volcanism.

AKNOWLEDGMENTS

Comments and criticisms from the Editor in Chief Ellen Thomas, Fabrizio Lirer and an anonymous reviewer were much appreciated and significantly improved this paper. Useful discussions with Michele Lustrino on Mediterranean volcanism were much appreciated. The research leading to this paper has been funded by Sapienza, University of Rome (Avvio alla Ricerca Project 2016 to Irene Cornacchia; Ateneo project 2016 to Marco Brandano; and by IGC-CNR to Samuele Agostini). Laura Tomassetti is sincerely thanked for the valuable help in the field. Giovanni Gaglianone and Paolo Di Giuseppe support in sedimentology and geochemistry laboratories was highly appreciated. All the data are reported in Tab. 4.1 and Tab. 4.2 and in the main text.

REFERENCES

Azizi, H. and **Moinevaziri, H.** (2009). Review of the tectonic setting of Cretaceous to Quaternary volcanism in northwestern Iran. *J. Geodyn.,* 47, 167-179.

Bertram, C. J. and **Elderfield, H.** (1993). The geochemical balance of the rare earth elements and neodymium isotopes in the oceans. *Geochim. Cosmochim. Acta,* 57, 1957-1986.

Blow, W. H. (1969). Late Middle Eocene to Recent planktonic foraminiferal biostratigraphy. In *Proceedings of the first international conference on planktonic microfossils*, 1, 199-422. EJ Brill, Leiden.

Brand, U. and **Veizer, J.** (1980). Chemical diagenesis of a multicomponent carbonate system-1: Trace elements, *J. Sed. Res.,* 50, 1219-1236.

Brandano, M. and **Corda, L.** (2011). The Lower Miocene spongolitic sequence of the Central Apennines: a record of the Burdigalian siliceous event in the Central Mediterranean. *Annalen des Naturhistorischen Museums in Wien. Serie A für Mineralogie und Petrographie, Geologie und Paläontologie, Anthropologie und Prähistorie*, 145-166.

Brandano, M. and **Policicchio, G.** (2012). Strontium stratigraphy of the Burdigalian transgression in the Western Mediterranean. *Lethaia,* 45, 315-328.

Brandano, M., Lipparini, L., Campagnoni, V. and **Tomassetti, L.** (2012). Downslope-migrating large dunes in the Chattian carbonate ramp of the Majella Mountains (Central Apennines, Italy). *Sed. Geol.,* 255, 29-41.

Brandano, M., Lustrino, M., Cornacchia, I. and **Sprovieri, M.** (2015). Global and regional factors responsible for the drowning of the Central Apennine Chattian carbonate platforms. *Geological Journal,* 50, 575-591.

Brandano, M., Cornacchia, I., Raffi, I. and **Tomassetti, L.** (2016a). The Oligocene–Miocene stratigraphic evolution of the Majella carbonate platform (Central Apennines, Italy). *Sed. Geol.,* 333, 1-14.

Brandano, M., Tomassetti, L., Sardella, R. and **Tinelli, C.** (2016b), Progressive deterioration of trophic conditions in a carbonate ramp environment: the *Lithothamnion* Limestone, Majella Mountain (Tortonian–early Messinian, central Apennines, Italy). *Palaios,* 31, 125-140.

Brandano, M., Cornacchia, I., Raffi, I., Tomassetti, L. and **Agostini, S.** (2017a). The Monterey Event within the Central Mediterranean area: The shallow-water record. *Sedimentology,* 64, 286-310.

Brandano, M., **Cornacchia, I.** and **Tomassetti, L.** (2017b). Global versus regional influence on the carbonate factories of Oligo-Miocene carbonate platforms in the Mediterranean area, *Mar. Petrol. Geol.,* 87, 188-202.

Brown, S. J. and **Elderfield, H.** (1996), Variations in Mg/Ca and Sr/Ca ratios of planktonic foraminifera caused by postdepositional dissolution: Evidence of shallow Mg-dependent dissolution, *Paleoceanography,* 11(5)*,* 543-551.

Burton, K. W. and **Vance, D.** (2000). Glacial–interglacial variations in the neodymium isotope composition of seawater in the Bay of Bengal recorded by planktonic foraminifera, *Earth Planet. Sci. Lett.,* 176(3)*,* 425-441.

Carminati, E. and **Doglioni, C.** (2005). Mediterranean tectonics. *Encyclopedia of geology,* 2*,* 135-146.

Carminati, E., **Lustrino, M.**, **Cuffaro, M.** and **Doglioni, C.** (2010). Tectonics, magmatism and geodynamics of Italy: what we know and what we imagine. *Journal of the Virtual Explorer,* 36(9)*,* 1-59.

Carminati, E., **Lustrino, M.** and **Doglioni, C.** (2012). Geodynamic evolution of the central and western Mediterranean: Tectonics vs. igneous petrology constraints. *Tectonophysics,* 579*,* 173-192.

Carminati, E., **Corda, L.**, **Mariotti, G.**, **Scifoni, A.** and **Trippetta, F.** (2013). Mesozoic syn-and postrifting evolution of the central Apennines, Italy: the role of triassic evaporites. *The Journal of Geology*, *121*(4), 327-354.

Carnevale, G., **Patacca, E.** and **Scandone, P.** (2011). Field guide to the post-conference excursions (Scontrone, Palena and Montagna della Majella). *RCMNS,* 1-99.

Carpenter, S. J. and **Lohmann, K. C.** (1992). Sr/Mg ratios of modern marine calcite: Empirical indicators of ocean chemistry and precipitation rate. *Geochim. Cosmochim. Acta,* 56(5)*,* 1837-1849.

Coccioni, R. and **Montanari, A.** (1992). The 'Livello Piero della Francesca' in the Umbria-Marche Apennines, Italy: a regional volcaniclastic marker bed at the boundary between the Bisciaro and the Schlier/Marne con Cerrogna formations (Lower Miocene). In: *Volume of Abstracts and Field Trips, Interdisciplinary Geological Conference on the Miocene Epoch with emphasis on the Umbria-Marche sequence (I.U.G.S., Subcommission on Geochronology, Miocene Columbus Project)*, edited by A. Montanari, R. Coccioni and G.S. Odin, Ancona, November 11-15, 1992, pp. 41-42.

Coccioni, R. and **Montanari, A.** (1994), L'orizzonte del Bisciaro. In: *Guide Geologiche Regionali, Appennino umbro-marchigiano*, BE-MA Editrice, pp. 36-38.

Cornacchia, I., **Andersson, P.**, **Agostini, S.**, **Brandano, M.** and **Di Bella, L.** (2017). Strontium Stratigraphy of upper Miocene *Lithothamnion* Limestone in the Majella Mountain (Central Italy) and palaeoenvironmental implications. *Lethaia,* 50(4), 561-575. doi:10.1111/let.12213.

Cosentino, D., **Cipollari, P.**, **Marsili, P.** and **Scrocca, D.** (2010). Geology of the central Apennines: a regional review. *Journal of the Virtual Explorer,* 36(11), 1-37.

Crescenti, U., **Crostella, A.**, **Donzelli, G.** and **Raffi, G.** (1969). Stratigrafia della serie calcarea dal Lias al Miocene nella regione marchigiano abruzzese: Parte II. Litostratigrafia, biostratigrafia, paleogeografia. *Soc. Geol. Ital Mem.,* 9*,* 343–420.

De Boer, B., **Van de Wal, R. S. W.**, **Bintanja, R.**, **Lourens, L. J.** and **Tuenter, E.** (2010). Cenozoic global ice-volume and temperature simulations with 1-D ice-sheet models forced by benthic $\delta^{18}O$ records. *Annals of Glaciology,* 51, 23-33.

Deino, A., **Channell, J.**, **Coccioni, R.**, **De Grandis, G.**, **DePaolo, D. J.**, **Fornaciari, E.**, **Emmanuel, L.**, **Laurenzi, M. A.**, **Montanari, A.**, **Rio, D.** and **Renard, M.** (1997). Integrated stratigraphy of the upper Burdigalian-lowerLanghian section at Moria (Marche region, Italy). In: *Miocene Stratigraphy: An Integrated Approach* (Eds A. Montanari, G.S. Odin and R. Coccioni), pp. 315–341. Elsevier Science B.V, Amsterdam, the Netherlands.

Dela Pierre, F., **Bernardi, E.**, **Cavagna, S.**, **Clari, P.**, **Gennari, R.**, **Irace, A.**, **Lozar, A.**, **Lugli, S.**, **Manzi, V.**, **Natalicchio, M.**, **Roveri, M.** and **Violanti, D.** (2011). The record of the Messinian salinity crisis in the Tertiary Piedmont Basin (NW Italy): the Alba section revisited. *Palaeogeogr., Palaeoclimatol. Palaeoecol.,* 310, 238-255.

de la Vara, A., **Meijer, P. T.** and **Wortel, M. J. R.** (2013). Model study of the circulation of the Miocene Mediterranean Sea and Paratethys: closure of the Indian Gateway. *Climate of the Past Discussions,* 4385-4424.

DePaolo, D. J. and **Wasserburg, G. J.** (1976). Nd isotopic variations and petrogenetic models. *Geophys. Res. Lett.*, 3*,* 249-252.

Dera, G., **Pucéat, E.**, **Pellenard, P. Neige, P.**, **Delsate, D.**, **Joachimski, M. M.**, **Reisberg, L.** and **Martinez, M.** (2009). Water mass exchange and variations in seawater temperature in the NW Tethys during the Early Jurassic: evidence from neodymium and oxygen isotopes of fish teeth and belemnites, *Earth Planet. Sci. Lett.,* 286*,* 198-207.

Di Stefano, A., **Foresi, L. M.**, **Lirer, F.**, **Iaccarino, S. M**, **Turco, E.**, **Amore, F. O.**, **Mazzei, R.**, **Morabito, S.**, **Salvatorini, G.** and **Aziz, H. A.** (2008). Calcareous plankton high resolution bio-magnetostratigraphy for the Langhian of the Mediterranean area. *Riv. Ital. Paleontol. Stratigr.,* 114(1), 51-76.

Di Stefano, A., **Baldassini, N.**, **Maniscalco, R.**, **Speranza, F.**, **Maffione, M.**, **Cascella, A.** and **Foresi, L.M.** (2015). New bio-magnetostratigraphic data on the Miocene Moria section (Northern Apennines, Italy): connections between the Mediterranean region and the North Atlantic Ocean. *Newsl. Stratigr.,* 48*,* 135–152.

Faure, G. (1986). *Principles of isotope geochemistry,* John Wiley and Sons, Chichester.

Flecker, R. and **Ellam, R. M.** (2006). Identifying late Miocene episodes of connection and isolation in the Mediterranean-Paratethyan realm using Sr isotopes. *Sed. Geol.,* 188–189*,* 189–203.

Flower, B. P. (1999). Palaeoclimatology: Warming without high CO_2? *Nature,* 399*,* 313-314.

Föllmi, K. B., Gertsch, B., Renevey, J. P., De Kaenel, E. and **Stille, P.** (2008). Stratigraphy and sedimentology of phosphate-rich sediments in Malta and south-eastern Sicily (latest Oligocene to early Late Miocene). *Sedimentology,* 55, 1029-1051.

Foresi, L. M., Mazzei, R., Salvatorini, G. and **Donia, F.** (2007). Biostratigraphy and chronostratigraphy of the Maltese Lower Globigerina Limestone Member (Globigerina Limestone Formation): new preliminary data based on calcareous plankton. *Bollettino della Società Paleontologica Italiana,* 46(2-3)*,* 175-181.

Frank, M. (2002). Radiogenic isotopes: tracers of past ocean circulation and erosional input. *Rev. Geophys*., 40, 28 pp.

Frijia, G. and **Parente, M.** (2008). Strontium isotope stratigraphy in the upper Cenomanian shallow-water carbonates of the southern Apennines: Short-term perturbations of marine 87 Sr/86 Sr during the oceanic anoxic event 2. *Palaeogeogr. Palaeoclimatol. Palaeoecol.,* 261*,* 15-29.

Frijia, G., Parente, M. Di Lucia, M. and **Mutti, M.** (2015). Carbon and strontium isotope stratigraphy of the Upper Cretaceous (Cenomanian-Campanian) shallow-water carbonates of southern Italy: Chronostratigraphic calibration of larger foraminifera biostratigraphy. *Cretaceous Res., 53,* 110-139.

Frost, C. D., O'Nions, R. K. and **Goldstein, S. L.** (1986). Mass balance for Nd in the Mediterranean Sea. *Chem. Geol.,* 55, 45-50.

Gattacceca, J., Deino, A., Rizzo, R., Jones, D. S., Henry, B. Beaudoin, B. and **Vadeboin, F.** (2007). Miocene rotation of Sardinia: new paleomagnetic and geochronological constraints and geodynamic implications. *Earth Planet. Sci. Lett.,* 258, 359–377.

Gradstein, F.M., Ogg, J.G. and **Smith, A.G.** (2004). *A Geologic Time Scale 2004.* Cambridge University Press, Cambridge, UK. 500 pp.

Goldstein, S. J. and **Jacobsen, S. B.** (1987). The Nd and Sr isotopic systematics of river-water dissolved material: Implications for the sources of Nd and Sr in seawater. *Chemical Geology: Isotope Geoscience section,* 66*,* 245-272.

Gueguen, E., Doglioni, C. and **Fernandez, M.** (1998). On the post-25 Ma geodynamic evolution of the western Mediterranean. *Tectonophysics,* 298*,* 259–269.

Guerrera, F., Tramontana, M., Donatelli, U. and **Serrano, F.** (2012). Space/time tectono-sedimentary evolution of the Umbria-Romagna-Marche Miocene Basin (Northern Apennines, Italy): a foredeep model. *Swiss Journal of Geosciences,* 105(3)*,* 325-341.

Guerrera, F., Martín-Martín, M., Raffaelli, G. and **Tramontana, M.** (2015). The Early Miocene "Bisciaro volcaniclastic event" (northern Apennines, Italy): a key study for the geodynamic evolution of the central-western Mediterranean. *International Journal of Earth Sciences*, 104(4), 1083-1106.

Henderson, G. M. (2002). New oceanic proxies for paleoclimate. *Earth Planet. Sci. Lett.,* 203(1)*,* 1-13.

Harzhauser, M. and **Piller, W. E.** (2007). Benchmark data of a changing sea — palaeogeography, palaeobiogeography and events in the Central Paratethys during the Miocene. *Palaeogeogr. Palaeoclimatol. Palaeoecol.*, 253, 8-31.

Harzhauser, M., Kroh, A., Mandic, O., Piller, W. E., Göhlich, U., Reuter, M. and **Berning, B.** (2007). Biogeographic responses to geodynamics: a key study all around the Oligo–Miocene Tethyan Seaway. *Zoologischer Anzeiger-A Journal of Comparative Zoology*, 246, 241-256.

Hilgen, F. J., Aziz, H. A., Krijgsman, H. W., Raffi, I. and **Turco, E.** (2003). Integrated stratigraphy and astronomical tuning of the Serravallian and lower Tortonian at Monte dei Corvi (Middle–Upper Miocene, northern Italy). *Palaeogeogr. Palaeoclimatol. Palaeoecol.,* 199, 229-264.

Hilgen, F., Aziz, H. A., Bice, D., Iaccarino, S., Krijgsman, W., Kuiper, K., Montanari, A., Raffi, I., Turco, E. and **Zachariasse, W. J.** (2005). The global boundary stratotype section and point (GSSP) of the Tortonian stage (Upper Miocene) at Monte Dei Corvi. *Episodes-Newsmagazine of the International Union of Geological Sciences*, 28, 6-17.

Holbourn, A., Kuhnt, W., Clemens, S., Prell, W. and **Andersen, N.** (2013), Middle to late Miocene stepwise climate cooling: Evidence from a high-resolution deep water isotope curve spanning 8 million years. *Paleoceanography*, 28, 688-699.

Holbourn, A., Kuhnt, W., Kochhann, K. G., Andersen, N. and **Meier, K. S.** (2015). Global perturbation of the carbon cycle at the onset of the Miocene Climatic Optimum. *Geology*, 43, 123-126.

Hüsing, S. K., Hilgen, F. J., Aziz, H. A. and **Krijgsman, W.** (2007). Completing the Neogene geological time scale between 8.5 and 12.5 Ma. *Earth Planet. Sci. Lett.*, 253(3), 340-358.

Hüsing, S. K., Kuiper, K. F., Link, W., Hilgen, F. J. and **Krijgsman, W.** (2009). Monte dei Corvi (Northern Apennines, Italy): a Mediterranean reference section for the Tortonian Stage. *Earth Planet. Sci. Lett.*, 282, 140–157.

Hüsing, S. K., Cascella, A., Hilgen, F. J., Krijgsman, W., Kuiper, K. F., Turco, E. and **Wilson, D.** (2010). Astrochronology of the Mediterranean Langhian between 15.29 and 14.17 Ma. *Earth Planet. Sci. Lett.,* 290(3), 254-269.

Ingram, B. L. and **Sloan, D.** (1992). Strontium isotopic composition of estuarine sediments as paleosalinity-paleoclimate indicator. *Science,* 255*,* 68-72.

Innocenti, F., Manetti, P., Mazzuoli, R., Pasquaré, G. and **Villari, L.** (1982). Anatolia and north-western Iran. In: Thorpe, R.S. (ed.) *Andesites*, John Wiley & Sons, New York, 327-349.

Jeandel, C. (1993). Concentration and isotopic composition of Nd in the South Atlantic Ocean. *Earth Planet. Sci. Lett.,* 117, 581-591.

Kocsis, L., Vennemann, T. W., Fontignie, D., Baumgartner, C. and **Montanari, A.** (2008). Oceanographic and climatic evolution of the Miocene Mediterranean deduced from Nd, Sr, C e O isotope compositions of marine fossils and sediments. *Paleoceanography, 23,* PA4211, doi:10.1029/2007PA001540.

Kocsis, L., Vennemann, T. W., Hegner, E., Fontignie, D. and **Tütken, T.** (2009). Constraints on Miocene oceanography and climate in the Western and Central Paratethys: O-, Sr-, and Nd-isotope compositions of marine fish and mammal remains. *Palaeogeogr. Palaeoclimatol. Palaeoecol.,* 271(1), 117-129.

Kouwenhoven, T.J., Morigi, C., Negri, A., Giunta, S. Krijgsman, W. and **Rouchy, J. M.** (2006). Paleoenvironmental evolution of the eastern Mediterranean during the Messinian: Constraints from integrated microfossil data of the Pissouri Basin (Cyprus). *Mar. Micropaleontol.,* 60*,* 17-44.

Krijgsman, W. and **Meijer, P.T.** (2008). Depositional environments of the Mediterranean "Lower Evaporites" of the Messinian salinity crisis: constraints from quantitative analyses. *Marine Geology*, 253, 73-81.

Iaccarino, S. M., Premoli Silva, I., Biolzi, M., Foresi, L. M., Lirer, F., Turco, E. and **Petrizzo, M. R.** (2007). Practical manual of Neogene planktonic foraminifera, *Biolzi, M., S M. Iaccarino, E., Turco, A., Checconi and R. Rettori (Eds), Perugia : International school on planktonic foraminifera.*

Lear, C. H., Rosenthal, Y., Coxall, H. K. and **Wilson, P. A.** (2004). Late Eocene to early Miocene ice sheet dynamics and the global carbon cycle, *Paleoceanography, 19,* PA4015. doi:10.1029/2004PA001039.

Lirer, F. (2000). A new technique for retrieving calcareous microfossils from lithified lime deposits. *Micropaleontology,*46(4)*,* 365-369.

Lohmann, G. P. (1995). A model for variation in the chemistry of planktonic foraminifera due to secondary calcification and selective dissolution. *Paleoceanography*, 10, 445-457.

Lustrino, M. and **Wilson, M.** (2007). The circum-Mediterranean anorogenic Cenozoic igneous province. *Earth-Sci. Rev.,* 81(1)*,* 1-65.

Lustrino, M., Morra, V., Fedele, L. and **Franciosi, L.** (2009). Beginning of the Apennine subduction system in central western Mediterranean: constraints from Cenozoic "orogenic" magmatic activity of Sardinia, Italy. *Tectonics, 28,* TC5016, doi:10.1029/2008TC002419.

Lustrino, M., Duggen, S. and **Rosenberg, C. L.** (2011). The Central-Western Mediterranean: anomalous igneous activity in an anomalous collisional tectonic setting. *Earth-Sci. Rev.,* 104(1), 1-40.

Mader, D., Montanari, A., Gattacceca, J., Koeberl, C., Handler, R. and **Coccioni, R.** (2001). $^{40}Ar/^{39}Ar$ dating of a Langhian biotite–rich clay layer in the pelagic sequence of the Conero Riviera, Ancona, Italy. *Earth Planet. Sci. Lett.,* 194, 111–126.

Manzi, V., Gennari, R., Hilgen, F., Krijgsman, W., Lugli, S., Roveri, M. and **Sierro, F. J.** (2013), Age refinement of the Messinian salinity crisis onset in the Mediterranean. *Terra Nova*, *25*, 315-322.

Martin, P. A., Lea, D. W., Mashiotta, T. A., Papenfuss, T., and **Sarnthein, M.** (1999). Variation of foraminiferal Sr/Ca over Quaternary glacial-interglacial cycles: Evidence for changes in mean ocean Sr/Ca?. *Geochemistry, Geophysics, Geosystems*, *1*(12).

Martín, J. M., Braga, J. C., Aguirre, J. and **Puga-Bernabéu, Á.** (2009). History and evolution of the North-Betic Strait (Prebetic Zone, Betic Cordillera): a narrow, early Tortonian, tidal-dominated, Atlantic–Mediterranean marine passage. *Sed. Geol.,* 216*,* 80-90.

Martini, E. (1971). Standard Tertiary and Quaternary calcareous nannoplankton zonation. In: Farinacci, A. (Ed.), Proceedings 2nd International Conference Planktonic Microfossils Roma: Rome (Ed. Tecnosci.) 2, 739–785.

Mattioli, M., Lustrino, M., Ronca, S. and **Bianchini, G.** (2012). Alpine subduction imprint in Apennine volcaniclastic rocks. Geochemical–petrographic constraints and geodynamic implications from Early Oligocene Aveto-Petrignacola Formation (N Italy). *Lithos,* 134-135, 201-220.

McArthur, J. M. (1994). Recent trends in strontium isotope stratigraphy. *Terra Nova,* 6*,* 331-358.

McArthur, J.M. and **Howarth, R. J.** (2004), Strontium isotope stratigraphy. In: A *Geologic Time Scale* (Gradstein, F., Ogg, J., Smith, A. eds), Cambridge University Press, Cambridge, 96-105.

McArthur, J. M., Howarth, R. J. and **Bailey, T. R.** (2001). Strontium isotope stratigraphy: LOWESS version 3: best fit to the marine Sr-isotope curve for 0–509 Ma and accompanying look-up table for deriving numerical age, *The Journal of Geology,* 109*,* 155-170.

McArthur, J.M., Howarth, R. J. and **Schields, G. A.** (2012). Strontium Isotope Stratigraphy, In: *The Geologic Time Scale 2012*. Gradstein F.M., Ogg J.G., Schmitz M.D., Ogg G.M. (eds). Elsevier: Amsterdam, 207-232.

Miller, K. G., Wright, J. D. and **Fairbanks, R. G.** (1991). Unlocking the ice house: Oligocene-Miocene oxygen isotopes, eustasy, and margin erosion, *Journal of Geophysical Research: Solid Earth,* 96(B4)*,* 6829-6848.

Montanari, A., Carey, S., Coccioni, R. and **Deino, A.** (1994). Early Miocene in the Apennine pelagic sequence: An inferred Sardinian provenance and implications for western Mediterranean tectonics. *Tectonics,* 13*,* 1120-1134.

Montanari, A., Beaudoin, B., Chan, L. S., Coccioni, R. Deino, A., DePaolo, D. J., Emmanuel, L., Fornaciari, E., Kruge, M., Lundblad, S., Mozzato, C., Portier, E,. Renard, M., Rio, D., Sandroni, P. and **Stankiewicz, A.** (1997b). Integrated stratigraphy of the middle to upper Miocene pelagic sequence of Conero Riviera (Marche region, Italy), In: *Miocene Stratigraphy: An Integrated Approach* (Eds A. Montanari, G.S. Odin and R.

Coccioni), pp. 410–450. Elsevier Science B.V, Amsterdam, the Netherlands.

Montanari, A., Bice, D. M., Capo, R. Coccioni, R., Deino, A., DePaolo, D.J., Emmanuel, L., Monechi, S. Renard, M. and **Zevenboom, D.** (1997a). Integrated stratigraphy of the Chattian to Mid-Burdigalian pelagic sequence of the Contessa Valley (Gubbio, Italy). In: *Miocene Stratigraphy: An Integrated Approach* (Eds A. Montanari, G.S. Odin and R. Coccioni), pp. 249-277. Elsevier Science B.V, Amsterdam, the Netherlands.

Morse, J.W. and **Mackenzie, F. T.** (1990). Geochemistry of sedimentary carbonates. In: *Developments in Sedimentology, 48,* 707 pp. Elsevier, Amsterdam.

Mutti, M., Bernoulli, D. and **Stille, P.** (1997). Temperate carbonate platform drowning linked to Miocene oceanographic events: Maiella platform margin, Italy, *Terra Nova, 9,* 122–125.

Mutti, M., Droxler, A. W. and **Cunningham, A. D.** (2005). Evolution of the Northern Nicaragua Rise during the Oligocene–Miocene: drowning by environmental factors. *Sed. Geol.*, 175(1), 237-258.

O'nions, R. K., Frank, M., Von Blanckenburg, F. and **Ling, H. F.** (1998). Secular variation of Nd and Pb isotopes in ferromanganese crusts from the Atlantic, Indian and Pacific Oceans. *Earth Planet. Sci. Lett.,* 155(1), 15-28.

Palmer, M. R. and **Edmond, J. M.** (1989). The strontium isotope budget of the modern ocean. *Earth Planet. Sci. Lett., 92,* 11-26.

Palmer, M. R. and **Elderfield, H.** (1985). Variations in the Nd isotopic composition of foraminifera from Atlantic Ocean sediments. *Earth Planet. Sci. Lett.,* 73(2-4)*,* 299-305.

Patacca, E. and **Scandone, P.** (2007). Geology of the southern Apennines. *Boll. Soc. Geol. Ital., 7,* 75-119.

Patacca, E., Scandone, P., Di Luzio, E., Cavinato, G. P. and **Parotto, M.** (2008). Structural architecture of the central Apennines: Interpretation of the CROP 11 seismic profile from the Adriatic coast to the orographic divide. *Tectonics, 27,* TC3006, doi:10.1029/2005TC001917.

Paul, H. A., Zachos, J. C., Flower, B. P. and **Tripati, A.** (2000). Orbitally induced climate and geochemical variability across the Oligocene/Miocene boundary. *Paleoceanography,* 15(5), 471-485.

Pekar, S. F. and **DeConto, R. M.** (2006). High-resolution ice-volume estimates for the early Miocene: Evidence for a dynamic ice sheet in Antarctica. *Palaeogeogr. Palaeoclimatol. Palaeoecol.,* 231(1), 101-109.

Piepgras, D. J. and **Wasserburg, G. J.** (1980). Neodymium isotopic variations in seawater. *Earth and Planetary Science Letters*, 50(1), 128-138.

Piepgras, D. J. and **Wasserburg, G. J.** (1987). Rare earth element transport in the western North Atlantic inferred from Nd isotopic observations. *Geochim. Cosmochim. Acta,* 51*,* 1257-1271.

Piepgras, D. J. and **Jacobsen, S. B.** (1988). The isotopic composition of neodymium in the North Pacific, *Geochim. Cosmochim. Acta,* 52, 1373-1381.

Pomiès, C., Davies, G.R. and **Conan, S. M. H.** (2002). Neodymium in modern foraminifera from the Indian Ocean: implications for the use of foraminiferal Nd isotope compositions in paleo-oceanography. *Earth Planet. Sci. Lett.*, 203, 1031-1045.

Popov, S. V., Rögl, F., Rozanov, A. Y., Steininger, F. F., Shcherba, I. G. and **Kovac, M.** (2004). Lithological-Paleogeographic maps of Paratethys. Late Eocene to Pliocene. *Courier Forschungsinstitut Senckenberg, 250,* pp. 46, maps 1-10 (annex).

Pucéat, E., Lécuyer, C. and **Reisberg, L.** (2005). Neodymium isotope evolution of NW Tethyan upper ocean waters throughout the Cretaceous. *Earth Planet. Sci. Lett., 236,* 705-720.

Raffi, I., Mozzato, C., Fornaciari, E., Hilgen, F. J. and **Rio, D.** (2003). Late Miocene calcareous nannofossil biostratigraphy and astrobiochronology for the Mediterranean region. *Micropaleontology*, *49*, 1-26.

Rögl, F. (1999). Mediterranean and Paratethys. Facts and hypotheses of an Oligocene to Miocene paleogeography (short overview). *Geol. Carpath.,* 50, 339–349.

Rosenbaum, G., Lister, G. S. and **Duboz, C.** (2002). Relative motions of Africa, Iberia and Europe during Alpine orogeny. *Tectonophysics*, 359, 117-129.

Roveri, M., Lugli, S., Manzi, V., Gennari, R. and **Schreiber, B. C.** (2014). High-resolution strontium isotope stratigraphy of the Messinian deep Mediterranean basins: Implications for marginal to central basins correlation. *Marine Geology*, *349*, 113-125.

Sant, K., Kirscher, U., Reichenbacher, B., Pippèrr, M., Jung, D., Doppler, G. and **Krijgsman, W.** (2017). Late Burdigalian sea retreat from the North Alpine Foreland Basin: new magnetostratigraphic age constraints. *Global and Planetary Change*, 152, 38-50.

Shackleton, N. J., Crowhurst, S. J., Weedon, J.P and **Laskar, J.** (1999). Astronomical calibration of Oligocene--Miocene time. *Philosophical Transactions of the Royal Society of London A: Mathematical, Physical and Engineering Sciences*, 357, 1907-1929.

Scher, H. D. and **Martin, E. E.** (2008). Oligocene deep water export from the North Atlantic and the development of the Antarctic Circumpolar Current examined with neodymium isotopes. *Paleoceanography, 23*, PA1205, doi:10.1029/2006PA001400.

Schildgen, T. F., Cosentino, D., Frijia, G., Castorina, F. Ö. Dudas, F., Iadanza, A., Sampalmieri, G., Cipollari, P., Caruso, A. and **Strecker, M. R.** (2014). Sea level and climate forcing of the Sr isotope composition of late Miocene Mediterranean marine basins. *Geochem. Geophys. Geosyst.*, 15, 2964-2983.

Sierro, F. J., Flores, J. A., Francés, G., Vazquez, A., Utrilla, R., Zamarreño, I., Herlenkeuser H. and **Barcena, M. A.** (2003). Orbitally-controlled oscillations in planktic communities and cyclic changes in western Mediterranean hydrography during the Messinian. *Palaeogeogr. Palaeoclimatol. Palaeoecol.*, *190*, 289-316.

Spivack, A. J. and **Wasserburg, G. J.** (1988). Neodymium isotopic composition of the Mediterranean outflow and the eastern North Atlantic. *Geochim. Cosmochim. Acta,* 52, 2767-2773.

Sprovieri, R., Di Stefano, E., and **Sprovieri, M.** (1996). High resolution chronology for Late Miocene Mediterranean stratigraphic events. *Rivista Italiana di Paleontologia e Stratigrafia, 102*, 77-104.

Steuber, T. (1999). Isotopic and chemical intra-shell variations in low-Mg calcite of rudist bivalves (Mollusca-Hippuritacea): disequilibrium fractionations and late Cretaceous seasonality. *International Journal of Earth Sciences*, 88, 551-570.

Stille, P., Steinmann, M. and **Riggs, S. R.** (1996). Nd isotope evidence for the evolution of the paleocurrents in the Atlantic and Tethys Oceans during the past 180 Ma. *Earth Planet. Sci. Lett.,* 144, 9-19.

Tachikawa, K., Jeandel, C. and **Roy-Barman, M.** (1999). A new approach to the Nd residence time in the ocean: the role of atmospheric inputs. *Earth Planet. Sci. Lett.,* 170, 433-446.

Taylor, A. S. and **Lasaga, A. C.** (1999), The role of basalt weathering in the Sr isotope budget of the oceans. *Chem. Geol.,* 161, 199-214.

Topper, R. P. M., Flecker, R., Meijer, P. T. and **Wortel, M. J. R.** (2011). A box model of the Late Miocene Mediterranean Sea: Implications from combined 87Sr/86Sr and salinity data. *Paleoceanography,* 26, PA3223, doi:10.1029/2010PA002063.

Vance, D., Scrivner, A. E., Beney, P., Staubwasser, M., Henderson, G. M. and **Slowey, N. C.** (2004). The use of foraminifera as a record of the past neodymium isotope composition of seawater. *Paleoceanography*, 19, PA2009, doi:10.1029/2003PA000957.

Vecsei, A., Sanders, D. G. K., Bernoulli, D., Eberli, G. P. and **Pignatti, J.** (1998). Cretaceous to Miocene sequence stratigraphy and evolution of the Maiella carbonate platform margin, Italy. In: *Mesozoic and Cenozoic Sequence Stratigraphy of European Basins, SEPM Special Publication, 60,* 53-74.

Veizer, J., Ala, D., Azmy, K., Bruckschen, P., Buhl, D., Bruhn, F. Carden, G. A. F., Diener, A., Ebneth, S., Godderis, Y., Jasper, T., Korte, C., Pawellek, F., Podlaha, O.G. and **Strauss, H.** (1999). $^{87}Sr/^{86}Sr$, $\delta^{13}C$ and $\delta^{18}O$ evolution of Phanerozoic seawater. *Chem. Geol.,* 161(1), 59-88.

Veizer, J., Buhl, D., Diener, A., Ebneth, S., Podlaha, O. G., Bruckschen, P., Jasper, T., Korte, C., Schaaf, M., Ala, D. and **Azmy, K.** (1997). Strontium isotope stratigraphy: potential resolution and event correlation. *Palaeogeogr. Palaeoclimatol. Palaeoecol.,* 132(1), 65-77.

Vezzani, L., Festa, A. and **Ghisetti, F. C.** (2010). Geology and tectonic evolution of the Central-Southern Apennines, *Italy. Geol. Soc. Am. Spec. Pap.,* 469, 1-58.

Wade, B. S., Pearson, P. N., Berggren, W.A. and **Pälike, H.** (2011). Review and revision of Cenozoic tropical planktonic foraminiferal biostratigraphy and calibration to the geomagnetic polarity and astronomical time scale, *Earth-Science Reviews*, 104, 111-142.

Weissert, H., Joachimski, M. and **Sarnthein, M. (**2008), Chemostratigraphy. *Newsl. Stratigr.,* 42(3), 145-179.

Woodruff, F. and **Savin., S.** (1991). Mid-Miocene isotope stratigraphy in the deep sea: high resolution correlations, paleoclimatic cycles, and sediment preservation. *Paleoceanography,* 6, 755–806.

Zachos, J., Pagani, M., Sloan, L., Thomas, E. and **Billups, K.** (2001). Trends, rhythms, and aberrations in global climate 65 Ma to present. *Science,* 292*,* 686-693.

Zachos, J. C., Dickens, G. R. and **Zeebe, R. E.** (2008). An early Cenozoic perspective on greenhouse warming and carbon-cycle dynamics. *Nature,* 451, 279-283.

5 Sr isotope stratigraphy of the upper Miocene *Lithothamnion* Limestone in the Majella Mountain, central Italy, and its paleoenvironmental implications

Irene Cornacchia[1], Per Andersson[2], Samuele Agostini[3], Marco Brandano[1], Letizia Di Bella[1]

1: *Dipartimento di Scienze della Terra, Sapienza Università di Roma, P. Aldo Moro 5, I-00185 Roma, (Italy).*

2: *Department of Geosciences Swedish Museum of Natural History, Box 50 007 SE-104 05 Stockholm (Sweden).*

3: *Istituto di Geoscienze e Georisorse (IGG) CNR, Via Moruzzi 1, 56124 Pisa (Italy).*

Published in *Lethaia* (2017), 50, 561-575.

Abstract

The $^{87}Sr/^{86}Sr$ isotope ratio has been widely used as a physical tool to date and correlate carbonate successions due to the long Sr residence time in comparison to the ocean mixing time. If this method works on oceanic successions, marginal basins may show different Sr isotope records in comparison to the coeval ocean one due to sea level variations, continental runoff and restricted water exchanges. In this work we present the $^{87}Sr/^{86}Sr$ isotope record of the upper Miocene carbonate ramp of the *Lithothamnion* Limestone (Majella Mountain, Central Apennines), as an example of the onset of restricted water exchanges between a marginal basin and the ocean water masses. The overall latemost Tortonian-early Messinian Sr isotope record of the *Lithothamnion* Limestone fits below the global reference line. This deviation has been interpreted as due to the strong control that fresh water input and enhanced continental runoff, linked to the migration of the Apennine accretionary wedge and foredeep system, have had on the central Adriatic water chemistry. These results imply that an accurate oceanographic and geodynamic framework along with diagenetic overprint investigation has to be taken into consideration prior to apply SIS on carbonate successions on marginal basins, even when facies analyses indicate fully marine conditions. This seems to be the case for the upper Miocene Central Mediterranean carbonate successions, but may have more general validity and be extended to other recent or past marginal basins.

5.1 Introduction

Strontium isotope ratios have been widely used during the last thirty years to date and correlate carbonate successions (e.g. Burke et al., 1982; De Paolo and Ingram, 1985; McArthur, 1994; Howart and McArthur, 1997; Mcarthur et al., 2001; 2012; Frijia and Parente, 2008; Brandano and Policicchio, 2012). This is because the Sr isotope ratio within the oceans has varied over geological time. The $^{87}Sr/^{86}Sr$ in sea water is mainly controlled by two different fluxes: continental weathering and ocean floor hydrothermal exchange and volcanism (Faure, 1986; Palmer and Edmond, 1989; Taylor and Lasaga, 1999). The first controlling factor tends to increase the $^{87}Sr/^{86}Sr$ ratio, while volcanism enters into the oceans huge amounts of light ^{86}Sr, lowering the overall Sr isotope signal. The Strontium Isotope Stratigraphy (SIS) lies on the assumption that the $^{87}Sr/^{86}Sr$ into the oceans has always been homogeneous on a geological time scale since the residence time of Sr into the ocean waters is ~10^6 years, thus much longer that the ocean mixing time, which is in the order of 10^3 years. Relying on these assumptions, a global reference curve of the $^{87}Sr/^{86}Sr$ isotope ratios has been reported for the Phanerozoic (McArthur et al., 2001; 2012), and calibrated with biostratigraphy and magnetostratigraphy, or other stratigraphic tools. Thus, the comparison between the measured $^{87}Sr/^{86}Sr$ values of a sample and the calibrated curve yields an age for the sample.

However, if this method can work in ocean settings, it has become evident that within marginal basins the values of $^{87}Sr/^{86}Sr$ ratio can significantly differ from the coeval global means, due to variable influences of fresh waters, continental run off, salinity changes and, eventually, local volcanism.

Analysing the Sr isotope record of the late Pleistocene succession of the San Francisco Bay estuary, Ingram and Sloan (1992) noted how it differed from the global Sr isotope ratio during sea-level lowstands and interpreted this difference as due to significant water salinity changes controlled by an increased fresh-water input. Andersson et al. (1992) show how the Sr isotope signal in the brackish Baltic Sea can be treated as a mixing between the riverine signature and the sea water, and how it can locally differ, due to the different lithologies drained by the fluvial systems. On longer time scales, and considering wider basins, Kocsis et al. (2008) interpret the lower $^{87}Sr/^{86}Sr$ ratios recorded in the lower Miocene carbonate successions of the central Mediterranean as due to the contemporary, highly explosive, subduction-related volcanism developed within the Western Mediterranean (Lustrino et al., 2009). If these results question the reliability of the SIS applied on marginal basins, on the other hand they imply that Sr isotopes can be a proxy of continental weathering and runoff and local palaeogeographic and palaeoceanographic reconstructions.

About 9-8 Ma, the $^{87}Sr/^{86}Sr$ isotope ratios of the Eastern and Northern Mediterranean marginal basins start to decrease below the global reference line, showing the maximum deviation within the Lower Evaporites, during the Messinian salinity crisis (Schildgen et al., 2014). This deviation has been interpreted as mainly due to sea level falls, together with basin uplift of the southern margin of Central Anatolia (Central Taurides), of the Apennines and the Sicilian Maghrebides, and thus to a progressive shallowing, which restricted the exchange of the eastern and the proto-Adriatic basins, with the main Mediterranean water body (Flecker and Ellam 2006; Topper et al., 2011, Schildgen et al., 2014). Different models have been published linking the late Miocene Mediterranean Sr isotope record to different controlling factors. For example, Flecker et al. (2002) and Flecker and Ellam (2006) propose a nondimensional steady state model where sea level changes seem to be the major controlling factor on $^{87}Sr/^{86}Sr$ isotope ratios. Sea level falls can lead to isolation and restrict water exchanges of marginal basins. On the contrary, Topper et al. (2011) provide a box-model with time independent equations inferring that Sr isotope variations are mostly affected by riverine input into restricted basins which lead to salinity changes.

In this work the Sr isotope record of the upper Miocene carbonate ramp succession, represented by the *Lithothamnion* Limestones (LL) cropping out in the Majella Mountain (Central Apennine, Italy) and in the exploration wells of Adriatic Sea (Brandano et al. 2016a), is presented. The LL offers an opportunity to study the evolution of a marginal basin within the Mediterranean such as the Adriatic Sea. This lithostratigraphic unit records the final steps of Apennine orogenesis when the proto-Adriatic area started developing. The aim of this work is to evaluate how the geodynamic evolution of this basin may have influenced the marine Sr isotope values and consequently impacted the SIS of the upper Miocene succession of the Adriatic area.

5.2 Geological setting

The Majella Mountain is a N-S/NW-SE oriented thrust-related anticline that plunges both North and South (Fig. 5.1A, B). It consists in the northern extension of the Apulia carbonate platform and, together with the Latium-Abruzzi, it represents one of the two carbonate platform domains of the Central Apennine fold-and-thrust-belt (Patacca et al., 2008; Vezzani et al., 2010). The Majella Mountain sedimentary succession consists in Upper Jurassic to upper Miocene limestones and dolostones (Crescenti et al., 1969). During the Mesozoic a steep, erosional escarpment separated the shallow-water carbonates from the basin, extending northward (Fig. 4.1C) (Vecsei et al., 1998). During the late Campanian, the platform prograded over the basin, since it was completely filled by onlapping sediments, and evolved into a distally steepened ramp with the adjacent slope (Vecsei et al., 1998; Mutti et al., 1996). The Paleogene evolution of the Majella platform is represented by Santo Spirito Formation characterised by a continuous sedimentation along the platform margin and the slope, while the top shows long-term hiatuses and discontinuous deposits (Vecsei et al., 1998). A discontinuity surface separates the Santo Spirito Formation from the overlying Bolognano Formation (late Rupelian-Messinian) that represents another carbonate ramp, developing above the shallow-water deposits of the former platform (Mutti et al., 1997; Brandano et al., 2012; 2016b). The Bolognano Formation has been divided into several informal members (Fig. 5.2) (Mutti et al., 1997; 1999; Carnevale et al., 2011; Brandano et al., 2012; 2016b). The first unit, Rupelian to late Chattian in age, is represented by the *Lepidocyclina* Limestones 1 (Brandano et al., 2012; 2016b). It mainly consists of cross-bedded packstone to graistone with Larger Benthic Foraminifera and represents a wide dune field developed within the middle ramp environment, under the action of strong northward, basinward-directed, storm-related currents (*Brandano et al.,* 2012). During the late Chattian-late Aquitanian time interval the *Lepidocyclina* Limestones 1 carbonate ramp drowned and it is overlain by a marly cherty unit, which represents the sedimentation on an outer ramp depositional environment, developed within the aphotic zone (Brandano et al., 2016b). From the late Aquitanian to the late Burdigalian the *Lepidocyclina* dominated carbonate factory faced a recovery (*Lepidocyclina* Calcarenites 2 of Brandano et al., 2012; 2016b), drowning eventually in the late Burdigalian. This event is marked by a phosphatic hardground surface cropping out throughout the entire Bolognano Formation. Two different units lie above this hardground surface: a bryozoan-dominated coarse calcarenitic unit, the thickness of which rapidly decreases northwards, laterally passing into a hemipelagic calcareous-marly unit. Both this units can be ascribed to the late Burdigalian-Serravallian time interval (Brandano et al., 2016b). Above the hemipelagic marly limestones the third shallow-water unit occurs: the *Lithothamnion* Limestone (Brandano et al., 2016a; Brandano et al., 2016b). The LL unit is capped by the deposition of the "*Turborotalita multiloba* hemipelagic marls" (Carnevale et al., 2011), followed by the

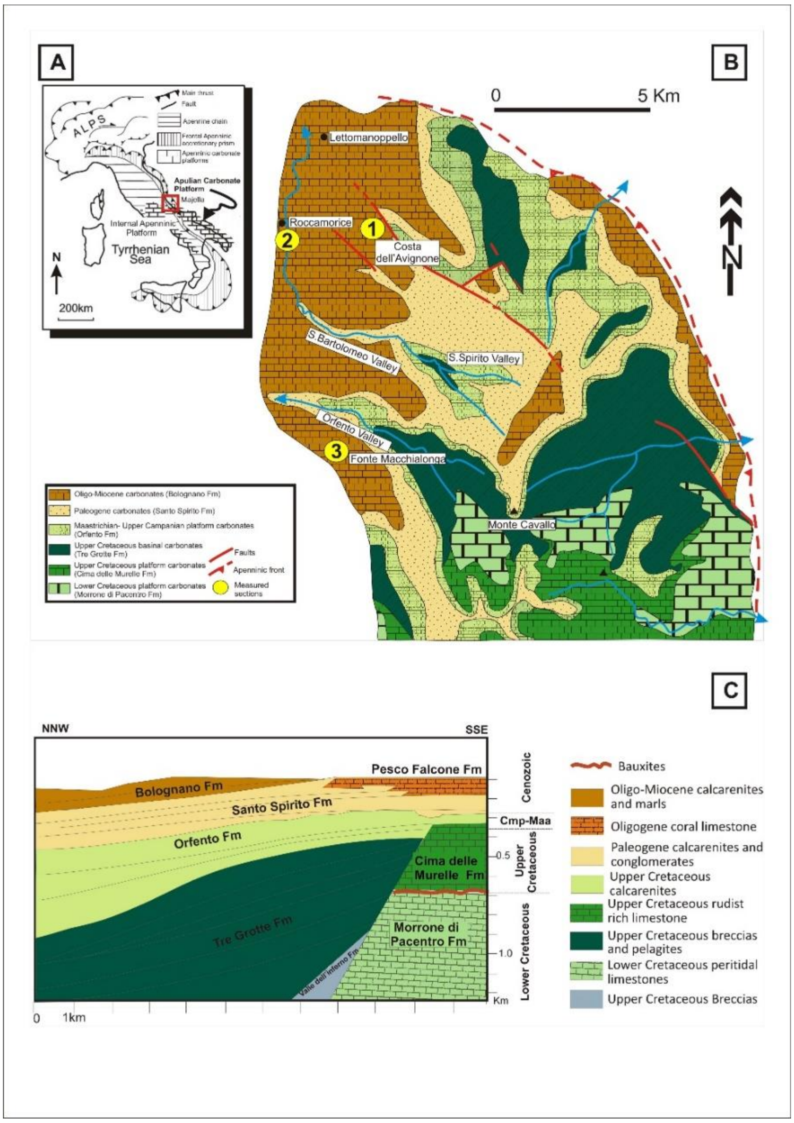

Fig. 5.1: A) Schematic geological map of Italy (modified after Pomar et al., 2004). B) Simplified geological map of the Majella Mountain (modified after Vecsei and Sanders 1999), with section locations. 1) Costa dell'Avignone; 2) Roccamorice; 3) Fonte Macchialonga. C) Schematic architecture of the Majella carbonate platform (modified after Vecsei et al., 1998).

Gessoso-Solfifera Formation (Crescenti et al., 1969). Lastly, during the early Pliocene, the Majella Mountain was involved into the foredeep system of the Apennine orogeny (Cosentino et al., 2010).

5.2.1 The Lithothamnion *Limestone*

The *Lithothamnion* Limestone (LL) unit is made by up to 30 m of limestones to marly limestones dominated by red algae and subordinated bivalves. The depositional model is consistent with a homoclinal ramp profile, characterised by a wide middle ramp environment dominated by red algae branches representing the maërl facies (Brandano et al., 2016a). The inner ramp is characterised by coral buildups, cropping out in the southernmost portion of the Majella Mountain (Danese, 1999), passing basinward to seagrass meadows that interfinger with the maërl facies. The outer ramp consists in bioturbated marly limestones and marls with pectinids, small benthic and planktonic foraminifera (Brandano et al., 2016a). Two main stratigraphic intervals may be recognised in the LL unit. The lower interval (lower LL) is dominated by red algal branches that decrease in the upper portion (upper LL) while the terrigenous input increases. The base of the upper LL is marked by the presence of the Bioclastic Packstone and the Red Algal Bindstone. Moreover, the uppermost portion is characterised by the presence of two different brachiopods-rich levels, where a population of *Terebratula sinuosa* has been identified (Sirna, 1996).

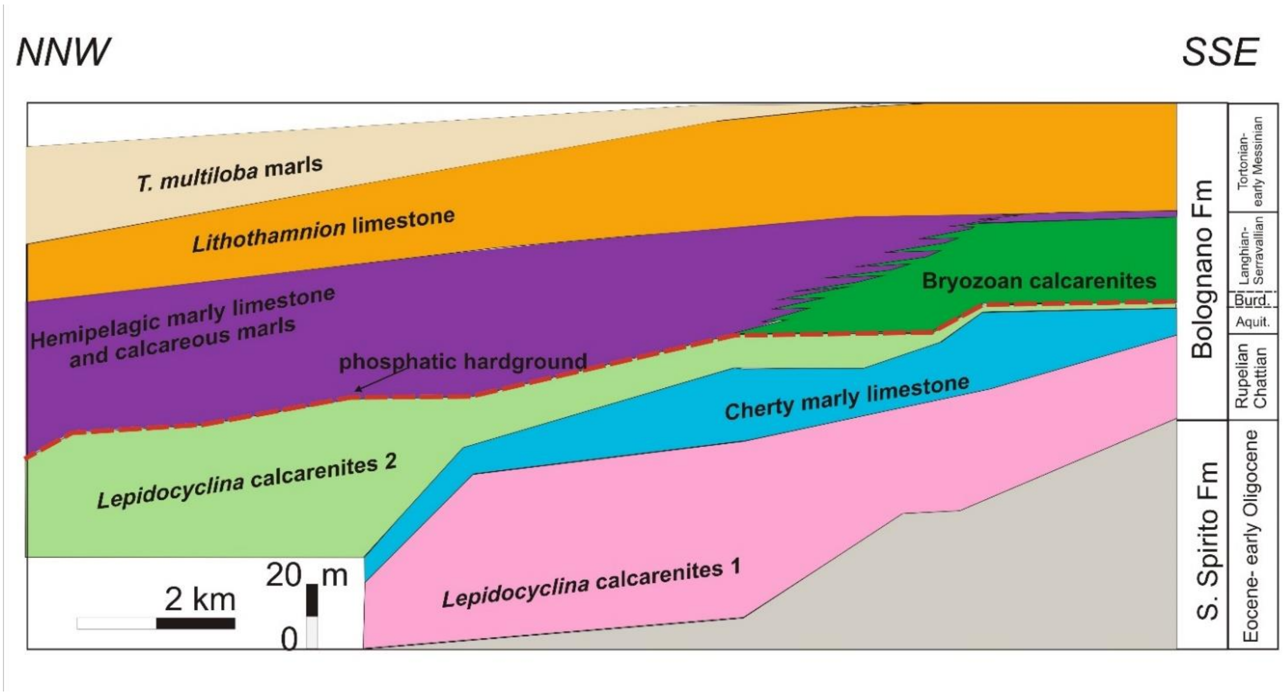

Fig. 5.2: Stratigraphic architecture of the Bolognano Formation (modified after Brandano et al., 2016b).

5.3 Material and Methods

Three stratigraphic sections, cropping out in the north-western sector of the Majella Mountain, have been sampled for Strontium Isotope Stratigraphy (SIS) and micropaleontological analyses. The first two sections crop out respectively within the

Lettomanoppello area (Costa dell'Avignone) and the Roccamorice village, while the third (Fonte Macchialonga) is exposed within the Orfento Valley (Fig. 5.1B, 5.3).

Ten different specimens of bivalves and brachiopods have been analysed for SIS. A complete diagenetic screening (trace element concentrations and stable isotope ratios) has been performed on the sampled shells. Mg, Mn, Fe, Sr and Ba concentrations have been measured on polished thin sections using the CAMECA electron microprobe of the Istituto di Geologia Ambientale e Geoingegneria (IGAG-CNR) at Sapienza, University of Rome. The same specimens have been powered with a hand-operated microdrill, using 0.5 mm Ø tungsten drill bits, avoiding the external and evidently altered portions, for both stable C and O and radiogenic Sr isotope ratios measures. Carbon and oxygen stable isotopes have been measured at the isotope geochemistry laboratory of the Istituto of Geologia Ambientale e Geoingegneria (IGAG-CNR) of Rome, using a gas chromatography-based Gas Bench II coupled with a FINNIGAN Delta Plus mass-spectrometer. The results were calibrated using the NBS19 carbonate standard. Both $\delta^{13}C$ and $\delta^{18}O$ values are reported on the Pee Dee belemnite (PDB) scale. The analytical error is ±0.1‰ based on replicate standards.

Sr isotope ratios have been measured at the Department of Geosciences of the Natural History Museum of Stockholm (NRM) using a Thermo Scientific TRITON mass spectrometer. Separation of Sr has been performed in Sr-spec and TRU resins mixed columns. Measured $^{87}Sr/^{86}Sr$ ratios have been normalized to $^{86}Sr/^{88}Sr=0.1194$. During the collection of the Sr isotope data 12 replicate analyses of the NIST SRM 987 standard gave an average value of 0.710226 ± 0.000014 (2σ) and all measured ratios have been corrected to this value.

The $^{87}Sr/^{86}Sr$ values of the unaltered samples have been converted to numerical ages using Version 4B: 08/04 of the Look-Up Table of Howarth and McArthur (1997); for details of 4B: 08/04 see McArthur and Howarth (2004). Minimum and maximum ages were calculated by combining the long-term standard error (2σ) of each measured $^{87}Sr/^{86}Sr$ value with the uncertainty of the strontium-isotope curve (Howarth and McArthur, 1997).

Five samples belonging to the upper portion of the LL have been analysed to identify their microfossil content for biostratigraphic purposes. The lithified samples were disaggregated first in acetic acid 80%, and then in an ultrasonic cleaner, according to the procedure described by Lirer (2000). The disaggregated material has been wet-sieved in a 63μm sieve to separate the clay fraction before the observation.

5.4 RESULTS

5.4.1 Stratigraphy of sampled sections

5.4.1.1 Costa dell'Avignone section

In this section only the lowest interval of the LL unit crops out (Fig. 5.3) (Annex A.11). In the Lettomanoppello area the LL overlays the hemipelagic marls and marly limestones unit described by Brandano et al. (2016b) (Fig. 5.2). The base of the section consists in a 1 m thick interval of a cross-bedded bioclastic packstone with bivalves and vertebrate bones (Figs. 5.3; 5.4A; 5.5A). This unit culminates in a lag deposit with bivalves where the most common genera are *Flabellipecten* and *Pecten*. This facies is overlain a 3 m thick interval represented by a free-living red algal branch floatstone to rudstone where the major

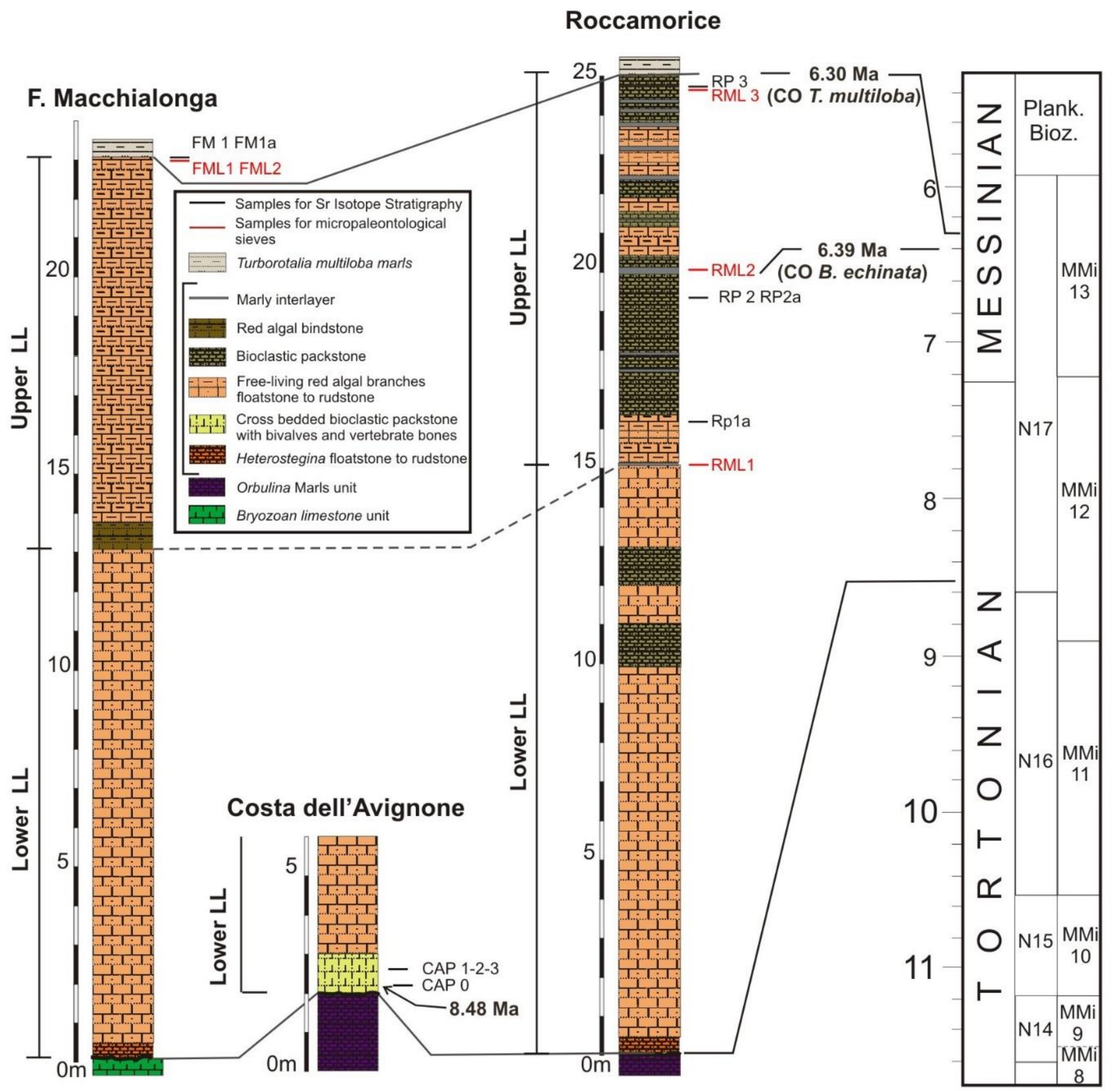

Fig. 5.3: Stratigraphic correlation of the measured sections, plotted against stratigraphic depth, and sample locations. Planktonic foraminifera N-zones are referred to Blow (1969), MMi-zones are according to Iaccarino (1985). The age of the base of the lower *Lithothamnion* Limestone is provided by SIS; ages of the CO of the *Bulimina echinata* and the *Turborotalita multiloba* are derived from Kouwenhoven et al. (2006).

components are coralline algae unattached branches characterised by a low-density branching, together with small rhodoliths. The matrix is represented by a poorly-sorted bioclastic packstone with small benthic and encrusting foraminifera.

Four pectinid shells (CAP0, CAP1, CAP2, CAP3) have been sampled from two different strata, 50 cm spaced one from another, belonging to the lower LL interval, cropping out at the base of the section (Fig. 5.3).

5.4.1.2 Roccamorice section

As in the Lettomanoppello area, also in the Roccamorice section the LL unit overlays the hemipelagic marls and marly limestones unit described by Brandano et al. (2016b) (Fig. 5.2) (Annex A.10).

Here the lower interval of LL consists of 20 cm thick bed of a *Heterostegina* floatstone to rudstone (Fig. 5.5B), followed by 15 m of a free-living branches floatstone to rudstone (Figs. 5.4B, C), alternated with a bioclastic packstone facies. The free-living red algal branch floatstone to rudstone consists in limestones to marly limestones dominated by unattached branches of coralline algae and small rhodoliths (Figs. 5.5C, D). The major components are usually dispersed in a poorly-sorted bioclastic matrix mostly made of small benthic foraminifera, together with encrusting foraminifera, which occasionally show hooked shapes.

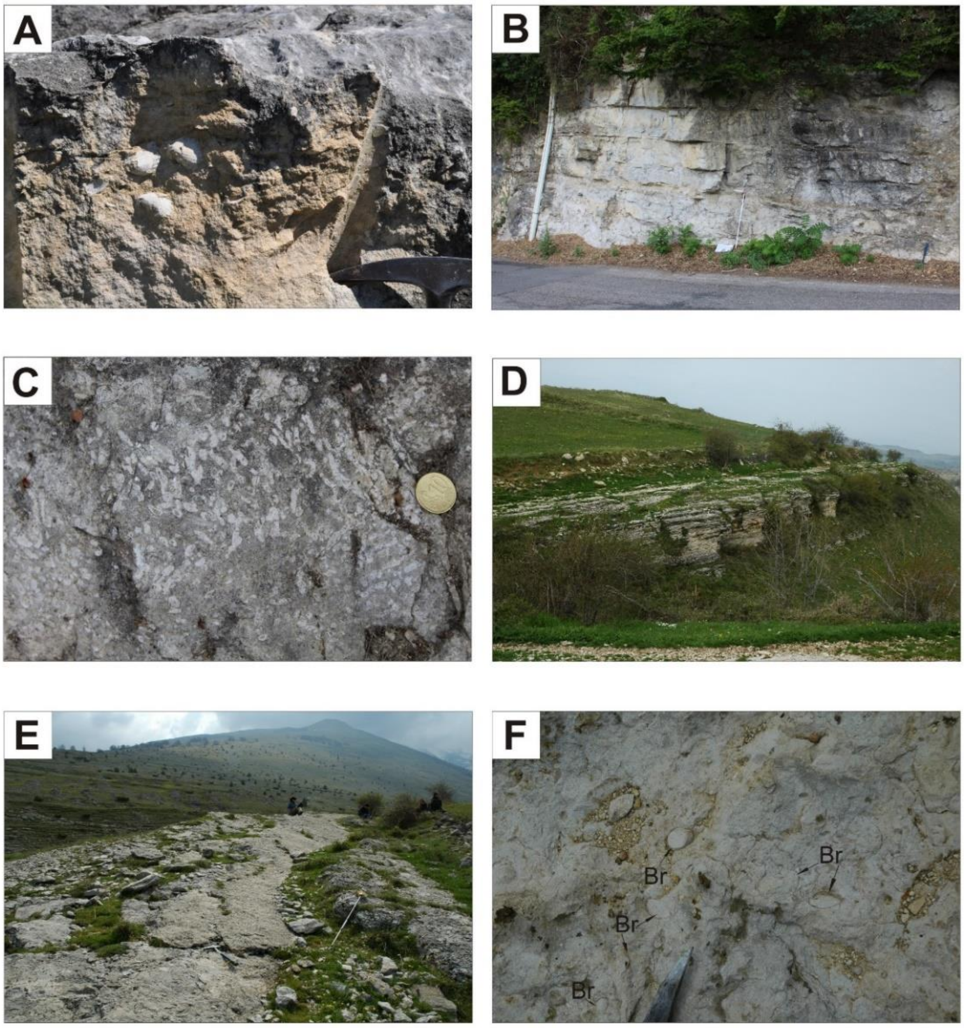

Fig. 5.4: Main lithofacies of the *Lithothamnion* Limestone (LL). A) Detail of *Pecten* specimens outcropping at the base of the lower LL interval in the Costa dell'Avignone section; B) Upper portion of the lower LL of the Roccamorice statigraphic section; C) Detail of the Free-living Red algal Branch Floatstone to Rudstone (maërl facies) of the lower LL in the Roccamorice section; D) Upper LL interval in the Fonte Macchialonga stratigraphic section; E) Brachiopod Floastone at the top of the LL unit outcropping in the Fonte Macchialonga stratigraphic section; F) Detail of the Brachiopod Floatstone in the Fonte Macchialonga section. For further information on the main lithofacies of the LL the reader is referred to Brandano et al. (2016a).

The bioclastic packstone, on the contrary, consists of 20 to 40 cm thick lenticular beds, usually poorly sorted. The main components are small benthic foraminifera as rotaliids, buliminids, encrusting foraminifera, planktonic foraminifera, serpulids, echinoid, bryozoan and bivalve fragments. Red algal fragments are usually subordinated. The upper LL is represented by 10 m of medium-grained bioclastic packstone. A constant increase of the terrigenous input is evident, as testified by few cm thick marly interstrata that interrupt the bioclastic packstone deposition.

Samples for SIS belong to three different layers (Fig. 5.3). Sample RP1a, collected 1.20 m above the base of the upper LL, is a pectinind shell. RP2 and RP2a and RP3 samples, belonging to two different brachiopod-rich

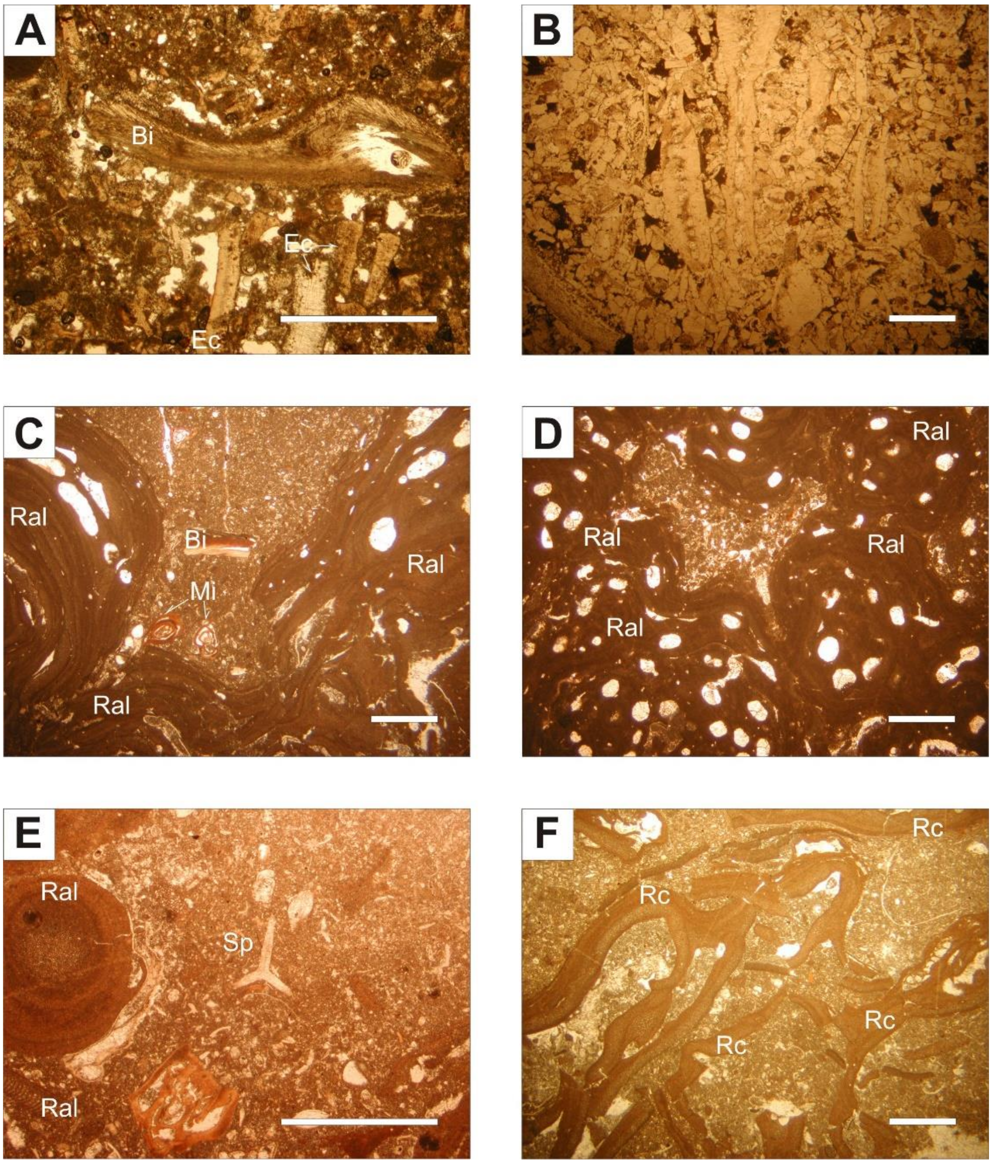

Fig. 5.5: Main microfacies of the *Lithothamnion* Limestone (LL). A) Cross bedded bioclastic packstone with bivalves and vertebrate bones; B) *Heterostegina* Floatstone; C-D-E) Free-living Red algal Branch Floatstone to Rudstone; F) Red algal Bindstone. Bi= bivalve fragment; Ec= echinoid fragment; Mi= miliolids; Ral= red algae; Rc= Red algal crust; Sp= sponge spicule. Scale bar= 1mm. For further information on the main microfacies of the LL the reader is referred to Brandano et al. (2016a).

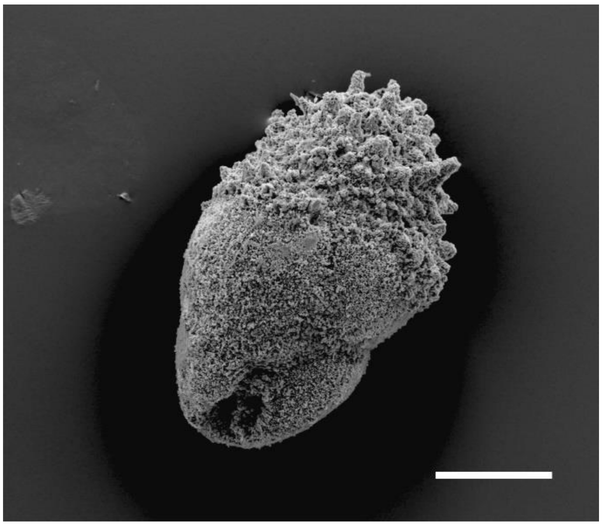

Fig. 5.6: Scanning electron micrograph of a *Bulimina echinata* specimen belonging to the Upper LL cropping out in the Roccamorice stratigraphic section. Scale bar= 100 μm.

intervals respectively at 11.40 m and at the top of the section, are *Terebratula sinuosa* brachiopods (Fig. 5.3).

Three different marly layers, the first one at the base of the upper LL, the second at 20 m and the third at the top of the section, have been sampled to analyse their microfossil content (samples RML1, RML2, RML3) (Fig. 5.3). All the samples show foraminiferal content with variable frequencies. In detail, RML1 and RML2 are characterised by typical infralittoral foraminifers represented mainly by *Elphidium* spp. (*E. complanatum*, *E. crispum*) and *Asterigerinata* spp. (e.g. *A. planorbis*). Particularly, RML2 shows a more abundant microfossil content with a better preservation in respect of the RML1 sample. In addition, in RML2 sample, a more diversified assemblage, characterised by epiphyte taxa like *Lobatula lobatula* and *Rosalina* spp., is recorded. Subordinately, infaunal taxa, belonging to *Brizalina/Bolivina* and *Bulimina* genera (e.g. *Bolivina arta, Bulimina aculeata, Bulimina echinata*) (Fig. 5.6), and agglutinated species, mainly represented by *Textularia* genus, are also present. Planktonic taxa are very rare or totally absent.

The upper sample of the section (RML3) shows a very low foraminiferal content. A sharp decrease of infralittoral taxa is recorded whereas only rare mud dwellers buliminids dominate the benthic assemblage; among these *Bulimina aculeata* and *Bulimina echinata* are found. The plankton fraction is very rare and represented by *Globigerinoides* spp. and small globigerinids.

5.4.1.3 Fonte Macchialonga section

Unlike in the Lettomanoppello and Roccamorice areas, within the Orfento Valley the LL lays on the Bryozoan calcarenites unit described by Brandano et al. (2016b) (Fig. 5.2) (Annex A. 12).

The lower LL in the Fonte Macchialonga section consists of 50 cm of the *Heterostegina* floatstone to rudstone, followed upward by 12.5 m of the free-living red algae floatstone to rudstone facies (Fig. 5.5E). The upper LL displays, at the base, a 70-cm thick stratum of a red algal bindstone. The red algal bindstone facies consists in a tabular bed of nodular limestones dominated by thin red algae crusts (Fig. 5.5F). The red algal bindstone is followed by 9.30 meters of free-living red algae branches floatstone to rudstone (Fig. 5.4D). As in the Roccamorice section, the upper LL shows a progressive increase of the terrigenous input. The top of the section consists in a bioturbated, marly floatstone with brachiopod shells, among which the *Terebratula sinuosa* is the most common species, and encrusting bryozoans (Fig. 5.4E, F). The brachiopod-rich level from the top of the section has been sampled for both SIS and biostratigraphic purposes. The microfossil content from FML1 and FML2 samples (upper portion of upper LL) (Fig. 5.3) is characterised by small benthic foraminifera belonging mainly to *Bulimina* and *Bolivina* genera among which *Bulimina echinata* and *Bolivina paralica* have been identified. Moreover, in both samples, rare specimens of *Valvulineria bradyana*, *Eponides* sp., *Guttulina* spp. and *Fissurina* spp. are found with frequent planktonic taxa like *Orbulina bilobata*, *O. universa*, *Globigerinoides* spp., and small globigerinids.

5.4.2 Screening for diagenetic overprint and SIS

Before applying SIS the preservation state of the samples must be assessed. Bivalves and brachiopods have been extensively used as proxies of the chemical composition of sea-water (Veizer et al., 1997; 1999; Wenzel, 2000; Brand et al., 2003; Immenhauser, 2016). Their L-Mg calcite shells, in fact, are quite resistant to diagenetic alteration (Brand and Veizer, 1980; Longmann, 1980; Morse and Mackenzie, 1990), thus they are considered a reliable proxy of the Sr isotope composition of the ambient water (Veizer et al., 1997; 1999; Steuber, 1999; McArthur, 1994; McArthur and Howarth, 2004; Frijia and Parente, 2008; Brandano and Policicchio, 2012; Frijia et al., 2015). The L-Mg calcite diagenesis tends to decrease the Sr concentrations of the shells, while Fe and Mn increase (Brand and Veizer, 1980). The Sr isotope ratio have been measured on different specimens of shallow-water Terebratula sinuosa brachiopods, the secondary shell layer of which consists of elongated calcite fibres that are resistant to diagenetic alteration (Veizer et al., 1999; Brand et al., 2003). According to Brand et al. (2003), who analysed trace elements composition on modern brachiopods from different oceans and the Mediterranean Sea, we have selected a 450 ppm of Sr as a cut-off threshold, as well as 200 ppm for Fe and Mn, to consider the brachiopod shells unaltered by diagenetic processes, thus reliable for SIS (Tab. 5.1) (Annex B.10). On the contrary, among the bivalves, pectinid shells have been demonstrated to be the most reliable ones to record the isotope composition of ambient water (Scasso et al., 2001; Brandano and Policicchio, 2012). In this case, according to Scasso et al. (2001), a cut-off threshold of 650 ppm of Sr, and of 200 ppm for Fe and Mn, has been chosen to determine diagenetic alteration of the samples (Tab. 5.1).

Oxygen isotope ratios measured on both the pectinid and brachiopod specimens show all positive values, ranging from +0.25‰ to +3.47‰, while carbon isotope values span from -0.33‰ to +1.92‰ (Tab. 5.1) (Annex B.10). These values all fall within the range of the marine precipitated carbonates (Weissert, 1989; Weissert et al., 2008 and references therein), thus a strong diagenetic overprint is excluded.

5.4.3 Sr isotope ratios and age model

The age of the LL can be constrained on the basis of the underlying and the overlying units. The Bryozoan calcarenites and the hemipelagic marls can be ascribed to the late Burdigalian-late Serravallian time interval (Merola, 2007; Brandano et al., 2016b).

Furthermore, the *T. multiloba* marls, which cap the LL, are early Messinian in age, as well as the upper LL (RML2), based on the occurrence of the *Bulimina echinata* (Sprovieri et al., 1996; Blanc-Valleron et al., 2002; Kouwenhoven et al., 2006; Violanti et al., 2013). Thus, the LL is Tortonian to early Messinian in age, although the absence of *B. echinata* in RML1 sample might be due to ecological factors. The foraminiferal assemblage (dominated by *Elphidium* and

Sample	Mg (ppm)	Mn (ppm)	Fe (ppm)	Sr (ppm)	Ba (ppm)	δ 13C (‰ VPDB)	δ 18O (‰ VPDB)
CAP0	1285,46	69,37	190,90	1009,98	219,52	1,92	1,10
CAP1	2074,10	8,86	118,80	552,18	101,76	0,76	0,64
CAP2	1047,90	73,51	185,38	516,24	183,20	1,33	0,67
CAP3	2596,61	141,46	79,91	1078,81	45,66	0,17	0,77
RP1a	2961,18	105,92	183,44	1099,49	64,24	-0,32	0,25
RP2	2323,96	10,63	68,09	654,15	0,00	-0,05	2,64
RP2a	983,91	121,87	75,55	657,15	74,05	-0,33	2,40
RP3	2032,58	146,49	113,58	263,62	100,83	0,73	1,63
FM1	2249,04	74,37	93,61	482,59	113,32	0,94	3,47
FM1a	7562,19	156,72	145,94	865,89	87,74	1,08	2,79

Tab. 5.1: Trace element concentrations profiles of Mg, Mn, Fe, Sr and Ba, reported as mean values of the pectinid and brachiopod shell samples. $\delta^{13}C$ and $\delta^{18}O$ values reported on the VPDB scale.

Asterigerinata spp.) suggests oligothrophic conditions and vegetated bottom not suitable for the euthrophic infaunal taxa like buliminids (Jorissen, 1987; Murray, 2006).
According to SIS, CAP 0 and CAP 3 pectinid samples, belonging to the base of the lower LL of the Costa dell'Avignone stratigraphic section, indicate respectively a 8.48 and 8.59 Ma age (Tab. 5.2) (Annex B.11). On the contrary, samples RP1a, RP2, RP2a, representative of the central and upper portions of the lower LL in the Roccamorice section, show dispersed age values, spanning from 9.75 Ma to 18.29 Ma. Lasty, samples FM1 and FM1a, belonging to the uppermost portion of the LL, in the Fonte Macchialonga section, indicate respectively an age of 10.09 Ma and 8.14 Ma (Tab. 5.2) (Annex B.11).

5.5 Discussion

5.5.1 Stratigraphy

The base of the LL can be ascribed to a late Tortonian age according to the $^{87}Sr/^{86}Sr$ values of CAP 0 and CAP 3 samples of the Costa dell'Avignone section (Fig. 5.3; Tab. 5.2). This age model is consistent with the published literature on this lithostratigraphic unit. Merola (2007) identifies the *Neogloboquadrina* group in the upper portion of the underlying lithostratigraphic unit (the *Orbulina* Marls or the hemipelagic limestones and calcareous marls unit as defined in Brandano et al. (2016b). The *Neogloboquadrina* group has been recognised in the Monte dei Corvi section (GSSP of the Tortonian stage) just below the Serravallian-Tortonian boundary (Hilgen et al., 2005). Thus, the base of the LL cannot be older than early Tortonian. According to this age model of the *Orbulina* Marls, Patacca et al. (2013) identify the discontinuity surface between the *Orbulina* Marls and the LL units as the maximum-regressive surface of the Tor2 Global T-R Sequence of Snedden and Liu (2011), dated at 9.32 Ma. The LL unit represents the following transgression phase during the Tor2 after 9.32 Ma (Patacca et al., 2013; Brandano et al., 2016a; 2016b). The upper interval of the LL can be referred to the early Messinian on the basis of the occurrence

	($^{87}Sr/^{86}Sr$)	$2\sigma_{mean}$ (*10^{-6})	($^{87}Sr/^{86}Sr$)[1]	2σ (*10^{-6})[2]	Minimum Age	Age (Ma)	Maximum Age	$(\varepsilon_{Sr})_{SW}$[3]	±
CAP0	0,708908	7	0,708927	14	7,34	8,48	9,43	-3,40	0,14
CAP3	0,708906	4	0,708925	14	7,41	8,59	9,49	-3,43	0,14
RP1a	0,708876	5	0,708895	14	9,33	9,75	10,15	-3,85	0,14
RP2	0,708679	6	0,708698	14	16,02	16,36	16,72	-6,63	0,14
RP2a	0,708547	4	0,708567	14	18,03	18,29	18,53	-8,47	0,14
FM1	0,708864	5	0,708883	14	9,49	10,09	10,74	-4,02	0,14
FM1a	0,708913	6	0,708932	14	7,17	8,14	9,25	-3,33	0,14

1)Corrected $^{87}Sr/^{86}Sr$ assuming a NBS 987 value of 0.710245 while our measured NBS 987 value was 0.710226±0.000014 (n=12).

2)External precision based on repeated measurements of NBS 987 during the course of the study gave a value 0.710226±0.000014 (n=12, 2SD).

3)Deviation from sea water $^{87}Sr/^{86}Sr$ in parts per 10 000 with an $^{87}Sr/^{86}Sr$ vale of 0.709168 as measured at GEO during the same period as the samples.

Tab. 5.2: $^{87}Sr/^{86}Sr$ values of the pectinid and brachiopod shell samples reported with related analytical error ($2\sigma_{mean}$); $^{87}Sr/^{86}Sr$ corrected ratios reported with the mean standard error (2σ) and the associated age values. Deviation from sea water $^{87}Sr/^{86}Sr$ (ε_{Sr}) in parts per 10 000 with an $^{87}Sr/^{86}Sr$ vale of 0.709168 as measured at GEO during the same period as the samples. Numerical ages are reported from McArthur et al. (2001; look up table version 4B: 08/04). Minimum and maximum ages were calculated by combining the long-term standard error (2σ) of each measured $^{87}Sr/^{86}Sr$ ratio with the uncertainty related to the strontium-isotope curve Howarth and McArthur, 1997).

of the *Bulimina echinata* (Sprovieri et al., 1996; Blanc-Valleron et al., 2002).

The $^{87}Sr/^{86}Sr$ ratios of the upper LL show very dispersed values giving an age that is not coherent with the stratigraphy, but being generally older than expected (Tab. 5.2; Fig. 5.7).

5.5.2 The role of palaeoceanography and palaeogeography on Sr isotope record

The difference between the central Mediterranean and the global Sr isotope values during early Messinian is likely due to the progressive establishment of restricted marine conditions within the LL carbonate ramp, which limited the water exchanges and the mixing with the larger Mediterranean water body and, consequently, the Atlantic Ocean. Mediterranean water circulation and chemistry has been affected by its geodynamic evolution during the Miocene. The closure of Indo-Pacific seaway started during the early Miocene, and definitely closed after the Langhian-Serravallian transition, leaving the Mediterranean Sea exchanging only with the Atlantic Ocean (Rögl, 1999; Kocsis et al., 2008) (Fig. 5.8). Kocsis et al. (2008) evidenced a Sr isotope anomaly trend, proposing restricted water circulation for the Mediterranean at least until 15 Ma. Successively, during the Messinian, the western connection with the Atlantic consisted in different short-living, tectonically-controlled, narrow straits and passages within the Betic area and the Rifian corridor (Betzler et al., 2006; Martin et al., 2009). In this oceanographic scenario, the Mediterranean basin starts facing progressive restricted conditions and partial isolation since 3 Myr prior to the onset of the Messinian salinity crisis, even if surface water salinity remains frankly marine up until 200 kyr prior the beginning of the deposition of the Lower Evaporites (Blanc-Valleron et al., 2002). Thus, the latemost Tortonian-early Messinian time interval is characterised by a large central Mediterranean water body which is still connected with the Atlantic Ocean; it maintains oligotrophic water conditions and a Sr isotope signature comparable with that of

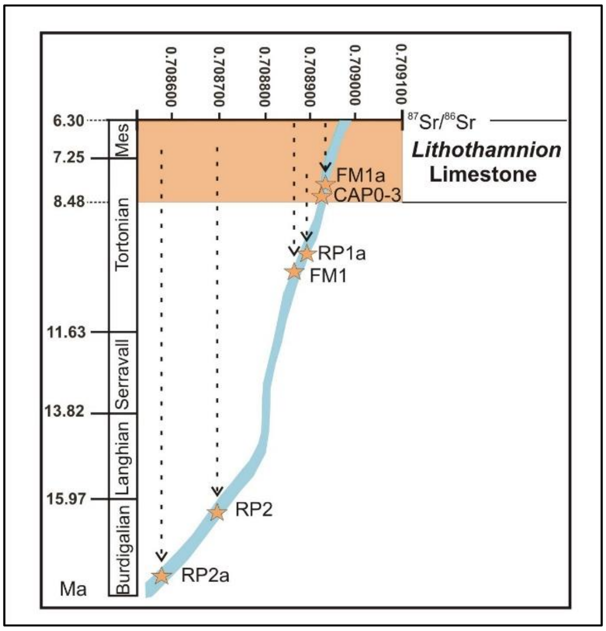

Fig. 5.7: Compilation of the Sr isotope data from this work. Light blue shaded region shows global sea water Sr isotope global reference line (from McArthur & Howarth, 2004). Orange column shows the stratigraphic position of the *Lithothamnion* Limestone (LL) unit according to the new age constraints: the 8.48 Ma for the base derives from new SIS data provided in this paper; the 6.30 Ma for the top refers to the CO of the *Turborotalita multiloba* according to Kouwenhoven et al. (2006). The orange stars represent the Sr isotope values of the measured samples. As it is shown in the figure, CAP 0 and CAP 3 samples fit with the age constraints of the LL, while the other samples show lower Sr isotope ratios in comparison to their age. The dashed indicators show how each sample is shifted from its correct stratigraphic position.

the mean global ocean, and within the range of the McArthur et al. (2001) reference line. Late Tortonian-early Messinian time interval is characterised by the development of different types of reefs within the Mediterranean area. The best examples are located in western Mediterranean, within the Betic, Balearic, Rif and Tell provinces (Braga et al., 1990; Esteban, 1996; Esteban et al., 1996; Braga and Martín, 1996; Pomar et al., 2004; 2012), but they have also been found in the central Mediterranean in the provinces of Toscana (Bossio et al., 1996), Calabria, Sicily and Malta (Pedley, 1996), and in the southernmost portion of the Apulia carbonate platform, in the Salento area (Bosellini, 2006). Marginal sub-basins have limited water exchanges with the main larger water mass body (Flecker and Ellam, 2006; Topper et al., 2011; Schildgen et al., 2014). In this context, the LL carbonate ramp succession records the evolution of trophic conditions in the proto-Adriatic marginal basin within the Mediterranean during late Miocene. This ramp is characterised by a completely different skeletal association, in comparison to the coeval Central Mediterranean platforms, dominated by coralline algae. This association has been interpreted as due to the evolving nutrient content of the central Adriatic waters. Brandano et al. (2016a) distinguish three main stages in the evolution of the LL. In the first stage the ramp established over the underlying hemipelagic marls and was subjected to repeated energy pulses within the inner ramp environment, very close to the vegetated area, where seagrass meadows established under oligotrophic conditions. The second stage is characterised by a progressive decrease of light penetration due to a progressive increase of fine continental derived sediments of the Apennine accretionary wedge. Seagrass meadows persisted within the inner ramp, interfingered with the maërl facies, which spread into the inner to middle ramp transition zone. The foraminiferal assemblage is dominated by *Amphistegina*, together with epiphytic small benthic foraminifera, indicating oligophotic conditions as well as a vegetated depositional environment. The third stage shows the decay of the trophic conditions faced in the ramp during the early Messinian, as testified by red algal growth form associated with an increase, towards the top of upper LL interval, of typical low oxygen foraminiferal taxa (*Bulimina* spp. and *Bolivina/Brizalina* spp., *Valvulineria bradyana*) tolerating abundant organic matter

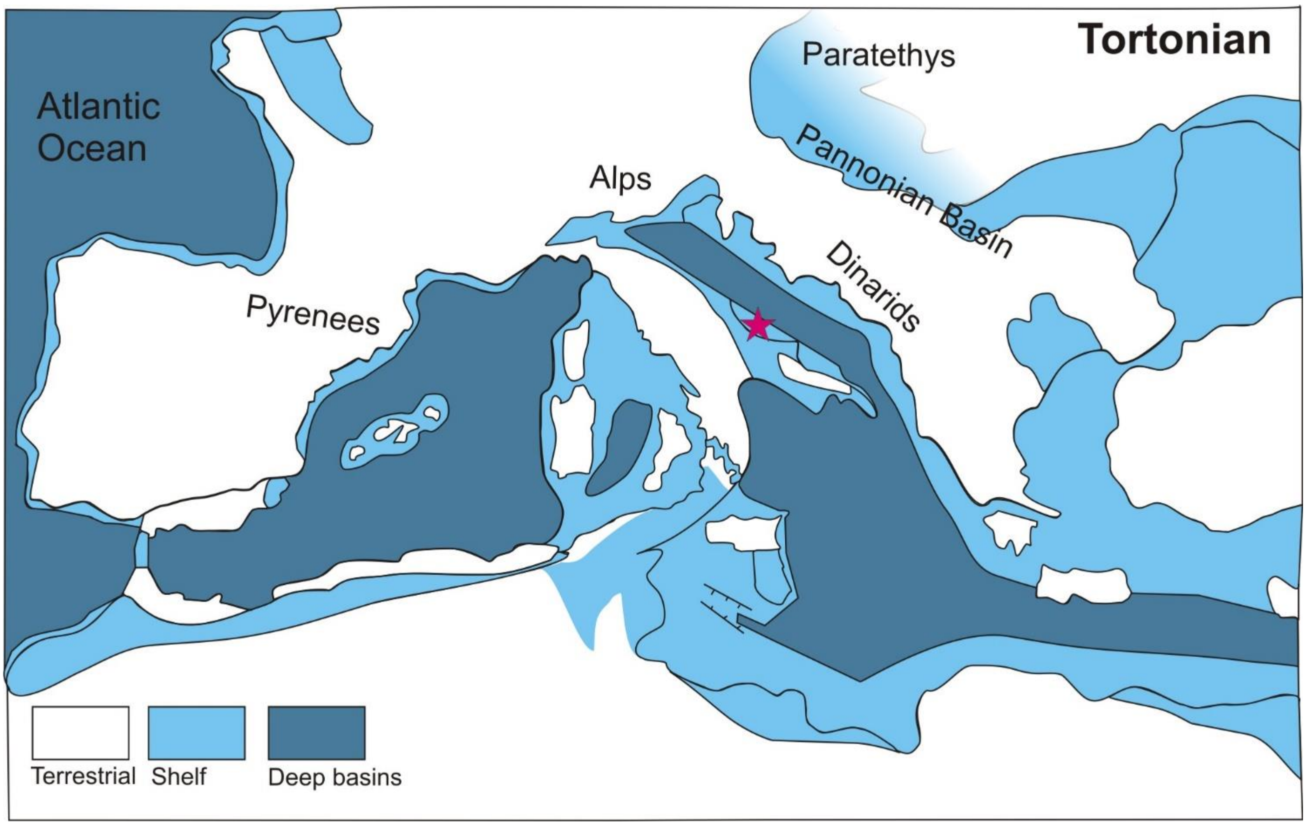

Fig. 5.8: Paleogeographic map of the Mediterranean area during the Tortonian with location of the Majella carbonate platform (modified after Carminati et al., 2010).

accumulation in dysoxic to anoxic conditions (Van der Zwaan, 1982; Jorissen, 1987, Kouwenhoven et al., 2006; Frezza and Carboni, 2009). This is confirmed also by the increase in the planktonic fraction of *Orbulina* spp. (mainly *O. bilobata*) commonly recorded in the upper pre-evaporitic succession (Suc et al., 1995; Sprovieri et al., 1996; Blanc-Valleron et al., 2002; Violanti et al., 2007) and in water masses rich in high nutrient levels (Hemleben et al., 1989; Robbins, 1988; Violanti et al., 2013). The increased nutrient content into the LL ramp has been referred to the Apennine accretionary wedge and foredeep system development and migration (Brandano et al., 2016a), which led to enhanced subsidence rates in the central Apennine platform domains and to an increased terrigenous input (Brandano and Corda, 2002). This is also suggested by the occurrence of agglutinated foraminiferal taxa (mainly Textularids) in the upper LL totally lacking in the underlying sample. Milli et al. (2007) showed that the first phase of the deposition of the turbidite succession of the Laga Basin is between 7.25 and 5.96 Ma, and it partially overlaps with the age the upper portion of the LL. Furthermore, in the late Miocene, the Adriatic Sea was an elongated, shallow shelf-basin where continental input arrived from the north. This particular setting is analogous of the nowadays Gulf of California (Mexico), where eutrophic water conditions are present in the northern sector. Here, bryozoan and mollusk dominate the skeletal assemblage. Moving southward, the nutrient content and organic matter of surface waters progressively decreases towards the southernmost portion of the gulf where corals develop into oligotrophic waters (Halfar et al., 2004; 2006). In the central portion of the gulf, within mesotrophic waters, red algae and mollusks are the main carbonate producers (Halfar et al., 2006). Similar to the present Gulf of California, the LL ramp developed under mesotrophic conditions due to the progressively increasing terrigenous input from the north. In addition, progressive eastward migration of the Apennine accretionary wedge supported the development of restricted circulation of proto-Adriatic Sea due to its physiography, which led to a subsequent minor input of ocean waters and an enhanced continental influence. This restricted circulation, in turn, led its water chemistry to be significantly different from the larger Mediterranean water body not only for the nutrient content, but also impacted the Sr isotope signal, as shown by its isotope signature, which is lower than the coeval early Messinian global reference line (Fig. 5.7). The deviation of LL Sr isotope values could be attributed to environmental factors, given that its Sr isotope record is pristine and not due to any deuteric alteration, such as a relevant diagenetic overprint, which can be excluded for the studied samples. A significant input of fresh water, and continental runoff within a restricted basin, can lower the $^{87}Sr/^{86}Sr$ of the proto-Adriatic seawater. Flecker and Ellam (2006) proposed a model where, in marginal Mediterranean sub-basins, only 50% of the water was of an Atlantic provenance, while the other half consisted in the riverine input, strongly affecting the local water chemistry and isotope signature. Schildgen et al. (2014) report Sr isotope values of different Mediterranean basins whose records show that, since the 9-8 Ma time interval, while the Central Mediterranean (Sicily, Malta, Cyprus) isotope signal is still strongly affected by the Atlantic influence, the eastern and the northern marginal basins are characterised by Sr isotope values lower than the contemporary mean Atlantic ones. Furthermore, the authors stated that this is due to the freshwater input and the continental derived sediments, together with the restricted circulation with the central Mediterranean large water body, that controls the Sr isotope signal of these basins. This interpretation is supported by Böhme et al. (2008) palaeoclimatic reconstruction of the late Miocene of the Southern-Western Europe, which faced a progressive increase of humidity and precipitation rates from 8 to 5.3 Ma. In this case, an increased riverine water inflow within small marginal basins must have lowered its $^{87}Sr/^{86}Sr$ ratios. The Sr isotope signature of rivers reflects the lithologies cropping out within the river catchment areas. Thus, on a global scale weathering and continental runoff tend to raise $^{87}Sr/^{86}Sr$ ocean isotope ratios, given the high $^{87}Sr/^{86}Sr$ of most riverine waters that uptake Sr mainly from continental rocks or sediments, which are, on average, characterised by relatively high Rb/Sr ratio and old ages. Within the Mediterranean different conditions were observed, since rivers had, and still have, mostly a northern catchment that drains (i) Mesozoic shallow-water carbonates successions, which are marked by lower $^{87}Sr/^{86}Sr$ ratios than the late Miocene mean ones (Topper et al., 2011), and, in some cases, (ii) sedimentary formation containing significant amount of volcanoclastic component (e.g. Mattioli et al., 2012), with a $^{87}Sr/^{86}Sr$ ratio lower than seawater. Thus, in the study area, an increased amount of the influx of freshwaters, which in the Mediterranean have a lower Sr isotope signature than ocean seawaters (Schildgen et al., 2014), will result in a lowering of $^{87}Sr/^{86}Sr$. This is also in agreement with the Sr input trend through ground water of the Modern

Western Mediterranean Sea (Trezzi et al., 2017). Investigating the Sr flux these authors show how the Sr input is higher than to the global ocean, and the $^{87}Sr/^{86}Sr$ ratio is overall lower, due to the carbonate source of Sr to groundwater discharging.

According to Flecker and Ellam (2006) a sea level drop or salinity changes are considered to be the main controlling factors producing a deviation of Sr isotope values in restricted basins with respect to the global ocean values. On the contrary, the investigated succession records fully marine conditions and a progressive deepening upward trend, evolving from the LL ramp to the hemipelagic *T. multiloba* marls before the Messinian crisis. In this case the physiography of the proto Adriatic basin, strictly linked to the tectonic evolution of the area as well as climate and related fluvial runoff, mainly controlled the water chemistry. This is in agreement with the deviation of the Sr isotope signal of the upper Tortonian hemipelagic record of the Umbria-Marche region (Northern Apennines). In this succession the Sr isotope ratios start deviating contemporary to the maximum uplift/exhumation rate of Apennine orogen (Montanari et al., 1997).

5.6 Conclusions

Biostratigraphic constrains associated with SIS indicate a late Tortonian to early Messinian age for the *Lithothamnion* Limestone ramp succession cropping out in the Majella Mountain. However, this succession evidences a failure of SIS during latemost Tortonian and early Messinian because of a regional deviation of Sr isotope ratios from the global reference line.

The overall lower Sr isotope signature in comparison to the oceanic one has been interpreted as a hint of the progressive onset of restricted water exchanges between the Adriatic basin and the larger Mediterranean water body due to the local tectonic evolution, the narrow physiography of the proto-Adriatic basin and its shallow water column. In this framework, the enhanced freshwater input and continental runoff due to the migration of the accretionary wedge of the Apennine orogeny controlled the Sr isotope composition of this marginal basin, even if there is no evidence of salinity or major sea-level changes.

These results imply that not only a diagenetic overprint has to be ruled out prior to apply SIS on carbonate successions, but also an accurate oceanographic and geodynamic framework has to be taken into account before applying SIS on marginal basin successions, as in the case of an upper Miocene, Central Apennines platform.

Aknowledgments

The researches leading to this paper received support from Synthesys Programme, which is financed by the European Union's Seventh Framework Programme (FP7/2007-2013) under grant agreement n°226506 (SYNTHESYS). Editor Peter Doyle and an anonymous reviewer are sincerely thanked for their comments and criticisms that improved the manuscript. The Majella National Park, in particular in the person of Dr. Elena Liberatoscioli, is sincerely thanked for the license to take samples within the park.

References

Andersson, P.S., **Wassenburg, G.J.** and **Ingri, J.** (1992). The sources and transport of Sr and Nd isotopes in the Baltic Sea. *Earth Planet. Sci. Lett.,* 113, 459-472.

Bernhard, J.M. and **Sen Gupta, B.K.** (1999). Foraminifera of oxygen-depleted environments. In Sen Gupta, B.K. (ed.): *Modern Foraminifera.* Kluwer Academic Publishers, Dordrecht, The Netherlands, 201–216.

Betzler, C., Braga, J. C., Martín, J. M., Sanchez-Almazo, I. M. and **Lindhorst, S.** (2006). Closure of a seaway: stratigraphic record and facies (Guadix basin, Southern Spain). *International Journal of Earth Sciences*, 95, 903-910.

Blanc-Valleron, M. M., Pierre, C., Caulet, J. P., Caruso, A., Rouchy, J. M., Cespuglio, G., Sprovieri, R., Pestrea, S. and **Di Stefano, E.** (2002). Sedimentary, stable isotope and micropaleontological records of paleoceanographic change in the Messinian Tripoli Formation (Sicily, Italy). *Palaeogeogr. Palaeoclimatol. Palaeoecol.,* 185, 255-286.

Blow, W. (1969). Late-Middle Eocene to Recent planktonic foraminiferal biostratigraphy. In: Bronniman, P., Renz, M.M. (Eds.), *Proceeding of the First International Conference on Planktonic Microfossils*, Genève 1967, pp. 199–421.

Böhme, M., Ilg, A. and **Winklhofer, M.** (2008). Late Miocene "washhouse" climate in Europe. *Earth Planet. Sci. Lett.,* 275, 393–401.

Bosellini, F.R. (2006). Biotic changes and their control on Oligocene-Miocene reefs: A case study from the Apulia Platform margin (southern Italy). *Palaeogeogr. Palaeoclimatol. Palaeoecol.,* 241, 393–409

Bossio, A. (1996). Rosignano reef complex (Messinian), Livornesi Mountains, Tuscany, Central Italy. In: E.K. Franseen, M. Esteban, W. Ward and J. Rouchy (Eds.) *Models for Carbonate Stratigraphy from Miocene Reef Complexes of Mediterranean Regions*. SEPM Concepts in Sedimentology and Paleontology, 5, 277-294.

Braga, J. C., Martin, J. M. and **Alcala, B.** (1990) Coral reefs in coarse-terrigenous sedimentary environments (Upper Tortonian, Granada Basin, southern Spain). *Sed. Geol.,* 66, 135-150.

Braga, J. C. and **Martín, J. M.** (1996). Geometries of reef advance in response to relative sea-level changes in a Messinian (uppermost Miocene) fringing reef (Cariatiz reef, Sorbas Basin, SE Spain). *Sed. Geol.,* 107, 61-81.

Brand, U., Logan, A., Hiller, N. and **Richardson, J.** (2003). Geochemistry of modern brachiopods: applications and implications for oceanography and paleoceanography. *Chemical Geology*, 198, 305-334.

Brand, U. and **Veizer, J.** (1980). Chemical diagenesis of a multicomponent carbonate system--1: Trace elements. *Journal of Sedimentary Research*, 50, 1219-1236.

Brandano, M. and **Corda, L.** (2002). Nutrients, sea level and tectonics: constrains for the facies architecture of a Miocene carbonate ramp in central Italy. *Terra Nova*, 14, 257–262.

Brandano, M. and **Policicchio, G.** (2012). Strontium stratigraphy of the Burdigalian transgression in the Western Mediterranean. *Lethaia*, 45, 315-328.

Brandano, M., Lipparini, L., Campagnoni, V. and **Tomassetti, L.** (2012). Downslope-migrating large dunes in the Chattian carbonate ramp of the Majella Mountains (Central Apennines, Italy). *Sed. Geol.,* 255-256*,* 29–41.

Brandano, M., Cornacchia, I., Raffi, I. and **Tomassetti, L.** (2016b). The Oligocene-Miocene stratigraphic evolution of the Majella carbonate platform (Central Apennines, Italy). *Sed. Geol.*, 333, 1-14.

Brandano, M., Tomassetti, L., Sardella, R. and **Tinelli, C.** (2016a). Progressive deterioration of trophic conditions in a carbonate ramp environment: the *Lithothamnion* Limestone, Majella Mountain (Tortonian-early Messinian, Central Apennines, Italy). *Palaios*, 31, 125-140.

Burke, W.H., Denison, R.E., Hetherington, E.A., Koepnick, R.B., Nelson, H.F. and **Otto, J.B.** (1982). Variation of $^{87}Sr/^{86}Sr$ throughout Phanerozoic time. *Geology*, 10, 516–519.

Carannante, G. and **Simone, L.** (1996). Rhodolith facies in the central-southern Apennines mountains, Italy. *SEPM*, 261-275.

Carminati, E., Lustrino, M., Cuffaro, M. and **Doglioni, C.** (2010). Tectonics, magmatism and geodynamics of Italy: what we know and what we imagine, In*: Beltrando, M., Peccerillo, A., Mattei, M., Conticelli, S., Doglioni, C. (Eds.), The Geology of Italy.* Journal of the Virtual Explorer, Electronic Edition, 36, paper 9. ISSN 1441–8142.

Carnevale, G., Patacca, E. and **Scandone, P.** (2011). Field guide to the post-conference excursions Scontrone, Palena and Montagna della Majella). *R.C.M.N.S. Interim Colloquium*, 4–5 March 2011, Scontrone (L'Aquila), Italy, pp. 1-99.

Cipollari, P. and **Cosentino, D.** (1995). Miocene unconformities in the Central Apennines: geodynamic significance and sedimentary basin evolution. *Tectonophysics,* 375-389.

Cosentino, D., Cipollari, P., Marsili, P. and **Scrocca, D.** (2010). Geology of the central Apennines: a regional review. *In* Beltrando M., Peccerillo A., Mattei M., Conticelli S., Doglioni C. (eds.): *The Geology of Italy. Journal of the Virtual Explorer*. Electronic Edition. ISSN 1441-8142, v. 36, paper 11.

Crescenti, U., Crostella, A., Donzelli, G. and **Raffi, G.** (1969). Stratigrafia della serie calcarea dal Lias al Miocene nella regionemarchigiano abruzzese: Parte II.

Litostratigrafia, biostratigrafia, paleogeografia. *Memorie della Società Geologica Italiana*, 9, 343–420.

Danese, E. (1999). Upper miocene carbonate ramp deposits from the southernmost part of Maiella Nountain (Abruzzo, Central Italy). *Facies*, 41, 41-54.

De Paolo, D.J. and **Ingram, B.L.** (1985). High-resolution stratigraphy with strontium isotopes. *Science*, 227, 938–941.

Esteban, M. (1996). An overview of Miocene reefs from Mediterranean areas: general trends and facies models. In: E.K. Franseen, M. Esteban, W. Ward and J. Rouchy (Eds.) *Models for Carbonate Stratigraphy from Miocene Reef Complexes of Mediterranean Regions*. SEPM Concepts in Sedimentology and Paleontology, 5, 3-53.

Esteban, M., Braga, J.C., Martín, J. and **De Santisteban, C.** (1996). Western Mediterranean reef complexes. In: E.K. Franseen, M. Esteban, W. Ward and J. Rouchy (Eds.) *Models for Carbonate Stratigraphy from Miocene Reef Complexes of Mediterranean Regions*. SEPM Concepts in Sedimentology and Paleontology, 5, 55-72.

Faure, G. (1986). Principles of isotope geochemistry. *John Wiley and Sons 6*, 8.

Flecker, R., and **Ellam, R.M.** (2006). Identifying late Miocene episodes of connection and isolation in the Mediterranean-Paratethyan realm using Sr isotopes. *Sed. Geol.,* 188–189, 189–203.

Flecker, R., de Viellers, S. and **Ellam, R. M.** (2002). Modelling the effects of evaporation on the salinity–$^{87}Sr/^{86}Sr$ relationship in modern and ancient marginal-marine systems: the Mediterranean Messinian Salinity Crisis. *Earth Planet. Sci. Lett.*, 203, 221-233.

Frezza, V. and **Carboni, M.G.** (2009). Distribution of recent foraminiferal assemblages near the Ombrone River mouth (Northern Tyrrhenian Sea, Italy). *Revue de Micropaléontologie,* 52, 43-66.

Frijia, G. and **Parente, M.** (2008). Strontium isotope stratigraphy in the upper Cenomanian shallow-water carbonates of the southern Apennines: Short-term perturbations of marine 87 Sr/86 Sr during the oceanic anoxic event 2. *Palaeogeogr. Palaeoclimatol. Palaeoecol.,* 261, 15-29.

Frijia, G., Parente, M., Di Lucia, M. and **Mutti, M.** (2015). Carbon and strontium isotope stratigraphy of the Upper Cretaceous (Cenomanian-Campanian) shallow-water carbonates of southern Italy: Chronostratigraphic calibration of larger foraminifera biostratigraphy. *Cretaceous Research,* 53, 110-139.

Halfar, J., Godinez-Orta, L., Mutti, M., Valdez-Holguín, J. E. and **Borges, J. M.** (2004). Nutrient and temperature controls on modern carbonate production: an example from the Gulf of California, Mexico. *Geology,* 32, 213-216.

Halfar, J., Godinez-Orta, L., Mutti, M., Valdez-Holguin, J. E. and **Borges, J. M.** (2006). Carbonates calibrated against oceanographic parameters along a latitudinal transect in the Gulf of California, Mexico. *Sedimentology,* 53, 297-320.

Hilgen, F., Aziz, H. A., Bice, D., Iaccarino, S., Krijgsman, W., Kuiper, K., Montanari, A., Raffi, I., Turco, E. and **Zachariasse, W. J.** (2005). The global boundary stratotype section and point (GSSP) of the Tortonian stage (Upper Miocene) at Monte Dei Corvi. *Episodes-Newsmagazine of the International Union of Geological Sciences*, 28, 6-17.

Howart, R. J. and **McArthur, J. M.** (1997). Statistics for strontium isotope stratigraphy with a look-up table version. The *Journal of Geology,* 105, 441-456.

Immenhauser, A., Schöne, B. R., Hoffmann, R. and **Niedermayr, A.** (2016). Mollusc and brachiopod skeletal hard parts: Intricate archives of their marine environment. *Sedimentology*, 63, 1-59.

Ingram, B. L. and **Sloan, D.** (1992). Strontium isotopic composition of estuarine sediments as paleosalinity-paleoclimate indicator. *Science,* 255, 68-72.

Jorissen, F.J. (1987). The distribution of benthic foraminifera in the Adriatic Sea. *Marine Micropaleontology,* 12, 21-48.

Kocsis, L., Vennemann, T.W., Fontignie, D., Baumgartner, C. and **Montanari, A.** (2008). Oceanographic and climatic evolution of the Miocene Mediterranean deduced from Nd, Sr, C e O isotope compositions of marine fossils and sediments. *Paleoceanography,* 23, PA4211.

Kouwenhoven, T.J., Morigi, C., Negri, A., Giunta, S., Krijgsman, W. and **Rouchy, J.M.** (2006). Paleoenvironmental evolution of the eastern Mediterranean during the Messinian: Constraints from integrated microfossil data of the Pissouri Basin (Cyprus). *Marine Micropaleontology,* 60, 17-44.

Iaccarino, S. (1985). Mediterranean Miocene and Pliocene planktic foraminifera. In: Bolli, H.M., Saunders, J.B., Perch-Nielsen, K. (Eds.), *Plankton Stratigraphy*. Cambridge University Press, Cambridge, pp. 283–314.

Lirer, F. (2000). A new technique for retrieving calcareous microfossils from lithified lime deposits. *Micropaleontology*, 46, 365-369.

Longman, M. W. (1980) Carbonate diagenetic textures from nearsurface diagenetic environments. *AAPG Bulletin,* 64, 461-487.

Martín, J. M., Braga, J. C., Aguirre, J. and **Puga-Bernabéu, Á.** (2009). History and evolution of the North-Betic Strait (Prebetic Zone, Betic Cordillera): a narrow, early Tortonian, tidal-dominated, Atlantic–Mediterranean marine passage. *Sed. Geol.,* 216, 80-90.

Mattioli, M., Lustrino, M., Ronca, S. and **Bianchini, G.** (2012). Alpine subduction imprint in Apennine volcaniclastic rocks. Geochemical–petrographic constraints and geodynamic implications from Early Oligocene Aveto-Petrignacola Formation (N Italy). *Lithos*, 134-135, 201-220.

McArthur, J. M. (1994). Recent trends in strontium isotope stratigraphy. *Terra Nova,* 6, 331-358.

McArthur, J. M., Howarth, R. J., and **Bailey, T. R.** (2001). Strontium isotope stratigraphy: LOWESS version 3: best fit to the marine Sr-isotope curve for 0–509 Ma and accompanying look-up table for deriving numerical age. *The Journal of Geology,* 109, 155-170.

McArthur, J.M. and **Howarth, R.J.** (2004). Strontium isotope stratigraphy. In: *A Geologic Time Scale* (Gradstein, F., Ogg, J., Smith, A. eds), Cambridge University Press, Cambridge, 96-105.

McArthur, J.M., Howarth, R.J. and **Schields, G.A.** (2012). Strontium Isotope Stratigraphy. In: In: *The Geologic Time Scale 2012.* Gradstein F.M., Ogg J.G., Schmitz M.D., Ogg G.M. (eds). Elsevier: Amsterdam, 207-232.

Merola, D. (2007). Biostratigrafia a foraminiferi planctonici dei depositi emipelagici dell'Oligocene Superiore/Miocene Inferiore (Calcari con Selce) e del Miocene Medio (Calcilutiti ad Orbulina) della Montagna della Maiella (Appennino centrale, Abruzzo). Unpublished PhD Thesis, Pisa.

Milli, S., Moscatelli, M., Stanzione, O. and **Falcini, F.** (2007). Sedimentology and physical stratigraphy of the Messinian turbidite deposits of the Laga basin (central Apennines, Italy). *Boll. Soc. Geol. It.,* 126, 255-281.

Montanari, A., Beaudoin, B., Chan, L.S., Coccioni, R., Deino, A., DePaolo, D.J., Emmanuel, L., Fornaciari, E., Kruge, M., Lundblad, S., Mozzato, C., Portier, E., Renard, M., Rio, D., Sandroni P. and **Stankiewicz, A.** (1997). Integrated stratigraphy of the Middle to Upper Miocene pelagic sequence of the Conero Riviera (Marche Region, Italy). In: *Miocene Stratigraphy: An Integrated Approach*, edited by A. Montanari, G. Odin, and R. Coccioni, Elsevier Science, Amsterdam, 409–450.

Morse, J.W. and **Mackenzie, F.T.** (1990). *Geochemistry of sedimentary carbonates. In: Developments in Sedimentology,* 48,707 pp. Elsevier.

Murray, J.W. (2006). *Ecology and Applications of Benthic Foraminifera.* Cambridge University Press. Cambridge. 426 pp.

Mutti, M., Bernoulli, D., Eberli, G.P. and **Vecsei, A.** (1996). Depositional geometries and facies associations in an upper Cretaceous prograding carbonate platform margin (Orfento supersequence, Maiella, Italy). *Journal of Sedimentary Research,* 66, 749–765.

Mutti, M., Bernoulli, D. and **Stille, P.** (1997). Temperate carbonate platform drowning linked to Miocene oceanographic events: Maiella platform margin, Italy. *Terra Nova*, 9, 122-125.

Mutti, M., Bernoulli, D., Spezzaferri, S. and **Stille, P.** 1999: Lower and Middle Miocene carbonate facies in the central Mediterranean: the impact of paleoceanography on sequence stratigraphy. In: *Harris, P., Saller, A., Simo, J., Handford, C.R. (Eds.), Advances in carbonate sequence stratigraphy: application to reservoirs, outcrops and models. SEPM, SP.,* 63, 371–384.

Patacca, E., Scandone, P., Di Luzio, E., Cavinato, G.P. and **Parotto, M.** (2008). Structural architecture of the central Apennines: Interpretation of the CROP 11 seismic profile from the Adriatic coast to the orographic divide. *Tectonics,* 27, TC3006, doi:10.1029/2005TC001917.

Patacca, E., Scandone, P. and **Carnevale, G.** (2013). The Miocene vertebrate-bearing deposits of Scontrone (Abruzzo, Central Italy): stratigraphic and paleoenvironmental analysis. *Geobios*, 46, 5-23.

Pedley, M. (1996). Miocene reef facies of the Pelagian region (Central Mediterranean). In: In: E.K. Franseen, M. Esteban, W. Ward and J. Rouchy (Eds.) *Models for Carbonate Stratigraphy from Miocene Reef Complexes of Mediterranean Regions.* SEPM Concepts in Sedimentology and Paleontology, 5, 247-260.

Pomar, L., Brandano, M. and **Westphal, H.** (2004). Environmental factors influencing skeletal grain sediment associations: a critical review of Miocene examples from the western Mediterranean. *Sedimentology*, 51, 627-651.

Pomar, L., Bassant, P., Brandano, M., Ruchonnet, C., & **Janson, X.** (2012). Impact of carbonate producing biota on platform architecture: insights from Miocene examples of the Mediterranean region. *Earth-Sci. Rev.,* 113, 186-211.

Robbins, L.L. (1988). Environmental significance of morphologic variability in open-ocean versus ocean-margin assemblages of Orbulina universa. *Journal of Foraminiferal Research*, 18, 326-333.

Rögl, F. (1999). Mediterranean and Paratethys. Facts and hypotheses of an Oligocene to Miocene paleogeography (short overview). *Geologica Carpathica*, 50, 339-349.

Scasso, R. A., McArthur, J. M., Del Rıo, C. J., Martınez, S. and **Thirlwall, M. F.** (2001): $^{87}Sr/^{86}Sr$ Late Miocene age of fossil molluscs in the 'Entrerriense'of the Valdés Peninsula (Chubut, Argentina). *Journal of South American Earth Sciences*, 14, 319-329.

Schildgen, T. F., Cosentino, D., Frijia, G., Castorina, F., Dudas, F. Ö., Iadanza, A., Sampalmieri, G., Cipollari, P., Caruso, A. and **Strecker, M. R.** (2014). Sea level and climate forcing of the Sr isotope composition of late Miocene Mediterranean marine basins. *Geochemistry, Geophysics, Geosystems,* 15, 2964-2983.

Sirna, G. (1996). Brachiopodi miocenici dei dintorni di Scanno e della Maiella. *Boll. Soc. Paleontol. It.,* 5, 184-196.

Snedden, J. W. and **Liu, C.** (2011). Recommendations for a uniform chronostratigraphic designation system for Phanerozoic depositional sequences. *AAPG bulletin*, 95, 1095-1122.

Sprovieri, R., Di Stefano, E., Caruso, A. and **Bonomo, S.** (1996). High resolution stratigraphy in the Messinian Tripoli Formation in Sicily. *Palaeopelagos,* 6, 415-435.

Steuber, T. (1999). Isotopic and chemical intra-shell variations in low-Mg calcite of rudist bivalves (Mollusca-Hippuritacea): disequilibrium fractionations and late Cretaceous seasonality. *International Journal of Earth Sciences*, 88, 551-570.

Suc, J.-P., Violanti, D., Londeix, L., Poumot, C., Robert, C., Clauzon, G., Gautier, F., Turon, J-L., Ferrier, J., Chikhi, H. and **Cambon, G.** (1995). Evolution of the Messinian Mediterranean environments: the Tripoli Formation at Capodarso (Sicily, Italy). *Review of Palaeobotany and Palynology,* 87, 51-79.

Taylor, A. S. and **Lasaga, A. C.** 1999. The role of basalt weathering in the Sr isotope budget of the oceans. *Chemical Geology*, 161, 199-214.

Topper, R. P. M., Flecker, R., Meijer, P. T. and **Wortel, M. J. R.** (2011). A box model of the Late Miocene Mediterranean Sea: Implications from combined 87Sr/86Sr and salinity data. *Paleoceanography*, 26, PA3223, doi:10.1029/2010PA002063.

Trezzi, G., Garcia-Orellana, J., Rodellas, V., Masqué, P., Garcia-Solsona, E. and **Andersson, P. S.** (2017). Assessing the role of submarine groundwater discharge as a source of Sr to the Mediterranean Sea. *Geochimica et Cosmochimica Acta,* 200, 42-54.

Vecsei, A., Sanders, D. G. K., Bernoulli, D., Eberli, G. P. and **Pignatti, J.** (1998). Cretaceous to Miocene sequence stratigraphy and evolution of the Maiella carbonate platform margin, Italy. In: *Mesozoic and Cenozoic Sequence Stratigraphy of European Basins, SEPM Special Publication*, 60, 53-74.

Veizer, J., Buhl, D., Diener, A., Ebneth, S., Podlaha, O. G., Bruckschen, P., Jasper, T., Korte, C., Schaaf, M., Ala, D. and **Azmy, K.** (1997). Strontium isotope stratigraphy: potential resolution and event correlation. *Palaeogeogr. Palaeoclimatol. Palaeoecol.,* 132, 65-77.

Veizer, J., Ala, D., Azmy, K., Bruckschen, P., Buhl, D., Bruhn, F., Carden, G.A.F., Diener, A., Ebneth, S., Godderis, Y., Jasper, T., Korte, C., Pawellek, F., Podlaha, O.G. and **Strauss, H.** (1999). $^{87}Sr/^{86}Sr$, $\delta^{13}C$ and $\delta^{18}O$ evolution of Phanerozoic seawater. *Chemical Geology*, 161, 59-88.

Vezzani, L., Festa, A. and **Ghisetti, F.C.** (2010). Geology and tectonic evolution of the Central-Southern Apennines, Italy. *Geological Society of America Special Papers,* 469, 1-58.

Violanti, D., Lozar, F., Natalicchio, M., Dela Pierre, F., Bernardi, E., Clari, P. and **Cavagna, S.** (2013). Stress-tolerant microfossils of a Messinian succession from the Northern Mediterranean basin (Pollenzo section, Piedmont, northwestern Italy). *Boll. Soc. Paleontol. It.,* 52, 45-54. Modena.

Weissert, H. (1989). C-isotope stratigraphy, a monitor of paleoenvironmental change: a case study from the Early Cretaceous. *Surveys in Geophysics*, *10*, 1-61.

Weissert, H., Joachimski, M. and **Sarnthein, M.** (2008). Chemostratigraphy. *Newsletter on Stratigraphy*, 42, 145-179.

Wenzel, B. (2000). Differential preservation of primary isotopic signatures in Silurian brachiopods from northern Europe. *J. Sed. Res.*, 70, 194-209.

6 Conclusions

In this work, the impact of carbon cycle perturbations on the Central Mediterranean carbonate successions from late Eocene to Miocene has been analysed. The complex interplay between the global forcing and the regional controlling factors that affected the carbonate production and the local isotope signature is widely discussed.

Carbon isotope curves of the Mediterranean successions from late Eocene to middle Miocene record the major global trends. The upper Eocene carbon isotope record of the Apula carbonate platform (Majella Mountain, Central Apennines) shows an overall decreasing trend, which marks the recovery from the carbon isotope anomaly contemporary to the Middle Eocene Climatic Optimum, and precedes the positive carbon isotope shift contemporary to the Oi-1 event. Accordingly, the pelagic $\delta^{13}C_{TOC}$ of the Umbria-Marche domain (Northern Apennines) records an increasing trend, which testifies for a reduced fractionation effect on carbon isotopes by the marine primary producers. However, the pelagic carbon isotope record of the upper Miocene is punctuated by several negative spikes between 36.5 and 36.0 Ma. These sharp and transient anomalies are mainly controlled by the oceanography of the Mediterranean during late Eocene. In fact, negative carbon isotope spikes are related to the westward subtropical Eocene Neo-Tethys current that entered from the Indian Gateway, bringing large amounts of deep-waters, rich in iron, triggering high productivity pulses. The Umbria-Marche carbon isotope curve, measured in the Massignano section, GSSP of the Eocene/Oligocene, records the onset of the shift related to the Oi-1 event, but not the entire perturbation. On the contrary, the platform record does not show any positive spike related to productivity pulses, nor any significant carbonate production change. The latter could be due to the investigated depositional environments. In fact, the studied portion of the Santo Spirito Formation (Majella Mountain, Central Apennines) identifies the lower middle and the outer ramp environments, developed within the aphotic zone, where only photo-independent biota live. However, a change in the composition of the carbonate factory can be inferred by the observation of the major components of the resedimented material. Across the Eocene-Oligocene transition, overall the Larger Benthic Foraminifera reduce, among them the ortophragminids disappear, while the red algae increase and the corals spread. Lastly, the Santo Spirito carbon isotope record does not document the positive shift related to the Oi-1 event, since the regular bedding is interrupted in the lower Oligocene by the occurrence of extensive slumps. These slumps, occurring over the entire ramp, represent the major evidence of the sea-level fall related to the onset of the Antarctica ice-sheet, which led to the deepening of the storm-weather wave base, favouring an increased instability on the ramp. Unlike the carbon isotope anomaly at the Eocene-Oligocene transition, the Monterey Event has been unequivocally identified in both the Central Apennines platforms (Latium-Abruzzi and Apula Platforms). A long-term positive excursion characterises the lower to middle Miocene carbon isotope curves of these platforms. An accurate chronostratigraphic framework, based on calcareous nannofossil biostratigraphy and Sr Isotope Stratigraphy, allowed to correlate at least two of the six carbon maxima identified in the deep-sea to the global record. The correlation of the shallow-water carbon isotope signal with the Umbria-Marche pelagic and the global record shows that the Monterey Carbon Isotope Excursion is four times wider in magnitude in the platform than in the pelagic record, and twice than the open-ocean signal. Lastly, in the middle to outer ramp environments of the Apennine Platforms, the Monterey event coincides with the spread of bryozoans, filter feeding organisms, favoured by the high trophic conditions of the waters during the middle Miocene climatic optimum. Furthermore, the high trophic conditions of the Mediterranean waters during middle Miocene must have been sustained also by regional causes, e.g. the subduction-related volcanism of the Sardinia-Corsica Block, coupled with the closure of the Indian Gateway between late Burdigalian and the Langhian. In turn, the high productivity of the bryozoan-dominated carbonate factory in the aphotic zone led to the development of low-angle ramps.

Sr and Nd isotope records of two hemipelagic carbonate successions of the Adriatic Domain (Northern and Central Apennines) indeed testify that the dynamic evolution of the Central Mediterranean had unequivocal impact on its water chemistry. The Sr isotope ratios deviate from the global reference line during three critical intervals: late Aquitanian, middle to late Burdigalian and the Messinian. In late Aquitanian, during a low-stand phase related to a glaciation, the increased continental runoff affected the Central Mediterranean seaweater, leading to a rise of the $^{87}Sr/^{86}Sr$ ratio in comparison to the global ocean signal. On the contrary, during middle to late Burdigalian, the Sr isotope signature of the Central Mediterranean is significantly lighter than the global signal due to the highly explosive subduction-related volcanic activity developed in the Western Mediterranean and within the overall circum-Mediterranean area. Lastly, during the Messinian, several sub-marginal basins of the Central Mediterranean, e.g. the proto-Adriatic basin, faced restricted water conditions testified by the Sr isotope ratios, which fall below the global reference line significantly before the Messinian salinity crisis.

The Miocene Nd isotope record testifies for the transition from a wide open Mediterranean basin, well connected with both the Atlantic and the Indo-Pacific Oceans, to the modern closed basin. The lower Miocene Nd isotope record documents that the major water mass entered the Mediterranean from the deep Indian Gateway, and that the Indo-Pacific Ocean mainly controlled the Central Mediterranean Nd isotope signature. In fact, the Cenozoic volcanism developed in the northern Indian Ocean affected the Mediterranean Nd isotope signal during Aquitanian. On the contrary, during middle Miocene, the Nd isotope ratios testify for a Central Mediterranean exchanging with the Paratethys, in particular during the sea-level high-stand linked to the Middle Miocene Climatic Optimum. During the Messinian, the Nd isotope datum is coherent with the Sr isotope record, indicating an overall Atlantic Ocean influence on the proto-Adriatic marginal basin, which was also partly contaminated by the local freshwater input and runoff. Lastly, the overall deviation of the Central Mediterranean Nd isotope record in comparison to the Oceans signal reflects the evolution and the physiography of the Mediterranean basin. The proximity of the land, also testified by the occurrence of hemipelagic rather than open-ocean deposits, is a major controlling factor on the seawater chemistry of the Central Mediterranean. Thus, the Mediterranean Nd isotope signature could never be the same as either one of the surrounding Oceans, but it will always be a mix of two opposite signals: the Atlantic and Indo-Pacific signatures and the main circulation patterns, and the local geodynamic evolution coupled with the volcanic activity. However, the comparison of the Mediterranean Nd isotope signature with the open ocean signals provides the information on which Ocean mainly affected the Mediterranean waters during the different stages of its evolution.

The onset of restricted water conditions in the proto-Adriatic basin is testified not only by the Central Apennine hemipelagic record, but also by the late Miocene platform record (*Lithothamnion* Limestone ramp, Majella Mountain). Biostratigraphic studies, coupled with Sr Isotope Stratigraphy, allowed to ascribe this shallow-water unit to the late Tortonian-early Messinian interval. However, the early Messinian Sr isotope record deviates from the global ocean reference line. This mismatch has been linked to the progressive onset of restricted conditions due to the eastward migration of the Apennine accretionary wedge, which controlled the narrow physiography of the proto-Adriatic basin, simultaneously favouring an increased freshwater input and sustaining high rates of runoff. These results imply that the Sr Isotope Stratigraphy has to be applied extremely carefully on marginal basins, even when facies analysis supports fully marine conditions, no significant salinity changes occur, and when any major diagenetic overprint can be ruled out.

To conclude, this work states that the global carbon isotope trends and perturbations occurred between late Eocene and middle Miocene are indeed recorded in the Central Mediterranean carbonate successions, but that the superimposed local factors, related to the geodynamic evolution of the Mediterranean area, masked or hampered the global climatic forcing, complicating the overall local carbonate successions records. Furthermore, this work intends to emphasize how an accurate biostratigraphic framework is necessary prior to apply chemostratigraphy on carbonate successions, in particular within marginal basins, since multiple regional factors may distort the response of carbonate systems to global forcings, potentially leading to mistakes and misinterpretations.

Aknowledgements

Despite this thesis carries my name first, it is indeed the result of a three-years long journey and a huge team effort. Many people, without whom nothing could have been possible, must be thanked.
Firstly, I do want to thank Marco Brandano, my tutor, guide and mentor throughout all the journey. I have met him when I was only a bachelor student, and since then he has always led me and advised me, never stopping to listen to my ideas and questions. It has been a challenge and a privilege to study and work with him in these years, during which I did grew up a lot, trying to follow his footsteps, even when it meant climbing hundreds of meters under the heavy rain.
Secondly, a great thank goes to my cotutors: Isabella Raffi and Samuele Agostini. Thanks to Isabella, who taught me how to see the invisible, and showed me, through her very own example, how to be a strong woman and a great researcher. Thanks to Samuele, who bet on me and on this project almost blindly, showing always a great enthusiasm for this research, totally new for him, and even greater patience for my never-ending questions. In Pisa, under the guidance of Samuele, I have learnt the very meaning of the word patience in the clean laboratory, and that no matter how little is your sample, atoms will always be littler.
Some great thanks go to Laura Tomassetti, whose work, collaboration and guidance have been nothing but essential. Firstly, her PhD laid the foundations to this research, opening a lot of scientific questions which we answered later together. Secondly, but not for importance, she has followed me through all these years, answering patiently and constantly to all my questions and my disparate doubts, in Rome as in the field.
A great thank is for the rewievers of this thesis: Helmut Weissert, Nereo Preto and Telm Bover-Arnal. I had the great opportunity to meet Helmi for the first time when I started the PhD, and in several other occasions during these years, and every time he has given me important feedbacks on my research, suggestions on things to be explored, and a good dose of encouragement to fulfil my goals and dreams. The suggestions of Nereo undoubtely improved this work and, most important, made me realise how many questions are still open, encouraging me to keep (re)searching. Last not least, the comments of Telm really improved this work and its form.
Michele Lustrino is sincerely thanked for all the support and helpfulness he showed me, finding always time to discuss the best analytical methods to reach a specific goal, to provide me the contacts of the best laboratories, to explore the evolution of the Mediterranean and of the geosciences. Most of all, he taught me, through his own example, how curiosity is the first engine of research.
Thanks to Mauro Brilli and Francesca Giustini, whom I have flooded with samples in their laboratory during these years, and never stopped welcoming and helping me.
Many thanks go indeed to Domenico “Mimmo” Mannetta for the amazing thin sections he provided, demonstrating for the umpteenth time how his work is more an art than a technique, and to Giovanni Gaglianone, who opened me the sedimentology laboratory for all the most disparate attempts I could imagine. Their support and help have been fundamental.
Thanks to Marcello Serracino for his patience in teaching me how to use a microprobe, and to Paolo Di Giuseppe, to whom the clean laboratory in Pisa has no secrets.

A great thank to my Sweden hosts, Per Andersson, whose collaboration has been stimulating and precious, Karin Wallner and Hans Schöberg, who opened me the laboratories, day and night, demonstrating how science is a passion first, and a teamwork secondly.
Thanks to all the co-authors of the papers, those included in the thesis and those that were preliminary but fundamental to it. Thanks to Letizia Di Bella, Adele Garzarella, Cristiano Ricci and Isabella Flores.
Last not least, thanks to the “Parco Nazionale della Majella” for providing the license to take samples within the park, and in particular to Elena Liberatoscioli, who valued this research from the beginning and followed it at every step.

Annex A Stratigraphic sections

A.1 Geological Map of the Majella Mountain

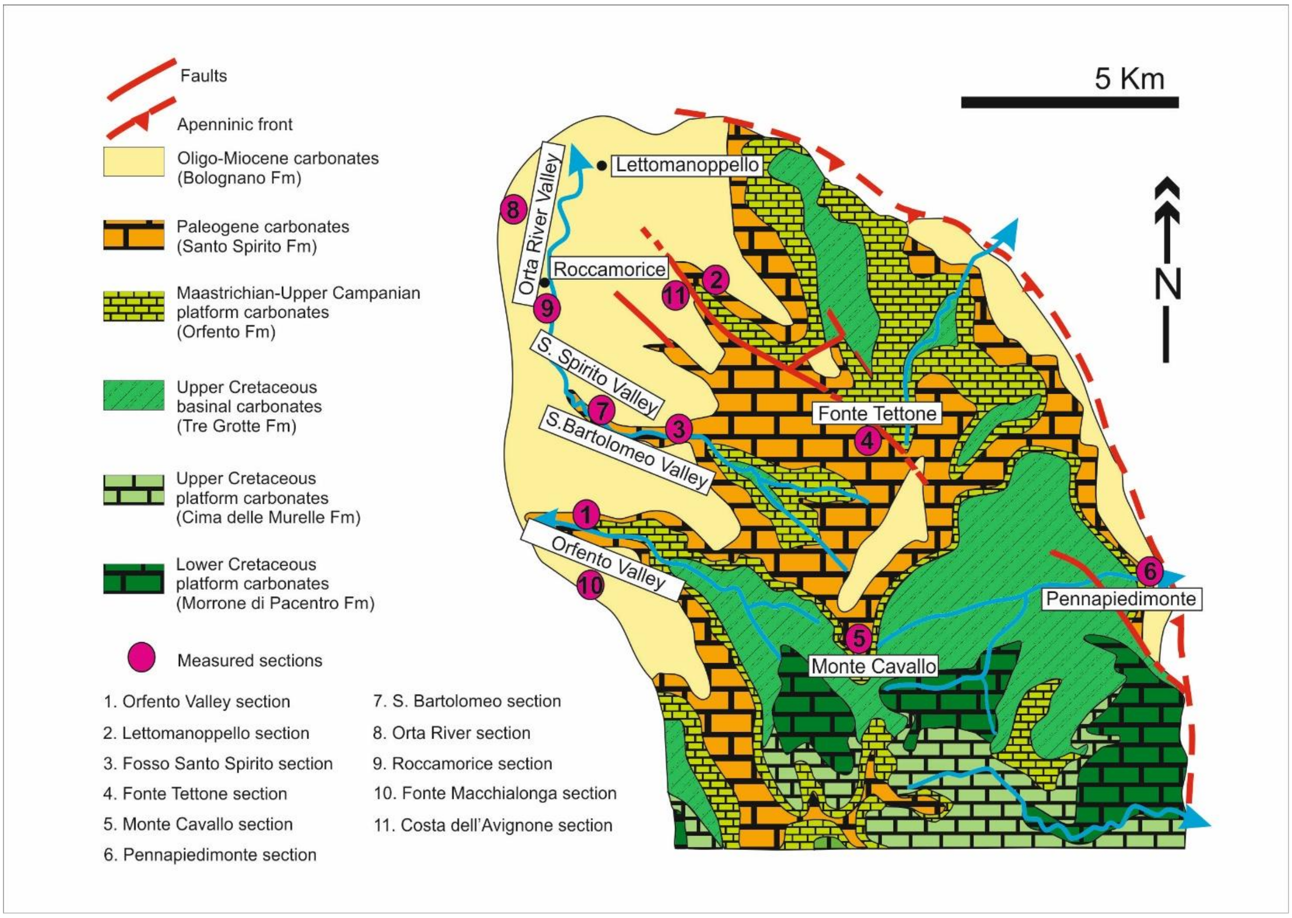

Fig. A.1. Geological map of the Majella Mountain (Central Apennines) with the locations of the measured sections (modified after Vecsei and Sanders, 1999).

A.2: Orfento Valley section

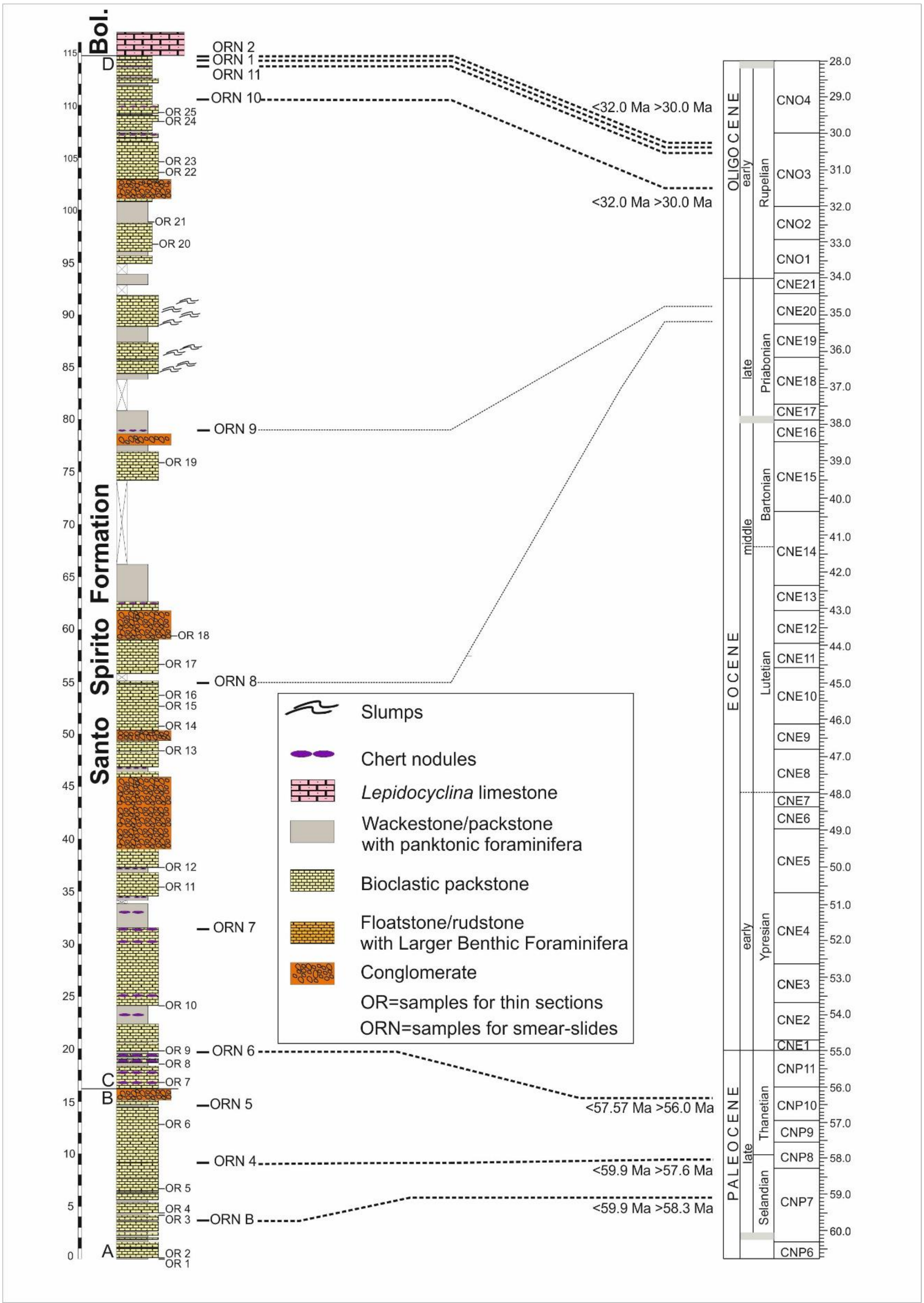

A.3: Lettomanoppello section

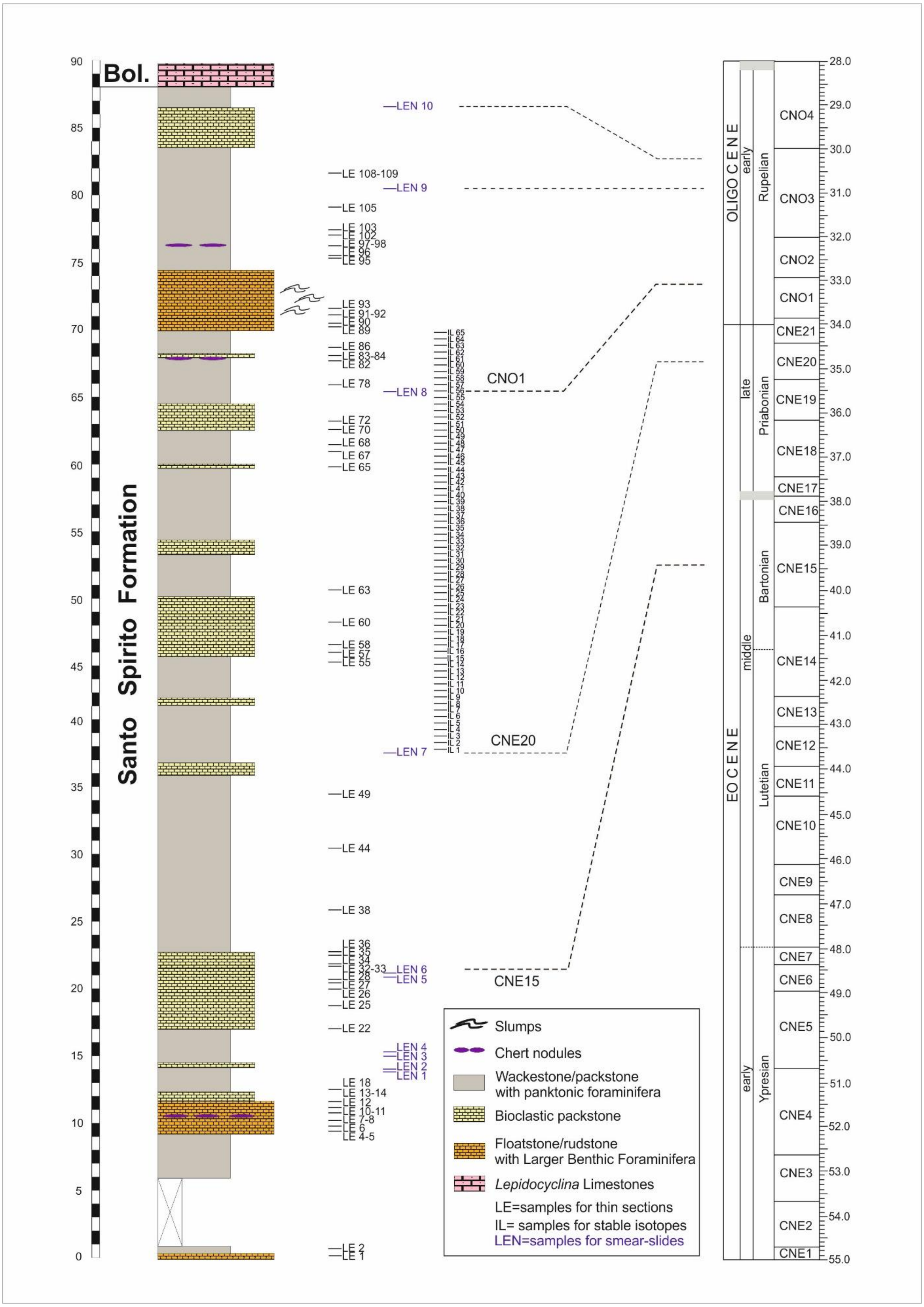

A.4: Fosso Santo Spirito section

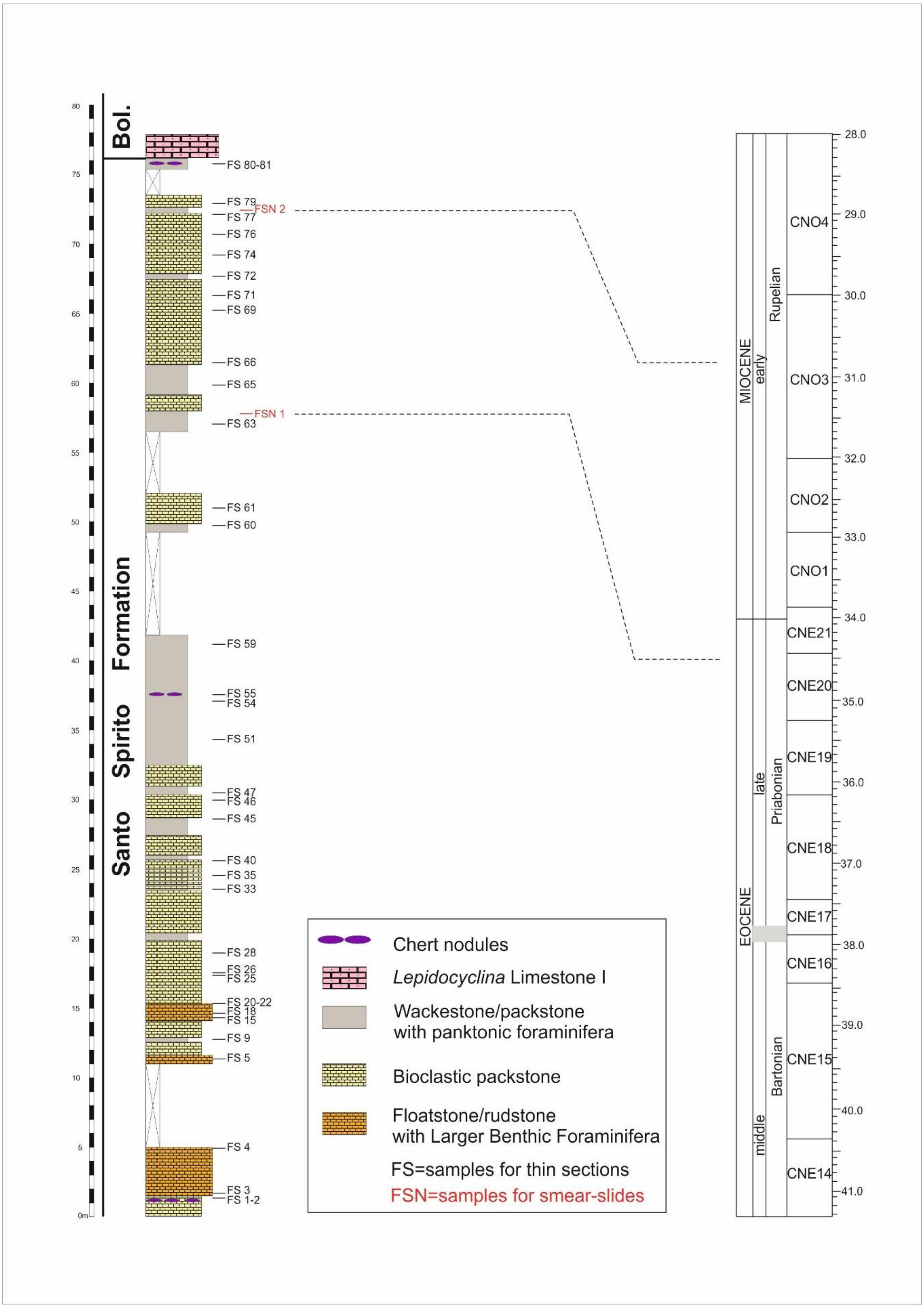

A.5: Fonte Tettone section

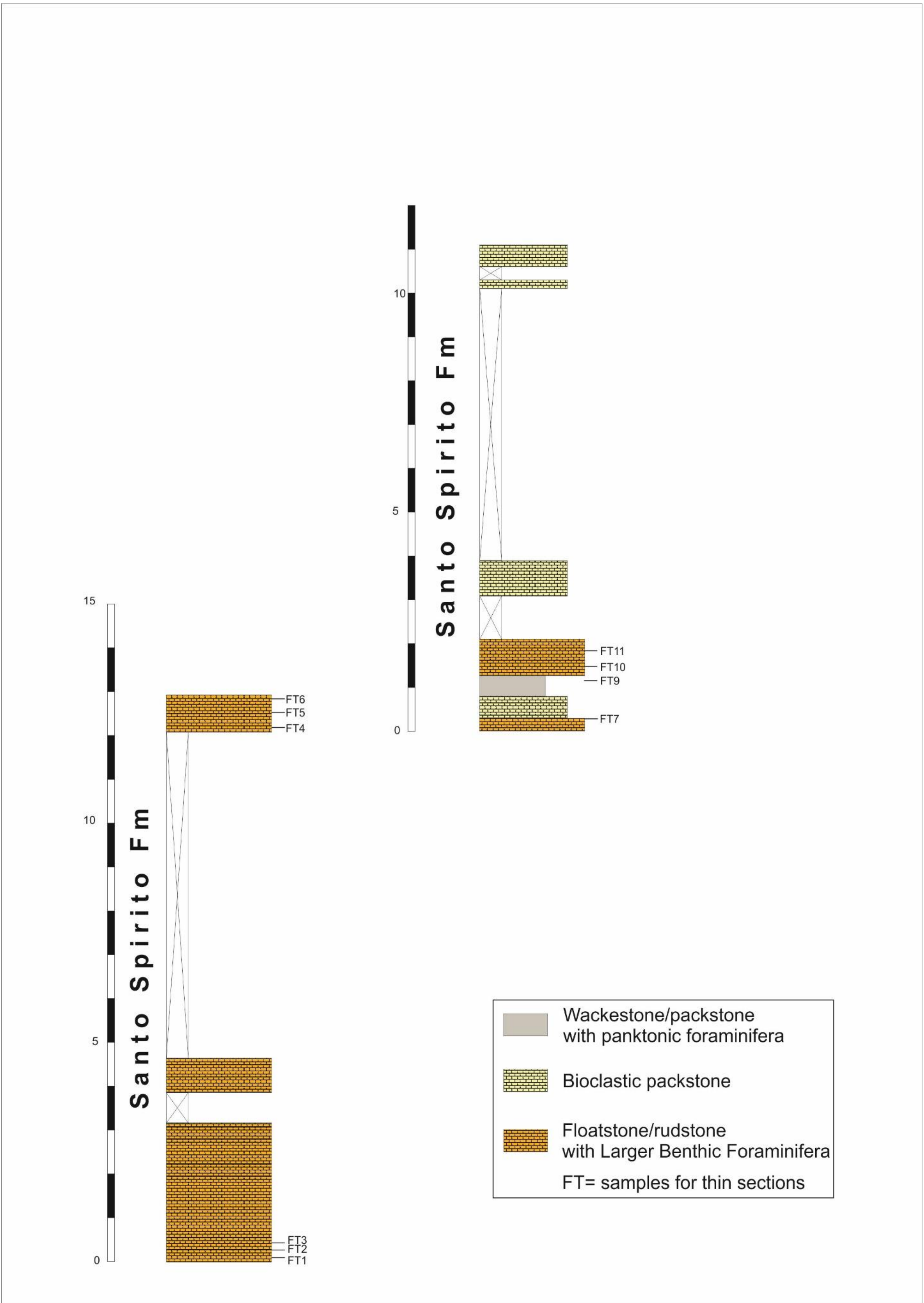

A.6: MONTE CAVALLO

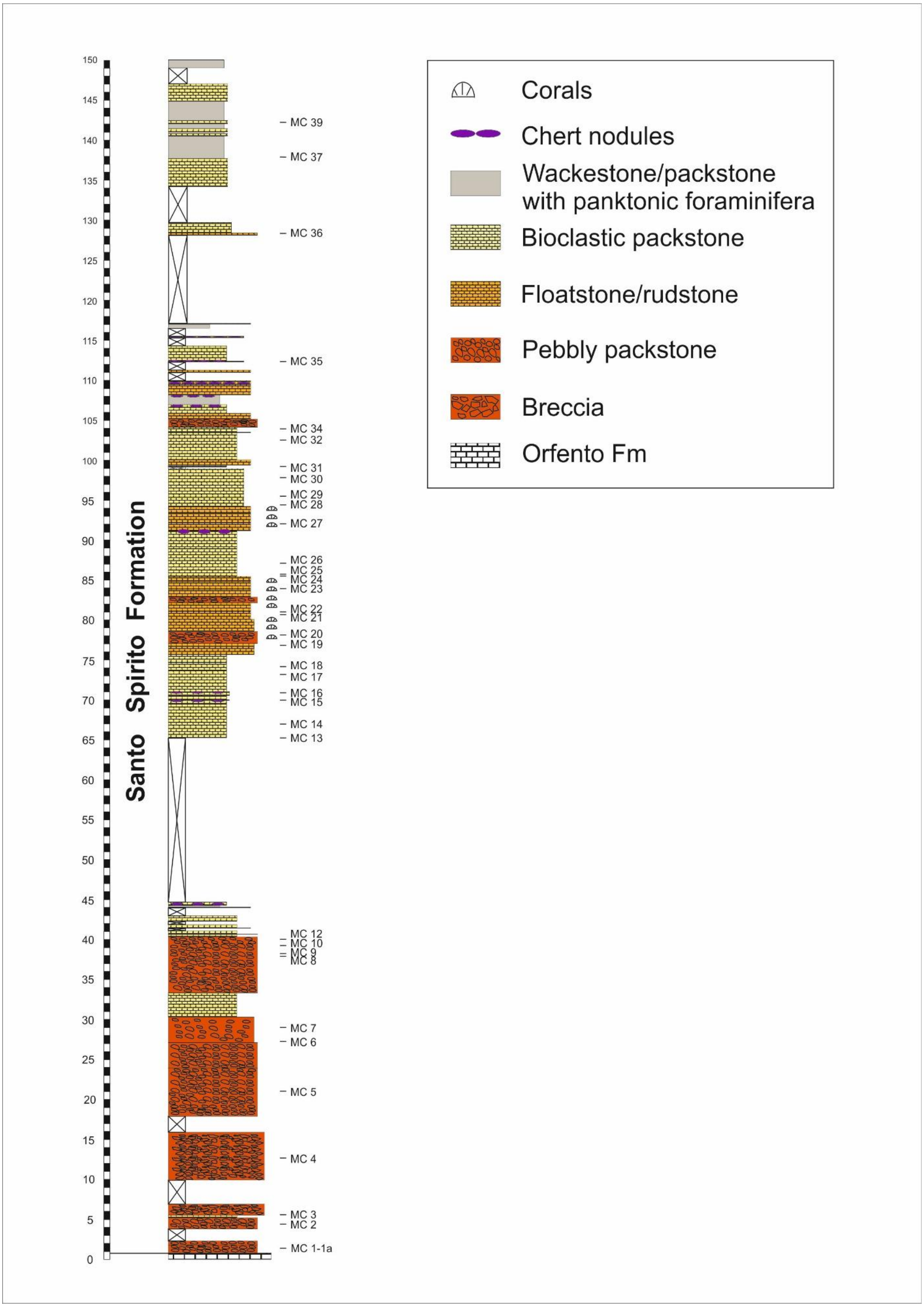

A.7: Pennapiedimonte section

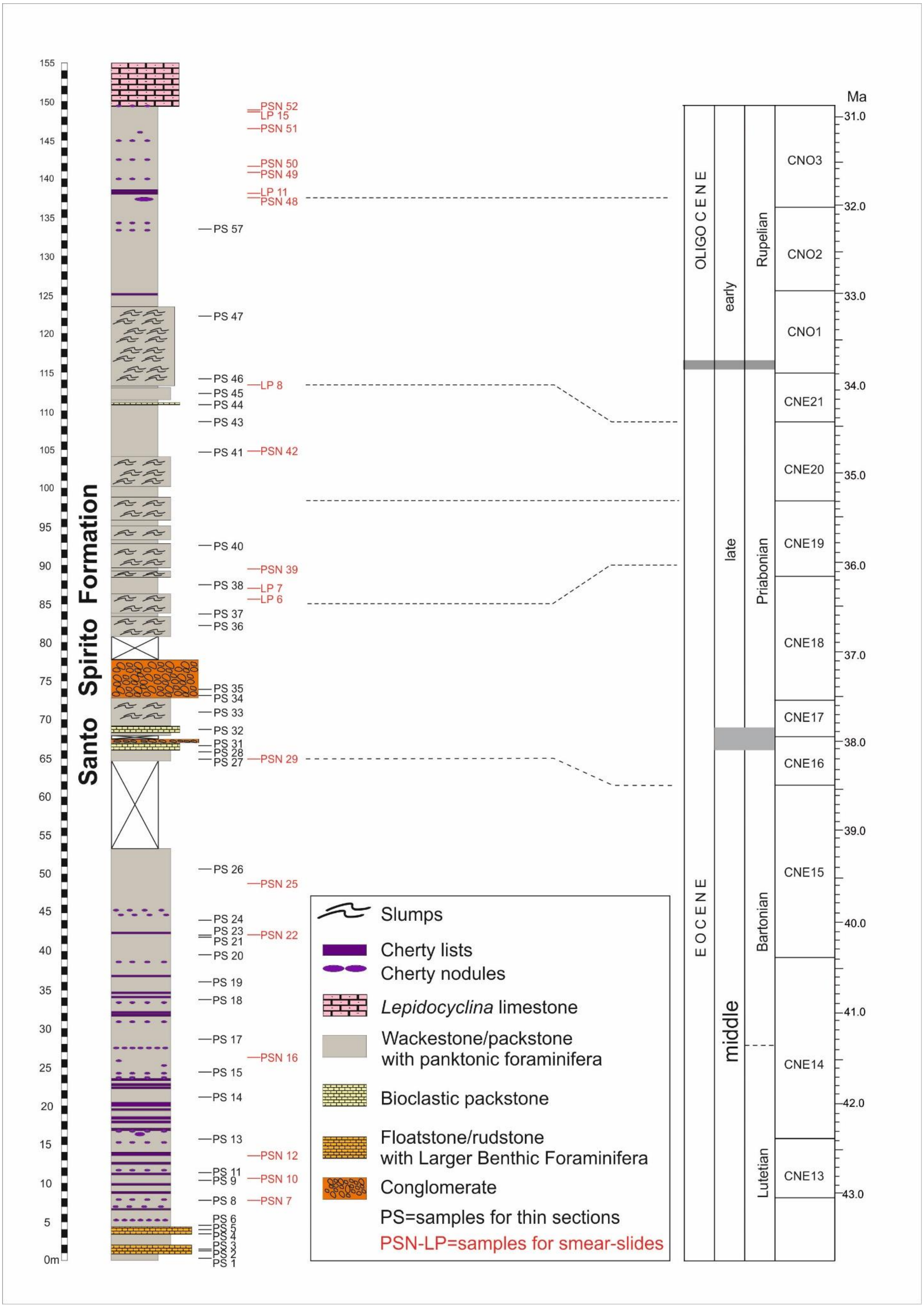

A.8: San Bartolomeo section

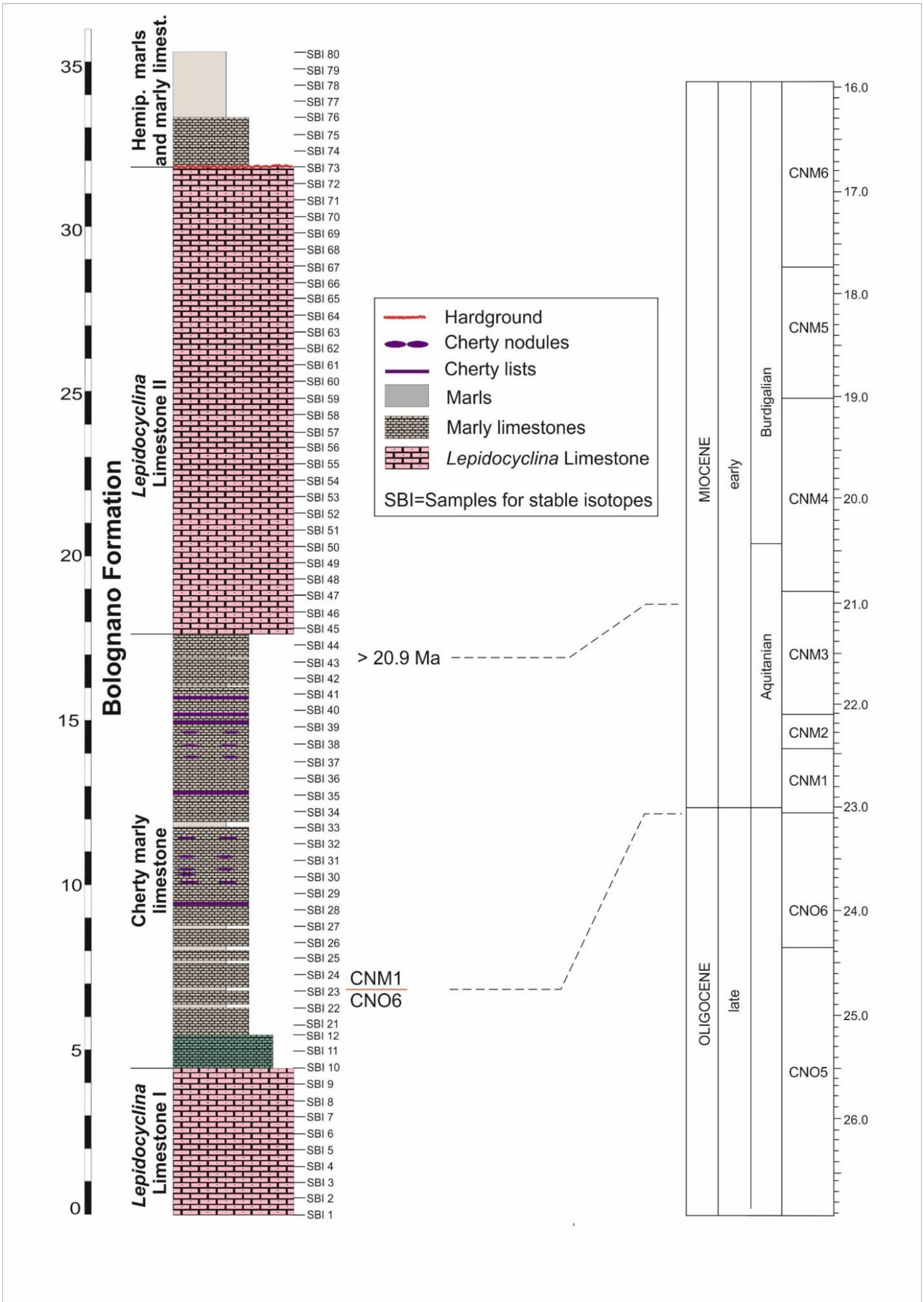

A.9: Orta River section

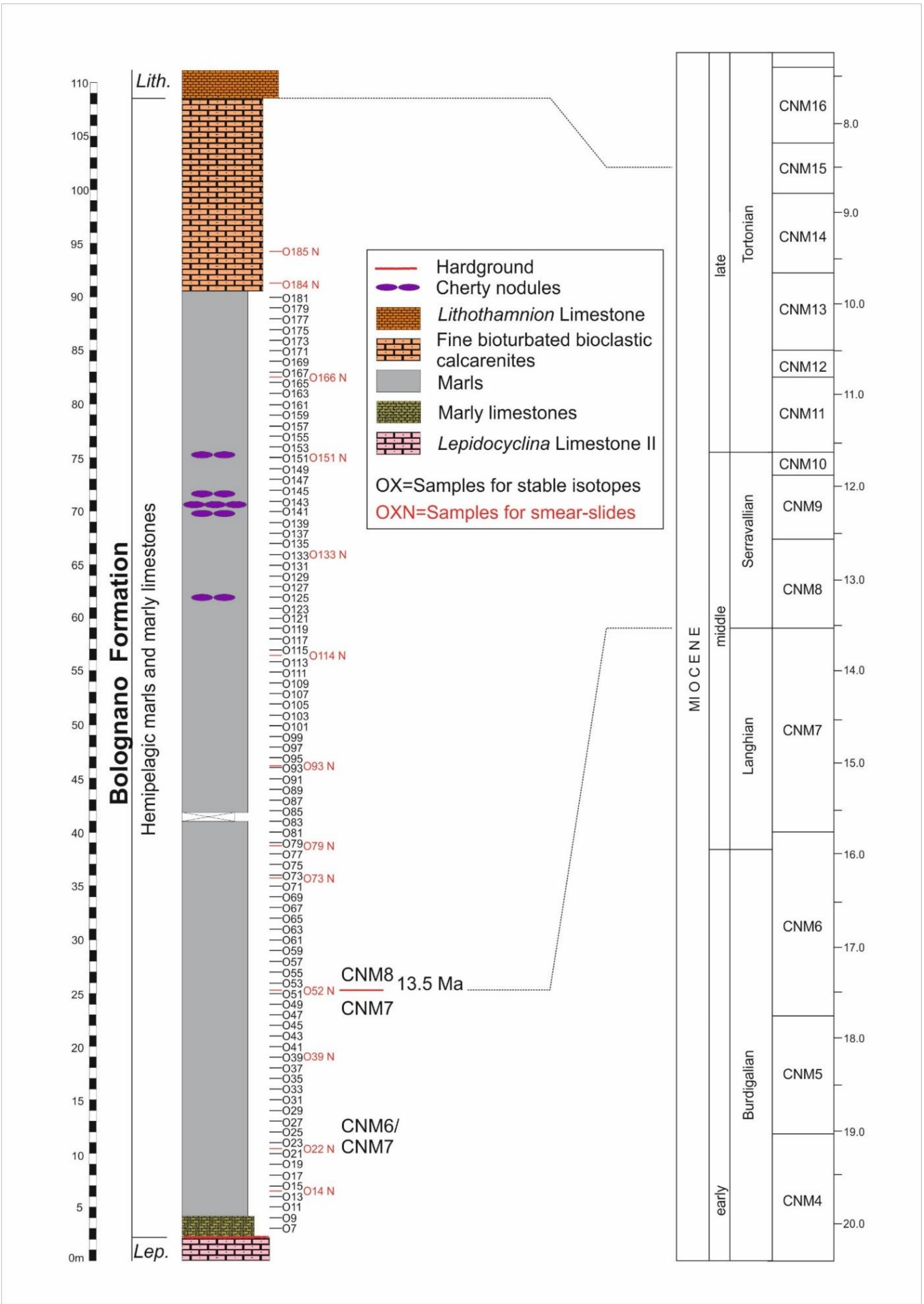

A.10: Roccamorice section

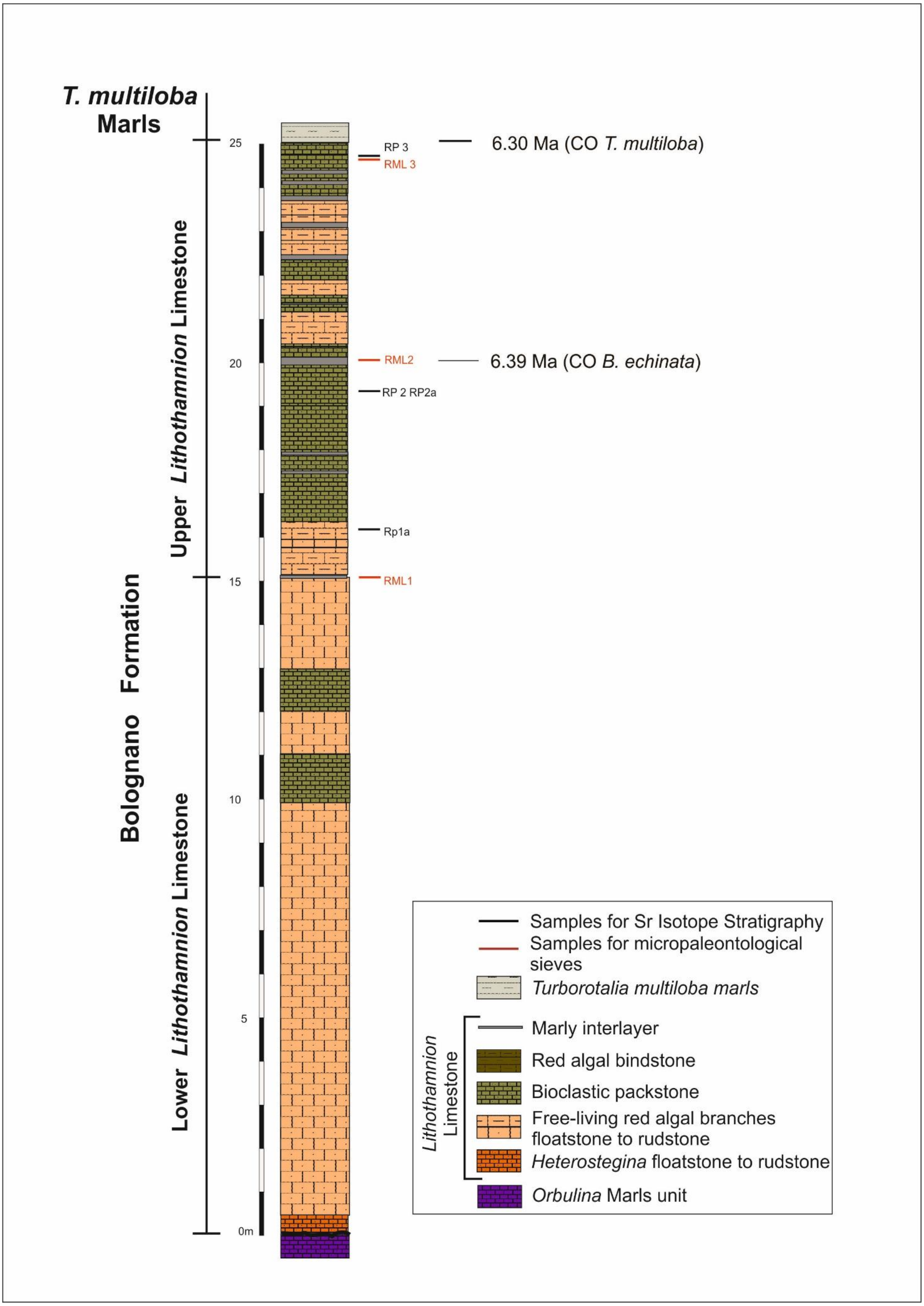

A.11: Costa dell'Avignone section

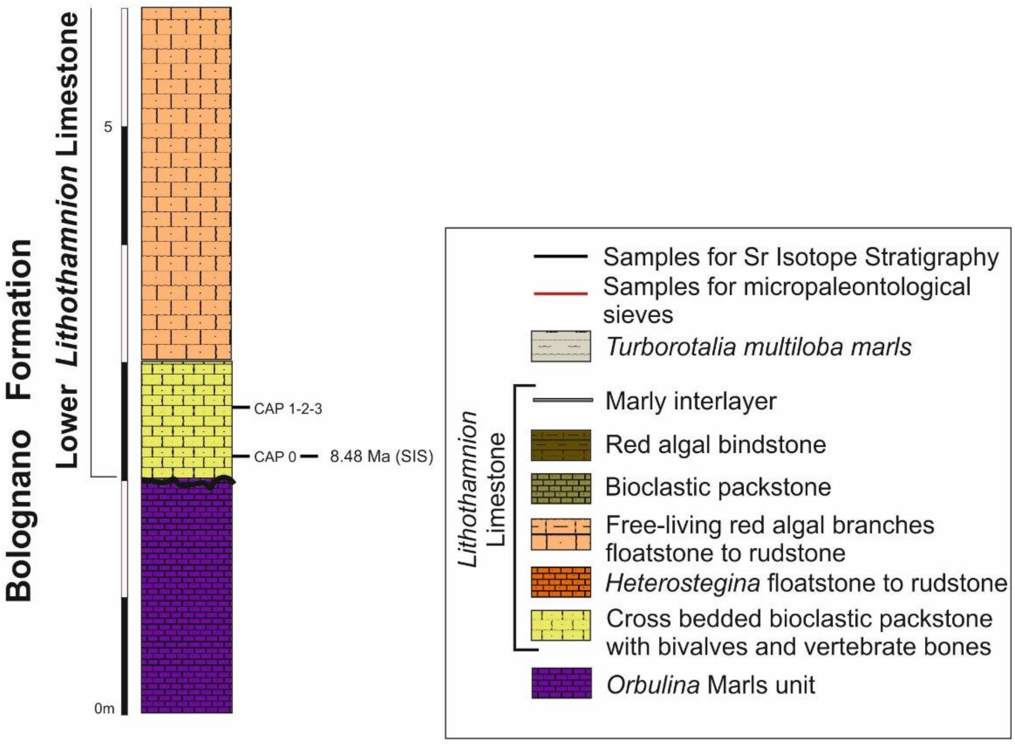

A.12: FONTE MACCHIALONGA SECTION

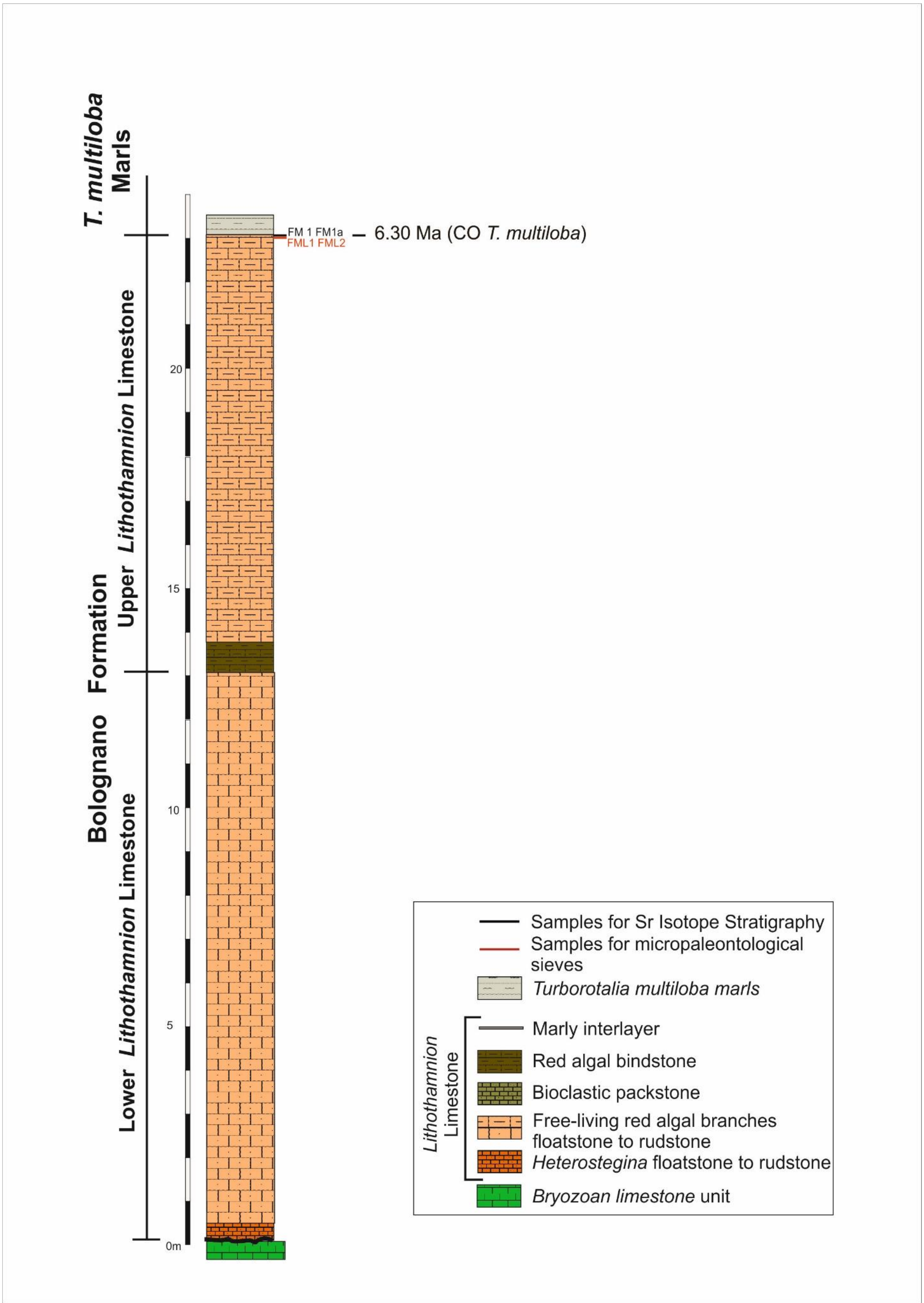

Annex B Detailed trace elements and isotope data

B.1: Carbon and oxygen isotope ratios of the Lettomanoppello section.

Sample	$\delta^{13}C$ (‰VPDB)	$\delta^{18}O$(‰VPDB)
IL1	1,44	-0,06
IL2	1,4	-0,20
IL3	1,45	-0,09
IL4	1,78	0,46
IL5	1,56	0,21
IL6	1,42	-0,06
IL7	1,58	0,48
IL8	1,77	0,64
IL9	1,72	0,79
IL10	1,87	0,89
IL11	1,86	0,74
IL12	1,61	0,95
IL13	1,62	0,80
IL14	1,41	0,55
IL15	1,49	0,60
IL16	1,46	0,28
IL17	1,30	0,08
IL18	1,52	0,33
IL19	1,44	0,66
IL20	1,78	1,04
IL21	1,68	1,09
IL22	1,33	0,70
IL23	1,34	0,03
IL24	1,53	0,62
IL25	1,55	0,71
IL26	1,61	0,48
IL27	1,78	0,79
IL28	1,05	0,30
IL29	1,05	0,06
IL30	1,08	0,32
IL31	1,06	0,02
IL32	0,99	0,02
IL33	1,19	-0,03
IL34	1,29	-0,35
IL35	0,91	-0,45
IL36	0,94	0,05

IL37	0,76	-0,15
IL39	1,02	0,08
IL40	0,83	0,16
IL41	0,99	0,02
IL42	0,98	0,02
IL43	0,81	-0,35
IL44	0,99	-0,15
IL45	1,04	0,25
IL46	0,95	0,26
IL47	1,23	0,05
IL48	1,12	0,17
IL49	1,02	0,39
IL50	0,98	0,43
IL51	0,70	0,03
IL52	1,07	0,07
IL53	1,44	0,21
IL54	1,45	0,22
IL56	1,04	0,52
IL57	0,93	0,19
IL58	0,93	0,09
IL59	1,02	0,09
IL60	1,2	0,05
IL61	0,79	-0,44
IL62	0,87	0,14
IL63	0,91	0,29
IL64	1,16	0,68
IL65	0,84	0,03

Table B.1: Carbon and oxygen isotope ratios of the Lettomanoppello section. All values are corrected to the international carbonate standard NBS19. Analitycal error is ±0,1‰ based on replicate standards.

B.2: Organic carbon isotope ratios of the Massignano Section

Sample	$\delta^{13}C_{org}$ (‰VPDB)
M0.5	-27,5
M1.0	-28,1
M1.5	-27,9
M2.0	-28,0
M2.5	-28,0
M3.0	-27,8
M3.5	-27,0
M4.0	-27,3
M4.5	-27,4
M5.0	-28,0
M5.5	-27,7
M6.0	-27,1
M6.5	-27,0
M7.0	-26,8
M7.5	-26,9
M8.0	-27,2
M8.5	-26,7
M9.0	-27,8
M9.5	-27,5
M10.0	-27,6
M10.5	-28,2
M11.0	-26,4
M11.5	-27,1
M12.0	-26,8
M12.5	-27,0
M13.0	-26,5
M13.5	-27,2
M14.0	-26,5
M14.5	-26,3
M15.0	-26,4
M15.5	-26,5
M16.0	-26,4
M16.5	-26,8
M17.0	-26,7
M17.5	-26,3
M18.0	-26,2
M18.5	-26,4
M19.0	-25,9
M19.5	-26,2

M20.0	-26,1
M20.5	-26,2
M21.0	-26,6
M21.5	-26,2
M22.0	-25,2
M22.5	-26,0
M23.0	-25,2

Table B.2: Organic carbon isotope ratios of the Massignano section. All the values are corrected to the IAEA-CH_6 and IAEA-CH_7 international standards. Analytical error is ±0,3‰ based on replicate standards.

B.3: Trace element concentration profiles of the Pectinid specimens of the Pietrasecca section

	PP1		PP2		PP3		PP4	
Element	mean	SD	mean	SD	mean	SD	mean	SD
Li	0,835	0,360624	< dl		0,995	0,595	0,805	0,007071
Be	0,653333	0,465009	< dl		< dl		< dl	
B	6,172	2,049773	3,396667	1,642809	7,07	0,849627	6,593333	1,468276
Na	630,67	131,4548	375,0467	83,74641	348,8867	36,021	819,4367	262,3503
Al	99,066	57,36787	4,486667	1,694704	79,57667	6,22932	72,77667	25,90306
Si	530,686	270,1157	130,15	19,47	274,6733	69,59013	240,1333	80,22953
K	317,432	140,355	213,5467	165,2453	138,4233	63,5159	272,05	65,34141
Sc	< dl		< dl		0,2195	0,0215	< dl	
Ti	12,908	14,41044	1,276667	0,604777	18,43	6,307392	10,2	3,861075
V	0,7906	0,355882	0,644667	0,190608	0,645	0,13436	0,307333	0,123961
Cr	1,764	0,979275	0,735	0,055	1,89	0,559345	1,686667	0,505404
Mn	*11,934*	*5,637915*	*26,22333*	*12,67071*	*12,04333*	*1,93524*	*23,97333*	*18,30796*
Fe	*1359,918*	*624,47*	*246,46*	*15,23718*	*664,9433*	*97,6135*	*269,5333*	*28,80373*
Co	0,5486	0,293866	0,172	0,059059	0,295667	0,052041	0,349	0,047624
Ni	11,472	9,350103	2,253333	0,618834	2,66	0,367786	2,4	0,726911
Cu	5,084	2,029847	6,03	3,058115	4,983333	1,319402	3,636667	0,891422
Zn	15,414	7,699856	11,95	2,107194	41,36667	4,609297	26,28667	6,792027
Ga	0,1324	0,110539	0,043	0,009	0,0895	0,0675	< dl	
Ge	< dl		0,3	0,03	< dl		0,266	0,048083
As	0,47925	0,33283	0,435	0,128906	0,242	0,108194	0,1935	0,05869
Rb	0,57	0,479831	0,140667	0,049101	0,263	0,078947	0,557667	0,240849
Sr	**1345,886**	**225,5528**	**1317,43**	**94,20783**	**571,8667**	**79,53033**	**991,7033**	**153,9171**
Y	0,11652	0,054437	0,163333	0,024513	0,371	0,062498	0,088233	0,023274
Zr	0,198	0,15982	0,0392	0,018396	0,230667	0,024554	0,222	0,096814
Nb	< dl		0,0092	0,004236	0,0251	0,010452	0,0233	0,014252
Cd	0,235333	0,168826	0,196667	0,073595	0,473667	0,082891	0,56	0,223383
In	0,0186	0,013294	0,006367	0,003088	0,023233	0,015675	0,063033	0,037655
Sb	0,075	0,07153	0,048	0,028	0,094333	0,033559	0,0845	0,019092
Cs	0,013375	0,006206	0,004	0,0012	0,0171	0,002286	0,018633	0,013154
Ba	4,498	1,105405	5,416667	1,226984	3,12	0,331361	3,846667	1,068379
La	0,19588	0,080849	0,105	0,007874	0,616667	0,083304	0,214333	0,108611
Ce	0,4296	0,248327	0,1202	0,052272	0,46	0,055227	0,362333	0,075302
Pr	0,05566	0,032353	0,007367	0,003512	0,070367	0,013514	0,016667	0,009571
Nd	0,09225	0,039084	0,087667	0,029273	0,234333	0,022291	0,074	0,029206
Sm	0,04175	0,020549	0,036267	0,019225	0,062333	0,031116	< dl	
Eu	< dl		< dl		< dl		< dl	
Gd	< dl		< dl		< dl		< dl	
Tb	< dl		< dl		< dl		< dl	
Dy	< dl		< dl		< dl		< dl	
Ho	< dl		< dl		< dl		< dl	
Er	< dl		< dl		< dl		< dl	

Tm	< dl		< dl		< dl		< dl	
Yb	< dl		< dl		< dl		< dl	
Lu	< dl		< dl		< dl		< dl	
Hf	< dl		< dl		< dl		< dl	
Ta	< dl		< dl		< dl		< dl	
Pb	0,3476	0,202447	0,294	0,051891	1,650667	0,632804	0,535667	0,164074
Th	0,01085	0,007529	0,003767	0,001994	0,017867	0,007858	0,011667	0,008376
U	0,6576	0,171061	0,131333	0,031372	0,622667	0,061478	0,210333	0,067099

	PP5		**PP6**		**PP7**		**PP8**	
Element	**mean**	**SD**	**mean**	**SD**	**mean**	**SD**	**mean**	**SD**
Li	1,66	0,565685	< dl		< dl		< dl	
Be	< dl		< dl		< dl		< dl	
B	10,18667	3,205001	2,373333	0,565184	2,91	1,705872	19,725	4,489725
Na	826,3067	111,4412	74,75	14,59925	100,0367	34,3955	278,1725	135,5826
Al	4,51	3,35671	208,76	88,15492	246,7133	91,92115	95,73	31,96317
Si	320,9	351,1227	369,9	263,7161	894,7133	300,7638	437,115	220,7216
K	38,73	7,125917	63,47333	35,44236	180,3733	19,1935	231,3075	53,08504
Sc	< dl		0,195667	0,047258	< dl		< dl	
Ti	< dl		38,70667	6,056586	17,20333	8,452161	10,045	3,33641
V	0,103	0,025239	1,114667	0,152179	1,778667	0,494209	0,58125	0,127126
Cr	1,88	0,692965	3,773333	1,680069	3,396667	1,224023	2,2775	1,202619
Mn	*8,066667*	*0,040415*	*32,85333*	*6,318199*	*31,94667*	*6,902147*	*6,44*	*2,614715*
Fe	*216,2267*	*15,32842*	*1326,273*	*144,018*	*974,24*	*140,7644*	*401,025*	*131,2112*
Co	0,229	0,029614	0,393333	0,020817	0,728333	0,338707	0,24875	0,123842
Ni	0,698	0,150373	7,07	8,860062	4,11	1,337423	19,635	33,54147
Cu	0,544333	0,141171	3,636667	1,375221	3,726667	1,037609	3,6225	2,91652
Zn	11,42333	0,885965	27,08667	9,923227	20,27667	5,398457	29,915	25,33169
Ga	0,059	0,042426	0,114333	0,01701	0,142	0,077272	< dl	
Ge	< dl		0,26	0,070711	< dl		< dl	
As	0,2915	0,026163	0,725	0,233345	1,656667	0,725695	0,211	0,083439
Rb	0,018	0,018809	0,263	0,174106	0,687	0,272721	0,4035	0,053057
Sr	**662,33**	**71,89904**	**291,8567**	**19,58748**	**316,1033**	**24,40703**	**1020,068**	**218,9436**
Y	0,154667	0,018502	0,514333	0,272188	0,581667	0,134031	0,15375	0,040705
Zr	0,064333	0,012503	0,311667	0,037314	0,582	0,233673	0,34025	0,157777
Nb	< dl		0,0592	0,036052	0,049733	0,018003	0,0406	0,02157
Cd	0,586667	0,333816	0,88	0,173494	0,793333	0,290918	1,0975	0,856052
In	< dl		< dl		< dl		< dl	
Sb	< dl		0,070333	0,024502	0,080333	0,067337	< dl	
Cs	< dl		0,017033	0,01742	0,055967	0,026087	0,040067	0,019194
Ba	2,503333	0,10504	4,05	0,753459	2,993333	0,487887	6,565	1,999608
La	0,117667	0,023502	15,55667	16,63303	0,693667	0,103413	0,243	0,117992
Ce	0,059267	0,020761	10,32	7,051092	0,849667	0,245017	0,5555	0,410296
Pr	0,0112	0,004359	0,093967	0,035392	0,0791	0,022242	0,02745	0,016167
Nd	< dl		0,374	0,090349	0,365	0,069087	0,1875	0,125646

Sm	< dl		0,112	0,127279	0,078333	0,012423	0,087333	0,068157
Eu	< dl		0,022433	0,006174	0,017	0,008479	< dl	
Gd	< dl		< dl		0,044	0,006245	< dl	
Tb	< dl		< dl		0,0106	0,001114	< dl	
Dy	< dl		< dl		0,054	0,013748	< dl	
Ho	< dl		< dl		0,020533	0,005718	< dl	
Er	< dl		< dl		0,041333	0,010263	< dl	
Tm	< dl		< dl		< dl		< dl	
Yb	< dl		< dl		< dl		< dl	
Lu	< dl		< dl		< dl		< dl	
Hf	< dl		< dl		< dl		< dl	
Ta	< dl		< dl		< dl		< dl	
Pb	0,431333	0,09888	1,050667	0,309684	0,695	0,120801	1,31025	0,953899
Th	< dl		0,033567	0,022566	0,025367	0,011617	0,019733	0,01236
U	0,132667	0,031786	0,451	0,236658	0,490333	0,098799	0,18975	0,040656

	PP9		**PP10**		**PP11**		**PP12**	
Element	**mean**	**SD**	**mean**	**SD**	**mean**	**SD**	**mean**	**SD**
Li	< dl		< dl		< dl		< dl	
Be	< dl		< dl		< dl		< dl	
B	2,616667	0,301054	3,336667	2,066551	7,87	5,484405	8,133333	1,56366
Na	75,43667	4,757314	82,93333	1,634391	489,0333	298,04	710,5333	344,8563
Al	330	54,50875	287,94	43,64088	91,7	60,26779	275,4633	185,5811
Si	896,2533	230,0261	754,69	140,2178	383,2933	148,0828	966,4233	452,0713
K	227,37	69,49581	196,6033	67,28184	124,6133	49,31703	629,3067	276,9114
Sc	0,103	0,042426	< dl		0,118	0,046293	0,172667	0,046458
Ti	19,32	5,767764	11,60333	2,493398	5,763333	3,959474	16,00333	10,729
V	1,114333	0,177725	1,472667	0,099626	0,775667	0,504397	2,97	0,775951
Cr	4,07	1,252158	1,54	0,443058	2,29	0,868504	6,723333	4,413891
Mn	*8,786667*	*0,558957*	*9,31*	*2,028078*	*13,09333*	*2,905896*	*19,19333*	*6,781109*
Fe	*431,8467*	*14,88676*	*417,6533*	*83,86747*	*455,5833*	*38,74103*	*994,2033*	*311,7317*
Co	0,205667	0,032517	0,195667	0,003786	0,272667	0,085734	0,435	0,292005
Ni	1,09	0,287924	1,173333	0,177858	2,41	0,84	5,553333	1,226553
Cu	1,288333	0,27587	1,031	0,313694	3,466667	0,883421	17,86	3,891683
Zn	9,573333	0,672483	6,713333	0,753746	31,37	2,823526	63,82333	29,17015
Ga	0,14	0,027495	0,186333	0,085149	0,074	0,049487	0,268333	0,114893
Ge	< dl		< dl		< dl		< dl	
As	0,77	0,261534	1,13	0,93723	0,55	0,228692	1,106667	0,392598
Rb	1,022667	0,384531	0,769667	0,079651	0,338333	0,241465	1,483	0,703795
Sr	**303,5067**	**26,52622**	**346,3867**	**21,89003**	**602,3367**	**149,7875**	**768,9633**	**350,1349**
Y	0,501667	0,016503	0,697	0,151486	0,3214	0,2839	0,791333	0,58644
Zr	0,319667	0,055788	0,261	0,005292	0,098	0,04078	0,516667	0,302451
Nb	0,119	0,034395	0,044	0,037084	0,0172	0,017746	0,069867	0,052876
Cd	0,77	0,052915	0,463333	0,135031	2,976667	1,625433	4,36	2,116436
In	< dl		< dl		< dl		0,047033	0,045965

Sb	0,127	0,158578	0,101667	0,040501	0,096667	0,016197	0,336	0,260085
Cs	0,076567	0,014527	0,062433	0,018597	0,019967	0,013367	0,0606	0,022429
Ba	3,62	0,587963	2,996667	0,555818	3,146667	0,237978	5,03	0,646452
La	0,688667	0,054638	0,643667	0,134805	< dl		0,947333	0,797146
Ce	0,671333	0,140976	0,674667	0,20292	< dl		1,239	0,808111
Pr	0,133067	0,025776	0,110433	0,025934	< dl		0,264133	0,306001
Nd	0,542333	0,088951	0,481	0,008185	< dl		< dl	
Sm	0,124333	0,061011	< dl		< dl		< dl	
Eu	< dl		< dl		< dl		< dl	
Gd	< dl		< dl		< dl		< dl	
Tb	< dl		< dl		< dl		< dl	
Dy	0,0493	0,039558	< dl		< dl		< dl	
Ho	< dl		< dl		< dl		< dl	
Er	< dl		< dl		< dl		0,087967	0,093989
Tm	0,009167	0,002178	< dl		< dl		0,010233	0,010289
Yb	< dl		< dl		< dl		< dl	
Lu	< dl		< dl		< dl		< dl	
Hf	< dl		< dl		< dl		< dl	
Ta	< dl		< dl		< dl		< dl	
Pb	0,734667	0,055429	0,745	0,14971	1,320667	0,454152	6,036667	3,559345
Th	0,045433	0,035885	0,044567	0,031028	0,02885	0,003465	0,044267	0,022673
U	0,744	0,112308	0,550333	0,026858	0,211333	0,0845	0,423667	0,345839

	PP13		PP14		PP15		PP16	
Element	mean	SD	mean	SD	mean	SD	mean	SD
Li	< dl		< dl		< dl		< dl	
Be	< dl		< dl		< dl		< dl	
B	12,85	3,6127	18,52667	6,099658	11,79333	3,980067	7,556667	6,924409
Na	1099,55	244,4793	922,6567	162,7436	646,9467	302,7093	436,9933	118,8628
Al	6,263333	2,484398	1720,683	858,3069	630,6133	530,5378	854,3967	690,6758
Si	55,29	22,14658	6708,487	2646,513	2755,513	1598,919	2377,597	2149,727
K	41,90333	8,474676	1962,667	1031,135	790,36	391,3224	569,9167	558,9753
Sc	0,061	0,014933	0,493333	0,190148	0,441667	0,202989	0,459	0,557506
Ti	4,036667	4,925133	127,03	72,29914	38,92333	41,11651	41,89333	34,43639
V	0,242667	0,035247	6,206667	3,69941	9,896667	6,5057	4,58	5,231262
Cr	0,97	0,650538	5,52	2,8366	11,68667	3,704839	5,953333	3,787629
Mn	*3,64*	*1,178474*	*196,31*	*15,17277*	*92,95667*	*29,70023*	*62,66333*	*14,34429*
Fe	*231,7*	*44,10421*	*2127,533*	*724,5319*	*2074,34*	*586,9365*	*1151,187*	*905,5985*
Co	0,139667	0,058688	2,293667	0,856195	1,182333	0,300442	9,193333	5,076045
Ni	1,072667	0,393936	13,03667	4,685193	8,02	1,610466	6,083333	2,225002
Cu	0,562667	0,286247	9,903333	3,158248	5,416667	0,996109	12,64	5,493232
Zn	6,936667	3,772669	66,43667	24,23037	40,07333	11,85705	72,57667	29,08056
Ga	< dl		0,991	0,463434	0,442333	0,093297	0,309	0,326758
Ge	< dl		< dl		0,393333	0,109697	< dl	
As	0,171	0,081062	0,536667	0,221435	4,636667	2,183125	< dl	

Rb	0,0526	0,028654	8,376667	4,377377	3,278667	2,468454	2,958333	2,656936
Sr	**997,2733**	**139,4339**	**1358,39**	**183,2197**	**1333,177**	**307,2154**	**908,3**	**101,8824**
Y	0,017267	0,013342	1,093667	0,387692	2,741667	0,701611	0,936	0,329774
Zr	0,0105	0,005693	3,583	3,359566	1,030333	0,610059	0,639333	0,372356
Nb	0,00205	0,000212	0,378667	0,212872	0,1421	0,166035	0,135667	0,096966
Cd	0,230667	0,047014	2,186667	0,323934	2,65	0,641561	3,576667	0,566598
In	< dl		0,039833	0,039259	0,022467	0,005155	0,03915	0,0408
Sb	0,037967	0,007919	0,124667	0,038991	0,422667	0,238764	0,272	0,195161
Cs	< dl		0,525	0,167538	0,173133	0,113004	0,274333	0,174809
Ba	2,921	1,378239	< dl		7,216667	0,548118	9,336667	3,158961
La	0,017833	0,008749	< dl		2,727333	0,509059	1,050333	0,678898
Ce	0,030567	0,027166	< dl		2,922333	1,427979	1,926333	1,585756
Pr	0,0063	0,00741	< dl		0,586667	0,133452	0,141733	0,146846
Nd	< dl		< dl		2,176667	0,674487	0,746	0,577761
Sm	< dl		< dl		0,323667	0,074527	0,2585	0,086974
Eu	< dl		< dl		< dl		< dl	
Gd	< dl		< dl		< dl		< dl	
Tb	< dl		0,026167	0,006962	< dl		< dl	
Dy	< dl		0,105667	0,016773	< dl		< dl	
Ho	< dl		< dl		< dl		< dl	
Er	< dl		< dl		< dl		< dl	
Tm	< dl		< dl		< dl		< dl	
Yb	< dl		< dl		< dl		< dl	
Lu	< dl		< dl		< dl		< dl	
Hf	< dl		< dl		< dl		< dl	
Ta	< dl		< dl		< dl		< dl	
Pb	3,306667	2,236836	4,926667	1,466163	4,643333	1,681497	3,926667	2,365255
Th	< dl		0,161	0,069735	0,095	0,017349	< dl	
U	0,1234	0,037178	0,384333	0,1132	6,396667	4,980224	0,789667	0,538547

Table B.3: Trace element concentration profiles, reported as mean values and standard deviations, of the pectinid shell samples of Pietrasecca section. All the mean values are reported in ppm. Number of measurements: n= 5 for PP1; n= 4 for PP8; n= 3 from PP2 to PP7 and from PP9 to PP16. dl = detection limit.

B.4: CARBON AND OXYGEN ISOTOPE RATIOS OF THE SELECTED PECTINID SPECIMENS OF THE PIETRASECCA SECTION

Sample	$\delta\ ^{13}C$ (‰ VPDB)	$\delta\ ^{18}O$ (‰ VPDB)
PP0	0,39	-1,20
PP1	-0,18	-0,24
PP2	0,46	-0,42
PP4	1,29	-0,14
PP5	1,58	-0,38
PP8	1,18	-0,89
PP13	1,92	-0,20
PP16	1,16	0,30

Table B.4: Carbon and oxygen isotope ratios of the pectinid specimens of the Pietrassecca section. $\delta\ ^{13}C$ and $\delta\ ^{18}O$ have been measured only on the well-preserved shells, according to the trace elements profile of Table B.3. All values are corrected to the international carbonate standard NBS19. Analitycal error is ±0,1‰ based on replicate standards.

B.5: SR ISOTOPE RATIOS OF THE SELECTED PECTINID SPECIMENS OF THE PIETRASECCA SECTION

Sample	$^{87}Sr/^{86}Sr$	2s.e.(*10^{-6})
PP0	0.708542	6
PP1	0,708616	9
PP2	0,708689	9
PP 2*	0,708684	17
PP5	0,708731	9
PP12a	0.708542	5
PP13	0,708780	6
PP 13*	0,708754	15
PP15	0.708855	4
PP16	0,708897	7
PP 16*	0,708898	9
PP 16*	0,708896	8
Eighteen replicate analyses of NIST 987 gave an average value of 0.710246±0.000011 (2 s.e.).		
2s.e. errors are in run errors.		
* = repeated samples		

Table B.5: $^{87}Sr/^{86}Sr$ values of the pectinid shell samples reported with related analytical error (2 SE).

B.6: Carbon and oxygen isotope ratios of the San Bartolomeo section

Sample	$\delta^{13}C$ (‰VPDB)	$\delta^{13}C$ (‰VPDB)
SBI 1	0,81	1,07
SBI 2	0,72	0,76
SBI 3	0,92	1,40
SBI 4	0,54	1,17
SBI 5	0,56	1,28
SBI6	0,27	0,99
SBI 7	0,40	1,19
SBI8	0,36	0,80
SBI9	0,52	0,85
SBI10	0,58	1,07
SBI11	0,49	0,58
SBI12	0,02	0,25
SBI 21	0,49	0,07
SBI22	0,67	0,41
SBI 23	0,72	0,53
SBI24	0,68	0,58
SBI 25	0,59	0,58
SBI26	0,43	0,11
SBI 27	0,55	0,22
SBI 28	0,51	0,39
SBI 29	0,44	0,53
SBI30	0,53	0,68
SBI31	0,25	0,14
SBI32	0,45	0,49
SBI 33	0,99	1,04
SBI 34	0,77	1,54
SB35	0,56	0,46
SBI 36	0,67	0,79
SBI 37	0,82	0,89
SBI38	0,79	0,96
SBI39	0,95	0,97
SBI40	0,48	0,35
SBI 41	0,92	0,79
SBI 42	0,61	0,45
SBI43	0,87	0,94
SBI 44	0,61	0,76
SBI 45	0,70	0,57
SBI46	0,74	0,56
SBI47	1,15	1,06
SBI 48	0,97	1,06
SBI49	1,22	1,07

SBI 50	0,93	0,98
SBI 51	1,27	1,29
SBI52	1,06	0,92
SBI 53	0,74	0,75
SBI 54	1,22	1,10
SBI55	1,10	0,96
SBI 56	1,25	1,53
SBI57	0,65	0,44
SBI58	0,38	0,80
SBI59	0,70	0,54
SBI60	0,79	0,67
SBI 61	0,89	0,38
SBI 62	1,23	0,81
SBI 63	0,65	1,13
SBI64	0,88	0,97
SBI 65	0,99	0,87
SBI 66	1,81	1,15
SBI67	1,26	1,22
SBI 68	1,40	1,35
SBI69	1,72	0,77
SBI70	2,12	0,56
SBI 71	2,65	1,04
SBI 72	1,91	1,13
SBI 73	2,40	1,42
SBI74	2,28	-0,24
SBI75	0,95	-0,04
SBI 76	1,40	-0,14
SBI77	1,21	-0,51
SBI78	1,37	-0,36
SBI79	1,21	-0,15
SBI 80	1,50	0,27

Table B.6: Carbon and oxygen isotope ratios of the San Bartolomeo section. All values are corrected to the international carbonate standard NBS19. Analitycal error is ±0,1‰ based on replicate standards.

B.7: Carbon and oxygen isotope ratios of the Orta River composite section

Sample	$\delta^{13}C$ (‰VPDB)	$\delta^{13}C$ (‰VPDB)
O-7	1,95	0,08
O-9	1,91	0,07
O-11	1,39	-0,24
O-13	1,35	0,00
O-15	1,34	0,05
O-17	1,35	0,06
O-19	1,50	0,15
O-21	1,77	0,16
O-23	1,38	-0,13
O-25	1,59	0,53
O-27	1,69	0,43
O-29	1,14	-0,15
O-31	1,42	0,29
O-33	1,57	0,47
O-35	1,40	0,20
O-37	1,08	-0,19
O-39	1,31	0,28
O-41	1,37	0,34
O-43	1,18	0,21
O-45	1,97	0,41
O-47	2,25	0,71
O-49	1,43	0,32
O-51	1,81	0,42
O-53	1,68	0,68
O-55	1,45	0,61
O-57	1,25	0,49
O-59	1,41	0,40
O-61	1,43	0,59
O-63	1,20	0,56
O-65	0,63	0,23
0-67	1,30	0,59
O-69	1,13	0,43
O-71	1,26	0,45
O-73	1,33	0,74
O-75	1,08	0,50
O-77	1,22	0,63
O-79	0,87	0,19
O-81	1,33	0,84
O-83	1,36	0,83
O-85	0,94	0,32
O-87	1,04	0,62

O-89	1,33	0,70
O-91	0,96	0,56
O-93	0,84	0,20
O-95	0,89	0,40
O-97	0,83	0,43
O-99	1,13	0,73
O-101	1,02	0,59
O-103	1,09	0,69
O-105	0,95	0,55
O-107	1,08	0,41
O-109	0,45	-0,06
O-111	0,79	0,46
O-113	0,87	0,76
O-115	0,57	0,84
O-117	0,55	0,67
O-119	0,74	0,77
O-121	0,67	0,71
O-123	1,13	1,04
O-125	1,01	0,76
O-127	0,63	0,76
O-129	0,89	1,02
O-131	0,84	0,78
O-133	0,90	0,88
O-135	1,05	0,72
O-137	0,53	0,35
O-139	0,82	0,28
O-141	1,32	0,54
O-143	1,08	0,12
O-145	0,56	0,27
O-147	0,37	0,06
O-149	0,70	0,56
O-151	0,56	0,24
O-153	0,46	0,15
O-155	0,50	0,03
O-157	0,56	0,30
O-159	0,56	0,20
O-161	0,67	0,18
O-163	0,61	0,28
O-165	1,03	0,60
O-167	0,75	0,58
O-169	0,46	0,54
O-171	0,69	0,90
O-173	0,45	0,63

O-175	0,17	0,43
O-177	0,24	0,15
O-179	0,46	-0,14
O-181	0,36	0,13

Table B.7: Carbon and oxygen isotope ratios of the Orta River section. All values are corrected to the international carbonate standard NBS19. Analitycal error is ±0,1‰ based on replicate standards.

B.8: Sr element concentration and carbon and oxygen isotope profiles of the foraminifera tests analysed in Chapter 4

Sample	Sr (ppm)	SD	Sr/Ca (mmmol/mol)	SD	δ ^{13}C (‰ VPDB)	δ ^{18}O (‰ VPDB)
RMI3	894,64	164,95	1,06	0,009	0,55	0,69
MDCI4	835,45	100,38	1,14	0,014	0,53	0,88
CAV	1183,84	321,55	0,92	0,014	0,8	0,17
MDCI1a	1057,00	278,19	1,19	0,012	1,07	0,09
VI1	1138,74	271,42	1,29	0,054	0,02	0,03
MO93	1133,10	296,06	1,28	0,061	0,08	-1,54
MO67	885,76	224,89	1,33	0,025	-0,4	-1,82
MO15	1138,17	260,38	1,18	0,022	-0,34	-2,04
P2	1155,09	187,56	1,30	0,037	-0,47	-1,45
P20	1021,48	94,26	1,02	0,008	-0,16	-1,8
CT47	786,41	298,67	1,37	0,064	-0,55	-2,08
CT36	1036,70	284,06	1,22	0,029	-0,09	-2,46
CT8	995,69	375,57	0,98	0,012	0,13	-1,96
CT3	938,61	157,56	1,03	0,010	0,98	-1,55
n= 4 for CT8, MO67, MO93						
n=5 for CT3, CT36, CT47, MO15, P2, P20, CAV, MDCI1a, MDCI4, RMI3						
n= 6 for VI1						

Table B.8: Sr element concentration profiles of the foraminifera tests analysed in Chapter 4. CT3, CT8, CT36, CT47 belong to the Contessa section (Annex). P20, P2, MO15, M67, MO93 belong to the Moria section (Annex). VI1, MDCIa, CAV, MDCI4 belong to the composite section La Vedova-Monte dei Corvi (Annex). RMI3 belongs to the Roccamorice section (Annex). Mean values and as Sr/Ca (mmol/mol) ratios. δ^{13}C and δ^{18}O values are corrected to the international carbonate standard NBS19. Analitycal error is ±0,1‰ based on replicate standards.

B.9: Sr and Nd isotope ratios of the foraminifera tests analysed in chapter 4

Sample	Sr	2s.e. ($*10^{-6}$)	Nd	2s.e. ($*10^{-6}$)	$(\varepsilon_{Nd})_t$	±
RMI3	0,708869	10	0,511895	47	-14,4	0,9
MDCI4	0,708832	9	0,512341	13	-5,6	0,3
CAVOLO	0,708793	9	0,512251	13	-7,3	0,3
MDCI 1a	0,708824	21	0,512344	19	-5,5	0,4
VI 1	0,708717	11	0,512244	10	-7,5	0,2
MO 93	0,708702	19	0,512445	7	-3,5	0,1
MO 67	0,708529	7				
MO 15	0,708415	7	0,51223	27	-7,7	0,5
P 2	0,708466	9	0,512271	13	-6,9	0,3
P 20	0,708656	18	0,512212	47	-8,0	0,9
CT 47	0,708252	6				
CT 36	0,708565	12	0,512355	19	-5,2	0,4
CT 8	0,708480	37	0,512348	7	-5,3	0,1
CT 3	0,708243	16				
Standard values	NIST 987		0,710232	19 2s.e. ($*10^{-6}$)		N=51
	J Nd i 1		0,512105	10 2s.e. ($*10^{-6}$)		N=25

Table B.9: Sr and Nd isotope ratios of the foraminifera test analysed in Chapter 4. All Sr isotope values are corrected to 0.710248, as reported by McArthur et al., 2001. Sr isotope values are not corrected by age, given very low Rb/Sr of analyzed samples. Nd isotope values are corrected by age assuming Sm/Nd ratio of samples same as seawater (0.122), as reported by Piepgras and Wasserburg (1980).

B.10: Trace element profiles and carbon and oxygen isotope ratios of the pectinid and brachiopod shells analysed in Chapter 5

Sample	Mg (ppm)	Mn (ppm)	Fe (ppm)	Sr (ppm)	Ba (ppm)	δ 13C (‰ VPDB)	δ 18O (‰ VPDB)
CAP0	1285,46	69,37	190,90	1009,98	219,52	1,92	1,10
CAP1	2074,10	8,86	118,80	552,18	101,76	0,76	0,64
CAP2	1047,90	73,51	185,38	516,24	183,20	1,33	0,67
CAP3	2596,61	141,46	79,91	1078,81	45,66	0,17	0,77
RP1a	2961,18	105,92	183,44	1099,49	64,24	-0,32	0,25
RP2	2323,96	10,63	68,09	654,15	0,00	-0,05	2,64
RP2a	983,91	121,87	75,55	657,15	74,05	-0,33	2,40
RP3	2032,58	146,49	113,58	263,62	100,83	0,73	1,63
FM1	2249,04	74,37	93,61	482,59	113,32	0,94	3,47
FM1a	7562,19	156,72	145,94	865,89	87,74	1,08	2,79

B.10: Trace element concentrations profiles of Mg, Mn, Fe, Sr and Ba and carbon and oxygen isotope ratios of the pectinid and brachiopod shell samples analysed in Chapter 5. $\delta^{13}C$ and $\delta^{18}O$ values are corrected to the international carbonate standard NBS19. Analitycal error is ±0,1‰ based on replicate standards.

B.11: Sr isotope ratios of the pectinid and brachiopod shells analysed in Chapter 5

Sample	($^{87}Sr/^{86}Sr$)	$2\sigma_{mean}$ (*10^{-6})	($^{87}Sr/^{86}Sr$)^{1}	2σ (*10^{-6})^{2}
CAP0	0,708908	7	0,708927	14
CAP3	0,708906	4	0,708925	14
RP1a	0,708876	5	0,708895	14
RP2	0,708679	6	0,708698	14
RP2a	0,708547	4	0,708567	14
FM1	0,708864	5	0,708883	14
FM1a	0,708913	6	0,708932	14

Table B.11: $^{87}Sr/^{86}Sr$ values of the pectinid and brachiopod shell samples reported with related analytical error ($2\sigma_{mean}$). 1) Corrected $^{87}Sr/^{86}Sr$ assuming a NBS 987 value of 0.710245 while our measured NBS 987 value was 0.710226±0.000014 (n=12). 2)External precision based on repeated measurements of NBS 987 during the study gave a value 0.710226±0.000014 (n=12, 2SD).